The Impact of Wind Generation on Power System Voltage Stability

Thesis presented for the Degree of

Doctor of Philosophy

at the University of Strathclyde.

by

Ibrahim Soliman Mohamed Naser

Supervisor: Professor K. L. Lo

Power Systems Research Group

Department of Electronic and Electrical Engineering

University of Strathclyde.

May 2013

Acknowledgement

First and foremost, all praise goes to Allah The Almighty, the only one God, for enlightening my way and directing me through each and every success I have ever reached or may reach. I would like to express my sincere gratitude to my supervisor, Professor K. L. Lo, Head of the Power Systems Research Group (PSRG), University of Strathclyde, Glasgow for his supervision and valuable guidance throughout my research period. His encouragement and help contributed greatly in my current achievements.

I also thank the Cultural Attaché and all the members of Libyan Embassy in London for their assistance and cooperation. My appreciation also goes to my sponsor, Ministry of Higher Education and Scientific Research in Libya, for offering me the full scholarship throughout the duration of my PhD study.

I wish to extend my gratitude to all the colleagues at PSRG for their kindness and readiness to help. A special thanks to Dr Abdullahi Garba for his help and support in various stages in this work through technical discussion or in other perspective issues that whenever I asked him for help or advise I found him very helpful. To friends Dr Thmvarit, Dr Chunyang Zhao, Umarin Sangpanich, Jingling Sun and Fahad Saeed for the valuable academic discussions and the help that they provided me during the days in Glasgow. Also, special thanks to Mr Ibrahim Abdulhadi in Advanced Electrical Systems Group, University of Strathclyde, for his help, advice and support in technical discussion in various stages or in other perspective issues.

Last but not least, I deeply appreciate the help and support of my wife and my children. Their encouragement, inspiration and unlimited love have contributed invaluably towards my PhD achievement. I also wish to thank my brothers and sisters who have been through with me all the period of this research work.

Abstract

The need for a reduction in pollution emissions, especially from electricity generating facilities, has led to an increased interest in electricity generation from renewable sources. Wind generation seems to be a favourable form of renewable generation considering the growth rate of wind generation. However, an increase in wind generation is influencing overall power system operation and planning in terms of voltage stability. Also, power flow pattern and system's dynamic characteristics change when large percentages of wind generation are connected to the grid. Wind generation is characterised by its variability and intermittency, and as such present major challenges to power system operators. Some of these challenges are examined in detail in this thesis. The main focus is on the impact of DFIG based wind generation on system voltage stability.

Therefore, the main contributions of this thesis are, first of all, the original methodology for determining a voltage collapse proximity indicator presented by Alammari and Kwok L Lo (1996) is developed further that considers the wind generator reactive power limits. Secondly, the thesis proposes a new assessment methodology regarding the wind generation impact on voltage stability of power systems, taking into consideration wind generation intermittency and load variations. In this methodology, a voltage collapse proximity indicator (VCPI) based on network loadability is used to investigate the contribution of wind generation to voltage stability. This thesis then develops a comprehensive methodology for calculating the power margin based on wind generation variability. In this methodology, the power stability margin is used to measure the impact of wind generation on system voltage stability.

In addition, the impact of wind generation intermittency and the penetration on system MWh losses based on system loadability is also investigated. In the simulation, wind data measured and collected for one month is used. To verify the analysis

methodologies, a variety of test networks are used. These range from a 3-bus system to the IEEE 14-bus system, IEEE 30-bus system, IEEE-118 bus system and the UKGDS test distribution network. These networks are used as sample test systems using recorded and generated wind data, and the wind sources are connected at different network locations. The commercial software Power World Simulator is used to obtain simulated results. Sets of results have been obtained for different wind condition cases for different systems which clearly demonstrate the validity and effectiveness of the developed analysis methods.

Declaration of Author's Right

Table of Contents

List of Figures

List of Tables

Glossary of Terms

DFIG	Doubly-Fed Induction Generator
DRSG	Direct Drive Synchronous Generator
ED	Economic Dispatch
FRT	Fault Ride-Through Capability
GWEC	Global Wind Energy Council
IGBT	Insulated Gate Bipolar Transistors
OPF	Optimal Power Flow
PCC	Point Common Coupling
SCIG	Squirrel Cage Induction Generator
TNO	Transmission Network Operator
UCTE	Union Coordination Transmission Electricity
UKGDS	United Kingdom Generic Distribution System
VCPI	Voltage Collapse Proximity Indicator
VSC	Voltage Source Converters
WF	Wind Farm
WG	Wind Generator
WP	Wind Penetration

Chapter 1

Introduction

1.1 Electrical Power System

The development of the power system over the years has produced an interconnection of large numbers of generators and transmission systems that serve different loads in the networks. To maintain stability of any power system, the demand and generation must be kept in constant balance, taking into account system losses.

In the recent years power systems are becoming more complex due to increased interconnections that being operated close to their transmission stability limits due to economics and environmental considerations; and increased penetration of power electronic interfaced renewable power plants with different dynamic characteristics compared to that of conventional synchronous machines. Traditional power systems consist of three main parts, power generation, and transmission and distribution networks, and its structure is shown in Figure 1.1.

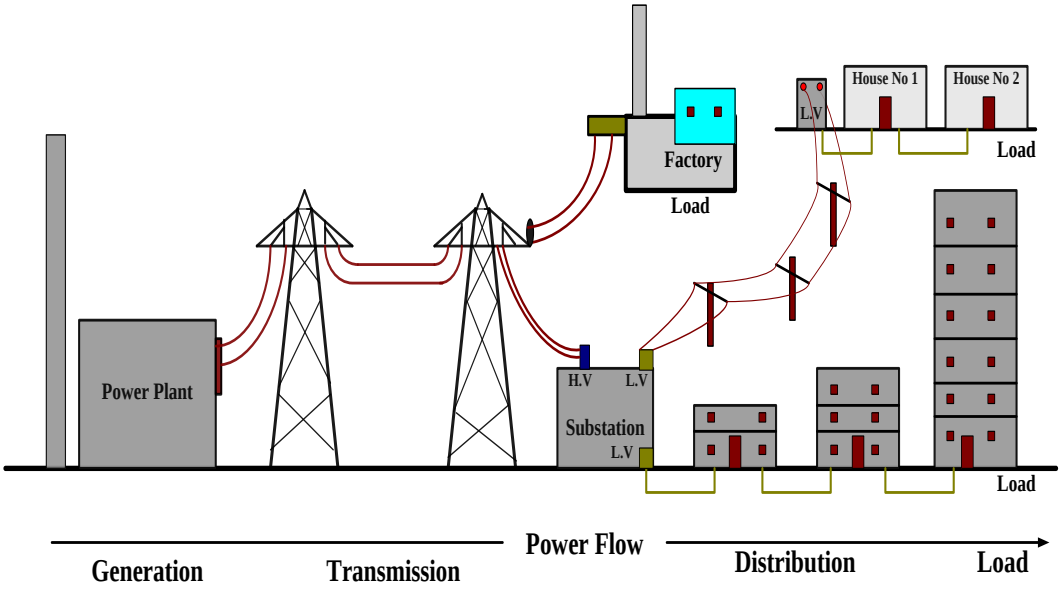

Figure 1.1: A traditional power system structure.

The demand for electrical energy in the world is increasing every year. The primary energy sources to meet this demand are fossil fuels (coal, oil, and natural gas), nuclear fission and water. The primary energy source such as coal is used to generate heat which is used in a steam-cycle to convert the thermal energy into mechanical energy, which is then to power electric generators.

Nuclear units are based on similar principle, but use nuclear fission as the input energy source. For hydro power, the gravitational (potential) energy of water in large reservoirs is converted into kinetic energy and then into mechanical energy using hydro turbine, which drives electric generators. A drawback of generating electricity from fossil fuels is their harmful environmental impact. They produce pollution by emitting toxic gases such as carbon dioxide (CO_2), sulphur oxides (SO_X) and nitrogen oxides (NO_X) [1]. Recently, many counties are encouraging the use of renewable clean energy sources such as solar cell and wind power due to environmental concern and the push for carbon-free power generation. Wind power has emerged as one of the viable forms of renewable and clean energy that can be used for electricity generation. For the operation of power systems with significant a mounts of renewable, the importance of conventional generation will remain or may increase even further in order to guarantee a reliable power supply. The transmission is made up of a high-voltage ac or any dc network, and is designed to transmit power from generation units to the load centres; the connections to load centres are normally through step-down power transformers. The transformers are used for voltage level matching.

Normally, distribution system uses medium and low-voltage levels (132kV/33kV/11kV) for electric power transmission over short distances. The distribution system connects the customer load with the transmission which is connected to supply centres. Originally, distribution system was designed as passive network with no generators were connected to it. Today distribution systems are no longer passive as number of renewable power plants are being connected directly it. At the present these renewable power plants are connected to low-voltage grid, with power rating ranging from several kilowatts to multi-megawatts. This influences the operation of the power system

networks, i.e. the power flow become more diverse and power generation at that levels makes them more active [2]. The variation of the daily load is roughly cyclic; the peak cycle could reach twice the base load (minimum load). Furthermore, most of the loads have daily, weekly, and seasonal variations. Consequently, there must be enough generating capacity available to meet these variations and the peak demand. Accordingly, the primary objective of an electric power system is to meet the load demand at the lowest cost with expectation of increased reliability and security of supply (virtually constant frequency and voltage).

Electricity generating companies and power system operators have the problem of deciding how best to meet the load demands that could vary daily and weekly. The short-term optimisation problem is how to schedule generation to minimize the total fuel cost or maximize the total profit over a predetermined period of typically a day, taking into account large number of constraints that must be satisfied. There are two related short-term optimisation problems, economic dispatch and unit commitment. Economic dispatch (ED) is the process of deciding what the individual power outputs should be of the scheduled generating units at each time-point. Unit commitment (UC) is the process of deciding when and which generating units at each power station to start-up and shut-down. [3]. ED-UC is challenged by wind power due to its variability which is difficult to predict, and uncertainties of the load.

1.2 Wind Power Generation and Its Impact on Power systems

The increasing interest in producing electricity using renewable resources is growing rapidly due to ability of these resources to reduce greenhouse gases. In some remote areas economic factor could be a major one. The size of wind turbines and wind farms are increasing and the influence of wind generation on power system stability is slowly becoming a major concern. The world wind energy total capacity has increased from 24,322 MW in 2001 to 239,000 MW in 2011 which is enough to cover 3% of the

world's electricity demands [4]. The world total installed wind capacity (MW) end 2011 is shown in Figure 1.2.

Wind power has become one of the most widely distributed and most developed renewable technologies worldwide. Wind power has a number of advantages that made it more attractive compared to other renewable energies such as relatively low investment cost, environmental friendly technology as it is not associated greenhouse emission, and sustainable in long term as wind is available in abundance on onshore and offshore. The principle behind the conversion of wind energy into electrical energy is not a new technique. History of wind generation goes back from the use of simple devices such as sail ships, grind grain and pump water etc, which are driven by aerodynamic drag forces [5].

A wind power generator has its own characteristics, such as randomness. Unlike conventional generation, the power output produced by a wind farm is not constant, but depends on the wind condition. A sudden change of wind speed can significantly alter the wind power output level and the condition of wind can change within a very short time interval. Due to this nature, wind power generation output is considered intermittent.

Connection of small amounts of intermittent power to grid has little effect on its operation; while large amounts of intermittent power may require upgrades or even a redesign of the grid infrastructure [6]. Due to this nature, may resulting fluctuations in power flow, frequency fluctuation, voltage fluctuation and available generation capacity due to the intermittent nature of wind can increase the complexity of system operation. In general, increased wind penetration will have the impacts on the operation of the system and, the effect is becoming increasingly.

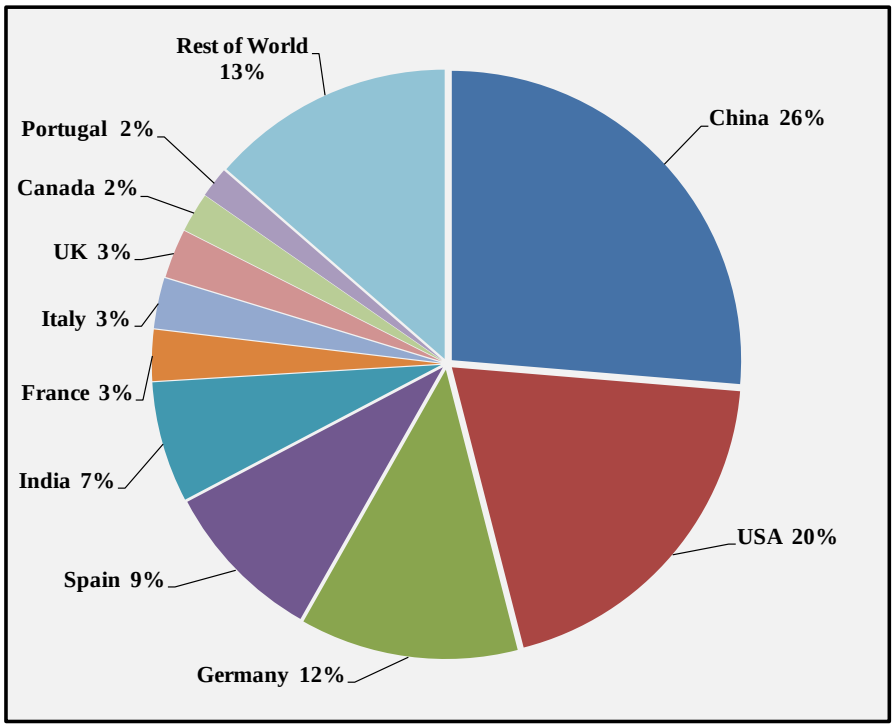

Figure 1.2: Total wind capacity end 2011 (MW).

The impacts of wind power on power systems can be divided into local impacts and system-wide impacts [7], taking into account the electrical aspects of wind turbines and the characteristics of the wind. Moreover, the connection of wind power challenges the planning and operation of the grid. In local impacts, as an individual small-scale wind power generator connected to distribution network, the impact of wind power generator mainly depend on network condition and the connected wind turbine type. And the effects become less noticeable with electrical distance from the source. The observed phenomena include changed line flows, changed voltage levels, increased fault currents, which complicate system protection, and maybe power quality problems such as flicker and harmonics [8]. System-wide impacts are largely results of the variability and limited predictability of the wind and mainly depend on a number of factors, including wind power penetration level, intermittent nature of wind generation, geographical dispersion of wind generation and the size of the electrical network [9]. As more wind power generations are installed in power system, the possible impacts wind

generation increase. A geographical dispersion of wind generator may reduce some of these impacts, however, especially if these are related to wind generation fluctuation.

1.3 Voltage Stability Problem

Special attention has been given to voltage stability especially in weak long lines and heavy loads. Voltage stability is considered to be the cause of recent blackouts in many electric utilities around the world [10]. The problem of blackout has been associated with system loadability and/ or credible contingencies such as loss of transmission lines or main generating equipment. Power system loadability is becoming increasingly important as the overall system load demand increases. When the load is increased, the bus voltage will decrease, and in the worst scenario, the voltage drop rapidly to a point beyond which the voltage is uncontrollable (voltage instability). As a results, voltage collapse leading to blackout. An important issue in the integration of large-scale wind farms is the power system' impact on voltage stability. When large wind farms are connected to the transmission network, voltage stability is one of the concerns, which affects system operation. For example, the key issue for a wind farm is the lack of reactive power support, which causes voltage instability in the power system.

1.4 Literature Reviews

This section summary the major researches previously conducted that related to the power system voltage stability problem, with the main focus on the studies that consider the impacts of wind generation on power system voltage stability**.**

1.4.1 Reviews of Voltage Stability

In recent years, voltage stability and voltage collapse is become important concern to the power systems planning engineers. The voltage collapse is often associated with contingencies like unexpected line and generator outages, insufficient local reactive power supply and increased load demands of the system [11]. A special report [12]

published in 2003 reported many voltage instability incidents have occurred around the world. The Europe blackout on November 4th 2006 [13] in UCTE (Union for the Coordination of Transmission of Electricity) inter connected power grid which coordinates 34 transmission system operators in 23 European countries. This blackout started with a 380 kV transmission line tripping. This blackout affected 15 Million people in Europe and 14.5 GW of load was interrupted in more than 10 countries. The IEEE defines voltage stability as the ability of a power system to maintain its voltage as the load admittance increases, load power will increase and so that both power and voltage are controllable [14].

A number of authors [15-16-17-18-19-20-21-22-23-24-25-26-27-28-29-30] have studied the problem of voltage stability and voltage collapse. One of the earliest works on voltage collapse is probably by Weedy (1968). In the investigation of voltage collapse, Weedy indicated that the induction motor load was the critical constituent of system loads, which was modelled by polynomial equations [15]. The proximity to voltage collapse can be estimated when the equivalent impedance of the receiving-end is equal to the Thevenin's equivalent impedance; this was demonstrated by Chebbo (1992). Chebbo proposed a voltage collapse proximity indicator based on the optimal impedance of the two-bus system generalized to actual system. For an N-bus system, however, the maximum power transferred to a load is reached when the impendence of the load equals the Thevenin's equivalent impedance of the network [25]. A voltage collapse proximity indicator (VCPI) derived by R. Alammari and K.L.Lo in (1996) is an extension of that described in [25] that proposes an algorithm based on network equivalent impedance that employs the PV-PQ sensitivity and "referencing" techniques to determine a constant equivalent impedance. Looking from the PQ node, the equivalent impedance of the power system network is constant regardless of the load level at the concerned PQ node [31]. Antonino *et al*. (2007) proposed two simple and efficient methods are proposed to estimate the distance to the voltage collapse of a radial distribution network; one which refers to the entire system loading, and the other which refers to the loading condition of the weakest node. One of the features of both methods

is that they do not require the calculation of the ***Z***-matrix in determining the parameters of the single-line equivalent system of the network and hence are computationally efficient. Both methods can be conveniently used jointly for on-line applications in order to assess the state of a distribution system from the viewpoint of voltage stability [23]. Yang *et al*. (2009) proposed an equivalent system model (ESM), which includes effects of both local network and system outside the local network. A new node voltage stability index called the equivalent node voltage collapse index (ENVCI), which is based on ESM and uses only local voltage Phasors, is presented [30]. This thesis extends the original method of [31] where voltage collapse proximity indicator is derived taken into account the reactive power output limitations of the wind turbine generators.

1.4.2 Reviews of Impact Wind Generation

The impact of wind generators on stability of the system has gained more importance with increasing wind penetration level. Wind generators may affect system stability in two ways. The first because of its intermittency; the second is wind generator instability due to a disturbance on power system network may lead to system instability. This literature review summaries research studies done related to the integration of wind power generation and power system stability and voltage stability. Wind generators can impact the rotor angle stability, voltage stability and frequency stability of the power system [32]. Voltage stability is another problem because of wind farm reactive power consumption. New wind farms technologies based on power electronics converters has made it possible to operate the generators in a way that enhances system voltage stability. A number of papers have investigated the impact of wind generation on system voltage stability [33-34-35-36-37-38-39-40-41-42-43].

Ch. Eping *et al*. (2005) focused on transient stability is-sues and analyses the impact of various aspects like generator technology, connection points, distributed generation etc. separately for getting a thorough understanding about the impact of these aspects on transient stability [33]. Chong Han *et al*. (2008) investigated the impact of static synchronous compensator (STATCOM) to facilitate the integration of a large wind

farm (WF) into a weak power system is studied [35]. Thrinh *et al*. (2008) investigated the impact of this wind power on voltage distribution levels. Theoretical expression of maximum power limited by voltage stability transfer through a grid is formulated using an exact representation of distribution line with ABCD parameters [41]. Abdelkader *et al*. (2009) proposed a simple method based on network reduction and graphical representation of the IG characteristics to determine the voltage stability region of the network in terms of wind power production and the available reactive power support. The proposed method determines the required remedial action. The graphical method proved its accuracy in indicating the system state and in quick estimation of an effective remedial action. It has been shown graphically and verified through numerical simulations that the voltage stability indicators based on the PQ model is not suitable for the case of IG. It has been also shown that the reactive power control of a WF does not only change quantitatively with variations in the WF output, but also qualitatively as the direction of reactive power support may be required to change [42]. Alonso, *et al*. (2009) presented a methodology for optimal placement of DG units in power networks to guarantee the voltage profile, maximize loadability conditions in normal and in contingencies situations. The methodology aims in finding the configuration, among a set of system components, which meets the desired system reliability requirements taking into account stability limits. Results shown in the paper indicate that the proposed formulations can be used to determine which the best buses are where the addition of small distributed generator units can greatly enhance the voltage stability of the whole network and power transfer capability under contingencies [43].

Nowadays, the problem of the long-term planning of voltage stability with the integration of wind generation in a power system is becoming more complicated, since both demands and wind generation outputs are variables. The most prominent problem of wind generation is intermittency, which presents a challenge for system operators to maintain the system stability and far from a critical voltage collapse point. Planning engineers must consider some scenarios to analyses the impact of wind generation intermittency and their penetration on system voltage stability. This problem poses some important questions –how far is the system from an unstable point or a collapse point

with fluctuation of wind generation output? What happens during large fluctuations in generation output affect system loadability? What is the impact of connecting wind generation to a weak bus or a strong bus? What is the impact of connecting a wind farm to the network at a single location or at multiple locations? What is the impact of variable system loading? What happens if load is increased at high wind generator output? And so on. This thesis aims to investigate these problems through the development of necessary tools and methodologies to conduct the analysis of voltage stability with wind generation intermittency.

1.5 Objectives of the Thesis

Wind generation is characterised by its intermittency and as such present major challenges to power system operators. Some of these challenges examined in detail in this thesis, the main focus is on the impact of DFIG based wind generation. The thesis objectives can be summarized as follows:

- To conduct comprehensive simulations to evaluate the impact of wind generation on voltage stability.
- To investigate the impact of the wind generation intermittency and their penetration on system voltage stability. Two different proximity indications are used to investigate the contribution of wind generation to voltage stability in power system, one of which is a voltage collapse proximity indicator based on network loadability. The second indicator is the power margin which is used to measure the margin between the voltage collapse point and the current operating point.
- To investigate the impact of wind generation intermittency and their penetration on system losses based on system loadability.
- To develop necessary tools and methodologies to conduct the analysis of voltage stability with wind generation intermittency.

- To validate analysis methodologies used in this thesis on a variety of network configurations, ranging from three-bus to 118-bus systems under different operational scenarios and conditions to obtain more practical simulation results.

1.6 Original Contributions of the Thesis

Based on the above objectives, the research in this thesis has achieved the following main original contributions:

- Identification and quantification of factors impacting network voltage stability. It has been established that the network voltage stability is sensitive to wind penetration level, fluctuation of wind generator output, system loadability, wind generator location (weak or strong area) and type of wind generator DFIG.
- Developed a new assessment of wind impact on voltage stability by considering wind and load variations.
- Implemented developed VCPI calculation procedure which takes into consideration the reactive power limitation of wind generators in the system, which identified a new reference bus when necessary which is required to determine the new equivalent system impedance. Due to the reactive power limitation of wind generators, this equivalent system impedance is not constant.
- A comprehensive methodology for calculating the power margin based on wind generation variability has been developed.
- Identification and quantification of factors affecting network losses in the presence of wind. The system losses can be influenced by wind penetration level, fluctuation of wind generator output, wind generator location and loading conditions.
- Verification of developed voltage stability analysis methodologies: By using the above developed methods, simulation and analysis of the voltage stability

problem in a power system with wind turbine generators is performed under different comprehensive simulation scenarios of wind generation output (wind generation intermittency and their penetration). This is achieved using 3-bus, UKGDS 61-bus, IEEE 30-bus and IEEE 118-bus systems.The improvement of voltage stability results shows a direct correlation to both the penetration level and the location of the wind generation.

1.7 Organisation of Thesis

The thesis is made up of seven chapters. The organisation is as follows:

Chapter 1 gives an introduction to the thesis, and highlights related research work, and presents the author's original contributions, organization of the thesis and a list of publications produced as result of the research work.

In chapter 2, a detailed presentation is given on wind technology development. Then it explores characteristics and performance of wind generators including the relationship between wind speed and power output. Next, it compares different types of wind generators. After that, it discusses the operation of doubly-fed induction generators (DFIG), control systems of wind generators, both of active and reactive power output features and reactive power support from voltage source converters.

In Chapter 3, the basic theory behind voltage stability and static load modeling are explained. Chapter 4 gives a detailed description of some of the related methods used in predicting voltage instability. Then chapter 4 develops a voltage collapse proximity indicator (VCPI) calculation procedure which takes into consideration the reactive power limitation of wind generators in the system. An illustrative 3-bus system example including one wind generator is used to test the method. The final section of this chapter shows the validity of this method by analyzing and presenting results of a voltage collapse proximity indicator with different wind penetration levels. Case studies including UKGDS a 61-bus radial distribution network, IEEE 30-bus and IEEE 118-bus systems are used to verify the methodology.

In Chapter 5, a proposed method is introduced on how voltage collapse proximity indicator (VCPI) can be calculated with variability of wind generation output based on simulation using optimal power flow. It then investigates the impact of the wind generation intermittency and its penetration on system voltage stability. Different scenarios have been selected and studied to analyse the behaviour of wind generators from the point view of voltage stability.

A comprehensive methodology for calculating the power margin based on wind generation variability has been developed in chapter 6. Then, a number of analyses are conducted to determine the impact of wind generation on voltage the stability margin under different conditions. The first analysis studies the influence of penetration levels. The second analysis studies the impact of fluctuating wind generator output. The final section of this chapter evaluates the impact of the fluctuation of wind generator output on power losses based on system loadability. Chapter 7 summaries the conclusions of this thesis and discusses possible future research work.

1.8 Publications

The following have been published or under review as result of the research work reported in this thesis:

1. I. S. Naser, A. Garba, O. Anaya-Lara, K. L. Lo, **"*Impact of Wind Generation on Voltage Stability in Low-Voltage Distribution Networks*"**, the 44th International Universities' Power Engineering Conference (UPEC2009), Glasgow, UK, 1-4 September 2009.

2. I. S. Naser, A. Garba, O. Anaya-Lara, K. L. Lo, **"*Voltage Stability of Transmission Network with Different Penetration Levels of Wind Generation*"**, The 45th International Universities' Power Engineering Conference (UPEC2010), Cardiff, UK, 31st August-3rd September 2010.

3. I. S. Naser, O. Anaya-Lara, K. L. Lo, **"*Study of the Impact of Wind Generation on Voltage Stability in Transmission Networks*"**, IEEE 4th International Conference on Electric Utility Deregulation Restructuring and Power Technology (DRPT 2011), pp. 39-44, Weihai, Shandong, China, 6-9 July 2011.

4. I. S. Naser, O. Anaya-Lara, K. L. Lo, **"*The Impact of Intermittent wind generation and their Penetration Level on System Voltage Stability*"**, Under Preparation for Journal Submission.

Chapter 2

Wind Power Generation

2.1 Introduction

In the past, the main power supply for the electrical industry came from conventional thermal power plants. These plants are mainly based on the combustion process of fossil fuels such as oil, coal and natural gas. Use of these primary fuels is not sustainable in the long term and also leads to the production of pollution such as CO_2, SO_X and NO_X. There is increasing interest in the production of electricity using renewable resources due to the ability of these resources to reduce greenhouse gases. There is also legislation requiring generators to limit their carbon emissions. There are a number of renewable energy technologies, including wind energy, wave power, tidal stream and solar technologies. Wind energy plays a major role in the generation of electricity from renewable energy resources. In the last 25 years, the total global wind generation installed capacity has increased almost 150 times [44].

Wind power is considered the most promising renewable energy source for the sustainable development of human society in the 21^{st} century. However, wind power generation still plays a small role when compared to conventional generation. The main disadvantage preventing large scale wind power generation is its intermittent nature. Unlike conventional generators, the output of wind turbine generators depends on the wind conditions. While the long term overall trends of wind speed can be predicated, it is still regarded as random in the short term [45]. A sudden change in wind speed will significantly change a wind turbine generator's output, even though such variation may only last for a very short time interval. As a result, wind speed can be described in a probability distribution form and the relationship between mean value and standard deviation can also be found. Furthermore, different parameters of probability distribution can be used depending on different situations. Any certain number of wind

speed data will be getting according to this probability distribution from original wind speed data for different research conditions.

The wind is available in abundance both on land (onshore) and at sea (offshore). A wind turbine generator is a device for extracting wind energy and transferring it into electrical energy. A wind farm usually consists of a high tower, a three bladed stall-regulated rotor and an induction or synchronous generator, as shown in Figure 2.1. The pattern and size of the wind turbine and generator is based on the wind characteristics. Wind generation can be divided into several types depending on the design of the rotor and generator, and wind generation can be a resource for both active and reactive power. Connecting a wind generator to a network can have negative effects, such as a new loading situation and changed power flow direction. Integration of a wind farm into a network can also affect the stability of the system. For this reason, grid operators have developed rules for connecting generators known as grid codes. These grid codes hold specific and useful information regarding wind farms that has motivated wind turbine generator manufacturers to amend their designs. Also, a wind turbine generator is equipped with a system control that can adjust active and reactive power or voltage values. Wind turbine generators can be modelled into two categories: a fixed speed with induction generator, and a variable speed generator in PQ or PV mode.

This chapter reviews the development of wind power generation and discusses the characteristics of wind and wind turbine generators which influence the performance of wind generation and power grids. First, it will summarise the current development of wind generation and introduce the situation of wind development in the world. The chapter will introduce Weibull Probability Distribution and then discuss the performance of wind turbines and induction generators, especially the doubly-fed induction generator (DFIG). Finally, it will discuss the impact of wind power generation on power system stability.

Figure 2.1: A Wind turbine with generator wind farm.

2.2 Wind Power Generation Development

Over the past decades, new power generation technologies have been developed which do not have the disadvantages of power generation technologies that use fossil fuels. Renewable energy technologies such as tidal and wave power, solar photovoltaics, biomass and wind power make use of natural energy sources (water flow, sunlight, biomass, wind) for the generation of electricity. Wind power is today the biggest renewable energy source used for electrical energy production and is one the best developed renewable energy sources. Its significance is growing rapidly throughout the world. The Global Wind Energy Council (GWEC) has reported on the installation of 42,000 MW of wind power in 2011. This brings the total worldwide installed capacity of wind generation to 239,000 MW, a 21.5% increase from 2010 figures [46]. Wind power has grown substantially from 24,322 MW in 2001 to 239,000 MW in 2011, as shown in Figure 2.2.

A report by the Global Wind Energy Council and Greenpeace International states that wind energy is capable of meeting 12% of all global power demand by 2020, and as

much as 22% by 2030. They are projecting 1,000 GW of installed wind power capacity worldwide by 2020 and 2,300 GW by 2030 [47]. Across the European Union area, the total capacity has reached 93,957 MW. The European target is 180,000 MW by 2020, of which 60,000 MW will be located offshore [48]. There has been a significant growth in interest in wind power generation throughout the world. The development of wind power generation is driven by the desire for environment protection, power supply security and economic benefits [49]. Amongst the countries of the world, China has kept its strong position in terms of wind power generation, reaching similar amounts as in previous years [50]. From among the 10 top countries with the highest amount of installed wind capacities, 6 European countries made the list, as shown in Table 2.1.

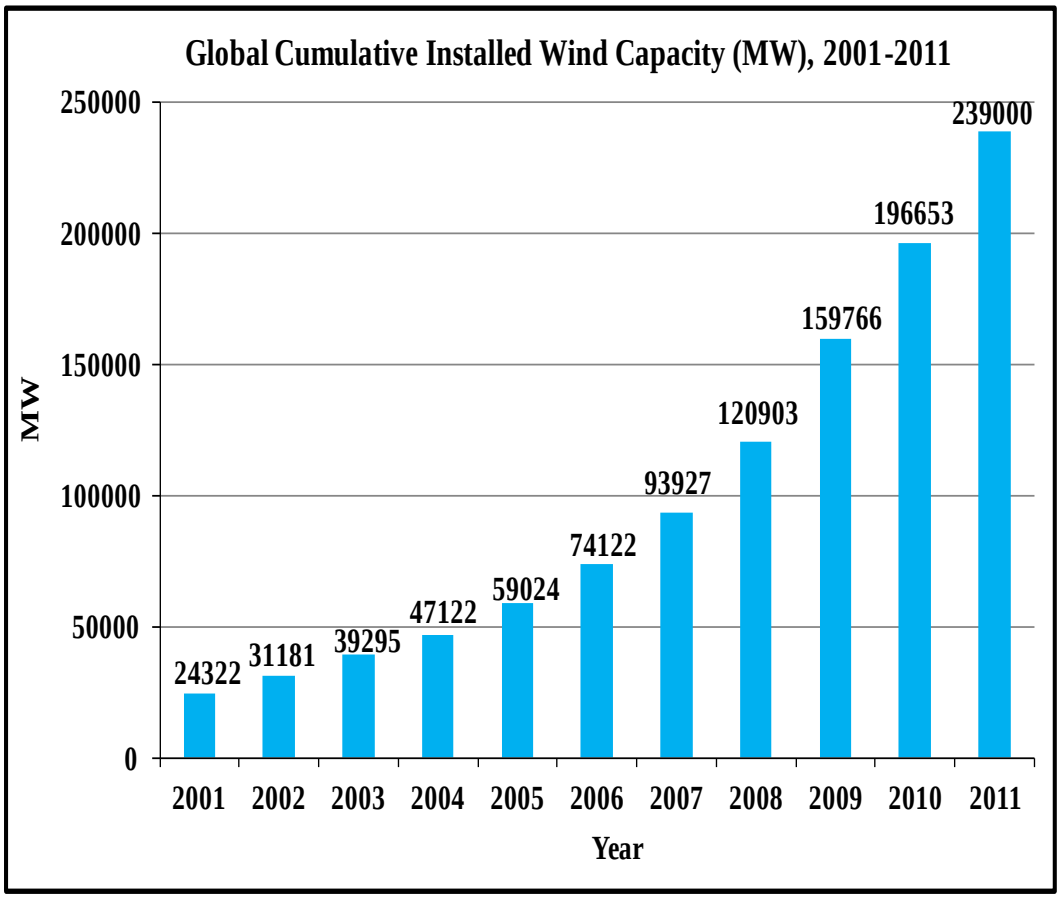

Figure 2.2: Global cumulative installed wind capacity 2001-2011 [46].

Table 2.1: Top 10 countries installed wind capacities.

Country	Wind (MW)	% World Total
China	62,733	26.3
USA	46.919	19.7
Germany	29,060,	12.2
Spain	21,674	9.1
India	16,084	6.7
France	6,800	2.8
Italy	6,747	2.8
UK	6,540	2.7
Canada	5,265	2.2
Portugal	4,083	1.7
Rest of the World	**(32,446)**	**(13.8)**
World Total	**239,000**	**100%**

The following introduces the wind development situation in the most representative countries in the world:

- **China**

China has a rich resource of wind energy and the Chinese government has released some new polices to stimulate and motivate the development of the wind power industry [51]. Today, China has become the largest wind energy provider worldwide, with its installed wind power capacity reaching 62.733 MW at the end 2011 [46]. The first wind farm was built by the Aviation Department and the government of Shangdong province in Rongcheng city in 1986.

The primary domestic wind turbine manufacturer in China is Goldwind from Xinjiang province. Established in 1998, Goldwind has been aggressively developing new technology and expanding its market share, accounting for 35% in 2006. Table 2.2 gives a separate overview of wind energy development in China from 2005 to 2011. In 2005, China's wind power capacity was 1,260 MW. By the end of 2008, it had jumped to 12,170 MW, or about 1.5% of China's total nameplate power generation capacity. By the end of 2010, China had expected another 41,800 MW of wind capacity to come online, surpassing the USA to make China the leader [52].

Table 2.2: MW of installed generating capacity since 2005 in China.

Year	2005	2006	2007	2008	2009	2010	2011
Capacity (MW)	1,260	2,599	5,912	12,170	25,100	41,800	62,733

In June 2010, the Shanghai East Sea Bridge Offshore Wind Farm, with an installed capacity of 102MW, went into operation, making it the country's first offshore wind farm to operate commercially. The price model for wind power from the government is very favorable to investment in wind and multiple wind farms, leading to different capacities of MW being built in China. With its large land mass and long coastline, China has exceptional wind resources. China aims to have 100 GW of on-grid wind power generating capacity by the end of 2015 [53].

- **USA**

Some reports that have been published over recent decades suggest that the USA is responsible for 25% of global greenhouse emissions, even though it has less than 5% of the world's population [54]. Wind energy is expanding rapidly in the United States, and over the five years to 2010, wind power has contributed towards approximately 35% of all new electric power capacity, and 2.3% of the U.S. electricity supply. The use of wind power in the U.S**.** has expanded rapidly over the last few years. Construction of new wind power generation capacity in 2011 totaled 6,810 MW, bringing the cumulative installed capacity to 46,919 MW. This capacity is exceeded only by China. Wind power grew from 2,578 MW in 2000 to more than 46,919 MW in 2011. Table 2.3 shows MW of installed generating capacity since 2005 [55].

Table 2.3: MW of installed generating capacity since 2005 in the USA.

Year	2005	2006	2007	2008	2009	2010	2011
Capacity (MW)	9,149	11,57	16,824	25,237	35,154	40,180	46,919

The Roscoe wind farm in Texas was the world's largest wind farm at completion with 627 wind turbines and a total capacity of 781 MW, which is enough to power more

than 250,000 average Texan homes [56]. There were 8,482 MW in 90 projects under construction in the third quarter of 2011. The U.S. Department of Energy's report 20% wind energy by 2030 envisioned that wind power could supply 20% of all U.S. electricity; offshore wind could provide 54,000 MW of generating capacity and 4% of the nation's capacity [57].

- **Germany**

Germany continues to lead Europe as the main wind energy country with 29,060 MW of installed capacity and wind power producing about 8% of Germany's total electrical power. More than 21,607 wind turbines are located in the German federal area and the country has plans to build more wind turbines. In 2011, the country added 1,884 MW, including 386 MW offshore [58]. Table 2.4 shows wind energy development in Germany from 2005 up to the year 2011. According to Table 2.4, total wind power capacities had increased more than 5 times by the end of 2011.

Table 2.4: MW of installed generating capacity from 2005-2011 in Germany.

Year	2005	2006	2007	2008	2009	2010	2011
Capacity (MW)	18,39	20,579	22,194	23,826	25,703	27,191	29,06

On 15 July 2009, the first offshore German wind turbine construction was completed. This turbine is the first of a total of 12 wind turbines (60 MW) for the Alpha Ventus offshore wind farm in the North Sea, and the government aims to deliver 10,000 MW of offshore capacity from the Alpha Ventus by 2020 [59].

- **United Kingdom**

The United Kingdom has long been regarded as one of the best places in Europe for wind energy development, and after a slow start, development over the last few years indicates that the UK has started to realise its wind power potential. From January 2011 to March 2012, 1,293 MW of new wind power capacity was brought online, taking the country's total installed wind power capacity to 6,540 MW, with 333 operational wind farms and 3,506 wind turbines in the UK [60]. The UK is ranked as the world's eighth

largest producer of wind power. Wind power has been grown substantially from 1,332 MW in 2005 to 6,540 MW in 2011, as shown in Table 2.5.

Table 2.5: MW of installed generating capacity from 2005-2011 in the UK.

Year	2005	2006	2007	2008	2009	2010	2011
Capacity (MW)	1,332	1,962	2,406	2,974	4,051	5,204	6,540

The majority of wind farms in the UK are located in Scotland (3167 MW), followed by England (2188.7 MW) and then Wales (530 MW). The UK became the leader in offshore wind power generation in October 2010 when it overtook Denmark. Walney offshore wind farm in the Irish Sea off Cumbria was opened on 22 February 2012 and is the largest offshore wind farm in the world at 367 MW, which is enough to provide power to up to 320,000 houses for a year. Table 2.6 shows the UK's capacity in terms of operational offshore wind farms. Wind power is expected to be of great significance in 2012, with the offshore wind industry potentially adding 5 farms with over 1,300 MW of generating capability [60]. The UK will require more than 7,500 offshore turbines by 2020, and it is planned that by 2020, 30% of the UK's energy supply will come from wind energy.

Table 2.6: List of the UK's capacities in operational offshore wind farms.

Farm Name	**Commissioned**	**Power (MW)**	**No Turbines**	**Notes**
Blyth Offshore	December 2000	4	2	Evaluation project
North Hoyle	December 2003	60	30	The UK's first major offshore wind farm
Scroby Sands	December 2004	60	30	
Kentish Flats	December 2005	90	30	
Barrow Offshore	May 2006	90	30	
Burbo Bank	October 2007	90	25	
Beatrice	August 2007	10	2	
Lynn Inner Dowsing	October 2008	194	54	
Rhyl Flats	December 2009	90	25	
Gunfleet Sands	April 2010	173	48	
Robin Rigg	April 2010	180	60	
Thanct	September 2010	300	100	The world's second offshore wind farm
Walney	February 2012	367	102	The world's largest offshore wind farm
Ormonde	February 2012	150	30	Commissioned 22 February 2012

- **Libya [61]**

Libya has joined the wind energy club with the construction of a 61.75 MW wind farm at Alfateh, near Dernah city on the country's north east coast. Alfateh wind farm is the first project for developing renewable energy in Libya. The proposed wind farm will be erected at a cost of around $150 million dollars and it will be complete in around 20 months. In 2004, measurements of wind speed were conducted and showed that there was great potential for wind energy production in Libya. The average wind speed at a 40 meter height is between 6-7.5 m/s, with this average wind speed being measured in different locations of the Libyan coast area. By 2015, the Libyan government's target and plan is to have several wind farms generating around 500 MW, with its overall target being to generate 1,000 MW of wind energy by 2020. Table 2.7 shows the wind farms currently under construction and projects in planning [61].

Table 2.7: A Summary of Wind Project Capacities in Libya.

Farm Name	Estimated Completion	Power (MW)	Notes
Alfateh	Stop worked as Libyan crisis (expect to complete early 2014)	120	Under construction (two stages)
Al Maqrun	2015-2020	240	Planning application submitted
Meslata and Tarhuna	2015-2020	250	Planning application submitted
Tazrbo and Gallo	2015-2020	120	Planning application submitted
Aliofra and Sabha	2015-2020	120	Planning application submitted

2.3 Requirements for Wind Farm Integration

In the past, wind farms connected to an electrical power system were small-scale in terms of capacity and the penetration level of wind power was small compared with the total installed generation. There were no special requirements for wind farm integration into a grid as their impact on power system network stability was very small and could be neglected. Wind farms were required to disconnect from the network under abnormal

operating conditions. Nowadays the situation has changed because of the dramatic increase in installed wind power. The increase in wind power penetration levels means that wind power plants have a considerable impact on power system stability, thus they must satisfy special requirements before being connected to a power system. Many countries, such as Germany, Spain and the UK, have issued new connection codes for wind farm connection. This section reviews the UK Grid Code requirements for wind farms. The new requirements state that wind farms must provide additional functionality, such as [62-63-64]:

- Steady-state and dynamic reactive power control and voltage control.
- Active power and frequency control.
- Fault ride-through capabilities.

2.3.1 Voltage and Reactive Power Control

Wind farms are required to be capable of regulating reactive power at their terminal in order to control the voltage at the point of common coupling (PCC). In the UK Grid Code, the reactive power requirement of the wind farm is defined as shown in Figure 2.3 [65]:

1. A wind farm must be able to supply rated MW output at any point between the limits 0.95 lagging and 0.95 leading at the point common coupling (PCC) with the UK transmission system.
2. With all plants in service, the reactive power limits defined at rated MW at lagging power factor will apply at all active power output levels above 20% of the rated MW output.
3. With all plants in service, the reactive power limits defined at MW at leading power factor will be applied at all active power output levels above 50% of the rated MW output. These reactive power limits will reduce linearly below 50% of

active power output unless the requirement to maintain the reactive power limits defined at rated MW at leading power factor down to 20% active power output.

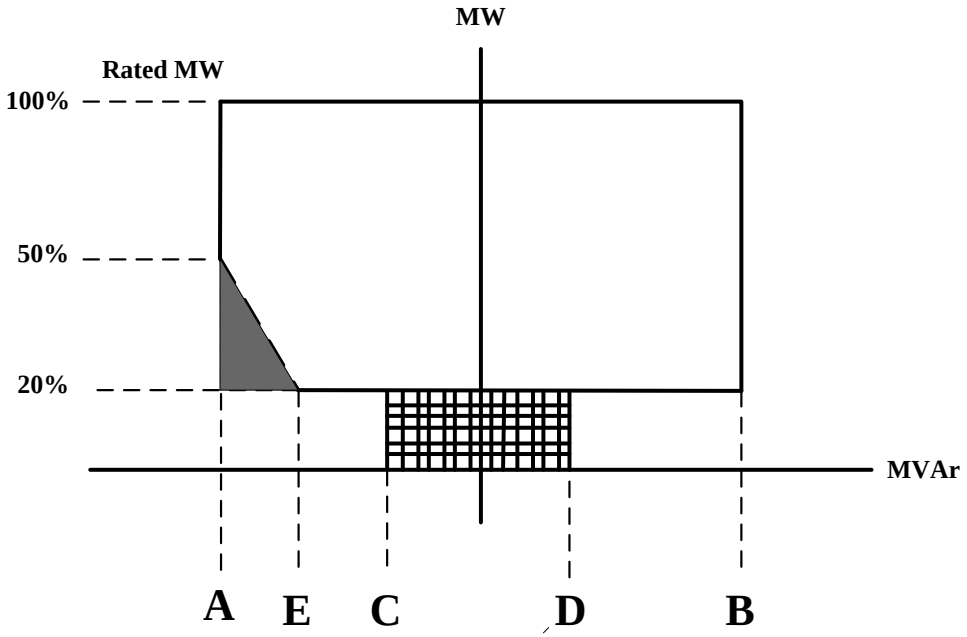

Point A is equivalent (in MVAr) to: 0.95 leading Power Factor at Rated MW output
Point B is equivalent (in MVAr) to: 0.95 lagging Power Factor at Rated MW output
Point C is equivalent (in MVAr) to: -5% of Rated MW output
Point D is equivalent (in MVAr) to: +5% of Rated MW output
Point E is equivalent (in MVAr) to: -12% of Rated MW output

Figure 2.3: Reactive power requirement for wind farm integration in the UK.

2.3.2 Frequency Control

Since an active power balance in the power system is strongly coupled to the frequency, any mismatch between the generation and demand may cause the system frequency to increase or decline, depending on the net difference between generation and demand. Primary frequency control installed in each generation plant is used to stabilize the frequency during sudden load changes. The power system operator starts, stops or adjusts the output of generating units in operation in order to support the primary control and re-schedule the generation of power plants. Figure 2.4 shows the frequency requirements of wind farms according to the UK Grid Code. Some of the

requirements concerning the relationship between the wind farm active power and the AC network frequency can be summarized as follows [65]:

- The wind farm must be able to operate continuously with constant active power output for the system frequency within 49.5 Hz and 50.5 Hz.
- The wind farm active power output should not be reduced by more than 5% for the system frequency changes within a range 49.5 Hz to 47 Hz.
- A wind farm must be able to operate continuously between 47-52 Hz for periods less than 30 seconds.

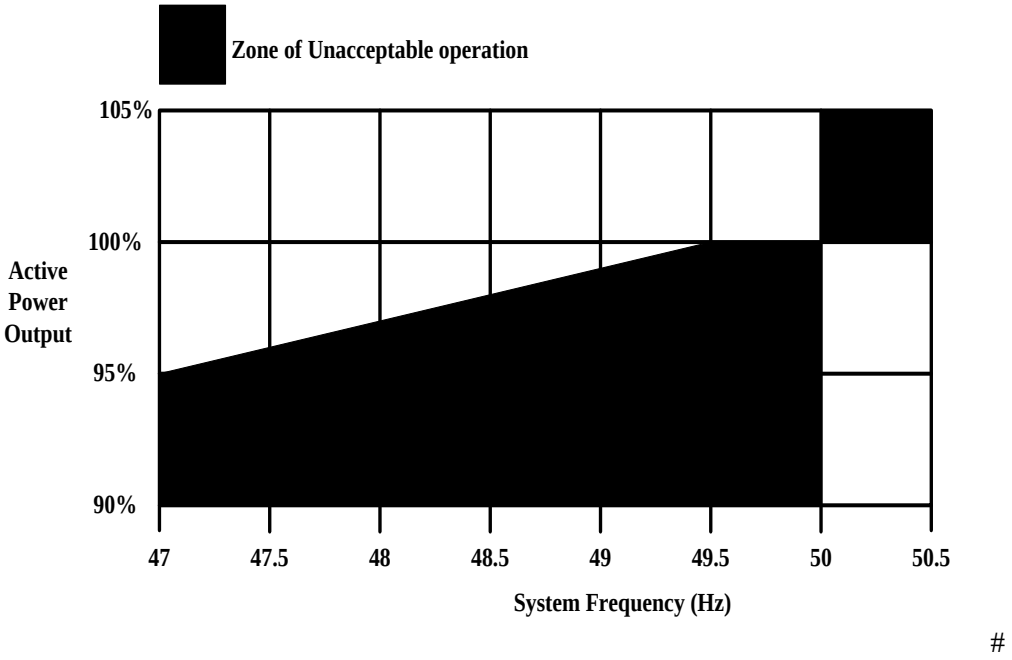

#

Figure 2.4: Frequency requirement for wind farm integration in the UK.

2.3.3 Voltage Level

Under steady state operation, wind farms must inject or consume reactive power in the range of $\pm 5\%$ at 400 kV, and $\pm 10\%$ for 275 kV and 132 kV and lower voltages.

This condition is not always applicable for 33 kV, as at this voltage level the reactive power injection or consumption is as specified in Figure 2.5.

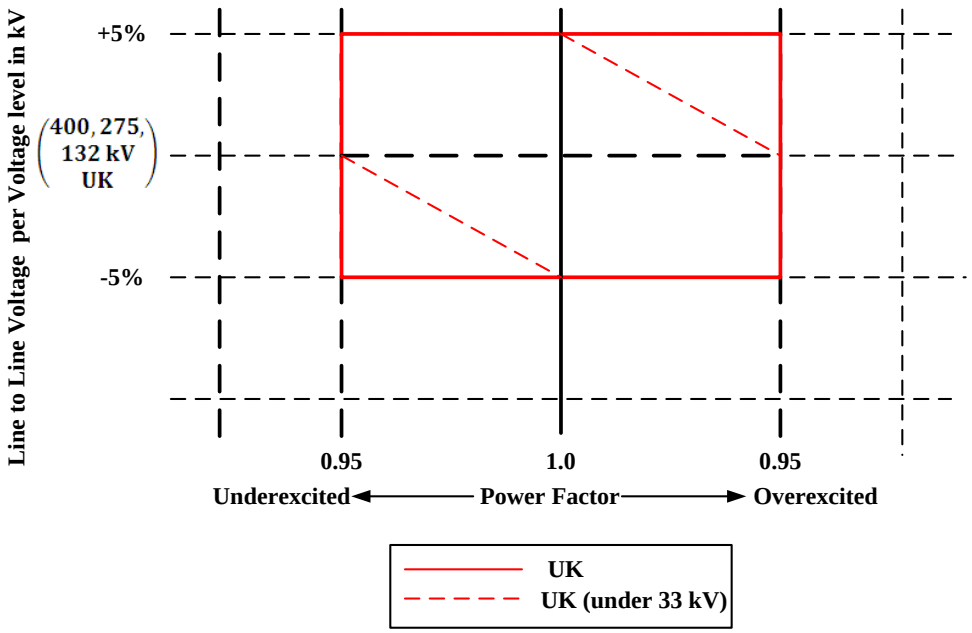

Figure 2.5: Requirements for power factor variation range in relation to the voltage according to UK codes.

2.3.4 Fault Ride-Through Capability

If the short circuit occurs somewhere in the network, the fault may extend across the system until the fault is terminated by circuit breakers. Some wind farms may not be able to remain stable and open their circuit breaker. In such a case the system needs the higher spinning reserve to prevent the risk of black out. An essential requirement in the UK Grid Code is that wind farms must remain connected to the system during the transmission system fault. The Fault Ride-Through Capability (FRT) can be defined as the ability of the generating unit or power converter to ride through different types of faults. The UK Grid Code FRT capability requirements are given below and summarized in Figure 2.6 [65]:

- The wind farm must remain transiently stable for the closed-up solid short-circuit with a duration of 140 ms for 400 kV. Also, a wind farm has to remain connected to the system for any dip duration on or above the heavy black line in Figure 2.6.
- The voltage at entry points must be restored to 90% of their pre-fault values within 0.5s.
- The terminal voltage of the wind farm should not be less than 15% of the nominal voltage during the fault period.
- During the fault period, the wind farms and DC converters must generate the maximum reactive power possible without exceeding their thermal ratings.

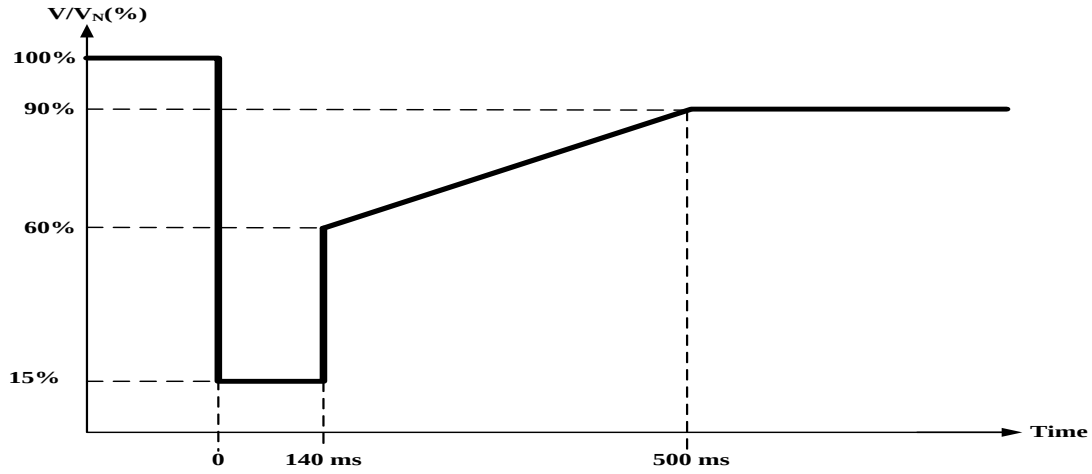

Figure 2.6: AC Fault Ride-Through Capability Requirement for Wind Farm Integration in the UK.

2.4 Wind Distribution

The most commonly used probability density function to describe wind speed is the Weibull function [66]. A probability density function is a function of a continuous variable whose integral over a region gives the probability that a random variable falls within the region [109].

The Weibull Distribution is described by the following probability density function:

$$f(\mathrm{v}) = \frac{\mathrm{k}}{\mathrm{c}}\left(\frac{\mathrm{v}}{\mathrm{c}}\right)^{\mathrm{k}-1} \mathrm{e}^{-(\mathrm{v}/\mathrm{c})^{\mathrm{k}}} \tag{2.1}$$

Where k is a shape parameter, c is a scale parameter and v is the wind speed. Hence, the average wind speed (or the expected wind speed) $\overline{\mathrm{v}}$ can be calculated from:

$$\overline{\mathrm{v}} = \int_0^{\infty} \mathrm{v}f(\mathrm{v})\mathrm{d}\mathrm{v} = \frac{\mathrm{c}}{\mathrm{k}}\Gamma\left(\frac{1}{\mathrm{k}}\right) \tag{2.2}$$

Where Γ is Euler's gamma function, i.e.

$$\Gamma(z) = \int_0^{\infty} \mathrm{t}^{\mathrm{z}-1}\mathrm{e}^{-\mathrm{t}}\mathrm{d}\mathrm{t} \tag{2.3}$$

If the shape parameter equals 2, the Weibull Distribution is known as the Rayleigh Distribution. For the Rayleigh Distribution, the scale factor c giving the average wind speed can be found from $\left(\mathrm{k} = 2, \text{and } \Gamma\left(\frac{1}{2}\right) = \sqrt{\pi}\right)$

$$\mathrm{c} = \frac{2}{\sqrt{\pi}}\overline{\mathrm{v}} \tag{2.4}$$

The wind speed probability density function is shown in Figure 2.7. The average wind speeds in Figure 2.7 are 5.4 m/s, 7.2 m/s, and 8 m/s [67].

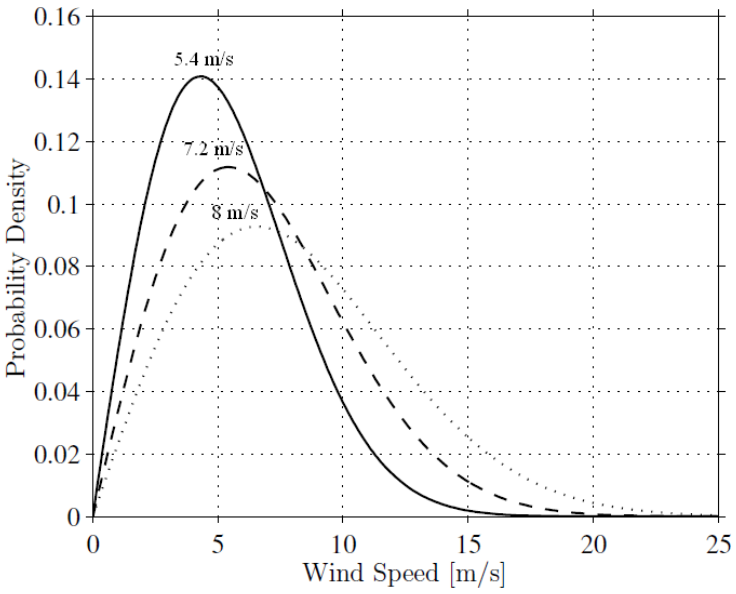

Figure 2.7: Probability Density of the Rayleigh Distribution (the average wind speeds are 5.4 m/s, 7.2 m/s, and 8 m/s.

2.5 Wind Turbine Operation Characteristics

A wind turbine is a machine that converts the wind's kinetic energy into rotary mechanical energy, which is then used to do work. In more advanced models, the rotational energy is converted into electricity, the most versatile form of energy, using a generator. The active power available from a wind generator is given by the expression below [68]:

$$P_{WG} = \frac{1}{2}\rho . A . C_p v_w^3 \tag{2.5}$$

Where P_{WG} is the power output from the wind, ρ is the air density, A is the turbine swept area, C_p is the coefficient of performance of the turbine, and v is the wind speed.

The value of C_p can be determined from equation 2.2 [69]:

$$C_p = \frac{1}{2}(\lambda - 0.022\beta^2 - 5.6)e^{-0.17\lambda i} \tag{2.6}$$

Where λ is the tip-speed and β is the blade pitch angle (degrees).

The C_p is not a constant for a given air foil, but rather is dependent on a parameter λ called the tip-speed ratio. The tip-speed ratio λ describes the relationship between the rotating blade tip speed and the wind speed given by:

$$\lambda = \frac{\omega R_w}{v_w} \tag{2.7}$$

Where R_w is rotor radius, ω is the rotational wind speed, and v is the wind speed. For small wind turbines, the turbine blades are fixed at a constant pitch angle, and for large ones the pitch angle can be changed in a certain range in order to get the maximum wind power output. The relationship curve between λ and C_p under different pitch-angles β is shown in Figure 2.8.

At both low and high tip speed ratios, the power coefficient is low so it will be ideal if the turbine can be operated at all wind speeds at a tip speed ratio λ in which area gives the maximum power coefficient.

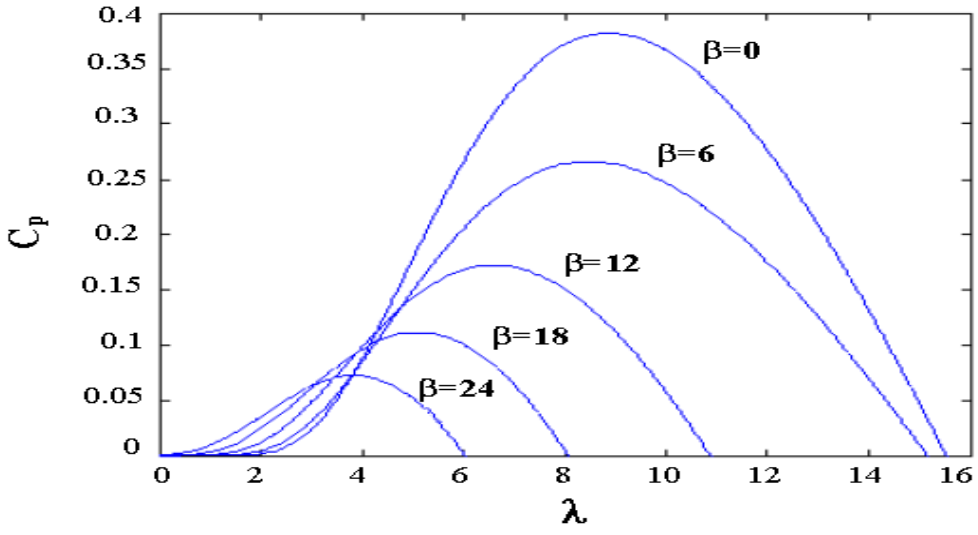

Figure 2.8: The Power Coefficients-Tip Speed Ratio Performance Curve for Different Pitch Angles.

The power output of the wind generator at time t is non-linear with wind speed v_t. The relationship between the power output of the wind generator and the wind speed is given by equation 2.3 and shown graphically in Figure 2.9 [70].

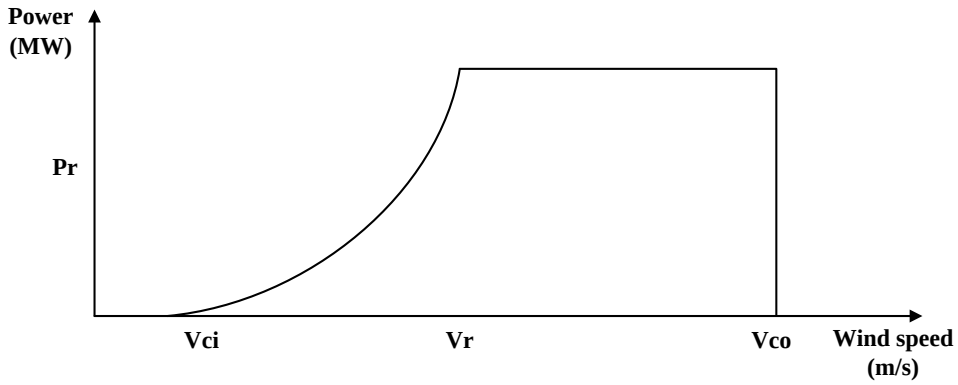

Figure 2.9: Wind Turbine Output Curve.

$$P_t = \begin{cases} 0 & 0 \le v_t \le v_{ci} \text{ or } v_t \ge v_{ci} \\ \left(A + Bv_t + Cv_t^2\right) P_r & v_{ci} \le v_t \le v_r \\ P_r & v_r \le v_t \le v_{co} \end{cases} \quad (2.8)$$

Where:

v_{ci} is cut-in speed

v_t is rated speed

v_{co} is cut-out speed

P_r is rated power

Typical values from most manufacturers of wind turbine generators for cut-in, rated and cut-out speeds are 4-5 m/s, 15 m/s, and 25 m/s, respectively. These values are typical for the VESTAS V90-3.0MW wind turbine. The constants A, B, and C are determined using the following equations [71]:

$$A = \frac{1}{(v_{ci} - v_r)^2}\left[v_{ci}(v_{ci} + v_r) - 4v_{ci}v_r\left(\frac{v_{ci} + v_r}{2v_r}\right)^3\right]$$

$$B = \frac{1}{(v_{ci} - v_r)^2}\left[4(v_{ci} + v_r)\left(\frac{v_{ci} + v_r}{2v_r}\right)^3 - (3v_{ci} + v_r)\right]$$

$$C = \frac{1}{(v_{ci} - v_r)^2}\left[2 - 4\left(\frac{v_{ci} + v_r}{2v_r}\right)^3\right]$$

Wind turbines are used to extract as much electrical energy from the wind as possible, so each part of the turbine has to be designed optimally for that goal. Optimal design is influenced by the modes of operation of the turbine, which are constant speed mode and variable speed mode. In constant speed mode, the rotational speed of the turbine is maintained at a constant level and tip speed ratio λ changes continuously. Alternatively, the turbine operating at variable speed mode can maintain the constant tip speed ratio required for the maximum power coefficient and can also rotate at the optimal rotational speed for each wind speed. Currently, the majority of wind turbines used are variable speed turbines. Variable speed operation mode improves the dynamic behavior of the turbine and the power production from variable speed turbines is higher than that of fixed-speed turbines [72].

2.6 Wind Turbine Induction Generator Performance

2.6.1 Wind Turbine Generator Types

The general working principle of the wind turbine consists of two conversion processes which are carried out by its main components: the rotor, which extracts the kinetic energy from the wind and converts it into a mechanical torque, and the generating system, which converts this torque into electricity, as shown in Figure 2.10.

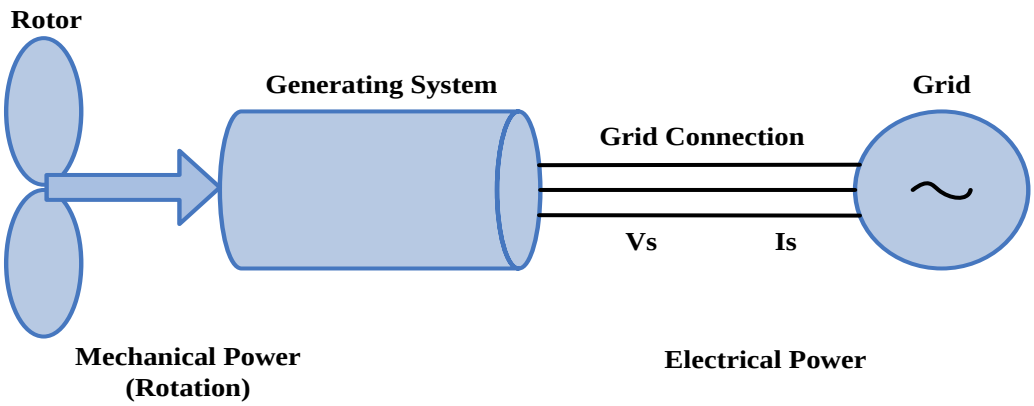

Figure 2.10: General Working Principle of Wind Turbine.

There are three different wind turbine generator concepts which are currently mainly applied in wind farms. The main differences between the concepts are the generating system and the aerodynamic efficiency limitations of the rotor during high wind speeds. The main wind turbines are:

- Squirrel Cage Induction Generator (SCIG)
- Doubly Fed (Wound Rotor) Induction Generator (DFIG)
- Direct Drive Synchronous Generator (DRSG)

The squirrel cage induction generator belongs to the fixed-speed types which are electrically simple devices consisting of an aero-dynamic rotor driving a low-speed shaft, a gearbox, a high speed shaft and an induction or asynchronous generator. The generator output, normally at low voltage, transmits power via vertical pendant cables to a switchboard and local transformer usually located at the tower base, as shown in Figure 2.11.

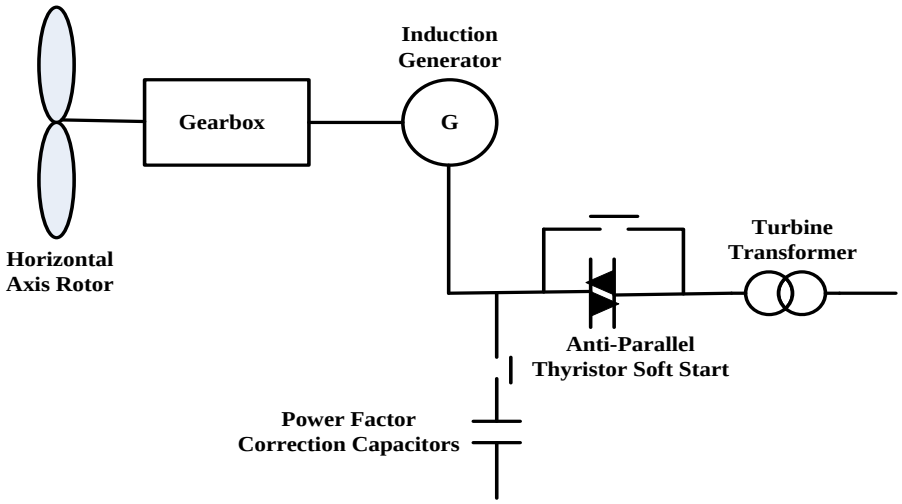

Figure 2.11: Schematic Diagram of a Fixed-Speed Wind Turbine.

A switched power factor correction capacitor is used to improve the power factor of the induction generator while an anti-parallel thyristor soft-start unit is used to energize the generator once its operating speed is reached. The function of the soft-start unit is to build up magnetic flux slowly and so minimize transient currents during energisation of the generator. Once energized, it brings the drive train to its operating speed [73].

The doubly fed induction generator and direct drive synchronous generator belong to the variable-speed wind turbines class. Their ability to comply with connection requirements and the reduction in mechanical loads achieved with variable-speed operation makes them very popular. They also provide key advantages such as reduction in mechanical stresses, dynamic compensation for torque and power pulsations caused by back pressure of the tower and improvement in power quality. In the following sections, the wind turbine generators types will be presented.

2.6.1.1 Fixed Speed Turbine Generator

In the early stages of wind power development, most wind farms were equipped with induction generators. The grid coupled squirrel cage induction generator, used in fixed speed wind turbines, has its blades connected to the hub, which is coupled via the

gearbox to a conventional squirrel cage induction generator, as shown in Figure 2.12 [74]. The generator is directly connected to the network and may have automatically switched shunt capacitors or a static VAR compensator for reactive power compensation, and possibly the soft start mechanism which is by-passed after the machine has been energized. The speed range of the turbine is fixed by the torque vs. speed characteristics of the induction generator. The squirrel cage induction generator (SCIG) always consumes reactive power because it has no separate field circuit, and so there is no direct control over reactive power [75]. This is undesirable in most cases, particularly in the case of large turbines and weak grids. Consequently, the reactive power consumption of the squirrel cage induction generator is nearly always partly or fully compensated by capacitors, as shown in Figure 2.6, in order to achieve the power factor close to unity.

The main advantages of fixed speed wind turbines with squirrel cage induction generators are that this type of wind generator is robust, easy to install and lower cost. Also, the generator operates in a fixed speed mode, providing stable frequency control. On the other hand, the squirrel cage induction generator has a number of disadvantages such as a lack of control possibilities for both real and reactive power, and gearbox failures because of larger power fluctuations translated to torque pulsations.

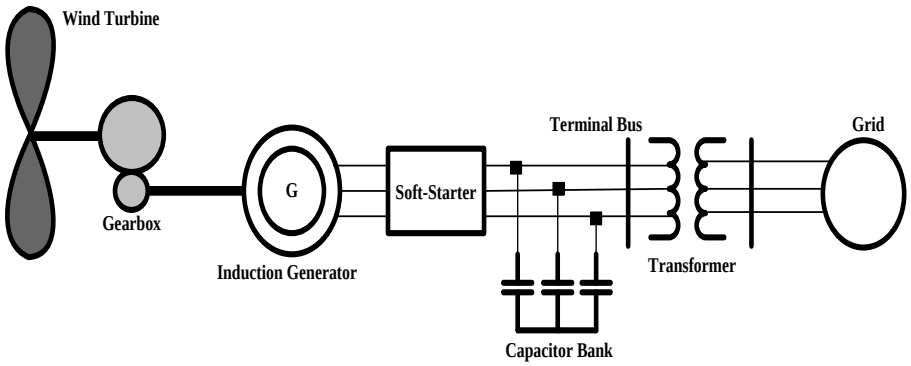

Figure 2.12: Fixed Speed Wind Turbine Generator.

2.6.1.2 Variable Speed Wind Turbine Generator

Several technologies and historical applications of the variable speed wind generator have been discussed in [76]. Variable speed concepts allow operation of the wind turbine at the optimum tip-speed ratio and hence at the optimum power coefficient for a wide wind speed range. The variable speed configuration is very flexible in that it can be used to control different parameters, namely active and reactive power, torque, power factor or terminal voltage. The variable speed wind turbine generator can act as the reactive power source or supply, in contrast to the fixed speed generator which always absorbs reactive power. The variable speed wind turbine also has a synchronous generator connected through a gearbox or a doubly fed (wound rotor) induction generator. The rotor winding is fed using the back-to-back voltage source converter. The wind turbine is coupled to the generator through a gearbox. In high wind speeds, the power extracted from the wind can be limited by pitching the rotor blades. The use of variable speed wind turbines is rising due to reasons such as the following:

- The power electronic modules used for variable speed operation of wind turbines are becoming cheaper and reliable.
- Variable speed wind turbines offer less fluctuations in power output because the large rotor inertia smoothes the variations in wind speed and thus reduces flicker problems
- Variable speed wind turbines offer a higher energy yield in comparison to constant speed turbines, as the optimal rotor speed for each wind speed can be achieved so that the rotor efficiency is improved. The increases in rotor efficiency outweigh the losses of the power electronic converter.
- Variable speed wind turbines offer extensive controllability of both active and reactive power, which is an advantage, particularly in remote locations and offshore.

Variable speed wind generators come in two types. Type one uses a synchronous generator with a power converter connected in series, as shown in Figure 2.13, which transforms the variable frequency as power into fixed frequency as power. This type of variable speed has several disadvantages, such as:

- ✓ The total system power is expensive because the power converter has to be rated at 1.0 p.u.
- ✓ Inverter output filters and electromagnetic interference filters are rated for 1.0 p.u. output, making filter design difficult and expensive.

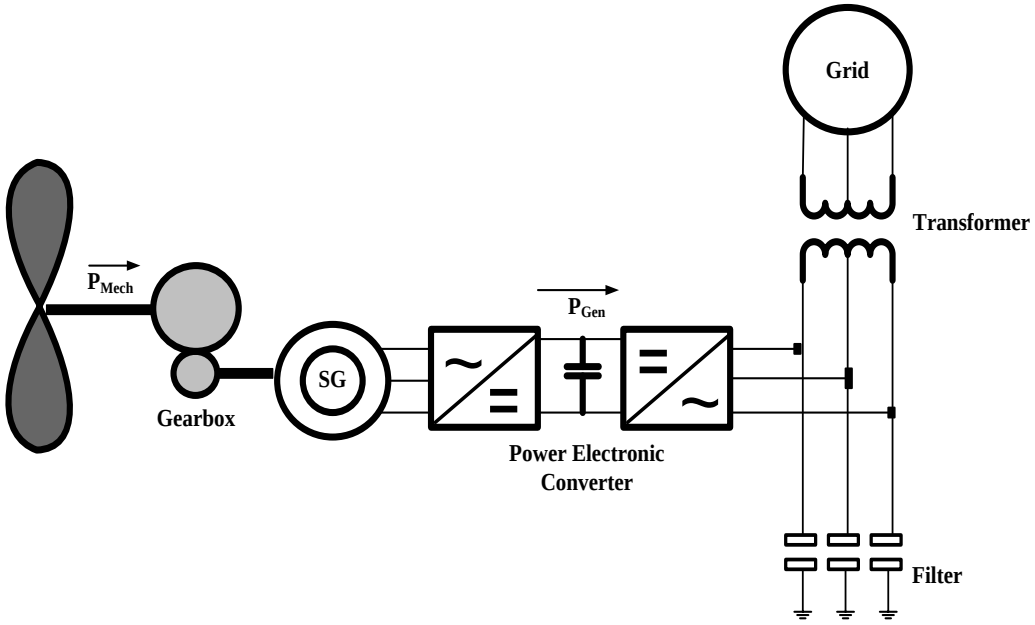

Figure 2.13: Direct-In-Line Wind Turbine System.

The second type for variable speed wind generators to use is the doubly fed induction generator (DFIG). The rotor winding is fed using a back-to-back voltage source converter, as shown in Figure 2.14. This type consists of the doubly fed induction generator with a four quadrant ac-to-ac converter based on insulated gate bipolar transistors (IGBTs) connected to the rotor windings. The wind turbine rotor is also

connected to the generator through the gearbox. In high wind speed, the power extracted from the wind is limited by pitching the rotor blades. The doubly fed (wound rotor) induction generator is a variant of the variable speed wind turbine. It uses a wound rotor induction generator with slip rings to take current into or out of the rotor winding, and variable speed operation is obtained by injecting a controllable voltage into the generator rotor at the slip frequency [77]. This type of wind turbine generator is one of the preferred technologies in wind generation applications as it supports a wide range of operations of wind speed. It also provides effective control of active and reactive power of the wind turbine generator since it uses back-to-back converters. Furthermore, the power converter system can perform as reactive power compensations and voltage support for the network. The doubly fed induction generator also has some advantages, such as [78]:

- It reduces the mechanical stress and optimizing power capture.
- A speed variation of $\pm$ 30% around synchronous speed can be obtained by use of the power converter of 30% of nominal generated power.
- It does not necessarily have to be magnetized from the power grid since it can be magnetized from the rotor circuit too.
- The size of the converter is not related to the total generator power but to the selected speed range and hence to the slip power.
- It is high quality, low noise, high efficiency.

However, the doubly fed induction generator is more complex than the squirrel cage induction generator, and hence increases the control blocks, such as pitch angle controller, rotor speed controller and converter with protection system blocks. Due to the improved efficiency of energy transfer from the wind, reduced mechanical stresses, system cost of three types of wind turbine generator and size, weight, radius of different wind turbines, and variable speed, wind turbines with DFIGs are the most suitable choice for many wind power systems. Thus, the wind turbine generator model in this

thesis is based on the DFIG model as a PV bus, which is operated in voltage controlled mode.

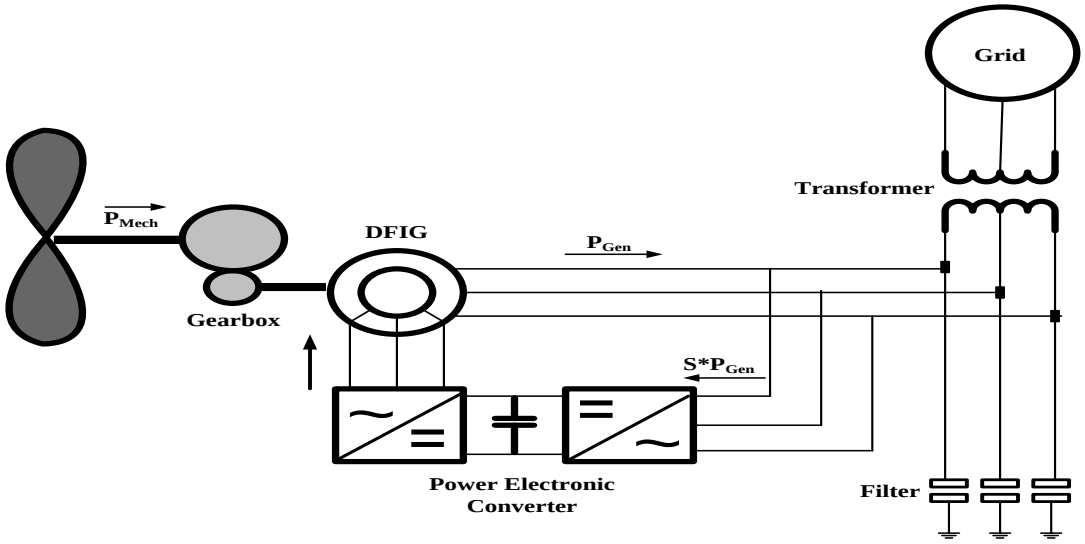

Figure 2.14: Doubly Fed Induction Generator Wind Turbine System.

2.6.2 Wind Turbine Doubly Fed Induction Generator (WTDFIG) [73]

Today new wind turbine technology integrates power electronics and control, making it possible for wind power generation to participate in active and reactive power control. The typical generator configuration for a new variable speed turbine is the doubly fed induction generator (DFIG) shown in Figure 2.15. This configuration consists of a wound rotor induction generator where the stator windings are directly connected to the grid and the rotor windings are connected to a back-to-back power converter. This back-to-back power converter is dimensioned for partial generator power and is able to operate bi-directionally. It uses a wound rotor induction generator with slip rings to take current into or out of the rotor winding, and variable speed operation is obtained by injecting the controllable voltage into the generator rotor at slip frequency [77]. As shown in Figure 2.15, the rotor winding is fed through the variable frequency power converter, typically based on two AC/DC insulated gate bipolar transistor (IGBT)

based voltage source converters (VSC) linked by the DC bus. The power converter decouples the network electrical frequency from the rotor mechanical frequency, enabling the variable speed operation of the wind turbine. The voltage source converter (VSC) produces an AC voltage that is controllable in magnitude and phase, similar to the synchronous generator or synchronous compensator. The VSC commutates independently of the AC-side voltage and consequently it can be used on the load-only system. This makes the VSC useful for rotor connection, wind farm connection and so forth.

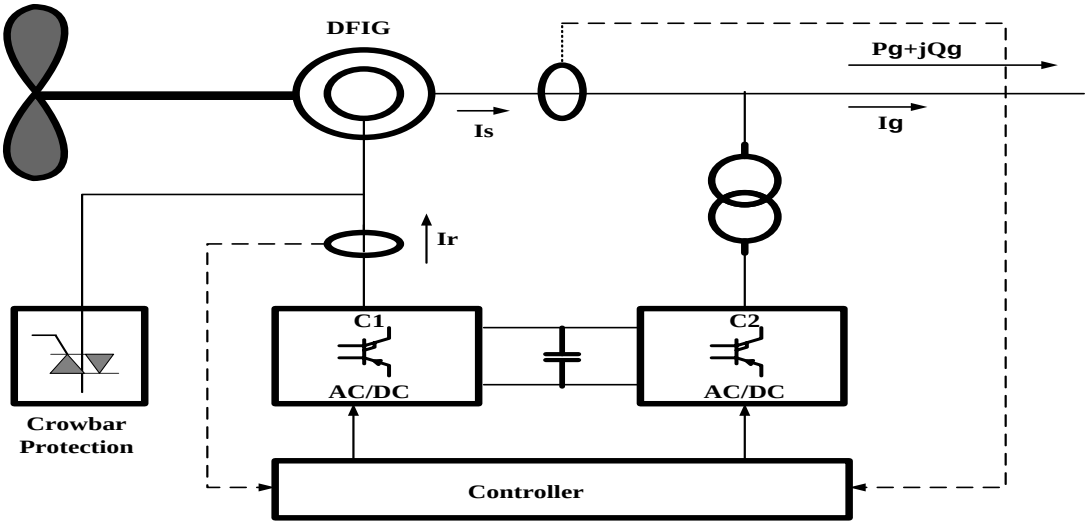

Figure 2.15: Typical Configuration of the DFIG Wind Turbine.

Converters (C1) and (C2) in Figure 2.15 are used to control the doubly fed induction generator wind turbine. A number of manufacturers use converter (C1) to provide torque/speed control, together with terminal voltage or power factor control for the overall system. Converter (C2) is used to maintain the DC link voltage and provide the path for power to flow to and from the AC system at unity power factor. The relationship between mechanical power, rotor electrical power and stator electrical

power in the doubly fed induction generator is shown in Figure 2.16, where P_m is the mechanical power delivered to the generator, P_r is the power delivered by the rotor, $P_{air\ gap}$ is the power at the generator air gap, P_s is the power delivered by the stator, and P_g is the total power generated and delivered to the network.

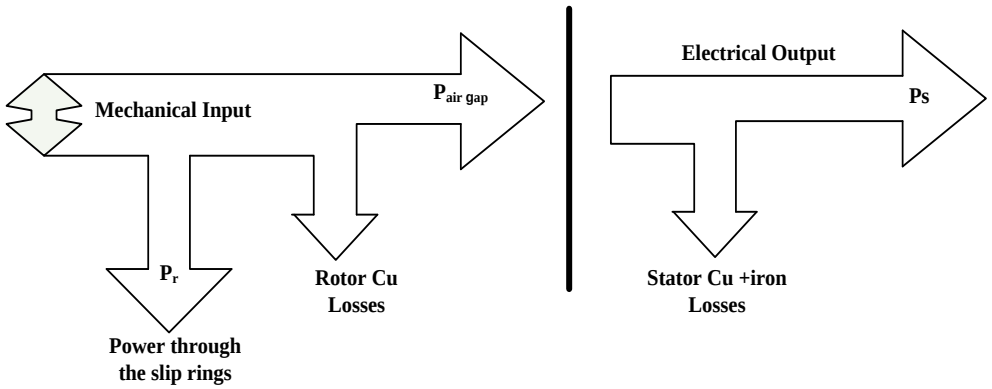

Figure 2.16: DFIG Power Relationships.

Once stator losses are neglected, from Figure 3.10 it follows:

$$P_{air\_gap} = P_s \tag{2.9}$$

Also, when rotor losses are neglected, then

$$P_{air\_gap} = P_{mech} - P_r \tag{2.10}$$

From equations 2.4 and 2.5, stator power P_s can be expressed as:

$$P_s = P_{mech} - P_r \tag{2.11}$$

Writing equation 2.6 in terms of the generator torque, T:

$$T\omega_s = T\omega_r - P_r \tag{2.12}$$

Re-arranging

$$P_r = -T(\omega_s - \omega_r) \tag{2.13}$$

The stator and rotor powers can then be related through the slip s as

$$P_r = -sT\omega_s = -sP_s \tag{2.14}$$

Where s is given in terms of ω_s and ω_r as

$$s = \frac{(\omega_s - \omega_r)}{\omega_s} \tag{2.15}$$

Combining equations 2.6 and 2.9, the mechanical power P_{mech} can be expressed as:

$$P_{mech} = P_s + P_r = P_s - sP_s \tag{2.16}$$

$$= (1 - s)P_s$$

The total power delivered to grid P_g is the addition of the stator and rotor power:

$$P_g = P_s + P_r \tag{2.17}$$

Figure 2.17 shows the general model structure of the variable speed wind turbine with the DFIG [79]. The model consists of several blocks, starting from the wind speed block, rotor model block and several others. The wind speed block bus an output as wind speed sequence. This block can either contain the wind speed model or the measured wind speed sequence from a site. The rotor model has an input as wind speed and output as mechanical power, which serves as an input to the generator model.

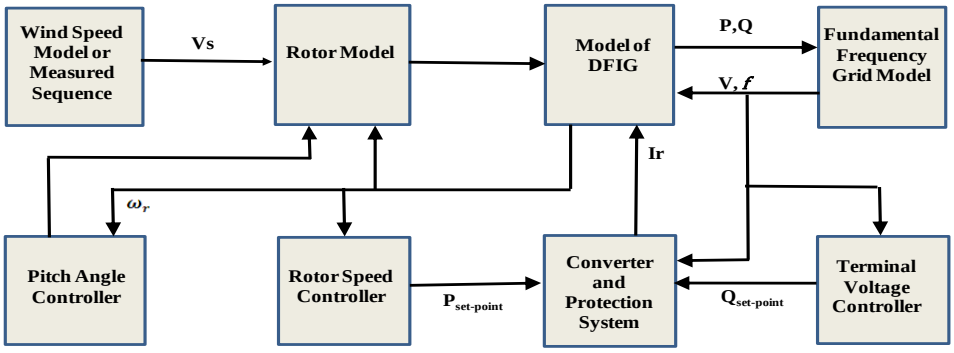

Figure 2.17: The General Model Structure of the Variable Speed Wind Turbine with a DFIG.

2.6.3 Equivalent Circuit of the Doubly Fed Induction Generator [80]

The equivalent circuit of the doubly fed induction generator, with inclusion of the magnetizing losses, can be seen in Figure 2.12. This equivalent circuit is valid for one equivalent Y-phase and for steady-state calculations. In the case that the doubly fed induction generator is Δ-connected, the machine can still be represented by this equivalent Y representation. In this section the $j\omega$ −method is adopted for calculations. Note that if the rotor voltage V_r in Figure 2.18 is short circuited then the equivalent circuit for the DFIG becomes the ordinary equivalent circuit for the cage-bar induction machine.

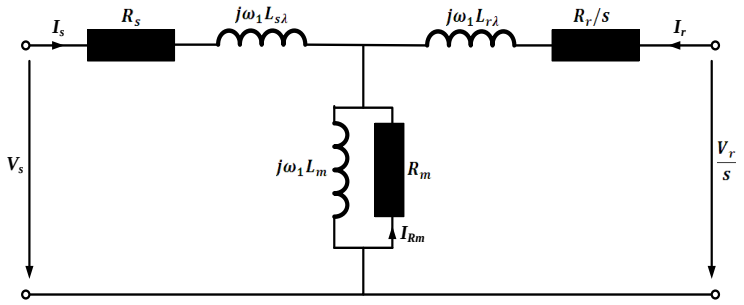

Figure 2.18: The Equivalent Circuit of the Doubly Fed Induction Generator.

Applying Kirchhoff's Voltage Law to the circuit in Figure 2.18 yields [76]:

$$V_s = R_s I_s + j\omega_1 L_{s\lambda} I_s + j\omega_1 L_m (I_s + I_r + I_{Rm}) \tag{2.18}$$

$$\frac{V_r}{s} = \frac{R_r}{s} I_r + j\omega_1 L_{r\lambda} I_r + j\omega_1 L_m (I_s + I_r + I_{Rm}) \tag{2.19}$$

$$0 = R_m I_{Rm} + j\omega_1 L_m (I_s + I_r + I_{Rm}) \tag{2.20}$$

Where V_s is the stator voltage, V_r is the rotor voltage, R_s is the stator resistance, R_r is the rotor resistance, R_m is a magnetizing resistance, $L_{s\lambda}$ is the stator leakage inductance, $L_{r\lambda}$ is the rotor leakage inductance, L_m is the magnetizing inductance, I_s is

the stator current, I_r is the rotor current , I_{Rm} is the magnetizing resistance current, ω_1 is the stator frequency, and s is the slip.

Then the equations describing the equivalent circuit, i.e., 2.13 and 2.15, can be rewritten as:

$$V_s = R_s I_s + j\omega_1 \Psi_s \tag{2.21}$$

$$\frac{V_r}{s} = \frac{R_r}{s} I_r + j\omega_1 \Psi_r \tag{2.22}$$

$$0 = R_m I_{Rm} + j\omega_1 \Psi_m \tag{2.23}$$

The mechanical power (P_{mech}) and the power losses (P_{loss}) of the induction machine can be found with:

$$P_{mech} = 3|I_r|^2 R_r \frac{1-s}{s} - 3\mathrm{Re}[V_r I_r^*] \frac{1-s}{s} \tag{2.24}$$

The resistive losses of the induction generator are:

$$P_{loss} = 3(R_s|I_s|^2 + R_r|I_r|^2 + R_m|I_{Rm}|^2) \tag{2.25}$$

Where the multiplication by 3 is due to the fact that the induction machine has three phases.

It is also possible to express the electro-mechanical torque, T_e, as:

$$T_e = 3n_p|I_m[\Psi_r I_r^*] \tag{2.26}$$

Where n_p is the number of pole pairs. Table 2.8 shows some typical parameters of the induction machine in per unit (p.u) [67].

Table 2.8: Typical Parameters of the Induction Machine in p.u.

	Small Machine 4 kW	Medium Machine 100 kW	Large Machine 800 kW
Stator and Rotor Resistance R_s and R_r	0.04 p.u.	0.01 p.u.	0.01 p.u.
Leakage Inductance $L_{s\lambda} + L_{r\lambda} \approx L_\sigma$	0.2 p.u.	0.3 p.u.	0.3 p.u.
Magnetizing Inductance $L_m \approx L_M$	2.0 p.u.	3.5 p.u.	4.0 p.u.

Figure 2.19 shows the shaft torque of an induction machine as the function of rotor speed when an induction machine is connected to the grid and has a short-circuited rotor, i.e., $V_r = 0$. As can be seen in Figure 2.19, the speed-torque characteristic is quite liner around synchronous speed, i.e., 1 p.u. If the rotor speed is below synchronous speed (positive slip) then the induction machine operates as the motor, and if the rotor speed is above synchronous speed (negative slip) then the induction machine runs as the generator.

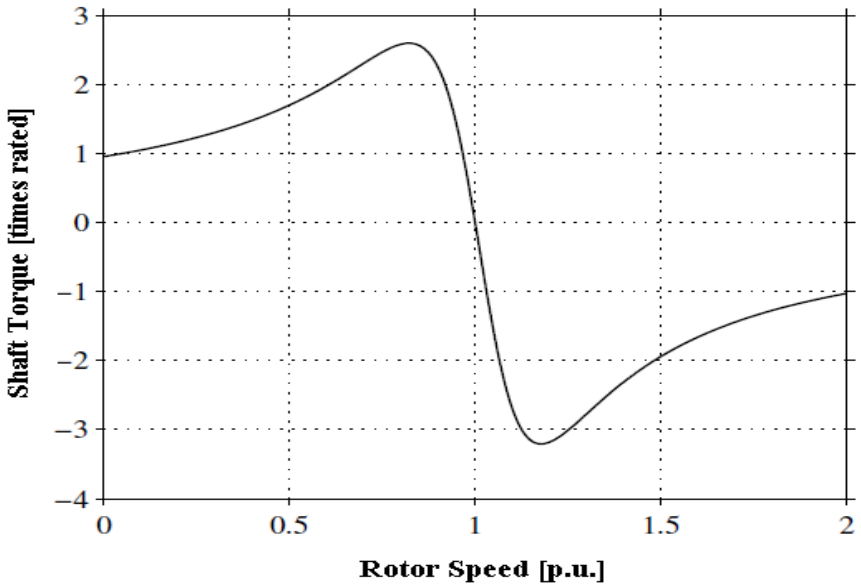

Figure 2.19: Shaft Torque of the Induction Machine with a Short-Circuited Rotor, $V_r = 0$, as the Function Rotor Speed.

2.6.4 DFIG Wind Turbine Control [73]

Control of the doubly fed induction generator is achieved through converters C1 and C2, as shown in Figure 2.15. The control system implemented by a number of manufacturers uses converter C1 to provide torque/speed control, together with terminal voltage or power factor (PF) control for the overall system. C2 is used to maintain the

DC link voltage and provide a path for rotor power flow to and from the AC system at unity power factor. The reactive power injection can be obtained from the stator-side converter C2. In a DFIG voltage control system, the rotor-side converter C2 is likely to be preferred over the converter C2. For purposes of analysis, simulation and control, the favored way of representing the DFIG is in terms of direct and quadrature (dq) axes, which form the reference frame that rotates at synchronous speed ($\omega_s = 2\pi f_s$). Adjusment of the dq-axis components of the rotor voltage provides the capability of independent control over two generator variables. This can be achieved in a variety of control systems. The control methodology knows as the current-mode control is commonly used where the dqaxis component of the rotor current is used to control terminal voltage (reactive power), and the q-axis component is employed to control the torque of the generator (active power).

2.6.4.1 Voltage Control

The basic implementation of a DFIG voltage controller is shown in Figure 2.20. In this system, the difference in magnitude between the terminal voltage reference $(V_{s_{ref}})$ and the actual terminal voltage (V_s) is used to generate a reference of the rotor current in the d-axis $(i_{dr_{ref}})$. A reference current $(i_{dr_{ref}})$ is compared with the actual value of the rotor current in the d-axis,(i_{dr}), to generate an error signal which is then processed by the standard PI controller. The required rotor voltage (V_{dr}) is obtained as the adding of PI controller output and the compensation term used to eliminate cross coupling between torque-and voltage control loops.

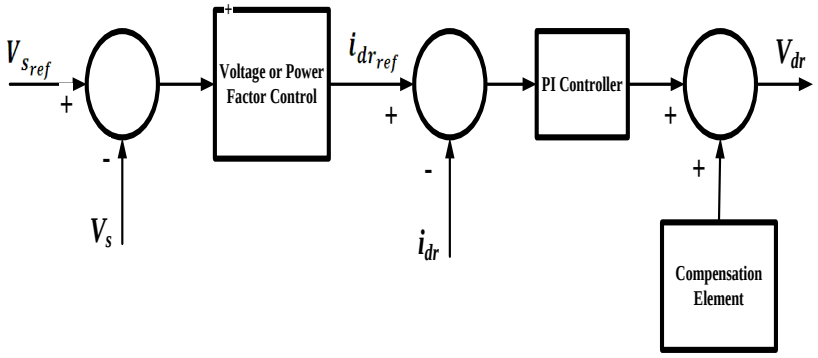

Figure 2.20: Voltage–Control Loop for the DFIG.

2.6.5 Reactive Power Support from the DFIG

The doubly fed induction generator is equipped with voltage source converters. As a result, C1 and C2 have the capability of generating or absorbing reactive power respectively and can be used as the reactive power sources to control the voltage at the grid terminals. Figure 2.21 shows the typical reactive power capability curve (P-Q characteristic) of the DFIG with variable speed wind turbine [81]. The reactive power capability of the doubly fed induction generator depends on converters C1 and C2 which means the maximum reactive and active power of the converters are limited by the maximum absolute current and the magnetizing current of the induction generator. From the P-Q characteristics, there are two special features:

1. The wind turbine generator can absorb more reactive power in an under-excited mode than max MVArs generation in an over-excited operation.

2. The wind turbine generator can support reactive power even if no active power is generated. Consequently, in low wind speed periods, when the wind turbine is still not running, the reactive power capability is available if the converter can be switched solely to the grid [82].

Although the doubly fed induction generator has certain reactive capacity, it still requires some reactive power support to maintain the voltage at the point of common

coupling with the power supply system's when the output of the wind power generation fluctuates. To meet the requirements of the interconnection to the network for large wind farms, it is often necessary to install reactive power compensation equipment such as FACT devices, a static var compensator (SVC) and a static synchronous compensator (STATCOM).

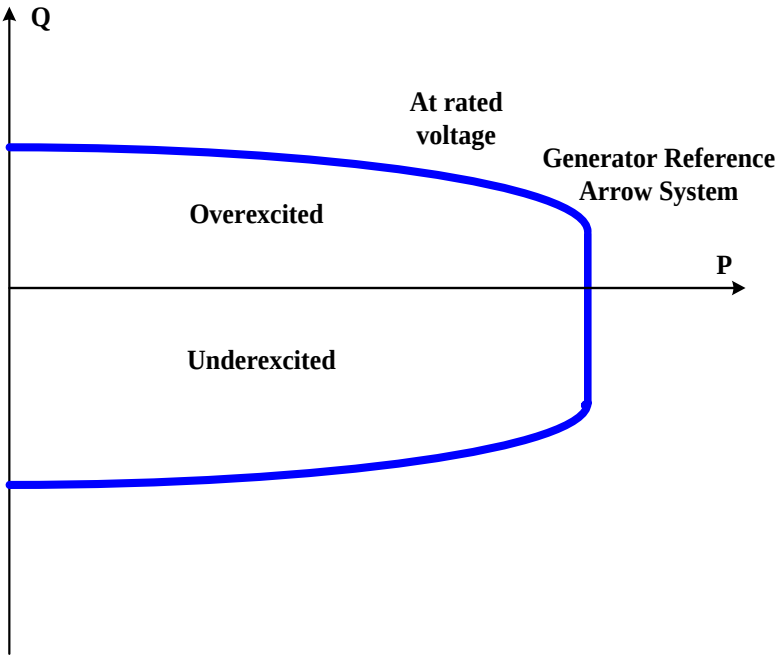

Figure 2.21: P-Q Characteristic of the DFIG.

2.6.6 Wind Turbine Generator Output

As introduced in section 2.3, the wind speed can be simulated by equation (2.2) and the wind turbine generator output can be calculated with equation (2.5). Figure 2.22 shows 120 hours of simulated wind farm output.

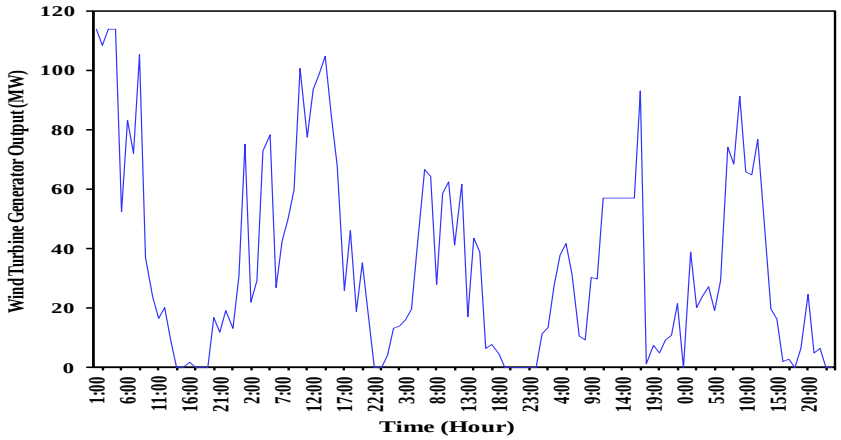

Figure 2.22: Wind Turbine Generator Output in 120 Hours.

2.7 Impact of Wind Turbine Generator on the Power System

The integration of a great amount of wind generation has a significant impact on a power system, primarily related to environmental, economical and reliability aspects. The impact of wind generation on power systems is consequently focused on numerous issues associated with power quality, stability, security and the operation of power systems.

- Wind turbine generators have certain impacts on power flow that can lead to reverse power flow and, as a result, the power system operation will become more complex. In addition, the power injection by a wind farm may cause power losses in the power network.

- The power quality is related to voltage variation and harmonic distortion in the power system. However, the incorporation of a wind turbine generator in a power system can affect the quality of the voltage supplied to customers. To decrease this impact, currently, variable speed wind turbines equipped with power electronics are widely used in wind energy conversion.

- System protection is greatly affected by a wind farm since the integration of wind power injection changes power flows; thus, conventional protection systems might fail under fault situations.

- All utilities have to maintain a stable and reliable voltage supply for customers within specific limits of frequency and magnitude. Connection of a wind farm may result in voltage stability problems, voltage levels changes, and frequency stability problems. The affects will be worse as the wind penetration levels increase. Recently, new requirements for wind farms have been introduced in order to keep power systems stable under numerous disturbances, such as low voltage ride through capability.

2.8 Conclusion

There is rising concern about increased emissions from conventional electricity generators. One of the ways to tackle this problem is to increase the generation of electricity from sources that produce little or no emissions. As a result, there has been an increase in the production of electricity from wind generation. For example, China's total wind generation capacity jumped from 1,260 MW in 2005 to 62,733 MW by the end 2011. Moreover, there has been a rapid development in the technologies used for wind turbine generators. The capacity of individual turbines has grown from a few kilowatts to more than 5 MW. This chapter has discussed the system facilities used to connect wind farms in order to meet the requirements set by the UK grid operator. It has also defined Weibull distribution, which is a probability distribution function of wind speed data that identifies the influences of the shape and scale parameters in the Weibull distribution on the probability curve. Wind turbine characteristics have also been discussed in this chapter, which has defined the relationship between wind speed and power output. Different wind turbine generators in current use have been presented. The doubly fed induction generator (DFIG), which is a variant of variable speed wind turbines, has been discussed in detail. The chapter has also discussed control systems for

wind generators to manage active and reactive power output, as well as reactive power support from voltage source converters. Finally, study of the impact of wind generators on power system operation has been reviewed. The proportion of wind turbines using a power electronic converter has remained relatively constant over the last decade. However, due to their good controllability and the decreasing costs of power electronics, an increasing market share of this generator technology is anticipated. In conclusion, this chapter has provided useful information about wind turbine generator technology and their future. DFIG type of generator has been selected for investigation in this research.

Chapter 3

Voltage Stability Theory

3.1 Introduction

The power system is said to be stable if it has the ability to remain in a state of operating equilibrium under normal operating conditions and to regain an acceptable state of equilibrium when subject to small disturbances. Recently there has been a significant increase in interest in the area of power system voltage stability analysis. The reason for this rising interest lies in the fact that losses of power supply due to collapse degrade system reliability and this in turn affects production and income. The ever increasing system demand increases the risk of voltage collapse. The development of the national economy of any country causes an increase in energy demand and electricity is the main form of energy heavily demanded by industry.

The voltage collapse phenomenon is known to be complex and localised in nature, although it has a widespread effect. A power system consists of several types of generators, long transmission lines, and support devices to supply power to customers. The nature of the demand depends on the consumer. It can be purely active power, as in domestic loads, or a combination of active power and reactive power in the case of industrial loads. A great deal of attention has been given to load modeling since the nature and characteristics of the load has an impact on the voltage stability of the system. In this chapter, the concept of voltage stability is presented. This includes basic definitions related to voltage stability and a brief discussion of voltage instability incidents to help demonstrate the causes and circumstances surrounding voltage collapse. The voltage-power relationship which is the topic of voltage stability is discussed in detail in section 3.4. The chapter also discusses power system load modelling.

3.2 Basic Concepts and Definitions

Power system stability may be defined as that property of a power system that enables it to remain in a state of operating equilibrium under normal operating conditions and to regain an acceptable state of equilibrium after being subjected to margin disturbance [83]. There are three forms of stability studies: rotor angle stability, voltage stability and frequency stability. The understanding of stability problems can be made much easier by classifying stability into various categories. The categories and subcategories of the power system stability problem are shown in Figure 3.1 [83]. The subsequent classification is based on a timescale which is divided into short term and long term elements.

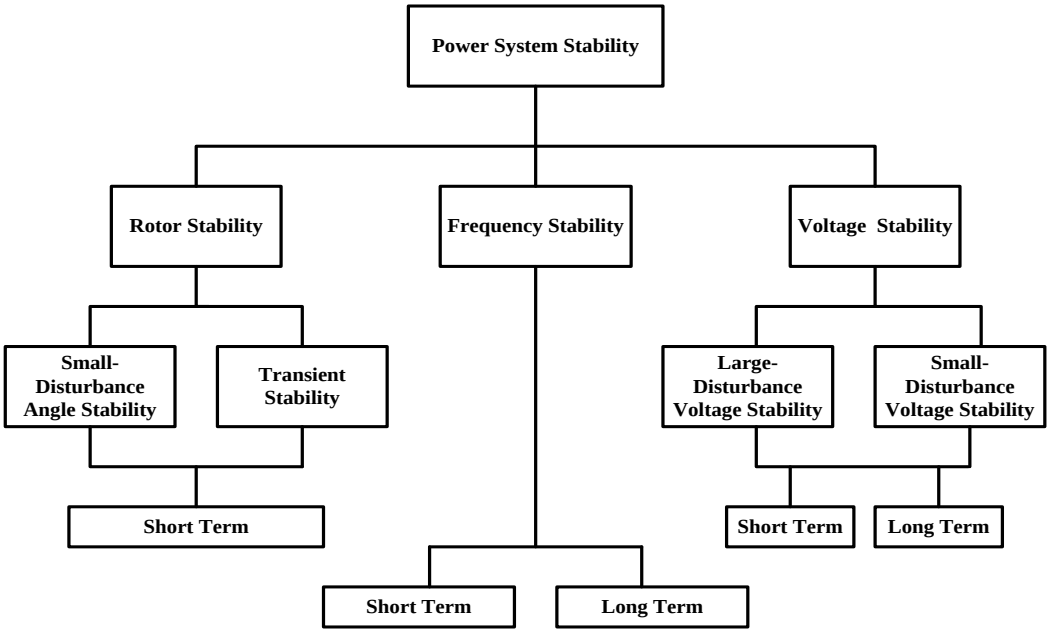

Figure 3.1: Classification of Power System Stability

Rotor angle stability is defined as the ability of interconnected synchronous machines of a power system to remain in synchronism after being subjected to a disturbance [84]. A synchronous generator connected to an infinite bus represented by its reactance used to study of rotor angle stability which involves the study of electromechanical oscillations in power systems. Rotor angle stability is divided into

small signal and transient stability. Small signal stability (or small disturbance stability) is the ability of power system to maintain synchronism under small disturbances in the form of undamped electromechanical oscillations. The character of a system response to small disturbances depends on a number of factors including the initial operating point, the transmission system strength, and the type of generator excitation controls used. The transient stability (or large disturbance rotor angle stability) is the ability of a power system to maintain synchronism when subjected to a severe transient disturbance. Stability depends on both the initial operating state of the system and the severity of the disturbance. The time frame of rotor angle stability is short term because the dynamics typically last for a few seconds [84].

Frequency stability refers to the ability of a power system to maintain a steady frequency following a severe system upset resulting in a significant imbalance between generation and load. Instability, which occurs in the form of sustained frequency swings, may lead to tripping of generating units or loads. Stability depends on the ability to maintain and restore equilibrium between system generation and load with minimum unintentional loss of load [83]. Serious system upsets generally result in large fluctuations in frequency, such as power flows, voltage and other system variables. Generally, frequency stability problems are associated with inadequacies in equipment responses, poor coordination of control and protection equipment, or insufficient generation reserve. As shown in Figure 3.1, frequency stability may be a short term or a long term phenomenon. During frequency fluctuation, the process characteristic times of devices and equipments will range from several seconds, such as under-frequency load shedding and generator controls and protections, to several minutes, such as prime energy supply systems and load voltage [83-84].

Voltage stability is a problem found in power systems which are heavily loaded, faulted or has a shortage of reactive power. The nature of voltage stability can be analysed by examining the production, transmission and consumption of reactive power. The problem of voltage stability concerns the whole power system, although it usually has a large involvement in one critical area of the power system. It is useful to classify

voltage stability into the following categories: large-disturbance voltage stability and small-disturbance voltage stability. Large-disturbance voltage stability refers to a system's ability to maintain steady voltages following large disturbances such as system faults. Small-disturbance voltage stability refers to the ability of a system to return to and maintain steady voltage when subjected to small perturbations such as incremental changes in system load. The time of interest for voltage stability problems vary from a few seconds to tens of minutes. Hence, voltage stability may be either a short term or a long term phenomenon, as shown in Figure 3.1. There are two terms that emerge in the voltage control problem, voltage stability and voltage collapse. The next section will describe voltage stability phenomena in detail.

3.3 Voltage Stability

The IEEE Power System Engineering Committee defines voltage stability as "the ability of the system to maintain voltage so that load admittance is increased, load power will increase, and so that both power and voltage are controllable" [85]. Voltage stability is concerned with the ability of a power system to maintain an acceptable voltage profile at all buses in the system under normal operating conditions, and after being subjected to a disturbance such as an increase in load demand or a change in system conditions. According to reference [86], "Voltage instability stems from the attempt of load dynamics to restore power consumption beyond the capability of the combined transmission and generation system"**.** Voltage instability is a local problem. However, the consequences of voltage instability may have widespread impact. Voltage collapse is defined as "the process by which voltage instability leads to uncontrollable voltage profile in a significant part of the system"**.** Voltage collapse may be characterised by the following system events [84]:

- A slow and steady decrease of voltage.
- The system cannot meet reactive power demands, since a change in the operating condition of the system requires reactive power, then a rapid voltage drop.

- It may be due to an increase in load during a particular time of day.
- Triggering of voltage collapse may be due to a loss of a transformer, loss of a transmission line or a loss of generation in any area.
- Under load tap changing (ULTC) action during low voltage conditions.
- Poor coordination between various control and protective systems.

It may be necessary at this point to provide some definitions of voltage stability and voltage collapse [84-87]:

- Disturbance in a power system: A disturbance is a sudden change or a sequence of changes in one or more of the parameters of a system, or in one or more of the operating quantities.
- Small-disturbance in a power system: A small-disturbance is a disturbance for which the equations that describe the dynamics of a power system may be linearised for the purpose of analysis.
- Large-disturbance in a power system: A large-disturbance is a disturbance for which the equations that describe the dynamics of a power system cannot be linearised for the purpose of analysis.
- Small-disturbance voltage stability: A power system at a given operating condition is small-disturbance voltage stable if, following any small-disturbance, voltage near loads is identical or close to pre-disturbance values.
- A voltage-stable power system: A power system at a given operating state, and subject to a given disturbance, is voltage-stable if voltage near loads approaches post-disturbance equilibrium values.
- A voltage-instable power system: Voltage instability is the absence of voltage stability and results in a progression of voltage magnitude.

If a power system lacks the capability to transfer a required amount of electrical power to loads then it is instable. The main factor causing voltage instability is the inability of a power system to meet demands for reactive power in heavily stressed systems to keep desired voltages. Other factors contributing to voltage stability are generator reactive power limits, load characteristics, characteristics of reactive power

compensation devices and the action of voltage control devices [86]. The reactive characteristics of AC transmission lines, transformers and loads restrict the maximum power of system transfers. A power system may lack the capability to transfer power over long distances or through high reactance due to the requirement of a large amount of reactive power at some critical value of power or distance.

3.3.1 Time Frames for Voltage Instability

Voltage instability spans a range in time from a fraction of a second to tens of minutes. Reference [88] recommends two time frames of voltage instability based on load characteristics: transient and longer-term. The time frame of the transient voltage instability is in seconds, whereas the time frame of the longer-term voltage instability varies from tens of minutes to hours. Figure 3.2 shows voltage stability phenomena and time responses.

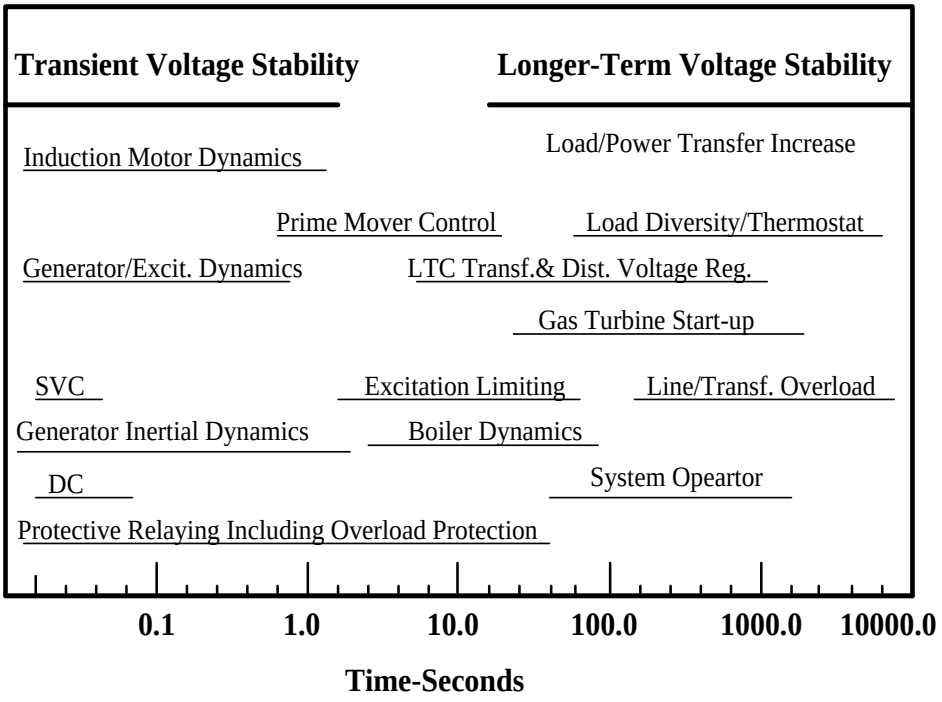

Figure 3.2: Voltage Stability Phenomena and Time Responses [88].

The figure shows the classification of voltage stability into transient and long term time frames. The time frame of transient voltage stability is a fraction of a second to about ten seconds. Transient voltage instability is caused by fast acting load components, such as induction motors. On the other hand, load pick-up associated with a heavily loaded system is an example of longer-term voltage instability, which is the focus of this thesis.

3.3.2 Incidents of Voltage Instability

Several blackouts have occurred in the last half century. The following are some of the major blackout events that have been reported [84-85-89-90-13-91]:

- New York City, November 9th, 1965. The first major blackout was in the United States, because of heavy loading conditions; one of five transmission lines tripped by backup relay low load level setting, thus tripping the remaining four transmission lines and diverting 1.7 GW load from other lines, over loading them and causing voltage collapse. This blackout affected 30 million people and New York City was in darkness for 13 hours.
- France, December 19th, 1978. 4.6 GW load rose in just one hour compared to 3 GW in the previous days. As a result, voltage deteriorated and reached a magnitude of 0.855 p.u in some 400 kV systems. The voltage collapse was triggered by the tripping of a major overloaded 400 kV line.
- Belgium, August 4th, 1982**.** A reactive power deficit combined with a series of generation outage caused voltage to decrease sharply and collapse. The time duration was less than 5 minutes.
- Tokyo City, July, 1987. This blackout occurred in Japan after noon during a hot summer day. Loads increased at a rate of 400 MW/minute and voltage decayed to reach 460 kV in the 500 kV systems, despite the connection of all available shunt capacitors. One hour later, collapse began and the load loss was about 8.2 GW.

- Western North American, United States, July 2nd, 1996. This blackout occurred due to the short circuit of a 1300 km series compensated 345 kV transmission line by flashover to a tree. The blackout affected 2 million people and caused a loss of 11.9 GW of load.
- US Canadian, August 14th, 2003. This blackout started with a 345 kV transmission line tripping due to a tree contact. Another line touched a tree after the first line was disconnected. At the same time, the computer software designed to warn operators was not functioning properly. All these reversed the power flow and caused a cascading blackout of an entire region. During this voltage collapse, 400 transmission lines and 531 generating units at 261 power plants tripped. This blackout affected 50 million people with a 63 GW of load interruption.
- The Europe Blackout, November 4th, 2006. This blackout occurred in the UCTE (Union for the Coordination of the Transmission of Electricity) inter-connected power grid which coordinates 34 transmission system operators in 23 European countries. The blackout started with a 380 kV transmission line tripping. The blackout affected 15 million people in Europe and 14.5 GW of load was interrupted in more than 10 countries.

- West of Scotland, Glasgow, UK, March 30th, 2009. A major power cut hit homes and businesses in Glasgow and parts of Western Scotland. The affected areas included the west end of Glasgow, Bearsden, Clydebank, Helensburgh, Dumbarton and as far afield as Lochgilphead and Oban. Arran was also affected from the outage. The power cut occurred at 16:20 and power was slowly restored between 17:20 and around 18:30.

- Southern California, USA, May 1st, 2011. Arizona and Baja California were left without power when a single transmission line in Arizona was lost, which led to a cascading series of failures. The blackout affected 2.7 million people across the two states.

- Cyprus, April 4th, 2012. A Blackout occurred in all Cyprus cities after Dhekelia Power Station failed (there was a lack of electric power from 04:42 to 09:20).

3.4 Power-Voltage Relationship [84-31]

The characteristics of voltage stability depend on the relationship between the power and voltage at the receiving end of a system. However, the power-voltage relationship can be illustrated by considering two terminal networks, as shown in Figure 3.3. It consists of a constant voltage source E supplying a load of impedance $Z_{Load}\angle\varphi$ through series line impedance $Z_s\angle\theta$.

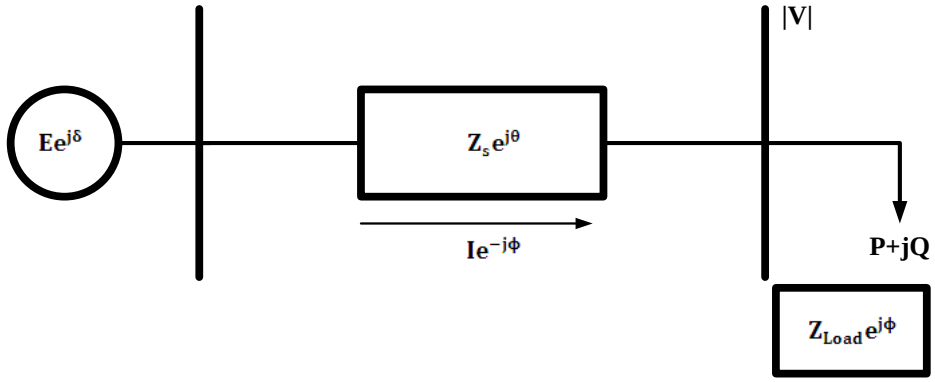

Figure 3.3: The Simple Two-Bus System for Illustration of Voltage Stability.

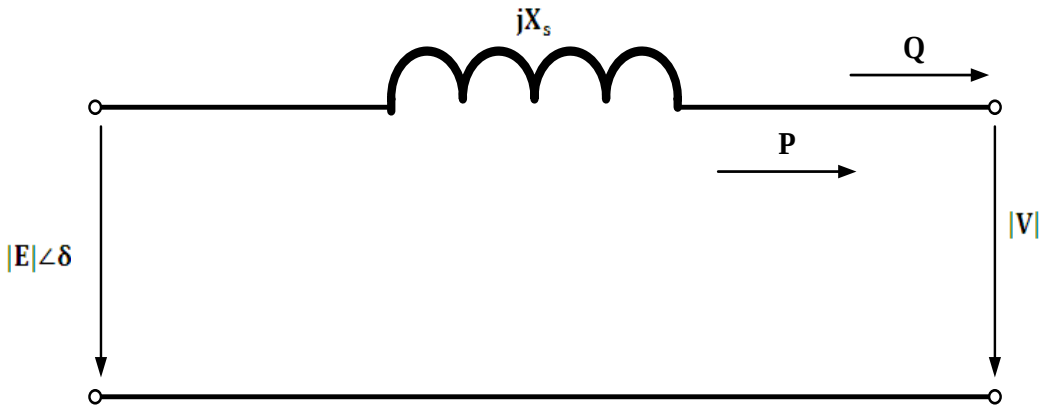

Figure 3.4: A Simple Transmission Line for Calculation of Power-Voltage Characteristics.

Load impedance is the function of active power and reactive power, and can be expressed in complex form as

$$Z_{Load} = \frac{|V|^2}{P - jQ} \tag{3.1}$$

The magnitude of the current flowing from the source to the load is given by

$$|I| = \frac{|E|}{\sqrt{(|Z_s|\cos\theta + |Z_{Load}|\cos\varphi)^2 + (|Z_s|\sin\theta + |Z_{Load}|\sin\varphi)^2}} \tag{3.2}$$

Equation (3.2) may be expressed as

$$|I| = \frac{|E|}{|Z_s|\sqrt{D}} \tag{3.3}$$

Where

$$D = 1 + \left(\frac{|Z_{Load}|}{|Z_s|}\right)^2 + 2\left(\frac{|Z_{Load}|}{|Z_s|}\right)\cos(\theta - \varphi)$$

The magnitude of the receiving-end voltage can be written as

$$|V| = |Z_{Load}||I| \tag{3.4}$$

Substituting equation (3.2) into equation (3.4) yields

$$|V| = \frac{|Z_{Load}|}{|Z_s|}\frac{|E|}{\sqrt{D}} \tag{3.5}$$

The power supplied to the load is given by

$$P = |V||I|\cos\varphi \tag{3.6}$$

Substituting equations (3.3) and (3.5) into equation (3.6) gives

$$P = \frac{|E|^2 |Z_{Load}| \cos \varphi}{D|Z_s|^2} \tag{3.7}$$

To make the results applicable to any value of E and Z_s, the power, voltage, and current can be normalized as follows:

The normalized power is

$$P_N = P/P_{max}$$

Where P_{max} is the maximum power that can be transmitted at the unity power factor. It is the power that is achieved when the voltage drop in the line is equal in magnitude to the receiving-end voltage; in other words, when $|Z_{Load}|$ is equal to$|Z_s|$. Therefore, the maximum power can be expressed as

$$P_{max} = \frac{|E|^2}{2|Z_s|(1 + \cos \theta)}$$

Then it follows from equation (3.7) that the normalised power can be written as

$$P = \frac{2 \cos \varphi (1 + \cos \theta)}{(|Z_s|/|Z_{Load}|) + |Z_{Load}|/|Z_s| + 2\cos(\theta - \varphi)} \tag{3.8}$$

The normalised voltage is defined as

$$v = |V|/|E|$$

From equation (3.5), it follows that

$$v = \frac{1}{(|Z_s|/|Z_{Load}|)\sqrt{D}} \tag{3.9}$$

The normalised current is defined as

$$i = |I|/(|E|/|Z_s|)$$

From equation (3.3), the normalised current can be expressed as

$$i = \frac{1}{\sqrt{D}}$$

Finally, the normalised impedance may be represented by

$$z = |Z_{Load}|/|Z_s|$$

The normalised current, voltage, and power are plotted by varying $|Z_s|/|Z_{Load}|$ (normalised admittance), as shown in Figure 3.5. As the load demand is increased, thus decreasing$|Z_{Load}|$, the load power *P* increases at a high slope at first and then at a low slope before reaching the maximum value($|Z_s| = |Z_{Load}|$), after which it decreases.

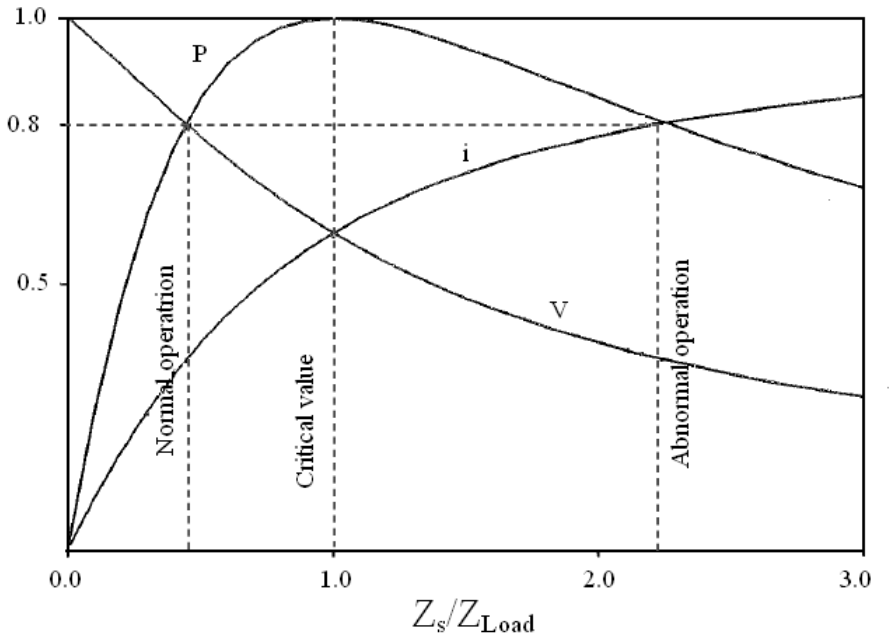

Figure 3.5: Receiving-end Voltage, Current, and Power as Functions of Load Demand ($\cos\varphi = 1.0, \tan\theta = 10.0$).

In addition, the power is the function of voltage and current; as the power demand is increased, the receiving-end voltage decreases, while the current flowing from the constant-voltage source increases. As long as $|Z_{Load}|$ is greater than$|Z_s|$, the rate of increase in the current dominates over the rate of decease in the voltage, and hence the power increases until it reaches its maximum. However, when $|Z_{Load}|$ becomes less

than$|Z_s|$, the decrease in voltage dominates over the increase of current and hence the power decreases. Based on the relationship between the power and voltage, two fundamental charts can be derived: the active power-voltage (P-V) and the voltage-reactive power (V-Q) characteristics. Consequently, the process of voltage collapse can be investigated from the study of the P-V and V-Q characteristics of the load, as demonstrated in the following sections.

3.4.1 Active Power-Voltage (P-V) Characteristics [84]

The relationship between the receiving-end real power and voltage for a constant, and for different values of power factors, are shown in Figure 3.6 and Figure 3.7, respectively. Plotted along the horizontal axis is the load real power, and along the vertical axis is the voltage. The graphs show that for each power factor there is a maximum transmissible power at the apogee of the curves. It can also be observed that for any value of power below the maximum there are two voltage solutions, represented by the upper and lower parts of the P-V curve. The upper part of the curve is the region of normal operation of power systems. It can be inferred from the P-V curves that the power factor has a great influence on the receiving-end voltage. Moreover, the very low lagging power factor reduces the maximum transmissible power.

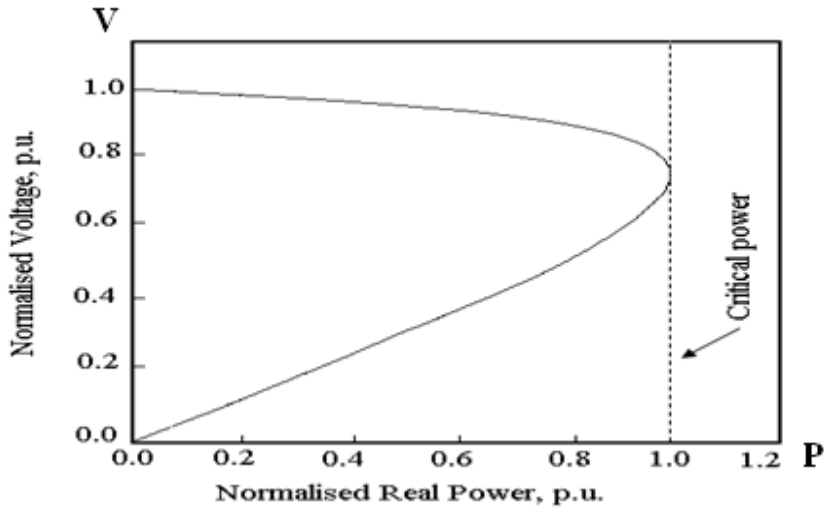

Figure 3.6: Power-Voltage Characteristics ($\cos\varphi = 1.0, \tan 10.0$).

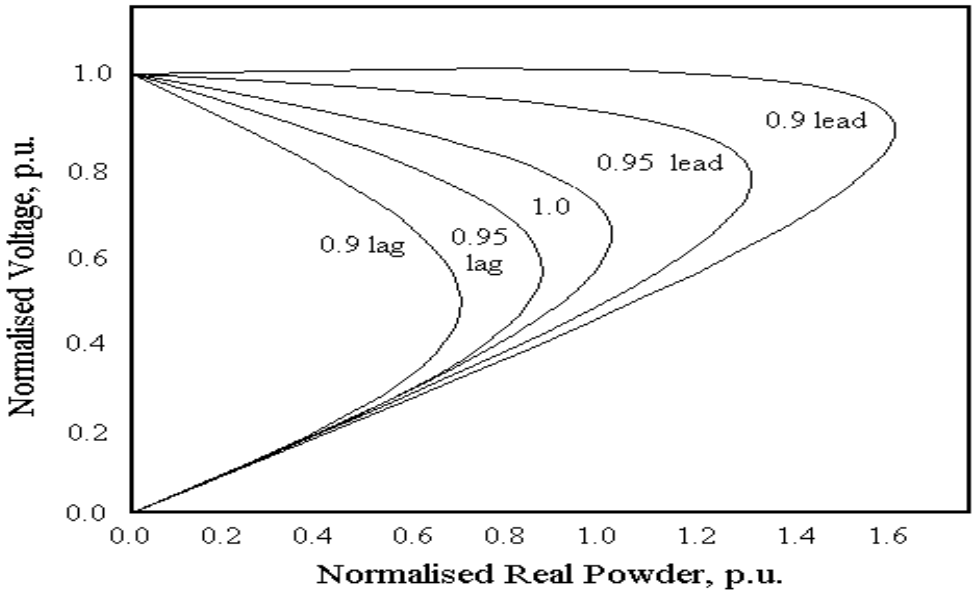

Figure 3.7: Power-Voltage Characteristics with Different Load-Power Factors($\tan\theta = 10.0$).

3.4.2 Voltage-Reactive Power (V-Q) Characteristics [84]

When there is a variable injection of reactive power into a system from any reactive power support device, such as synchronous condensers or static var compensators, a more useful chart is the voltage-reactive power curve (V-Q). These curves are called in some literature Q-V curves; however, the V-Q terminology will be used here to stress that the voltage (in the abscissa) rather than the reactive power is the independent variable. To obtain a general expression of the V-Q characteristics of the system, consider the circuit in Figure 3.4, from which the equations of power governing the circuit (eliminating the resistance) can be written as follows:

The expression of the active power is represented as

$$P = \frac{|E||V|}{X_s}\sin\delta \tag{3.10}$$

The expression of the reactive power is simply

$$Q = \frac{|E||V|}{X_s}\cos\delta - \frac{|V|^2}{X_s} \tag{3.11}$$

Normalise the variables of equations (3.10) and (3.11) based on the short circuit power, $|E|^2/X_s$ with the following expressions:

The normalised active power is given as

$$p = \frac{PX_s}{|E|^2} = \frac{|V|}{|E|}\sin\delta \tag{3.12}$$

The normalised reactive power is stated as

$$q = \frac{QX_s}{|E|^2}$$

or

$$q = \frac{|V|}{|E|}\cos\delta - \frac{|V|^2}{|E|^2} \tag{3.13}$$

The normalised voltage is simply

$$v = \frac{|V|}{|E|} \tag{3.14}$$

Combining equations (3.10, 12, and 14) and rearranging, it follows that the normalised real power can be written as

$$p = v\sin\delta \tag{3.15}$$

Similarly, the normalised reactive power can be represented by

$$q = v\cos\delta - v^2 \tag{3.16}$$

Then it follows that

$$p^2 + q^2 = (v\sin\delta)^2 + (v\cos\delta - v^2)^2 \tag{3.17}$$

Using the trigonometric identity,

$$\sin^2\delta + \cos^2\delta = 1$$

The per unit normalised power can be written as

$$p^2 = v^2 - (v^2 + q)^2$$

For an injection of reactive power, the sign of *q* must be changed, therefore

$$p^2 = v^2 - (v^2 - q)^2 \tag{3.18}$$

Rearranging equation (3.18), the normalised reactive power injection, q, can be simply stated as

$$q = v^2 - \sqrt{v^2 - P^2} \tag{3.19}$$

The relationship in equation (3.19) is plotted in Figure 3.8. It shows the general v-q curves for several values of p; voltage is the independent variable and the abscissa variable. Each curve represents the relationship between the reactive power and the voltage at the receiving-end. However, for a given value of real power, there are two values of voltage represented by the right and left parts of the curve; the part right of the minima of the curve represents the stable operation and the part to the left of the minima represents an unstable operation. Nevertheless, the minima are the point at which the derivative dq/dv is zero. Accordingly, the v-q curve determines the reactive power margin (MVAr distance) from the operating point to the critical state (minima of the

curve). As shown in Figure 3.8, the left side of the v-q curves end at the point where *p* = v. In other words, all the v-q curves lie in the area between the curve $q = v^2$ (i.e. p = v) and $q = v^2 - v$ (i.e. p = 0), as suggested by equation (3.19).

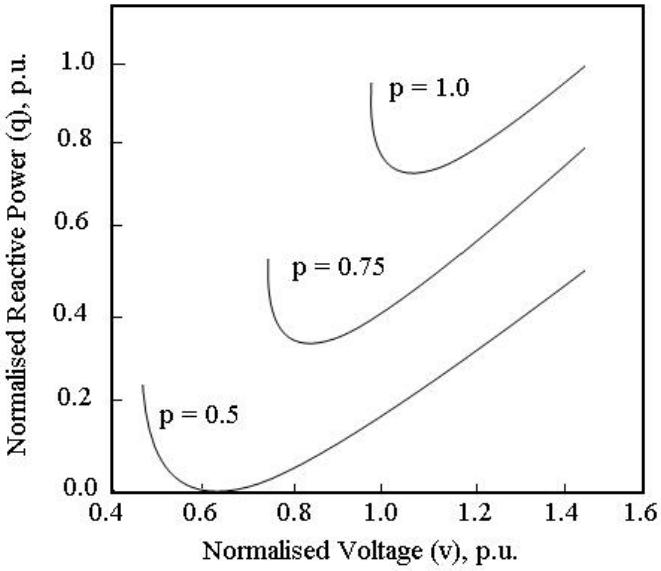

Figure 3.8: Voltage-Reactive Power (v-q) Characteristics with Different Values of Real Power.

Based on the descriptive analysis, Figure 3.9 shows the boundary ($0 \leq p \geq v$) of the v-q curves. The local minimum curve is obtained by differentiating equation (3.19) and equating to zero as follows:

$$\frac{dq}{dv} = 2v - \frac{v}{\sqrt{v^2 - p^2}}\ 0 \tag{3.20}$$

Solving for v, the normalised voltage is simply

$$v = \sqrt{p^2 + \frac{1}{4}} \tag{3.21}$$

Substituting equation (3.21) into (3.19) and rearranging yields

$$q = v^2 - \frac{1}{2} \tag{3.22}$$

This relationship contains all the minimum points of the v-q curves and can be called the curve of minima, as shown in Figure 3.10.

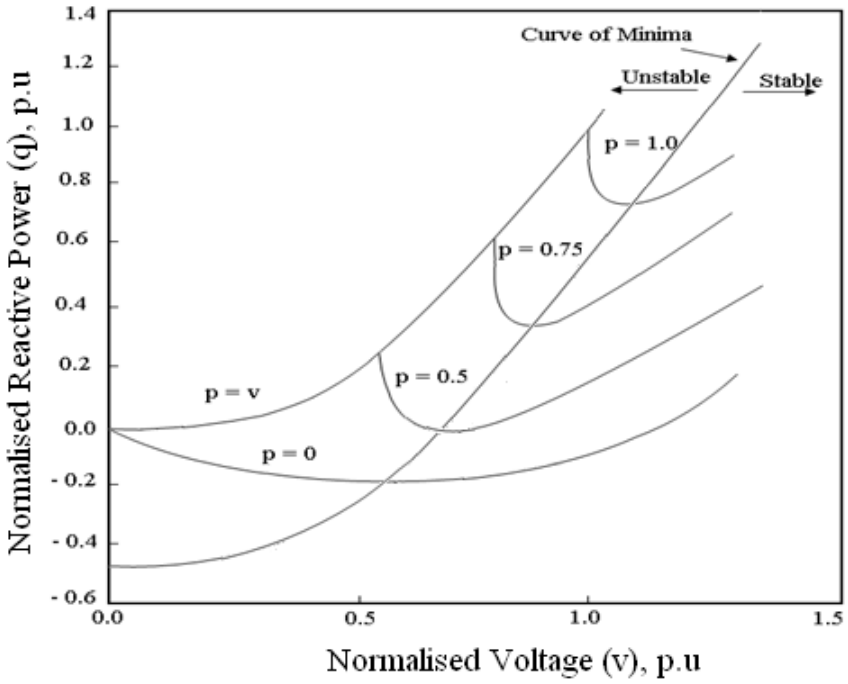

Figure 3.9: The v-q Characteristics with the Minimum Local Curve for Different Values of Real Power

3.5 Classification of Buses

For load flow studies it is assumed that the loads are constant and that they are defined by their real and reactive power consumption. It is further assumed that the generator terminal voltages are tightly regulated and therefore constant. The main objective of the load flow is to find the voltage magnitude of each bus and its angle when the powers generated and loads are pre-specified. There are three major buses used in power flow, as shown in Figure 3.10 and Table 3.1 below:

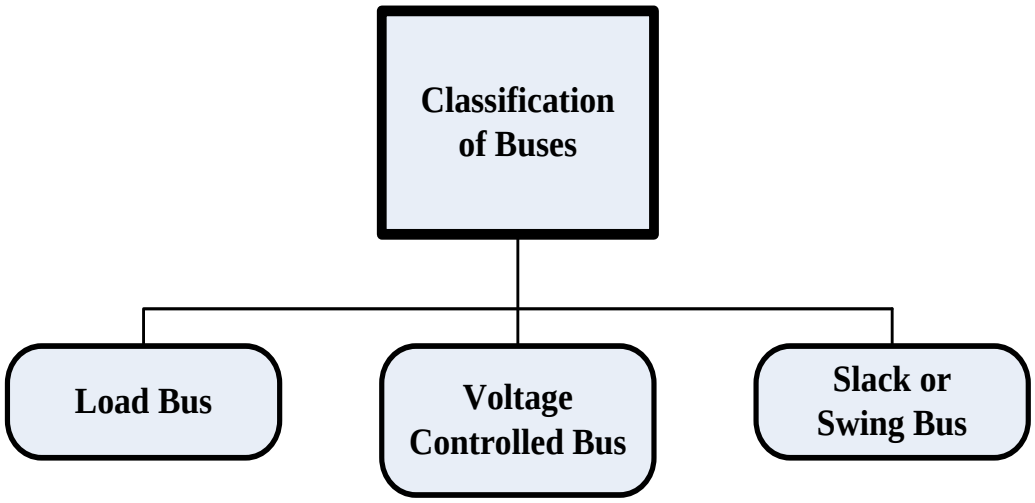

Figure 3.10: Classification of Buses

Table 3.1: Bus Types

Bus Type	P	Q	V	Angle
Load Bus (PQ Bus)	*	*	X	X
Voltage Controlled (PV Bus)	*	X	*	X
Slack Bus or Swing Bus	X	X	*	*

(X): Variable Unknown

(*): Variable Known

- Load bus: In this bus no generator is connected and hence the generated real power P_{Gi} and reactive power Q_{Gi} are taken as zero. The load drawn by this bus is defined by real power $-P_{Li}$ and reactive power $-Q_{Li}$ in which the negative sign accommodates for the power flowing out of the bus. This is why this bus is sometimes referred to as the P-Q bus. In other words, the P-Q bus is often known as a load bus because it has real and reactive powers set to a specific value; both voltage and angle at the bus must be calculated.

- Voltage controlled bus**:** This is the bus where the generator is connected. Therefore the power generation in such a bus is controlled through the prime mover while the terminal voltage is controlled through generator excitation. Keeping the input power constant throughout the turbine-governor control and keeping the bus voltage constant using automatic voltage regulator, the constant P_{Gi} and $|V_i|$ for this bus can be specified. This is why such a bus is also referred to as a P-V bus. It is to be noted that the reactive power supplied by the generator Q_{Gi} depends on the system configuration and cannot be specified in advance (depending on regulation, generator connected to such a bus will inject or consume reactive power at their $-Q < Q < +Q$ limit). Furthermore, it has to find the unknown bus angle.

- Slack or swing bus: Usually this bus is numbered 1 for load flow studies. This bus sets the angular altitude references for all other buses. However, it sets the reference against which angles of the other bus voltages are measured. For this reason the angle of this bus is usually chosen as (0°). Also, it is assumed that the magnitude of the voltage of this bus is known.

Consider a typical load flow problem in which all load demands are known. Even if the generation matches the sum total of these demands exactly, the mismatch between generation and load will persist because of the (I^2R) losses. As the (I^2R) loss of the line depends on the current which, in turn, depends on the magnitudes and angles of voltages of the two buses connected to the line, it is rather difficult to estimate the loss without calculating the voltages and angles. Consequently, the generator bus is usually chosen as the slack bus without specifying its real power. It is assumed that the generator connected to this bus will supply the balance of the real power required and the line losses.

3.6 Load Modelling in Voltage Stability

Over the last decade, a great deal of attention has been given to load modelling. This section throws some light on load modelling. The definition of load is given first followed by static and dynamic load modelling. Static modelling can be classified into three models:

1. Constant power
2. Constant impedance
3. Constant current

On the other hand, the dynamic load model is a function of time and is simulated by differential equations.

3.6.1 Definition of Load

The term 'load' can have several meanings in power system engineering [92], namely the following:

a. Load device: the device connected to a power system, which consumes power.
b. Generator load: the power output of a generator or generating plant.
c. System load: total active and reactive power consumed by all devices connected to a power system.
d. Bus load: a portion of a system that is not explicitly represented in the system model but is treated as if it were a single power-consuming device connected to the bus.

The definition of bus load above includes all connected load devices, distribution transformers, subtransmission feeders, shunt capacitors and customer wiring and appliances. Moreover, 'load characterise' refers to a set of parameters, such as power factor or variation of power with voltage, that characterise the behaviour of a specified load. A load model is a mathematical representation of the relationship between load bus voltage (magnitude and frequency) and the power (active and reactive) flowing into a

bus load. Load modelling is classified into two models: static and dynamic. A static load model is represented by algebraic equations while a dynamic model is represented by differential equations.

3.6.2 Static Load Model [93]

A general load characteristic of the busbar may be adopted such that the MW loading of this bus is a function of the voltage and frequency.

$$P = P_0 \left(\frac{V}{V_0}\right)^{\alpha_v} \left(\frac{\omega}{\omega_0}\right)^{\alpha_\omega} \tag{3.23}$$

The reactive power expression is

$$Q = Q_0 \left(\frac{V}{V_0}\right)^{\beta_v} \left(\frac{\omega}{\omega_0}\right)^{\beta_\omega} \tag{3.24}$$

Where the subscript 0 refers to nominal values, P_0 is the nominal active power, Q_0 is the nominal reactive power, V_0 is the nominal voltage, ω is the angular frequency, α and β are the characteristic parameters of the load. Based on the characteristic parameters of the load, the static load model can be classified into three categories, namely constant power, constant current, and constant impedance loads. Equations (3.23) and (3.24) provide useful means to determine various load models by varying the characteristics of the load. Reference [93] has identified the characteristic load parameters for some loads, which can be combined to give the resultant load characteristics at the busbar. For example, a group of M homogenous loads at busbar i, each load with the characteristic of α_{ij} and a nominal power of P_{ij}, has an overall characteristic of

$$\alpha_i = \sum_{j=1}^{M} \alpha_{ij} \frac{P_{ij}}{P_i} \tag{3.25}$$

The following table shows typical values of characteristic load parameters [93]:

Load	α_v	α_ω	β_v	β_ω
Filament Lamp	1.6	0	0	0
Florescent Lamp	1.2	-1.0	3.0	-2.8
Heater	2.0	0	0	0
Reduction Furnace	1.9	-0.5	2.1	0

However, the dependency on frequency is usually neglected in voltage stability because voltage usually changes much more than frequency. Also, the sensitivity of frequency is not related directly to voltage instability.

3.6.2.1 Constant Power Load Model

In a constant power or constant MVA load model, the power (real and reactive) does not vary with changes in the load voltage. Therefore, the active and reactive power are represented simply by their initial values as

$$P = P_0$$

$$Q = Q_0$$

Where P_0 and Q_0 are the nominal active and reactive power respectively.

Examples of constant power loads are adjustable speed drives and devices with regulated power supplies.

3.6.2.2 Constant Current Load Model

In a constant current model, the power varies directly with the voltage magnitude.

The proper expression for active power is

$$P = P_0 \left(\frac{|V|}{|V_0|} \right)$$

For reactive power it is

$$Q = Q_0 \left(\frac{|V|}{|V_0|} \right)$$

Examples of constant current loads are discharge lighting such as florescent, mercury vapour, sodium vapour, and other similar types such as street lighting.

This load extinguishes when the voltage reaches about 0.8 per unit, and may drop to zero during faults [92].

3.6.2.3 Constant Impedance Load Model

The power of a constant impedance load model varies with the square of the voltage magnitude. It can also be called a constant admittance load model.

Active power can be simply stated as

$$P = P_0 \left(\frac{V}{V_0} \right)^2$$

The reactive power expression is

$$Q = Q_0 \left(\frac{V}{V_0} \right)^2$$

Thermostat-controlled loads such as space heaters, water heaters, and soldering machines are examples of constant impedance loads. However, when voltage drops, the reduction in heat output from such loads will be sensed by the thermostat and the ‘on’ part of the cycle will be extended automatically. Due to the extended ‘on’ period at a lower voltage, more thermostats are in the ‘on’ mode at any given instant at low voltage, therefore the total load is the same as it is at normal voltage.

The constant power, constant impedance, and constant current models are graphically represented in Figure 3.11. Plotted along the horizontal axis is the voltage magnitude and along the vertical axis is the load (active or reactive). It can be seen in the figure that the constant power model is independent of the voltage, while the constant

impedance and current loads are dependent on the voltage magnitude. However, when the voltage equals the nominal value, the three load models are equal. When the load is a function of voltage (constant impedance and constant current models), any decrease of voltage from the initial state (nominal value) results in a decrease in load, and the constant impedance model has the lowest consumption of load. In contrast, for a given voltage greater than the nominal value, the constant impedance model draws the highest load. Therefore, the constant impedance model is the least severe case in voltage stability, whereas the constant power model is the most severe case.

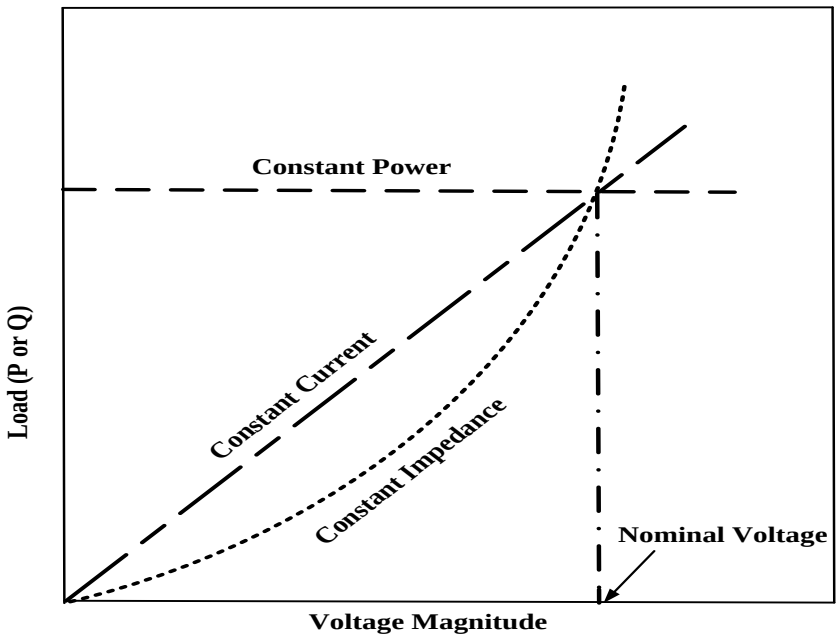

Figure 3.11: Characteristic of Different Load Models.

3.6.3 Dynamic Load Models

There are many cases where it is necessary to account for dynamic load components. Induction motors, which are the main power consumption in industrial loads, must be represented as dynamic devices. These devices are fast acting load components, i.e. they respond rapidly to match their mechanical load within a few

seconds following a sudden change in voltage. When the voltage falls sharply, the reactive power of the induction motor increases and contributes to the voltage collapse problem. In the following section, the mathematical modelling of an induction motor is presented.

3.6.3.1 Modelling of Induction Motors [94-95]

Induction motors form the workhorse of the electric power industry, therefore modelling of induction motors is important for transient voltage stability. In this section a mathematical model is developed for an induction machine. An induction machine carries alternating currents in both the stator and rotor windings. When there is a relative motion of the stator field and the rotor, voltages are 'induced' in the rotor windings. The current in each rotor winding is equal to the induced voltage divided by the impedance of the rotor circuit. However, the torque is produced as a result of the reaction of the rotor current with the stator field. To develop a positive torque, the rotor speed must be less than the speed of the stator field (synchronous speed). The rotor speed is related to the stator speed by the slip, which is defined as

$$s = \frac{\omega_s - \omega_r}{\omega_s} \tag{3.26}$$

Where s is the slip of induction motor, ω_s and ω_r are the synchronous and rotor speed respectively. With no load the motor operates with negligible slip; however, if mechanical load is applied then the slip increases.

Induction motor equations are derived from the equivalent circuit of the induction motor, which is shown in Figure 3.12. The input electrical active power is represented by

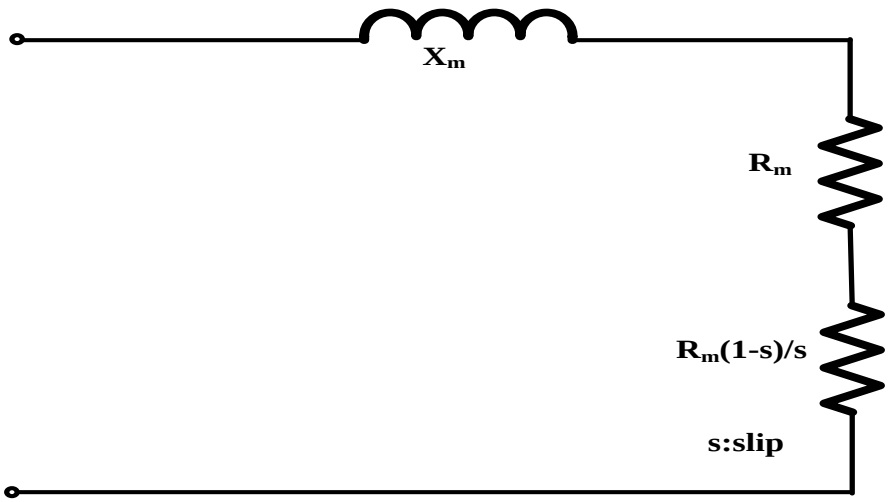

Figure 3.12: Induction Motor Equivalent Circuit [94].

$$P_e = \frac{R_m}{slip\left(\left(\frac{R_m}{slip}\right)^2 + X_m^2\right)}\left(V_{rl}^2 + V_{im}^2\right) \tag{3.27}$$

The input reactive power can be written as

$$Q_e = \frac{X_m}{\left(\left(\frac{R_m}{slip}\right)^2 + X_m^2\right)}\left(V_{rl}^2 + V_{im}^2\right) \tag{3.28}$$

Where R_m and X_m are the resistance and reactance of the equivalent circuit of the induction motor respectively, neglecting the stator's resistance, and V_{rl} and V_{im} are the real and imaginary parts of the bus voltage respectively.

The relationship between the mechanical and electrical power is represented by

$$P_e(1 - slip) = P_m \tag{3.29}$$

Where P_e and P_m are the electrical and mechanical power respectively. The dynamic equation of the induction motor is described as the function of slip (the derivation is given in Appendix A). It can be simply written as [94]:

$$\frac{d(slip)}{dt} = \frac{1}{\Phi\omega_0^2}\left(\frac{P_m}{1 - slip} - P_e\right) \tag{3.30}$$

Where t is the time in seconds and Φ is the moment of inertia of the rotor in kg-m^2.

$\omega_0 = 2\pi f_0$, where f_0 is the frequency of the power system in hertz.

However, the slip varies from 0 at no load to 1.0, at which point the motor stalls. Hence, for any disturbance in the electrical power input, the value of the slip together with the load characteristic (power-voltage curve) is the measure of voltage stability for the induction motor load. However, the slip can be obtained at any instance of time by solving the dynamic differential equation using the well-known Runge-Kutta method.

The results are depicted in Figure 3.13. The figure shows the power-voltage (P-V) curve and the load characteristic curve at different values of the motor slip. Plotted along the vertical axis is the voltage of the busbar at which the induction motor load is connected, and along the horizontal axis is the active power load. The P-V curve is plotted at unity and 0.9 power factor lagging respectively. It is easy to see that the curve with lagging power factor has a lower voltage stability limit than the one with unity power factor. Following any disturbance (e.g. a decrease in electrical power), the slip is increased with time. Consequently, the operating point falls along the P-V curve towards the voltage stability limit at the apogee of the curves; this is transient voltage stability.

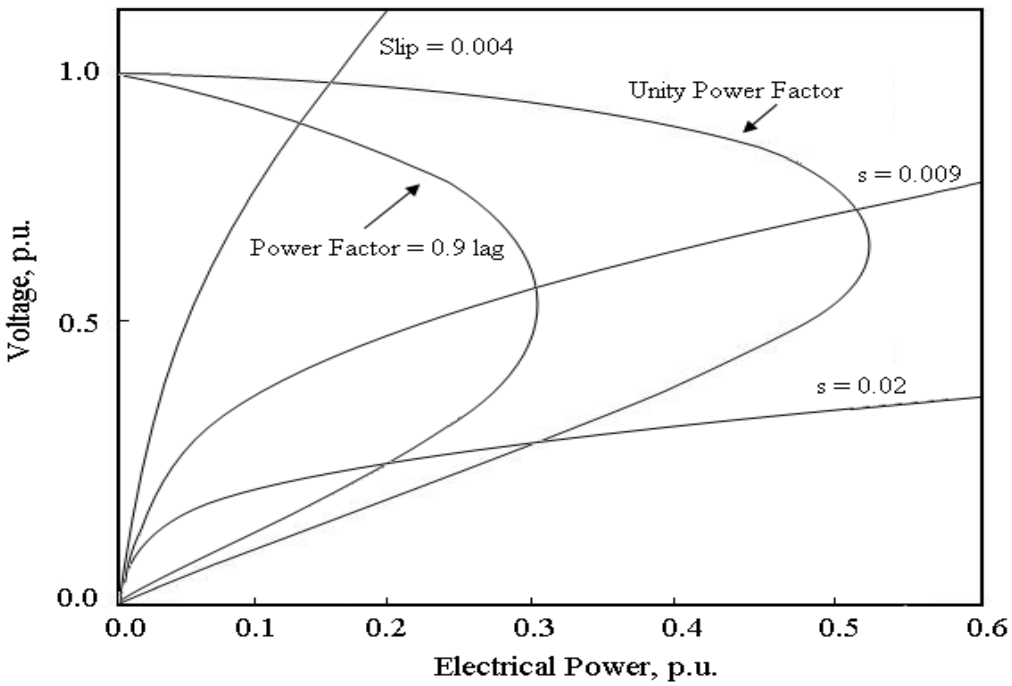

Figure 3.13: Power-Voltage Curve and Load Characteristic Curve for Induction Motor [13].

3.7 Conclusion

An understanding of the voltage stability problem has been established with an explanation made from various points of view. The first section of this chapter introduced the basic concepts and categories of power system stability, which are based on the dynamic performance of the power system. It also briefly described and compared the different categories of stability: rotor angle stability, frequency stability and voltage stability. Voltage stability was examined in more detail, including giving the definition of voltage stability, voltage instability and voltage collapse. The time frames involved in the development of a voltage collapse were also examined for operator intervention purposes. Short term or transient changes which lead to voltage collapse cannot be dealt with by manual intervention and thus require automatic mitigation methods. However, for mid-term and long-term voltage collapse incidents, operator

intervention is possible. Since load variation scenarios play a major role in voltage collapse, load increase scenarios are studied when considering mid-term and long-term voltage collapse during stability analysis. This chapter also provided a descriptive analysis of the relationship between power (active and reactive) and voltage at the receiving-end. This chapter has made the following findings:

- Voltage stability is related to load areas and load characteristics.
- Voltage stability depends on the relationship between power transfer and receiving-end voltage.
- The power factor plays a significant role in the voltage-power characteristics of the system.
- The reactive power margin of the power system can be obtained from the study of the Q-V curves.

Finally, this chapter reviewed the load representation for static and dynamic performance. Concise but adequate theoretical background was presented to explain the various constituent parts of the load model. Loads are classified into two categories: static and dynamic loads. The static load model expresses the characteristics of the load at any instance of time as an algebraic function of bus voltage. On the other hand, the dynamic load model is simulated by differential equations and is a function of time. It can also be concluded that the constant power representation of loads is the most severe case from a long-term voltage stability viewpoint, and this thesis focuses on the worst case scenario.

Chapter 4

Predicating Methodologies for Voltage Instability

4.1 Introduction

After defining voltage collapse and its symptoms, there is a need to look into existing methods of analysis. A number of researched methods are used to estimate the proximity to voltage instability [23-24-25-28-30-96-97-98-99-100-101]. This chapter restricts itself to the mathematical formulation of some existing voltage stability indices. The chapter first describes the mathematical formulation of voltage stability indices. Three different methodologies related to long-term voltage stability will be presented in the next section. The three methods are the Voltage-Reactive Power (V-Q) Index by (Mansour) [102], the (L) Indicator by (Kessel) [103], and the Voltage Collapse proximity Indicator (VCPI) by (Alammari) [26]. Secondly, the original methodology for determining a voltage collapse proximity indicator presented by Alammari and K Lo (1996) is developed further. It is developed to calculate the voltage collapse proximity indicator that considers the wind generator reactive power limits. This also takes into account the need for a new reference bus to determine the new equivalent system impedance. Due to the reactive power limitation of wind generators, this equivalent system impedance is not constant as suggested by Alammari and Lo's method [26]. The procedure of the proposed method is explained and then a 3-bus system to determine the voltage collapse proximity indicator (VCPI) is given. Finally, the UKGDS 61-bus, IEEE-14 bus system, IEEE-30 bus and IEEE-118 bus systems are used to demonstrate the capability of the proposed method and to investigate the voltage collapse indicator (VCPI) with different penetration levels of wind generation.

4.2 V-Q Index [103]

Based on the voltage-reactive power relationship, a voltage stability indicator is proposed by Mansour and Kundur (1991). In this method, the voltage-reactive power (V-Q) sensitivity of each load bus is calculated using the Jacobian matrix associated with the power flow equations, which can be written as

$$P = f(\delta, V) \tag{4.1}$$

$$Q = g(\delta, V) \tag{4.2}$$

The above equations may be represented in the following form

$$\begin{bmatrix} \Delta P \\ \Delta Q \end{bmatrix} = \begin{bmatrix} J_{P\delta} & J_{PV} \\ J_{Q\delta} & J_{QV} \end{bmatrix} \begin{bmatrix} \Delta\delta \\ \Delta V \end{bmatrix} \tag{4.3}$$

Let $\Delta P = 0$, then from equation (4.3)

$$\Delta Q = \left[J_{QV} - J_{Q\delta} J_{P\delta}^{-1} J_{PV}\right]\Delta V \tag{4.4}$$

or

$$[\Delta Q] = [J_R][\Delta V] \tag{4.5}$$

Where

$$J_R = \left[J_{QV} - J_{Q\delta} J_{P\delta}^{-1} J_{PV}\right] \tag{4.6}$$

Rearranging equation (4.5) gives

$$[\Delta V] = [J_R]^{-1}[\Delta Q] \tag{4.7}$$

The i^{th} diagonal element of $[J_R]^{-1}$ is the V-Q sensitivity of the bus i and positive values of all diagonal elements are an indication of stable operation. The smaller the sensitivity value, the more stable the system. However, as the stability of bus i decreases, the magnitude of the i^{th} diagonal increases and becomes infinity at the stability limit.

4.3 The L Indicator [102]

The method called the L indicator, aimed at the detection of voltage instability, is proposed by Kessel and Glavitsch (1986). It uses the information of the normal load flow and varies in the range between zero (no load) and one (voltage collapse). The method was derived from the two-bus system where one of the nodes is the slack and the other is the PQ node. The model and the method are extended to the multi-machine power system. The L stability indicator can be computed for each node; the maximum value (closest to one) is an indication of proximity to voltage collapse.

The voltage stability indicator at the bus j, as proposed by Kessel and Glavitsch, is expressed as

$$L_j = \left| \frac{\sum_{i \in \alpha_G} F_{ji} V_i}{V_j} \right| \tag{4.8}$$

Where α_G is the set of generator buses and F_{ji} is the element in matrix [F] which is determined by

$$[F] = -[Y_{LL}]^{-1}[Y_{LG}] \tag{4.9}$$

Where $[Y_{LL}]$ and $[Y_{LG}]$ are the sub-matrices in the bus admittance matrix which connects the injected currents I and voltages V of different buses in the system, as in the following relationship

$$\begin{bmatrix} I_L \\ I_G \end{bmatrix} \begin{bmatrix} Y_{LL} & Y_{LG} \\ Y_{GL} & Y_{GG} \end{bmatrix} \begin{bmatrix} V_L \\ V_G \end{bmatrix} \tag{4.10}$$

Where the subscripts L and G indicate the load and generator buses respectively.

4.4 Voltage Collapse Proximity Indicator [26]

Based on the system loadability, a voltage collapse proximity indicator (VCPI) was derived by Alammari and Lo in (1996), which was an extension of that described by

Chebbo (1992) [23]. It was defined as the ratio of the system equivalent impedance to the equivalent load impedance. In Alammar's method, an algorithm for calculating network equivalent impedance was proposed; it employed PV-PQ sensitivity and "referencing" techniques to determine constant equivalent impedance and assumed that generators produce unlimited reactive power. Looking from the PQ node, the equivalent impedance of the power system network is constant regardless of the load level at that node. The voltage collapse proximity indicator (VCPI) calculated in Alammar's method is the ratio of the system equivalent impedance to the load equivalent impedance and it is expressed as

$$\mathrm{VCPI} = \frac{Z_{ie}}{Z_i} \tag{4.11}$$

The value of the VCPI varies from zero at no load to 1.0 at the maximum loadability.

Where Z_{ie} is the system equivalent impedance for the node i and Z_i is the load equivalent impedance for node i.

4.5 Proposed Method: VCPI Taking Into Account the Reactive Power Limitation of the Wind Generator

When the reactive power limitations of wind turbine generators in the system are taken into consideration, it can be observed that power systems with enough reactive power wind generators have higher power and voltage margins, in contrast with systems where reactive power limits of the wind generators are reached. Once the wind generator reaches its reactive power limit it can no longer offer any further support to the demand. System voltage stability is becoming increasingly important in power systems as overall system demand increases. The main reason for voltage instability in a power system is a reactive power deficit caused by a change in the operating conditions, such as variations in real and reactive loading. In general, when both real and reactive loads are increased, the voltage magnitude gradually decreases and the voltage drops rapidly to the point

beyond which a voltage is controllable. This point is known as the point of voltage collapse. The voltage collapse that results from an incident of voltage instability may be caused by a number of factors.

This chapter investigates the problem of longer-term voltage instability when the reactive power limitation of wind generators is taken into consideration and a system reaches its maximum loading. In this section, the original methodology used to determine a voltage collapse proximity indicator (VCPI) presented by Alammar and Lo (1996) [26] is developed to derive the voltage collapse proximity indicator considering the reactive power output limitations of wind generators. Alammar and Lo indicated that the equivalent impedance of a power system, as seen from a PQ node, is constant regardless of the load level at the concerned PQ node. This cannot be a valid model for simulation when wind generators are connected to a network. Due to the reactive power limitation of wind generators, this equivalent system impedance is not constant. The main extension to Alammar and Lo's method proposed in this thesis can be summarized as follows:

- Assessment of the relationship between the voltage collapse proximity indicator and the reactive power contribution, taking into account reactive power limitations of wind turbine generators and the system equivalent impedance. This is not the case in to original proposed's method. In addition, it did not consider wind generation and assumed that conventional generators produced unlimited reactive power. This condition cannot be applied for wind generators such as the doubly-fed induction generator (DFIG) because the reactive power output of wind generators is limited by design to take into account the rating of the power electronics interface and to avoid generators over heating due to over excitation.
- The VCPI calculation procedure takes into consideration the reactive power limitation of wind generators in the system. The wind generator is assumed to be a doubly fed induction generator (DFIG), which has a reactive power control capability. In this assessment, DFIG is modelled as a PV bus and is operated with maximum and minimum power factors of 0.95 leading (capacitive VAr) and

0.95 lagging (inductive VAr). For these limitations, DFIG can be used as a reference to PQ buses when it operates within its reactive power capability.

- Once a wind generator reaches its reactive power limit it can no longer be used as a reference bus; consequently, a new PV reference bus must be found using the same sensitivity technique, which is required to determine a new equivalent system impedance. Moreover, the reference bus may change several times depending on the reactive power limitation of wind generations, which is required to determine new equivalent system impedance for each change of the reference bus until the collapse point is found.
- Due to the reactive power limitation of wind generators, system impedance is not a constant, as shown in Figure 4.1.

Figure 4.1 below demonstrates the relationship between the reactive power contributions of all generators, including the reactive power limitation of wind generation, the VCPI and the system equivalent impedance, when wind speed is assumed to be constant and the wind farm is at maximum output MW. Initially, node 2 (WG) is used as a reference bus and the load power at bus 3 is increased gradually, which results in an increase of system reactive power demand. It can be observed that the wind generation reaches its reactive power output limit at point B_1. During this period, the equivalent system impedance is $Z_{ie(A-B)}$. Once the limitation is reached, it is necessary to choose a different reference bus, and in this case it was chosen to be node 1 (Slack bus) at point C_1; then the load increase continues. This change in reference bus necessitates the calculation of new equivalent impedance, which is $Z_{ie(C-D)}$. The change of equivalent system impedance is independent of load change as a result of changing the reference bus.

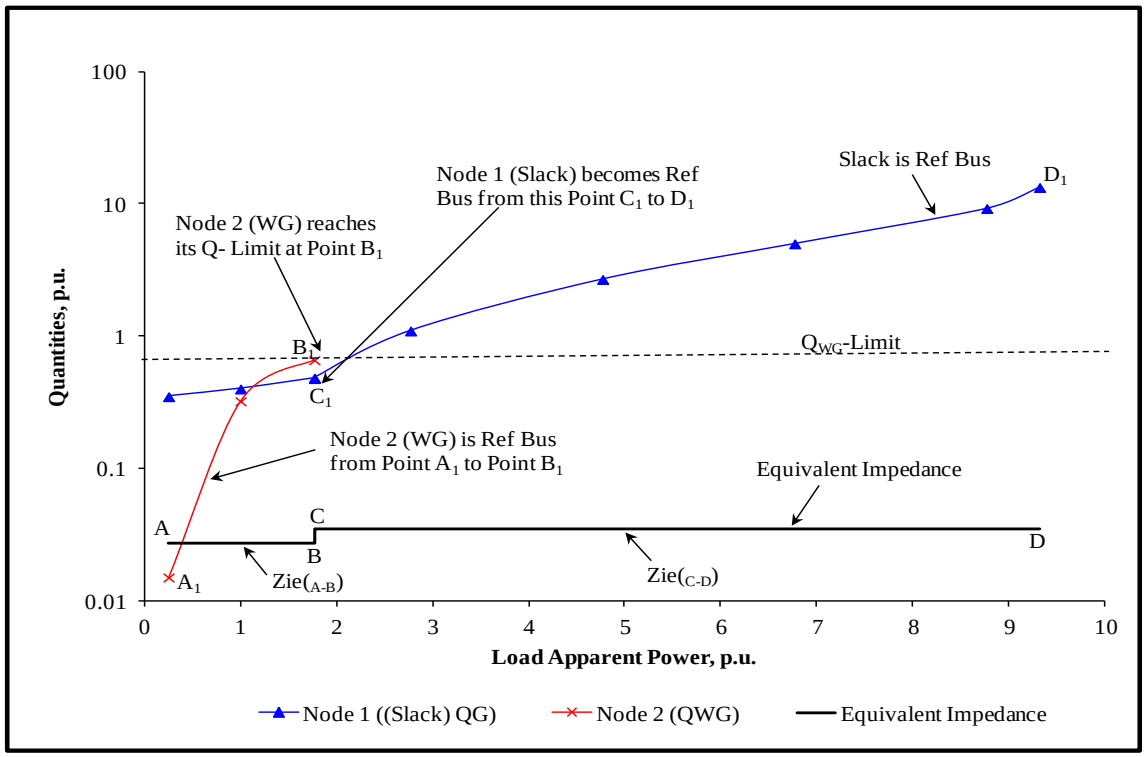

Figure 4.1: The relationship between the reactive power contributions of generators, the VCPI and the system equivalent impedance at 5% wind penetration. The wind speed is assumed to be constant and the wind farm is at maximum output.

4.6 Determination of Voltage Collapse Proximity Indicator (VCPI)

Among several voltage stability indices, the voltage collapse proximity indicator (VCPI) is one of the most important indices that can be used to establish voltage collapse at any point in the power system network. This indicator can be determined by looking into the power system from any chosen load bus in the network. In this manner, any multi-machine power system can be reduced to an equivalent system that comprises of one voltage source connected to a load bus. After taking into account the reactive power limitation of wind power generators, this thesis proposes a voltage collapse proximity indicator and reduction procedure for calculating system impedance. The detailed procedures for calculation of VCPI are described in the following subsections.

4.6.1 Calculation of Impedance of the Load at Node i

For ease of representation and solution, the complex power at each load and generation buses in the system are represented with their equivalent admittances, with the appropriate signs to differentiate between load and generation. The equivalent load admittance at bus i can be written in terms of complex power and voltage magnitude as follows

$$Y_i = \frac{S_i^*}{|V_i|^2} \tag{4.12}$$

Where S_i^* is the conjugate complex power at bus *i*. So, the equivalent load impedance can be written as

$$Z_i = \frac{|V_i|^2}{S_i^*} \tag{4.13}$$

The column vector of the equivalent load/generation admittances is formed as follows

$$[Y_{Load}]^t = [Y_1 \quad Y_2 \quad \dots \quad Y_N]$$

Where N is the total number of buses in the system.

4.6.2 PV-PQ Sensitivity and Selection of Reference Buses

Sensitivity is defined as the ratio$\Delta x/\Delta y$, where Δx represents a small change in dependent variable x and Δy denotes a small change in independent variable or controllable y. In power systems, the sensitivity of PV to PQ buses is normally defined in terms of reactive power when reactive power limitations of wind generators are considered, hence determining the system voltage stability. This section derives a direct sensitivity solution in terms of reactive power between PV and PQ buses. Using power flow equations, the real and reactive power injections at bus *i* can be written as follows

$$P_i = \sum_{j=1}^{N} |V_i||V_j| \left|Y_{ij}\right| \cos\left(\delta_i - \delta_j - \theta_{ij}\right)$$

$$Q_i = \sum_{j=1}^{N} |V_i||V_j| \left|Y_{ij}\right| \sin\left(\delta_i - \delta_j - \theta_{ij}\right)$$

Where

$|V_i|\angle\delta_i$ is the voltage at bus i

$|Y_{ij}|\angle\theta_{ij}$ is the admittance of the line i-j

$|Y_{ii}|\angle\theta_{ii}$ is the summation of all admittances that are connected to bus i

The partial derivative of the reactive power with respect to the voltage is

$$\frac{\partial Q_i}{\partial V_{j(j\neq i)}} = |V_i||Y_{ij}| \sin\left(\delta_i - \delta_j - \theta_{ij}\right)$$

and

$$\frac{\partial Q_i}{\partial V_i} = \sum_{\substack{j=1 \\ j\neq i}}^{N} |V_j||Y_{ij}| \sin(\delta_i - \delta_j - \theta_{ij}) + 2|V_i||Y_{ii}| \sin(-\theta_{ii})$$

The proper expression for reactive power sensitivity is developed based on the assumption that in a transmission system where the lines are predominantly inductive, there is a strong relationship between voltage and reactive. Therefore a system nodal equation in a decoupled load flow is valid and can be written in matrix form as

$$[\Delta Q] = \left[\frac{\partial Q}{\partial V}\right] [\Delta V] \qquad (4.14)$$

Separating the generator (G) and the load (L) of $[\Delta Q]$, the equation becomes

$$\begin{bmatrix}\Delta Q_G\\ \Delta Q_L\end{bmatrix} = \begin{bmatrix}\frac{\partial Q_G}{\partial V_L}\\ \frac{\partial Q_L}{\partial V_L}\end{bmatrix}[\Delta V_L] \tag{4.15}$$

If we define

$$[S_G] = \left[\frac{\partial Q_G}{\partial V_L}\right]$$

and

$$[S_L] = \left[\frac{\partial Q_L}{\partial V_L}\right]$$

then it follows

$$[\Delta Q_G] = [S_G][\Delta V_L] \tag{4.16}$$

$$[\Delta Q_L] = [S_L][\Delta V_L] \tag{4.17}$$

For the power system of N_G generated buses and N_L load buses, the dimensions of S_G and S_L are $N_G \times N_L$ and $N_L \times N_L$ respectively.

Combining and rearranging equations (4.16) and (4.17) yields,

$$[\Delta Q_G] = [S_G][S_L]^{-1}[\Delta Q_L] \tag{4.18}$$

Defining

$$[S] = [S_G][S_L]^{-1},$$

Then $[S]$ represents the sensitivity matrix and has a dimension of $N_G \times N_L$. It contains the sensitivity of the reactive power of the generator buses to that of the PQ buses. The sensitivity is a measure of the PQ bus reactive power dependency on the PV bus, and $[S]$ is the matrix which directly relates the reactive power generation with reactive load. Elements of the S matrix indicate the sensitivity of the PV buses to

reactive loads in the PQ buses. The large S_{ij} indicates the i^{th} PV bus is more sensitive to reactive load at the j^{th} PQ bus. The PV bus which is the most sensitive to the variation of load at the PQ bus is called a reference to that PV bus.

$$[S] = \begin{bmatrix} S_{11} & \cdots & S_{1N_L} \\ \vdots & \vdots & \vdots \\ S_{N_G 1} & \cdots & S_{N_G N_L} \end{bmatrix}$$

For each load, there must be at least one reference in the network; the system must run with at least one voltage control. A voltage control node is considered to be a reference node when it satisfies the following two conditions:

- It is directly connected to the PQ node. In other words, if $|Y_{Bus}(i,j) > 0$, then node i is a reference to j, where i is a PV and j is a PQ node. This condition is applied if more than one generator is connected to the same PQ bus.
- It is the most sensitive to the PQ node, i.e. its sensitivity S_{ij} is dominant when $|S_{ij}| > 50\%$. If there is no$S_{ij} > 50\%$ then there must be more than one PV node considered a reference bus. In this case, the sensitivity is arranged from the higher S_{ij} to the lower S_{ij}, and then adding the elements of each row of matrix S starting from the highest S_{ij} until the summation becomes greater than or equal to 50%. The PV nodes, the sensitivities of which are counted in this summation, are taken as references.

Once the references have been defined, we can determine the system equivalent impedance. When the wind generator is considered as a reference bus to a certain PQ bus in the network and the load demand at this PQ bus is increased gradually, an increase in the reactive power of the wind generator occurs. Once a wind generator reaches its reactive power limit it can no longer be used as a reference bus. Consequently, another PV reference bus must be found using the same sensitivity technique.

4.6.3 Calculation of the Equivalent Impedance of the Network

In order to establish an equivalent system for a multi-machine power system looking from node i, the following steps are necessary:

- Bus admittance matrix $[Y_{Bus}]$ must be calculated using lines data.

$$Y_{Bus} = \begin{bmatrix} Y_{11} & Y_{12} & \cdots & Y_{1N} \\ Y_{21} & Y_{22} & \cdots & Y_{2N} \\ \vdots & \vdots & \vdots & \vdots \\ Y_{N1} & Y_{N2} & \cdots & Y_{NN} \end{bmatrix}$$

Y_{ii} : The self-admittance (diagonal term) is equal to the sum of the primitive admittance of all the components connected to node i.

Y_{ij} : The ijth element of the Y_{Bus} (off-diagonal element) is equal to the negative of the primitive of all components connected between nodes i and j. If there is no line between i and j, this term is set to zero.

Add to the diagonal term of $[Y_{Bus}]$ the admittance of the injected active and reactive power of the system nodes, including the load and generation power at node i, so that the new system admittance matrix $[Y_{System}]$ that includes load and generated power can be expressed as:

$$\text{diag}[Y_{System}] = [Y_{Bus}] + [Y_{Load-i}],$$

Where $[Y_{Load-i}]$ the admittance of the injected active and reactive power at all nodes, including the injected power at node i.

- Delete the row and column in the matrix $[Y_{System}]$ that contains the reference nodes that have been identified in step 4.6.2.
- Invert the system admittance matrix to obtain the system impedance matrix $[Z_{System}]$.

- Element Z_{ii} in the diagonal of $[Z_{System}]$ represents the system equivalent impedance for node i. Hence, Z_{ii} will be called Z_{ie} or $Z_{ie(A-B)}$. The value of equivalent impedance remains constant as long as the reference bus is able to provide the necessary reactive power needed for system stability.

Once a reference bus reaches its reactive power limit it can no longer be used as a reference bus during the voltage collapse process. Consequently, at this point a new PV reference bus must be found, which is required to determine new equivalent system impedance $Z_{ii(new)}$ for node i. Hence, $Z_{ii(new)}$ will be called $Z_{ie(new)}$ or $Z_{ie(C-D)}$. The new value of equivalent impedance will be constant as long as a new reference bus provides enough reactive power for the system until the collapse point is found.

4.6.4 Calculation of the VCPI

The bus voltage collapse proximity indicator is defined as the ratio of the system equivalent impedance to the load equivalent impedance of that bus.

$$\mathrm{VCPI} = \frac{Z_{ie}}{Z_i} = \frac{Z_{ie(A-B)}}{Z_i} \tag{4.19}$$

When VCPI is approaching zero it means the system is stable. The system becomes marginally unstable when VCPI approaches unity (the critical point). Beyond this point the voltage of the bus may collapse, and as a consequence the system may become unstable.

4.7 Illustrative Example

To assess and clarify the effectiveness of the proposed method, the following numerical example is presented. Each step of the proposed method is presented in detail.

4.7.1 Three-Bus Two-Generator System Including One Wind Generator

This subsection aims to describe the steps necessary during assessment of the voltage collapse problem using the proposed VCPI in a typical modern power system that includes wind generation. In this assessment the test network shown in Figure 4.2

will be used for illustration. This test system consists of conventional synchronous and wind-turbine generators G and WG respectively, and three busses. The system parameters, including loads and transmission line constants, are shown in Figure 4.2. The system is analysed using Optimal Power Flow (OPF) and the voltage magnitude of the slack generator is set at 1.0 p.u. The total system generation capacity is 145 MW, with capacity of the wind generator connected to bus 3 representing only 20% of total generation mix 29MW. The wind generator is assumed to be a doubly fed induction generator (DFIG) which has reactive power control capability. In this assessment, DFIG is modelled as a PV bus and operated with maximum and minimum power factors of 0.95 leading (capacitive VAr) and 0.95 lagging (inductive VAr). These power factors can be attained with an aggregate DFIG model having reactive power capability of ±9.15 MVAr for the 29 MW wind farm. This reactive power range is calculated based on wind farm size. The per-unit powers and voltages of the test network in the power system model of Figure 4.2 are listed in Table 4.1.

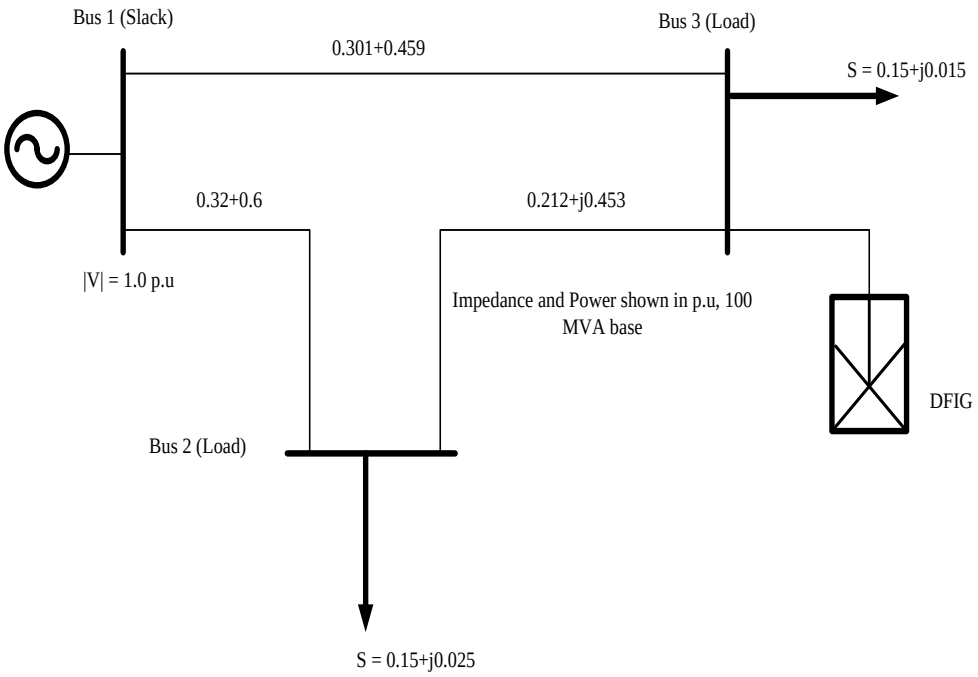

Figure 4.2: The model system of the 4.7.1 case study.

Table 4.1: The per unit power and voltage profile at the base case.

Bus Name	Load Voltage V∠δ	Load Power, p.u		Load Admittance Y_{Load}
		P	Q	
Bus 1	1.0 ∠0.0°	-0.0137	-0.0426	-0.0136-j0.0425
Bus 2	0.973∠-1.34°	0.15	0.025	0.1589+j0.0226
Bus 3	1.0 ∠1.31°	-0.14	0.01009	-0.1401+j0.00707

DFIG can be used as a reference to the nearest PQ buses when it operates within its reactive power capability. When it reaches its reactive power limits it becomes a PQ bus. In this case, another PV 'reference' must be found using the sensitivity technique previously described. In this illustrative example, constant wind speed is assumed where the wind turbine generator produces maximum power (29 MW). Table 4.2 shows the sensitivity of the PV buses to the PQ buses in the case of no load. It can be seen from Table 4.2 that the summation of the sensitivities is 1.0. As bus 3, where DFIG is connected, has the largest sensitivity value of (0.592 > 50%), it has been selected as the reference bus for PQ bus 2. Bus 3 remains a reference bus for bus 2 until it reaches its reactive power limits as load at bus 2 increases.

Table 4.2: The reference nodes and the sensitivity of the PQ to the PV buses for 3-bus system at no load.

PQ Bus	Sensitivity: PV Buses are 1 (Slack) and 2 (WG)			Ref Bus
	Bus 1	Bus 3	Sum of Sensitivity	
2	0.4096	0.592	1.001	3

Once the reactive power limitation of bus 3 is reached at point B, another PV bus (which is the slack bus in this example) becomes a reference bus for PQ bus 2, and bus 3 will be converted to a PQ bus. Figure 4.3 illustrates the variation in apparent power load demand at bus 2 with the sensitivity of generator buses in the system. It can be observed that bus 3 is considered a reference for load bus 2 during initial loadings until it reaches its reactive power limit (bus 3 is a reference bus from point A to point B). At this point, the slack bus has the higher sensitivity and consequently it becomes a reference for bus 2 (the slack bus becomes a reference bus from point C_1 to point D_1). Figure 4.4 shows the

variation of apparent power demand for load bus 2 with generator reactive power contributions. The results displayed in Figure 4.4 show that when the load apparent power increases at constant power factor, the reactive power generated by the reference bus (wind generation) increases until it reaches its limit. At this point another PV bus (slack bus in this case) becomes the reference bus and the process continues.

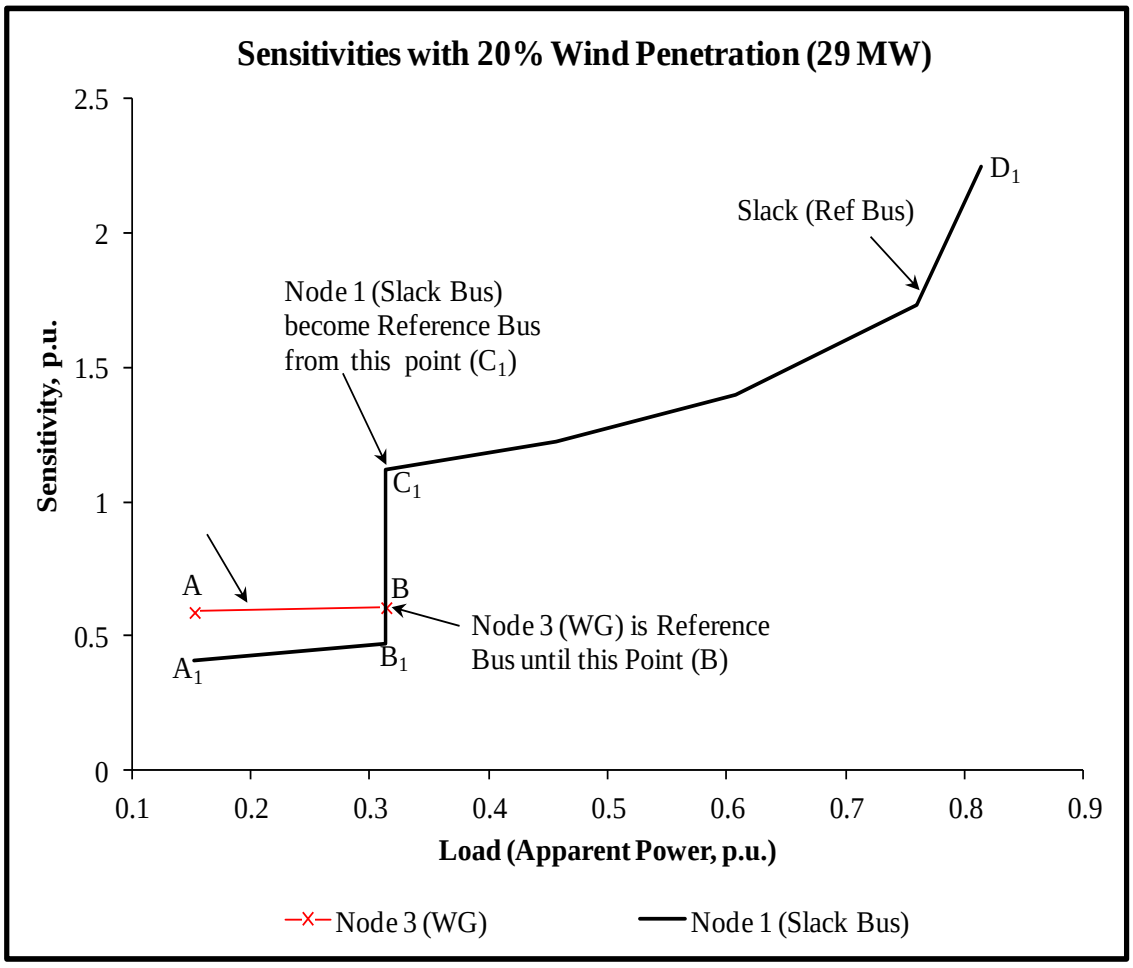

Figure 4.3: The variation of apparent power load demand at bus 2 with the sensitivity of generator buses in the system. The wind speed is assumed to be constant and the wind farm is at maximum output.

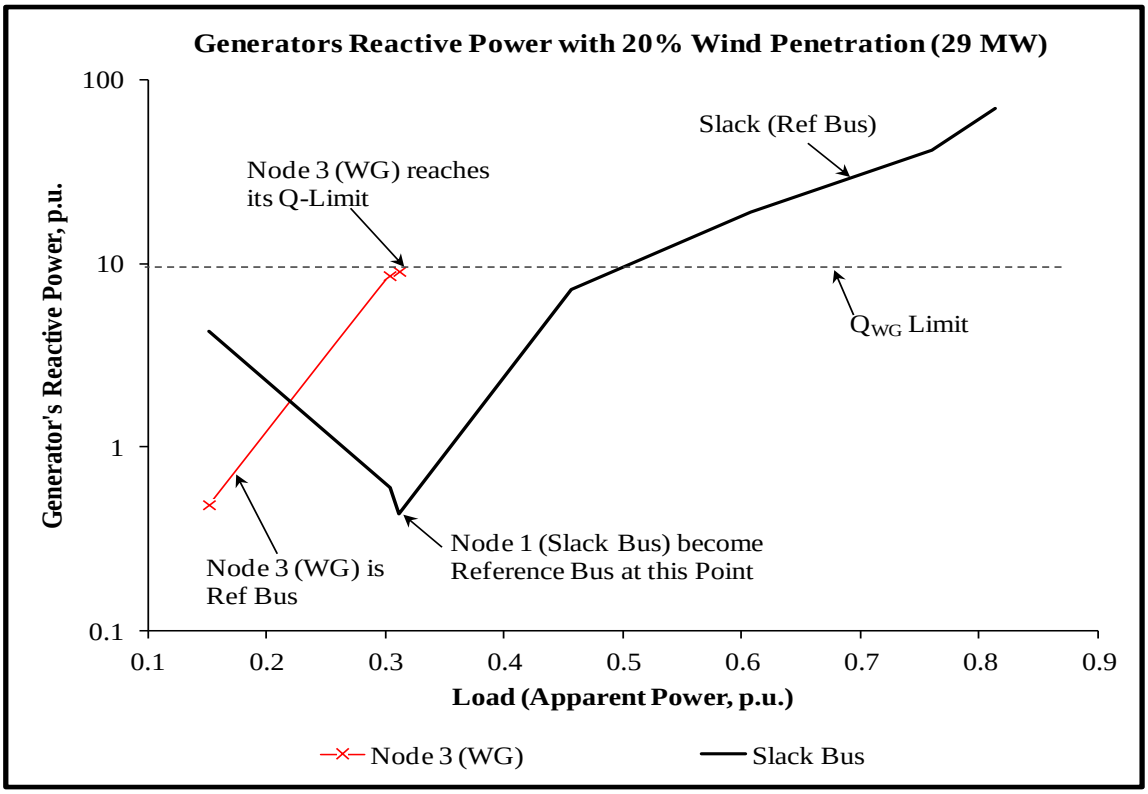

Figure 4.4: The variation of apparent power demand for load bus 2 with generator reactive power contributions. The wind speed is assumed to be constant and the wind farm is at maximum output.

To investigate the relationship between the proposed voltage collapse proximity indicator and the load voltage and power at bus 2, the wind turbine generator is operated at maximum output (140 MW) and the load at bus 2 is increased gradually at constant power factor up to the point where the load flow has diverged. The bus admittance matrix $[Y_{Bus}]$ of the test network in Figure 4.2 is

$$Y_{Bus} = \begin{bmatrix} 1.69 - j2.82 & -0.69 + j1.3 & -1.0 + j1.52 \\ -0.69 + j1.3 & 1.54 - j3.11 & -0.85 + j1.81 \\ -1.0 + j1.52 & -0.85 + j1.81 & 1.85 - j3.33 \end{bmatrix}$$

The equivalent load impedances (except for the concerned bus 2) are now added to the diagonal of $[Y_{Bus}]$ to form the system admittance matrix $[Y_{System}]$, as described in

step (4.3.3). It can be noticed from the sensitivity table 4.2 that bus 3 (WG) is a reference bus to PQ bus 2 during initial load, therefore column 3 and row 3 must be deleted, and $[Y_{System}]$ becomes

$$Y_{Bus} = \begin{bmatrix} 1.676 - j2.862 & -0.69 + j1.3 \\ -0.69 + j1.3 & 1.54 - j3.11 \end{bmatrix}$$

The system impedance matrix during initial load is

$$[Z_{System}] = [Y_{System}]^{-1}$$

$$\begin{bmatrix} Z_{11} & Z_{12} \\ Z_{12} & Z_{22} \end{bmatrix} = \begin{bmatrix} 0.1887 + j0.3199 & 0.0762 + j0.1379 \\ 0.0762 + j0.1379 & 0.1585 + j0.3176 \end{bmatrix}$$

During this period the system equivalent impedance of bus 2 is $Z_{22} = Z_{ie(A-B)}$ = 0.1585+j0.3176 p.u., with a magnitude of 0.354 per unit at 20% penetration level of wind. This value of $Z_{ie(A-B)}$ is kept constant as the load at bus 2 increases gradually until the reference bus reaches reactive power limit. When reactive power limitation of the wind turbine generator connected to bus 3 is reached, new equivalent system impedance must be calculated based on the new reference bus. The slack bus is the new reference (because it satisfies the condition for a reference bus). The reactive power limitation of the reference bus is reached as the load at bus 2 increases at constant power factor up to 30.9MW. At this point, new equivalent load impedances (except for bus 2 concerned) are now added to the diagonal of $[Y_{Bus}]$ to form the new system admittance matrix $[Y_{New\ system}]$. As the slack bus becomes a reference to PQ bus 2, column 1 and row 1 of the resulting matrix are deleted, and the $[Y_{New\ system}]$ becomes

$$Y_{New\ System} = \begin{bmatrix} 1.54 - j3.11 & -0.85 + j1.81 \\ -0.85 + j1.81 & 1.7086 - j3.4037 \end{bmatrix}$$

The new system impedance matrix is

$$[Z_{\text{New system}}] = [Y_{\text{New system}}]^{-1}$$

$$\begin{bmatrix} Z_{22} & Z_{23} \\ Z_{32} & Z_{33} \end{bmatrix} = \begin{bmatrix} 0.1907 + j0.3662 & 0.1051 + j0.1896 \\ 0.1051 + j0.1896 & 0.1756 + j0.3327 \end{bmatrix}$$

The new system equivalent impedance of bus 2 (row 1 X column 1) is $Z_{22} = Z_{ie(C-D)}$ = 0.1907+j0.3662, with a magnitude of 0.4128 p.u, and this value remains constant as long as the slack is able to provide the necessary reactive power needed for system stability. As the load at bus 2 is increased, the load impedance decreases until it reaches the value of the system equivalent impedance at the maximum loadability. Figure 4.5 shows the variation of the load at bus 2 with the voltage collapse proximity indicator (VCPI) when wind generation is connected to bus 3. It is worth noting that with larger system studies, the reference bus may change several times depending on the reactive power limitations of wind generations. Therefore, it is necessary to identify the reference bus that must be selected when the reactive power limit of the reference bus is reached.

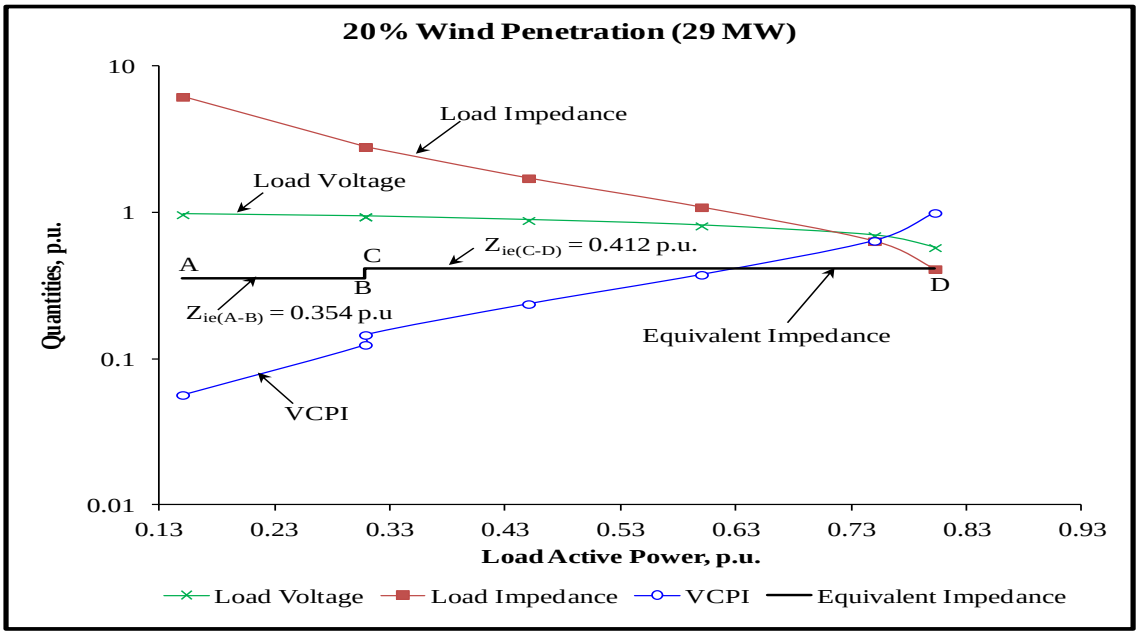

Figure 4.5: The variation of quantities with load at bus 2 with 20% wind penetration. The wind speed is assumed to be constant and the wind farm is at maximum output.

4.8 Case Studies and Results Analysis

The method proposed to calculate the voltage collapse proximity indicator (VCPI) presented in this thesis can be applied to any system by considering the reactive power limitation of wind generators. In this section, IEEE-14 bus system, IEEE-30 bus system, IEEE-118 bus system and 61-bus radial distribution network are used to demonstrate the validity of the proposed method and to investigate the VCPI with different wind penetration levels.

4.8.1 Test Systems

4.8.1.1 IEEE-14 Bus Test System

The proposed method of VCPI was applied on the modified IEEE-14 bus system as shown in Figure 4.6. Detailed data about the system are shown in Appendix A [104]. The system consists of five generators which supply power to 11 loads through a 69/13.8 kV. The total generation capacity is 1300 MW and peak load is 935 MW. The test system was modified by connecting one wind farm at bus 10. The test system was modelled using the PowerWorld®Simulator. The modified test system was analyzed using an AC Optimal Power Flow (OPF). The wind farm consists of several variable speed wind turbines each of 1.5 MW; each DFIG generator within the wind farm is operated to maintain its terminal voltage at 1.0 p.u.

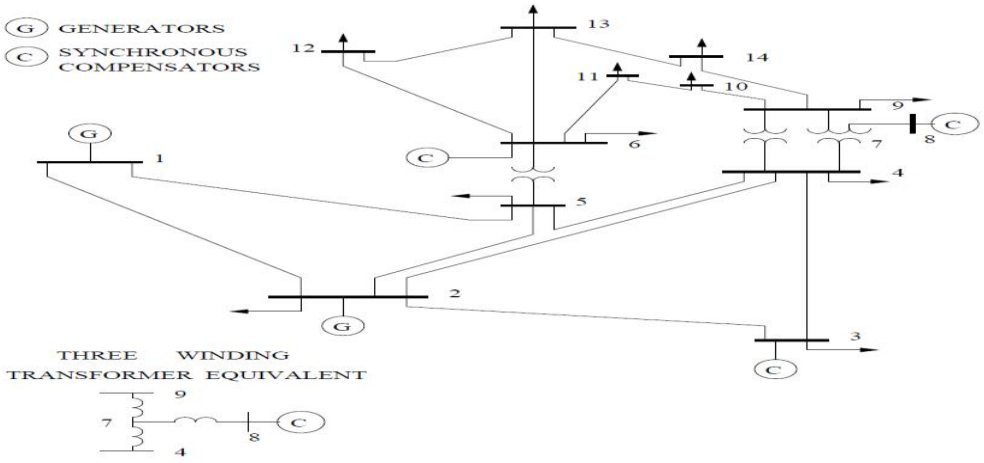

Figure 4.6: One-line diagram of IEEE-14 bus system.

4.8.1.2 IEEE-30 Bus Test System

A single line diagram of the IEEE-30 bus system is shown in Figure 4.7. Detailed data about the system are shown in Appendix B [104]. The test system was modified by connecting wind generation and was modelled using the PowerWorld®Simulator, as shown in Figure 3. The modified test system was analyzed using an AC Optimal Power Flow (OPF). The test system consists of six generators which supply power to 21 loads through a 132/33 kV substation. The total generation capacity is 1000 MW and peak load is 820 MW. One wind farm is connected to bus 14. The wind farm consists of several variable speed wind turbines each of 1.5 MW, and each DFIG generator within the wind farm is operated to maintain its terminal voltage at 1.0 p.u.

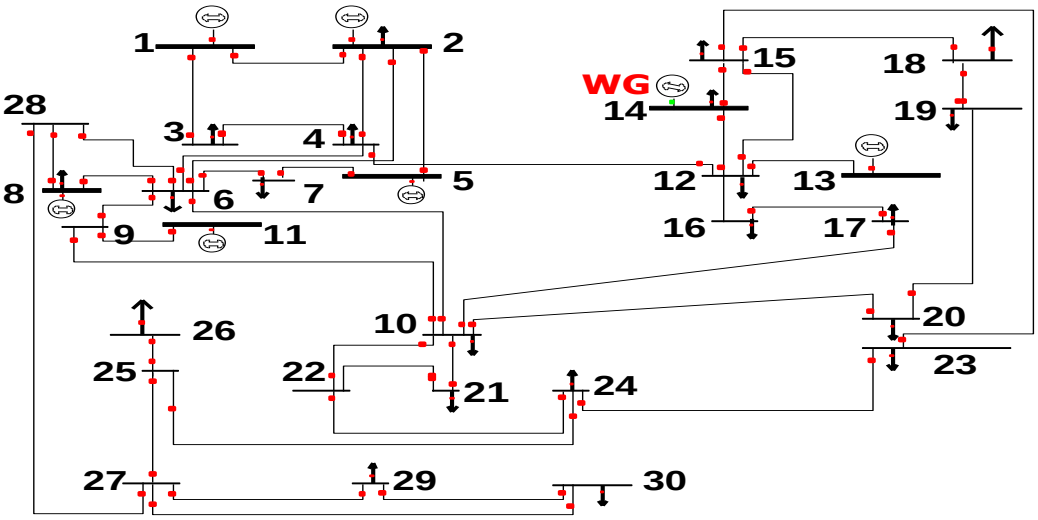

Figure 4.7: Single line diagram of the modified IEEE-30 bus test system.

4.8.1.3 IEEE-118 Bus Test System

In order to test the validity of the proposed VCPI method on a bigger system, the IEEE-118 bus test was modified by connecting wind generation to bus 51. Then in the second simulation run, two wind generations were connected to bus 45 and bus 51, as shown on the single line diagram of Figure 4.8. The modified IEEE-118 bus test system consists of 118 buses, 54 conventional generators with a modified total generating capacity of 10,000 MW, and 91 loads with a peak value of 7,100 MW. There are 194

lines connected in the network. Detailed data about the system are provided in Appendix C [104].

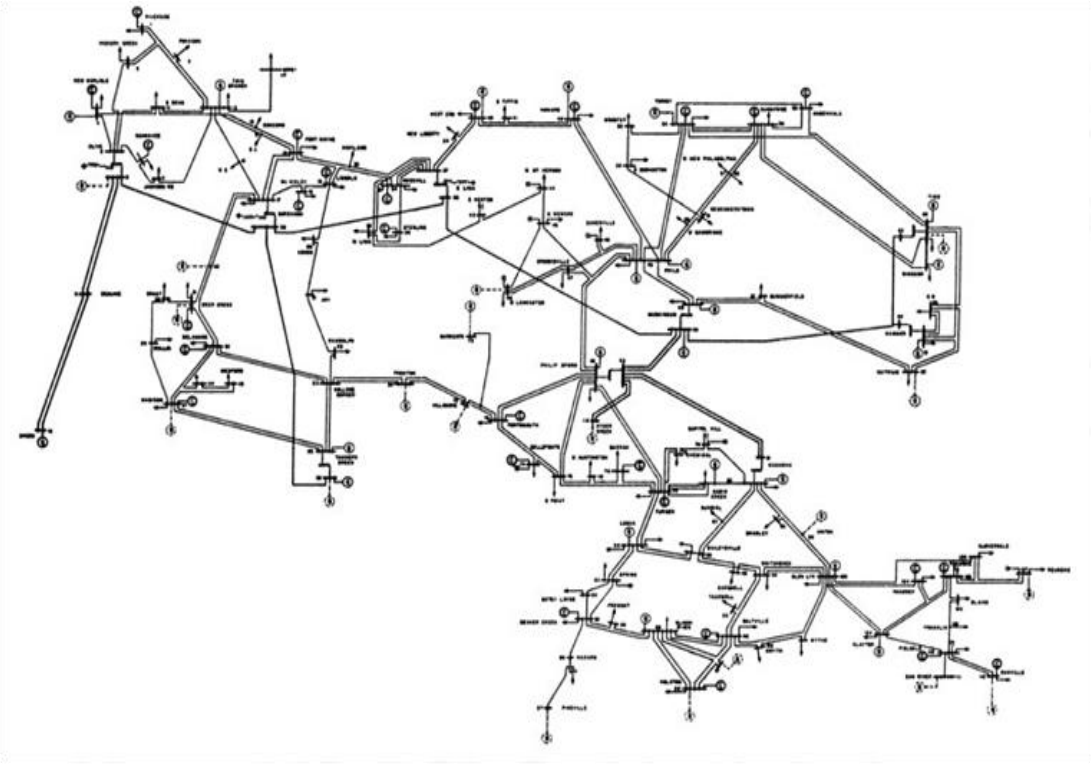

Figure 4.8: One line diagram of IEEE-118 bus system.

4.8.1.4 A 61 bus radial distribution network

A modified 61 bus radial distribution network test system was modelled in PowerWorld®Simulator. Figure 4.9 shows the 61 bus radial distribution network with two thermal generators which supply power to the 18 load points through a 132/33/kV substation. The voltage level at the loads is 11.0 kV and the total load is 58 MW. The total generation capacity is 80 MW. Detailed data about the system are provided in Appendix D [105]. One wind farm is connected at bus 311, and the size of each wind turbine is 1.5 MW.

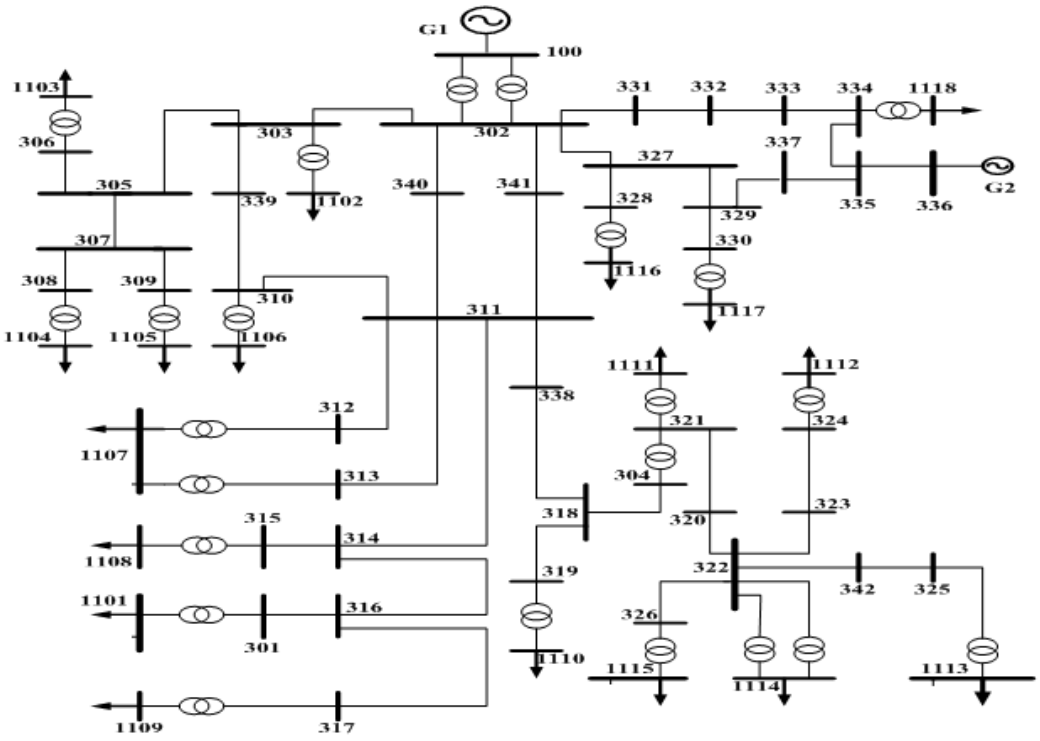

Figure 4.9: Single line diagram of the modified 61 bus radial distribution network.

4.9 Simulation Scenario

The simulation was carried out using PowerWorld®Simulator, and the modified tests systems were analyzed using an AC Optimal Power Flow (OPF). In these systems, the wind generators are assumed to be doubly fed induction generators (DFIG) which have reactive power control capabilities. In this assessment, DFIG is modelled as a PV bus and operated with maximum and minimum power factors of 0.95 leading (capacitive VAr) and 0.95 lagging (inductive VAr). In order to determine the voltage collapse proximity indicator (VCPI), the wind speed is considered to be constant and wind generators are at maximum output during the simulation until the VCPI reaches the value of 1.0 beyond which the voltage collapses.

The VCPI is calculated taking into account the level of wind penetration with a gradual increase of load in a single bus until the collapse point, while other load buses in the system remain unchanged. Nodes 11, 12 and 14 from the IEEE-14 bus system, nodes 12, 16, 20 and 23 from the IEEE-30 bus system, nodes 44, 52 and 58 from the IEEE-118 bus system, and buses 45, 50 and 52 from the 61 radial distribution network are selected. The selection covers a wide range of locations in the test system to validate the calculation method. It is assumed that the wind speed is constant during the analysis.

4.10 Results and Discussion

For the first part of the analysis, in order to determine a VCPI at this point it is necessary to define the sensitivities of PV nodes to all PQ buses when the reactive power limitation of the wind generator in the system is taken into consideration. When the wind generator reaches its reactive power limit, it can provide no more assistance as the load is increased. As mentioned above, the wind speed is constant during simulation and the wind generator output is at maximum. Due to load increase at the PQ bus, the wind generator reaches its reactive limit. It then can no longer be the reference bus and another PV reference must be found using the sensitivity technique.

The reference nodes and the sensitivity of the PV to the PQ buses for the IEEE-14 bus, IEEE-30 bus, and IEEE-118 bus systems and the 61 radial distribution network are defined using the sensitivity technique which is described in section 4.6.2. Tables 4.3, 4.4 and 4.5 show the sensitivity of the PV buses to the PQ buses at no load for the test systems with 20% wind penetration level. Tables 4.6, 4.7, 4.8 and 4.9 show the sensitivity of the PV reference buses to the PQ buses with different wind penetration levels at no load. It can be seen from tables 4.3, 4.4 and 4.5 that the summation of the sensitivities in any row in the table is 1.0.

The column with the heading “Ref” shows the reference nodes, the sensitivity summation of which dominates the overall sensitivity. Furthermore, the PV (wind generator) which is selected to be the reference to the load bus when the system is unloaded (no load) is expected to maintain its highest sensitivity and be the reference regardless of the load variation at the PQ bus. Once the wind generator reaches its reactive power limit, it is converted into a PQ bus and is no longer used as a reference. In figures 4.10, 4.11, 4.12, and 4.13, the horizontal axis represents the load variation (apparent power) and the vertical axis represents the sensitivity of the generator buses, including wind generators in the system.

It can be seen from Figure 4.10 that the wind generator node (node 51, IEEE-118 bus system) has a higher sensitivity compared to other PV nodes (nodes 49, 54, and 56) in the system during initial loading. Once the wind generator has been selected as a reference for the PQ bus 52, it will remain the most sensitive in spite of the load variation at the bus until it reaches its reactive power limit. During this period, the equivalent system impedance is called $Z_{ie\ (A\text{-}B)}$. Once the limitation of the reactive power wind generator is reached, two PV buses become the reference buses from points C_1 and C_2, which are buses 49 and 54. This change in reference buses requires the calculation of new equivalent impedance, called $Z_{ie\ (C\text{-}D)}$, and the process continues.

Figures 4.14, 4.15, 4.16 and 4.17 show the variation of apparent power demand with the reactive power contributions of the generators, including wind generators in the system. The results show that when the apparent power load increases at constant power factor, as shown in Figure 4.14, the reactive power of the reference bus (wind generator, bus 51) increases until it reaches its limit. At that point, it can no longer be of any assistance to the demand. Then another PV bus takes over the referencing from this point, buses 49 and 54 become references and the process continues.

Table 4.3: The reference nodes and the sensitivity of the PQ to the PV buses for IEEE-14 bus system at no load, with one wind farm connected at bus 10 with 20% wind penetration level. The wind speed is assumed to be constant and the wind farm is at maximum output 260 MW.

PQ Node No	Sensitivity: PV buses are G1(slack), G2, G3, G6, G8, WG10						Sum of Sensitivity	Ref
	G1	G2	G3	G6	G8	WG10		
4	0.1063	0.3522	0.2080	0.1111	0.0596	0.1642	1.001	G2,G3
5	0.1850	0.3665	0.1268	0.1934	0.0364	0.1001	1.008	G2,G6
7	0.0365	0.1253	0.0784	0.0718	0.4063	0.2861	1.004	G8,WG10
9	0.0240	0.0822	0.0514	0.0917	0.1778	0.5759	1.003	WG10
11	0	0	0	0.4576	0	0.5432	1.001	WG10
12	0.0052	0.003	0	0.9454	0.0113	0.0396	1.005	G6
13	0.0036	0.0124	0.0078	0.8567	0.0269	0.0946	1.002	G6
14	0.0152	0.0522	0.0326	0.4366	0.1129	0.3505	1.00	G8,WG10

Table 4.4: The reference nodes and the sensitivity of the PQ to the PV buses for IEEE-30 bus system at no load, one wind farm connected at bus 14 with 20% wind penetration level. The wind speed is assumed to be constant and the wind farm is at maximum output 200 MW.

PQ Node No	Sensitivity: PV buses are G1(Slack),G2,G5,G8,G11,G13, WG14							Sum of Sensiti	Ref Bus
	G1	G2	G5	G8	G11	G13	WG14		
3	0.2811	0.2280	0.0543	0.3162	0.0326	0.0521	0.0407	1.005	G1,G8
4	0.1373	0.2716	0.0650	0.3791	0.0384	0.0638	0.0483	1.003	G2,G8
6	0.0542	0.1715	0.0990	0.5676	0.0512	0.0321	0.0294	1.005	G8
7	0.0321	0.1083	0.4721	0.3275	0.0315	0.0197	0.0179	1.006	G5,G8
9	0.0313	0.0786	0.0509	0.3014	0.3908	0.0779	0.0756	1.006	G8,G11
10	0.0321	0.1032	0.0525	0.3082	0.2073	0.1421	0.1593	1.004	G8,G11

12	0.0376	0.0763	0.0227	0.1032	0.0519	0.4129	0.2936	0.998	G13,WG14
15	0.0291	0.0673	0.0249	0.1254	0.0752	0.2304	0.4538	1.006	G13,WG14
16	0.0371	0.0798	0.0354	0.2043	0.1255	0.3066	0.2176	1.006	G13,WG14
17	0.0365	0.1026	0.0476	0.2842	0.2265	0.1671	0.1345	0.999	G8,G11
18	0.0316	0.0615	0.0346	0.1853	0.1349	0.2107	0.3443	1.002	G13,WG14
19	0.0332	0.0902	0.0405	0.2106	0.1584	0.1732	0.2946	1.0	G8,WG14
20	0.0341	0.0437	0.0436	0.2583	0.1814	0.1744	0.2594	0.997	G8,WG14
21	0.0352	0.0935	0.0507	0.3081	0.2501	0.1312	0.1402	1.008	G8,G11
22	0.0367	0.0885	0.0498	0.3156	0.2438	0.1193	0.1481	1.001	G8,G11
23	0.0316	0.0817	0.0347	0.2072	0.1138	0.2238	0.3072	1.00	G13,WG14
24	0.0351	0.0893	0.0482	0.3163	0.1749	0.1172	0.2239	1.005	G8,WG14
25	0.0389	0.0934	0.0312	0.4635	0.1117	0.1051	0.1582	1.002	G8,WG14
26	0.0375	0.0917	0.0299	0.4821	0.1085	0.1116	0.1427	1.004	G8,WG14
27	0.0411	0.1028	0.0690	0.5431	0.0762	0.0628	0.1031	0.999	G8
28	0.0417	0.1412	0.0759	0.6309	0.0472	0.0320	0.0329	1.001	G8
29	0.0411	0.1330	0.0692	0.5646	0.0695	0.0233	0.1043	1.005	G8
30	0.0413	0.1333	0.0693	0.5653	0.0697	0.0245	0.1046	1.004	G8

Table 4.5: The reference nodes and the sensitivity of the PQ to the PV buses for a 61-radial distribution network at no load, one wind farm connected to a network at bus 12 with 20% wind penetration level. The wind speed is assumed to be constant and the wind farm is at maximum output 16 MW.

PQ Node No	Sensitivity: PV buses are G1(Slack) , WG12 and G38 G1	WG12	G 38	Sum of Sensitiv	Ref
2	0	1.0038	0	1.0038	WG12
3	0.6786	0.26362	0.05781	1.0	G1
4	0.67795	0.26434	0.05775	1.0	G1
6	0.68313	0.26468	0.05819	1.006	G1

7	0.68313	0.26468	0.05819	1.006	G1
8	0.68542	0.26019	0.05839	1.004	G1
9	0.68542	0.26019	0.05839	1.004	G1
10	0.70684	0.23195	0.06021	0.999	G1
11	0.30357	0.67213	0.02734	1.003	WG12
13	0	1.00292	0	1.0029	WG12
14	0	1.00357	0	1.0035	WG12
15	0	1.00244	0	1.0024	WG12
16	0	1.00250	0	1.0025	WG12
17	0	1.00283	0	1.0028	WG12
18	0	1.00283	0	1.0028	WG12
19	0	1.00165	0	1.0016	WG12
20	0	1.00165	0	1.0016	WG12
21	0	1.00087	0	1.0008	WG12
22	0	1.00087	0	1.0008	WG12
23	0	1.00098	0	1.0009	WG12
24	0	1.00092	0	1.0009	WG12
25	0	1.00092	0	1.0009	WG12
26	0	1.00159	0	1.0015	WG12
27	0	1.00225	0	1.0022	WG12
28	0.52816	0.21985	0.25249	1.0005	G1
29	0.52816	0.21985	0.25249	1.0005	G1
30	0.48666	0.19623	0.31717	1.0	G1,G38
31	0.48666	0.19623	0.31717	1.0	G1,G38
32	0.63907	0.26213	0.1008	1.002	G1
33	0.60668	0.24713	0.15219	1.006	G1

34	0.54716	0.22762	0.22522	1.0	G1
35	0.51341	0.20701	0.27957	1.0	G1
36	0.43565	0.1586	0.40885	1.003	G1,G38
37	0.38175	0.13749	0.48576	1.005	G1,G38
39	0	1.0011	0	1.0011	WG12
40	0.50145	0.4723	0.03025	1.004	G1
41	0.34083	0.63644	0.02903	1.006	WG12
42	0.46056	0.51685	0.02759	1.005	WG12
43	0	1.0022	0	1.0022	WG12
44	0	1.0074	0	1.0074	WG12
45	0	1.0069	0	1.0069	WG12
46	0.70507	0.28531	0.00952	0.9999	G1
47	0.68313	0.27644	0.04043	1.0	G1
48	0.68542	0.27736	0.03812	1.0009	G1
49	0.70002	0.29101	0.00877	0.9998	G1
50	0.30428	0.6792	0.01652	1.0	WG12
51	0	1.00433	0	1.0043	WG12
52	0	1.00891	0	1.0089	WG12
53	0	1.00283	0	1.0028	WG12
54	0	1.00165	0	1.0016	WG12
55	0	1.00155	0	1.0015	WG12
56	0	1.00219	0	1.0021	WG12
57	0	1.00298	0	1.0029	WG12
58	0	1.00226	0	1.0022	WG12
59	0	1.00238	0	1.0023	WG12
60	0.54524	0.21985	0.23491	1.0	G1

61	0.48666	0.19623	0.32011	1.003	G1, G38
62	0.51341	0.20701	0.28158	1.002	G1

Table 4.6: The PV reference buses' sensitivity to PQ buses for IEEE-14 bus system with different wind penetration levels at no load. The wind speed is assumed to be constant and the wind farm is at maximum output for each wind penetration level.

PQ Node No	Sensitivity: PV buses are G1 (slack), G2, G3, G6, G8, WG10		
	Reference bus for each wind penetration level		
	10% wind penetration	20% wind penetration	30% wind penetration
4	G2,G3	G2,G3	G2,G3
5	G2,G6	G2,G6	G2,G6
7	G6,G8	G8,WG10	G8,WG10
9	G6,G8	WG10	WG10
11	G6	WG10	WG10
12	G6	G6	G6
13	G6	G6	G6
14	G6	G6,WG10	G6,WG10

Table 4.7: The PV reference buses' sensitivity to PQ buses for IEEE-30 bus system with different wind penetration levels at no load. The wind speed is assumed to be constant and the wind farm is at maximum output for each wind penetration level.

PQ Node No	Sensitivity: PV buses are G1 (Slack), G2, G5, G8, G11, G13, WG14		
	Reference bus for each wind penetration levels		
	10% wind penetration	20% wind penetration	30% wind penetration
3	G1,G8	G1,G8	G1,G8
4	G2,G8	G2,G8	G2,G8
6	G8	G8	G8
	G5,G8	G5,G8	G5,G8

7	G8,G11	G8,G11	G8,G11
9	G8,G11	G8,G11	G8,G11
10	G13	G13, WG14	G13, WG14
12	G8,G13	G13, WG14	G13, WG14
15	G8,G13	G13, WG14	G13, WG14
16	G8,G13	G8, G11	G8, G11
17	G8,G13	G13, WG14	G13, WG14
18	G8,G13	G8, WG14	G8, WG14
19	G8,G13	G8, WG14	G8, WG14
20	G8,G11	G8, G11	G8, G11
21	G8,G11	G8, G11	G8, G11
22	G8,G13	G13, WG14	G13, WG14
23	G8,G13	G8, WG14	G8, WG14
24	G8,G13	G8, WG14	G8, WG14
25	G8,G13	G8, WG14	G8, WG14
26	G8	G8	G8
27	G8	G8	G8
28	G8	G8	G8
29	G8	G8	G8
30			

Table 4.8: The PV reference buses' sensitivity to PQ buses for IEEE-118 bus system with different wind penetration levels at no load. The wind speed is assumed to be constant and the wind farm is at maximum output for each wind penetration level.

PQ Node No	Sensitivity: PV buses are G4, G6, G8, G10, G12, G15, G18, G19, G24, G25, G26, G27, G31, G32, G34, G36, G40, G42, G46, G49, WG51, G54, G55, G56, G59, G61, G62, G65, G66, G69 (Slack), G70, G72, G73, G74, G76, G77, G80, G82, G85, G87, G89, G90, G91, G92, G99,G100, G103, G104, G105, G107, G110, G111, G112, G113, G116		
	Reference bus for each wind penetration levels		
	5% wind penetration	10% wind penetration	15% wind penetration
1	G12	G12	G12
2	G12	G12	G12
3	G12	G12	G12
5	G4	G4	G4
7	G6	G6	G6
9	G8	G8	G8
11	G12	G12	G12
13	G12	G12	G12
14	G12	G12	G12
16	G12	G12	G12
17	G15,G113	G15,G113	G15,G113
20	G19	G19	G19
21	G19	G19	G19
22	G19,G24	G19,G24	G19,G24
23	G24,G25	G24,G25	G24,G25
28	G27	G27	G27
29	G31	G31	G31
30	G8,G26	G8,G26	G8,G26

33	G15	G15	G15
35	G36	G36	G36
37	G34	G34	G34
38	G34,G65	G34,G65	G34,G65
39	G40	G40	G40
41	G40	G40	G40
43	G34	G34	G34
44	G46,G49	G46,G49	G46,G49
45	G46	G46	G46
47	G49	G49	G49
48	G49	G49	G49
50	G49	G49	G49
52	WG51	WG51	WG51
53	G54	G54	G54
57	G56	G56	G56
58	WG51	WG51	WG51
60	G61	G61	G61
63	G61,G59	G61,G59	G61,G59
64	G61	G61	G61
67	G66	G66	G66
68	G116	G116	G116
71	G70,G73	G70,G73	G70,G73
75	G74,G76	G74,G76	G74,G76
78	G77	G77	G77
79	G77	G77	G77
81	G80,G116	G80,G116	G80,G116

83	G82	G82	G82
84	G85	G85	G85
86	G85	G85	G85
88	G89	G89	G89
93	G92	G92	G92
94	G92,G100	G92,G100	G92,G100
95	G82,G100	G82,G100	G82,G100
96	G80,G82	G80,G82	G80,G82
97	G80	G80	G80
98	G80	G80	G80
101	G100	G100	G100
102	G92	G92	G92
106	G105	G105	G105
108	G105	G105	G105
109	G110	G110	G110
114	G32	G32	G32
115	G27,G32	G27,G32	G27,G32
117	G12	G12	G12
118	G76	G76	G76

Table 4.9: The PV reference buses sensitivity to PQ buses for for a 61-radial distribution network with different wind penetration levels at no load. The wind speed is assumed to be constant and the wind farm is at maximum output for each wind penetration level.

PQ Node No	Sensitivity: PV buses are G1 (Slack), WG12, G38		
	Reference bus for each wind penetration levels		
	10% wind penetration	20% wind penetration	30% wind penetration
2	WG12	WG12	WG12
3	G1	G1	G1
4	G1	G1	G1
6	WG12	WG12	WG12
7	G1	G1	G1
8	G1	G1	G1
9	G1	G1	G1
10	G1	G1	G1
11	G1	G1	G1
13	WG12	WG12	WG12
14	WG12	WG12	WG12
15	WG12	WG12	WG12
16	WG12	WG12	WG12
17	WG12	WG12	WG12
18	WG12	WG12	WG12
19	WG12	WG12	WG12
20	WG12	WG12	WG12
21	WG12	WG12	WG12
22	WG12	WG12	WG12
23	WG12	WG12	WG12
24	WG12	WG12	WG12

25	WG12	WG12	WG12
26	WG12	WG12	WG12
27	WG12	WG12	WG12
28	WG12	WG12	WG12
29	G1	G1	G1
30	G1	G1	G1
31	G1, G38	G1, G38	G1, G38
32	G1, G38	G1, G38	G1, G38
33	G1	G1	G1
34	G1	G1	G1
35	G1	G1	G1
36	G1	G1	G1
37	G1, G38	G1, G38	G1, G38
39	G1, G38	G1, G38	G1, G38
40	WG12	WG12	WG12
41	G1	G1	G1
42	WG12	WG12	WG12
43	WG12	WG12	WG12
44	WG12	WG12	WG12
45	WG12	WG12	WG12
46	G1	G1	G1
47	G1	G1	G1
48	G1	G1	G1
49	G1	G1	G1
50	WG12	WG12	WG12
51	WG12	WG12	WG12

52	WG12	WG12	WG12
53	WG12	WG12	WG12
54	WG12	WG12	WG12
55	WG12	WG12	WG12
56	WG12	WG12	WG12
57	WG12	WG12	WG12
58	WG12	WG12	WG12
59	WG12	WG12	WG12
60	G1	G1	G1
61	G1, G38	G1, G38	G1, G38
62	G1	G1	G1

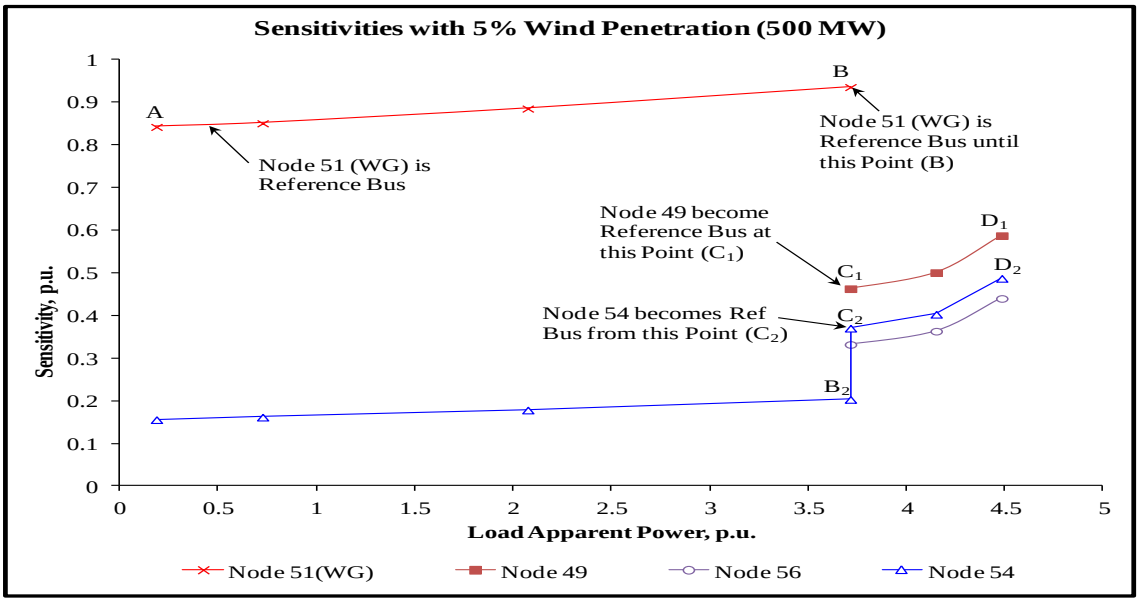

Figure 4.10: The variation of apparent power load demand at bus 52 (IEEE-118 bus system) with the sensitivity of generator buses in the system, and limited wind generator reactive power. The wind speed is assumed to be constant and the wind farm is at maximum output.

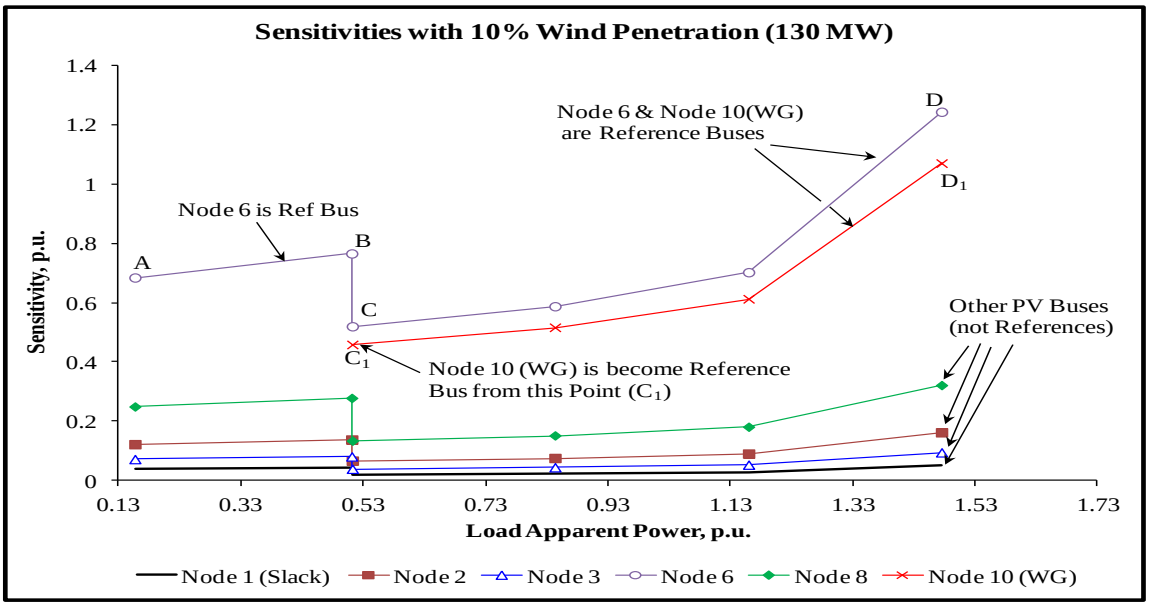

Figure 4.11: The variation of apparent power load demand at bus 14 (IEEE-14 bus system) with the sensitivity of generator buses in the system, and limited wind generator reactive power. The wind speed is assumed to be constant and the wind farm is at maximum output.

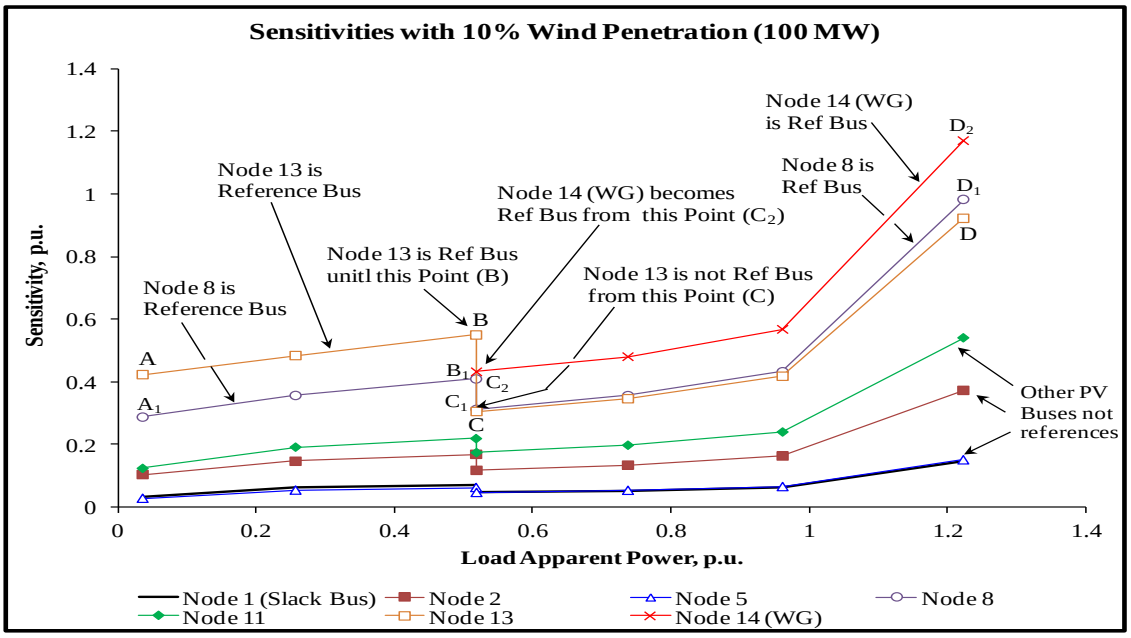

Figure 4.12: The variation of apparent power load demand at bus 23 (IEEE-30 bus system) with the sensitivity of generator buses in the system, and limited wind generator reactive power. The wind speed is assumed to be constant and the wind farm is at maximum output.

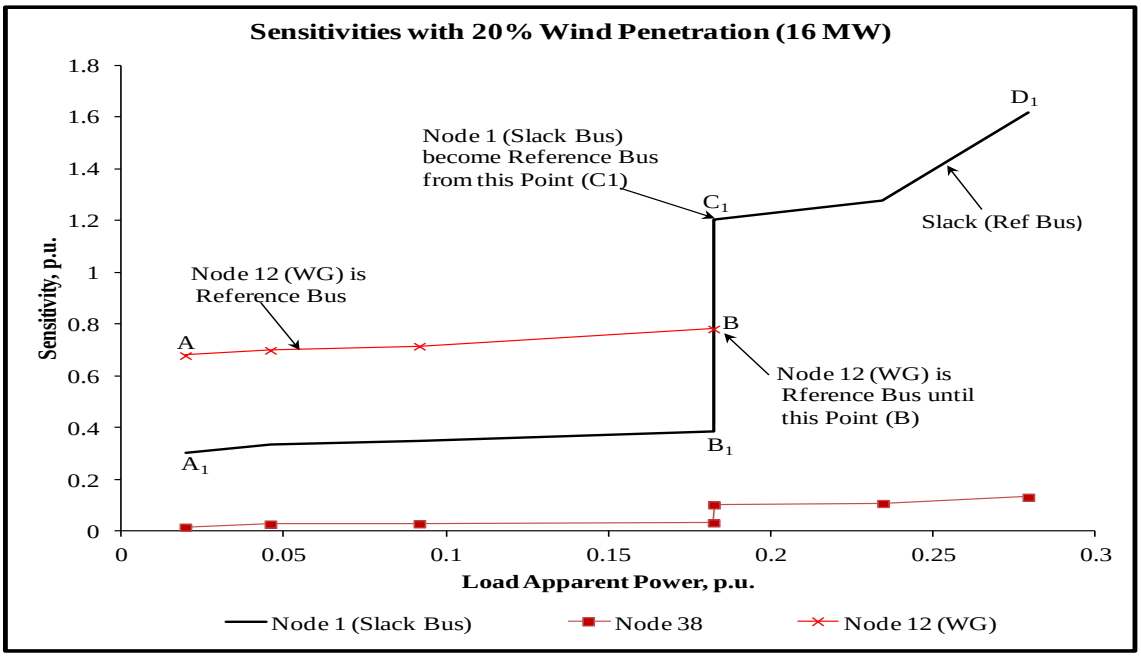

Figure 4.13: The variation of apparent power load demand at bus 50 (61-radial distribution network) with the sensitivity of generator buses in the system, and limited wind generator reactive power. The wind speed is assumed to be constant and the wind farm is at maximum output.

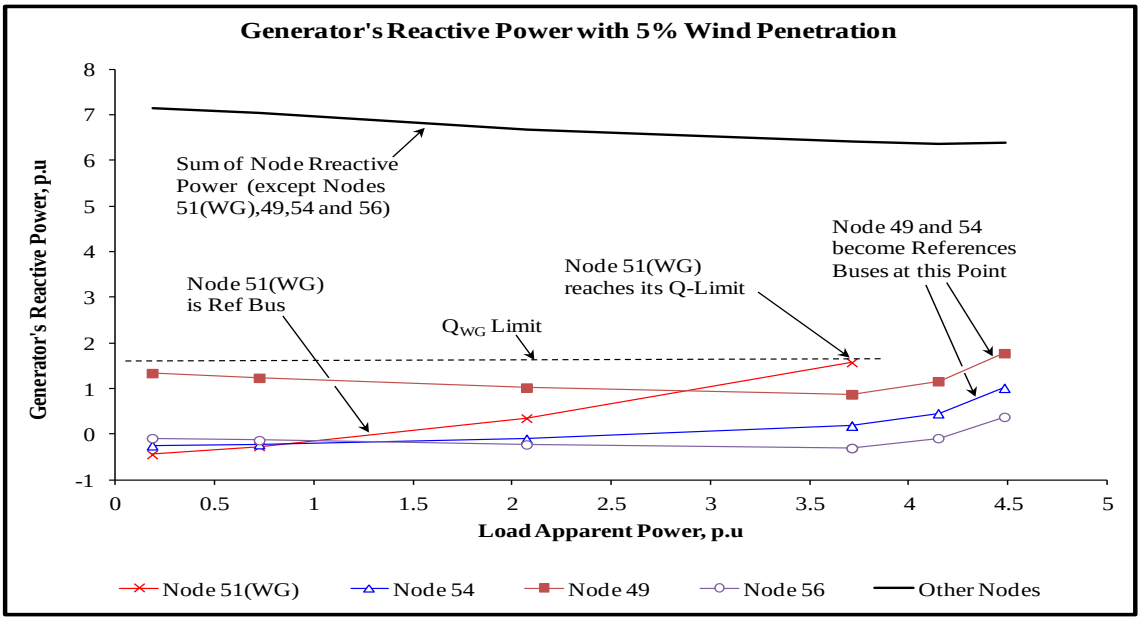

Figure 4.14: The variation of apparent power load demand at bus 52 (IEEE-118 bus system) with generators' reactive power contributions in the system, and limited wind generator reactive power. The wind speed is assumed to be constant and the wind farm is at maximum output.

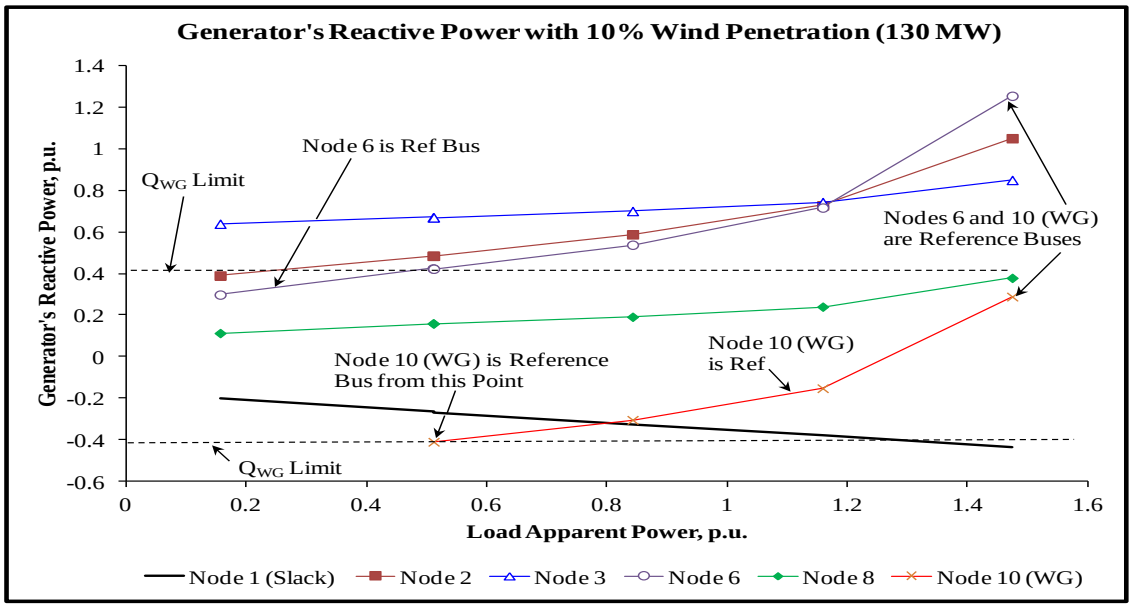

Figure 4.15: The variation of apparent power load demand at bus 14 (IEEE-14 bus system) with generators' reactive power contributions in the system, and limited wind generator reactive power. The wind speed is assumed to be constant and the wind farm is at maximum output.

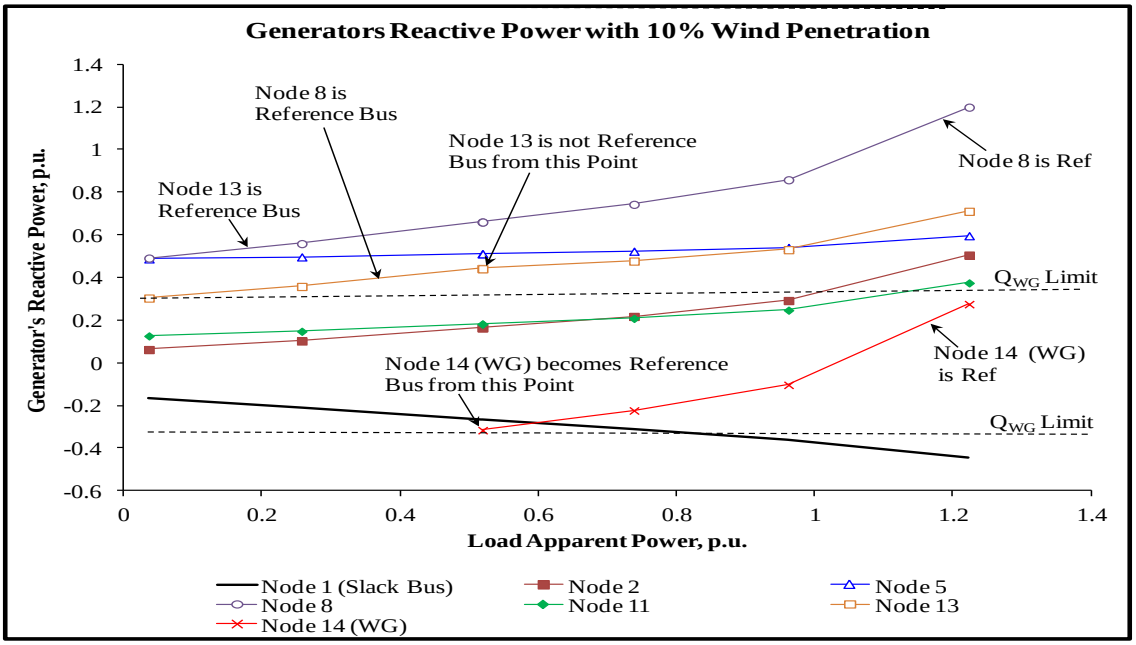

Figure 4.16: The variation of apparent power load demand at bus 23(IEEE-30 bus system) with generators' reactive power contributions in the system, and limited wind generator reactive power. The wind speed is assumed to be constant and the wind farm is at maximum output.

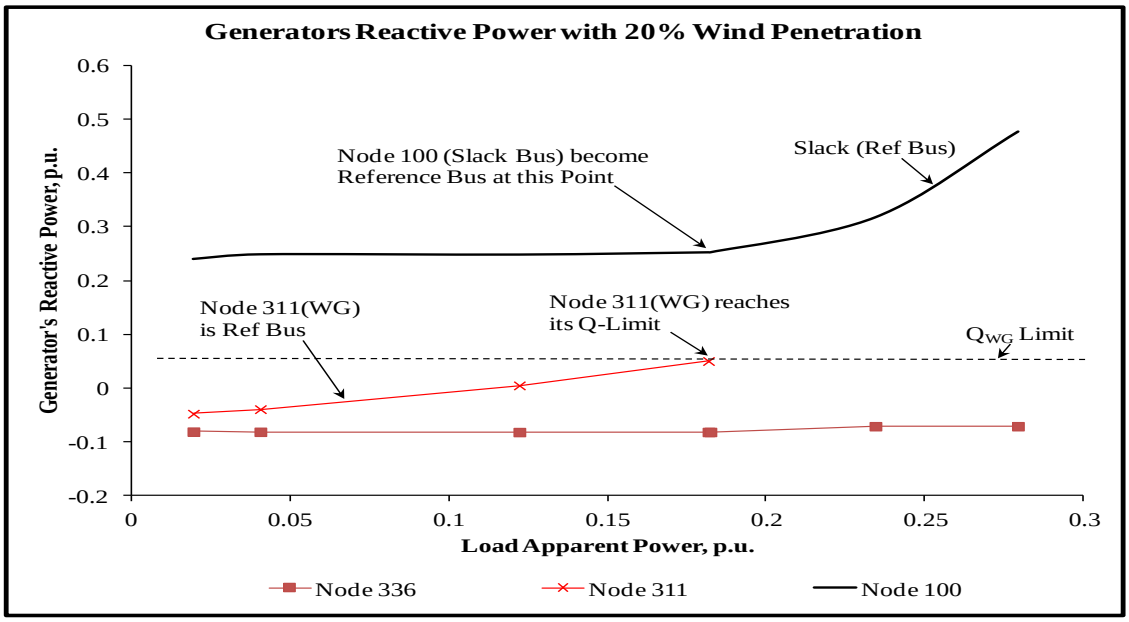

Figure 4.17: The variation of apparent power load demand at bus 50 (61-radial distribution network) with generators' reactive power contributions in the system, and limited wind generator reactive power. The wind speed is assumed to be a constant and wind farm is at maximum output.

For the second part of the analysis, an investigation of the behavior of the voltage collapse proximity indicator at the node is conducted. The load at that node is increased gradually until the voltage collapse point is reached. The wind speed is assumed to be constant, the wind generator is operated at maximum output and the load at a single bus is increased gradually at constant power factor up to the point where the load flow has diverged. To assess the relationship between the voltage collapse proximity indicator and the load power, the voltage and the system equivalent impedance takes into consideration the reactive power limitation of wind generators in the system. Several tests have been conducted at nodes 11, 12 and 14 from the IEEE-14 bus system, nodes 12, 16, 20 and 23 from the IEEE-30 bus system, nodes 44, 52 and 58 from the IEEE-118 bus system, and buses 45, 50 and 51 from the 61 radial distribution network. Figures 4.18 to 4.30 show the relationship between the VCPI and the above mentioned quantities when the single load is increased gradually at different wind penetration levels. In the

single load change test, the ratio of the system equivalent impedance to the equivalent load impedance is used as the voltage collapse proximity indicator (VCPI).

The results displayed in Figure 4.18 show that when the active and reactive load are increased at the concerned bus 52 (IEEE-118 bus system) at constant power factor, the equivalent load impedance is decreased and the VCPI is increased. The system equivalent impedance ($Z_{ie\ (A\text{-}B)}$ = 0.0526 p.u.) remains constant until the reference bus (wind generation) reaches its reactive power limit. After this, new system equivalent impedance ($Z_{ie\ (C\text{-}D)}$) is calculated ($Z_{ie\ (C\text{-}D)}$ = 0.0961 p.u.), which also remains constant until the collapse point. When the system reaches its loadability limit, the magnitude of the equivalent load impedance of the bus equals the value of the system equivalent impedance. As a result, the voltage collapse proximity indicator reaches the value of 1.0, beyond which voltage collapse occurs.

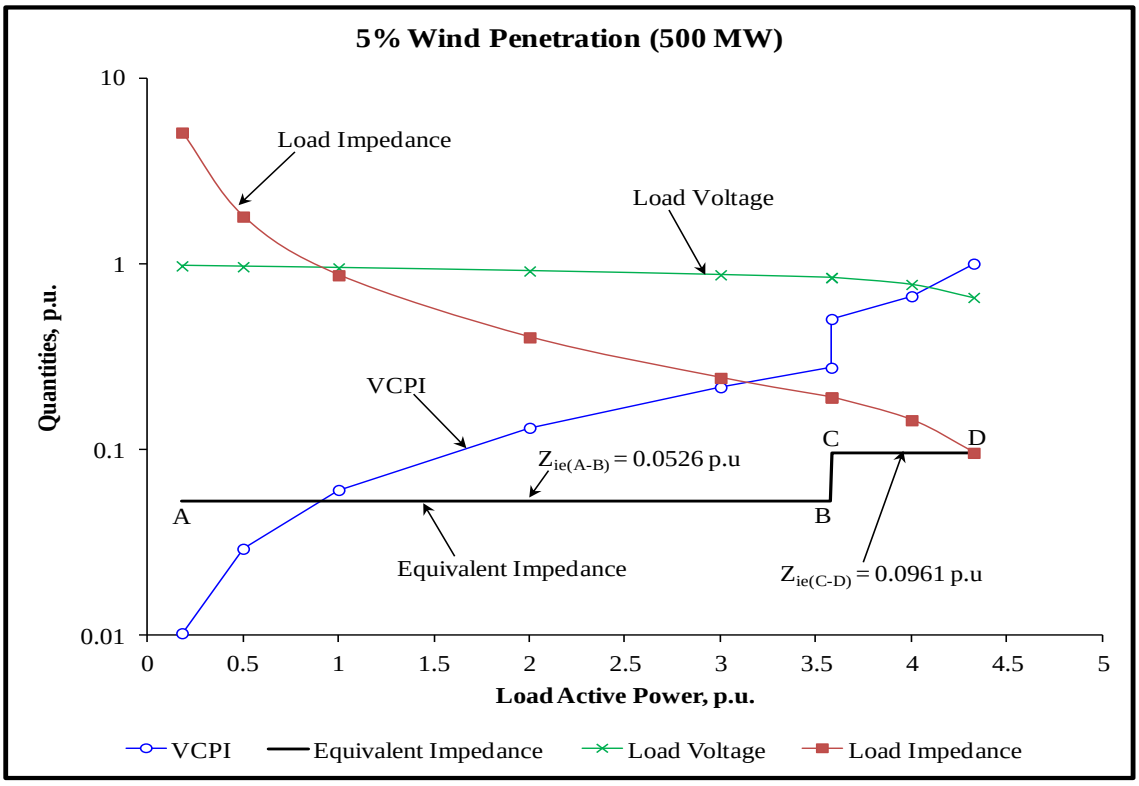

Figure 4.18: The variation of quantities with the load at bus 52 (IEEE-118 bus system) with 5% wind penetration. The wind speed is assumed to be constant and the wind farm is at maximum output.

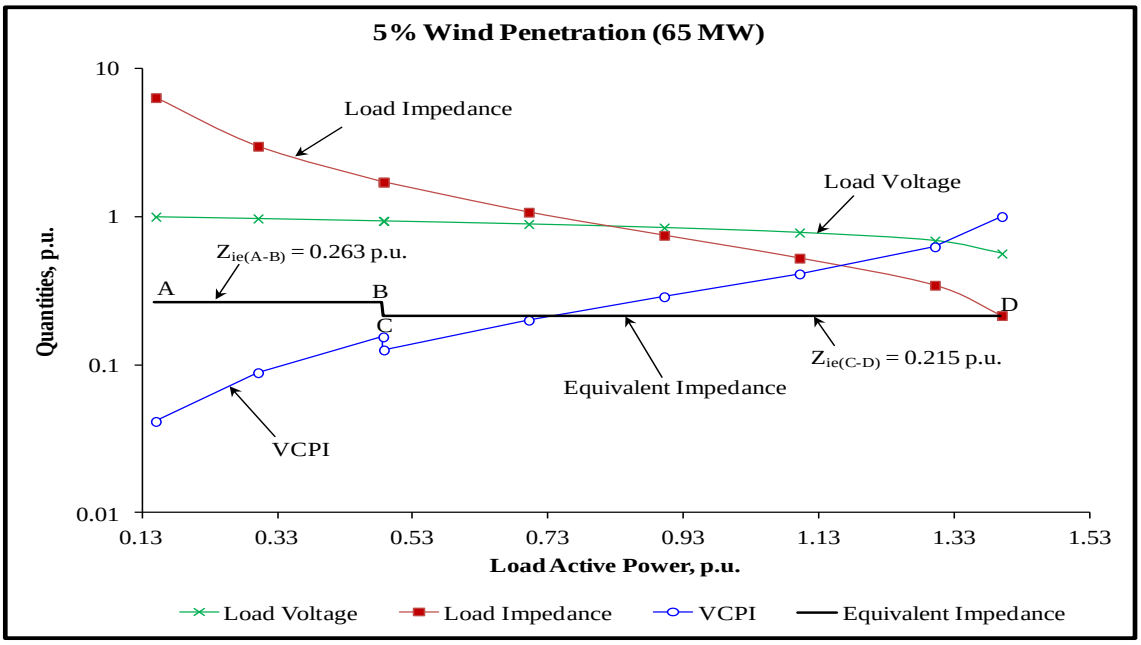

Figure 4.19: The variation of quantities with the load at bus 14 (IEEE-14 bus system) with 5% wind penetration. The wind speed is assumed to be constant and the wind farm is at maximum output.

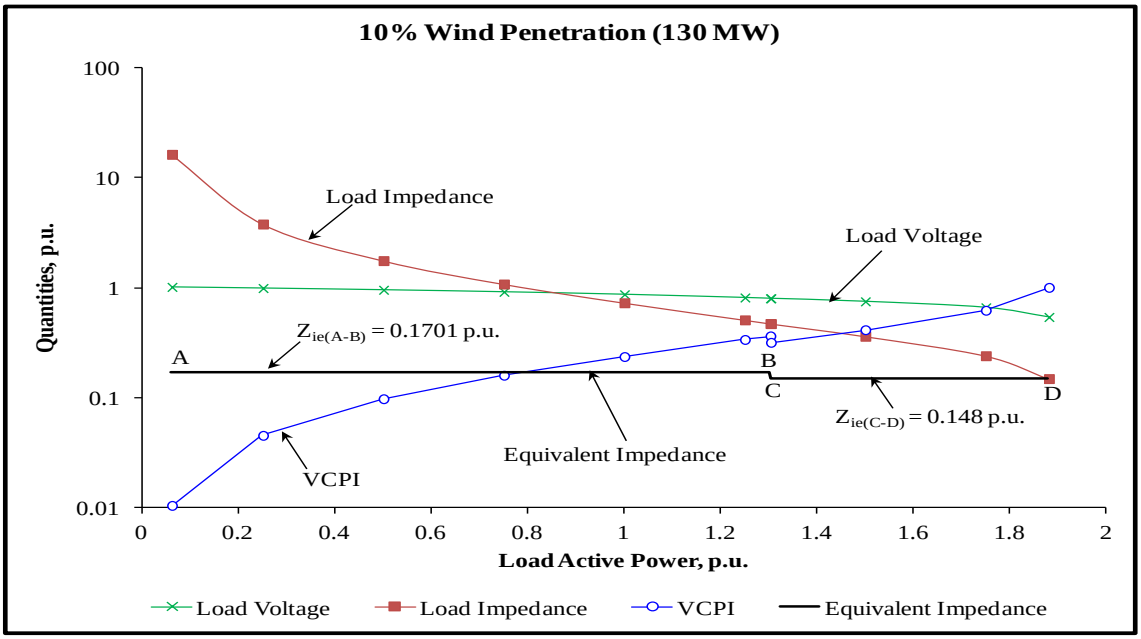

Figure 4.20: The variation of quantities with the load at bus 12 (IEEE-14 bus system) with 10% wind penetration. The wind speed is assumed to be constant and the wind farm is at maximum output.

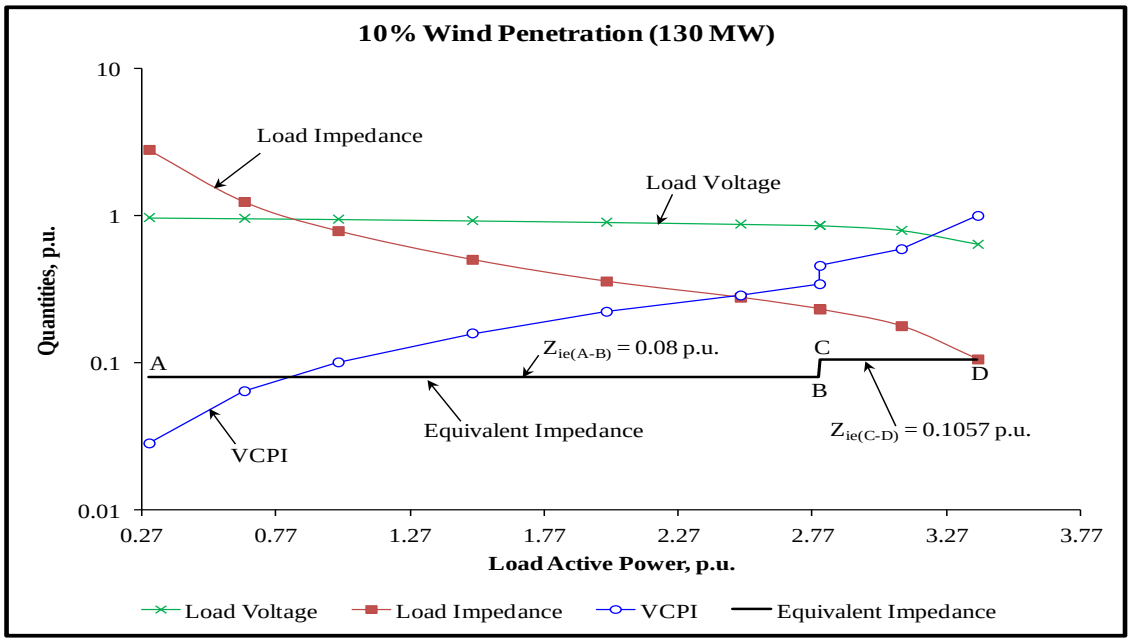

Figure 4.21: The variation of quantities with the load at bus 11 (IEEE-14 bus system) with 10% wind penetration. The wind speed is assumed to be constant and the wind farm is at maximum output.

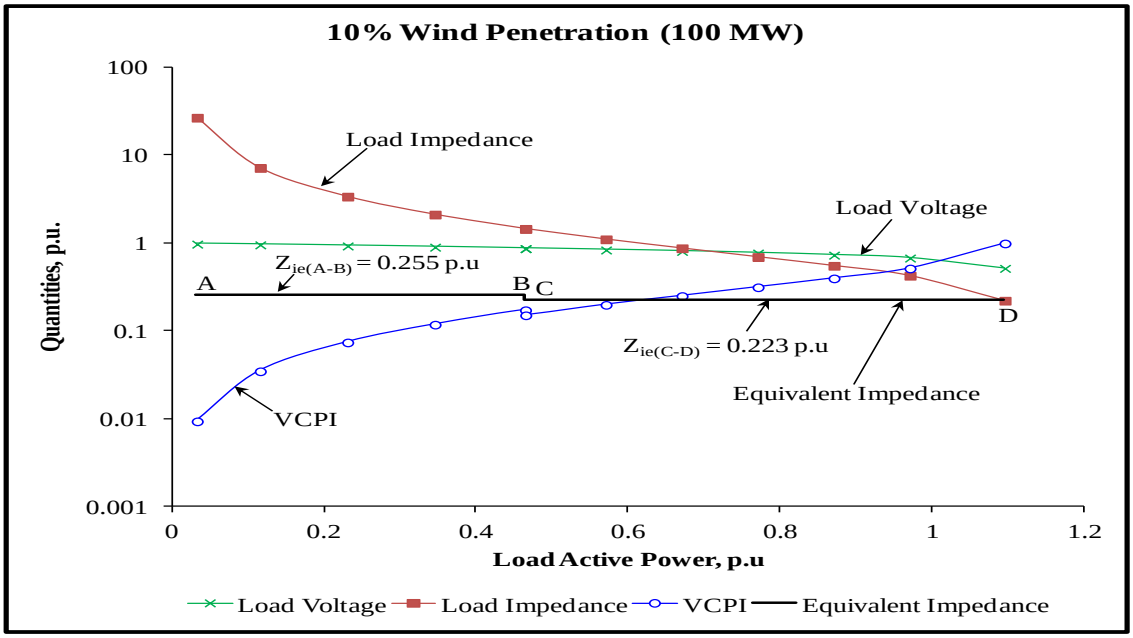

Figure 4.22: The variation of quantities with the load at bus 23 (IEEE-30 bus system) with 10% wind penetration. The wind speed is assumed to be constant and the wind farm is at maximum output.

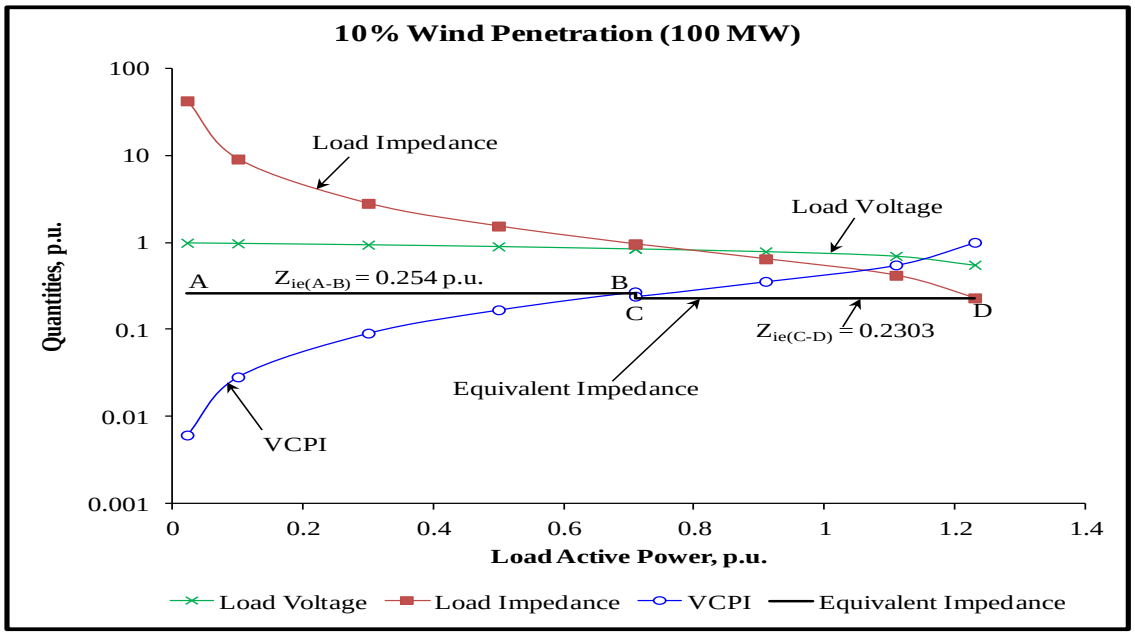

Figure 4.23: The variation of quantities with the load at bus 20 (IEEE-30 bus system) with 10% wind penetration. The wind speed is assumed to be constant and the wind farm is at maximum output.

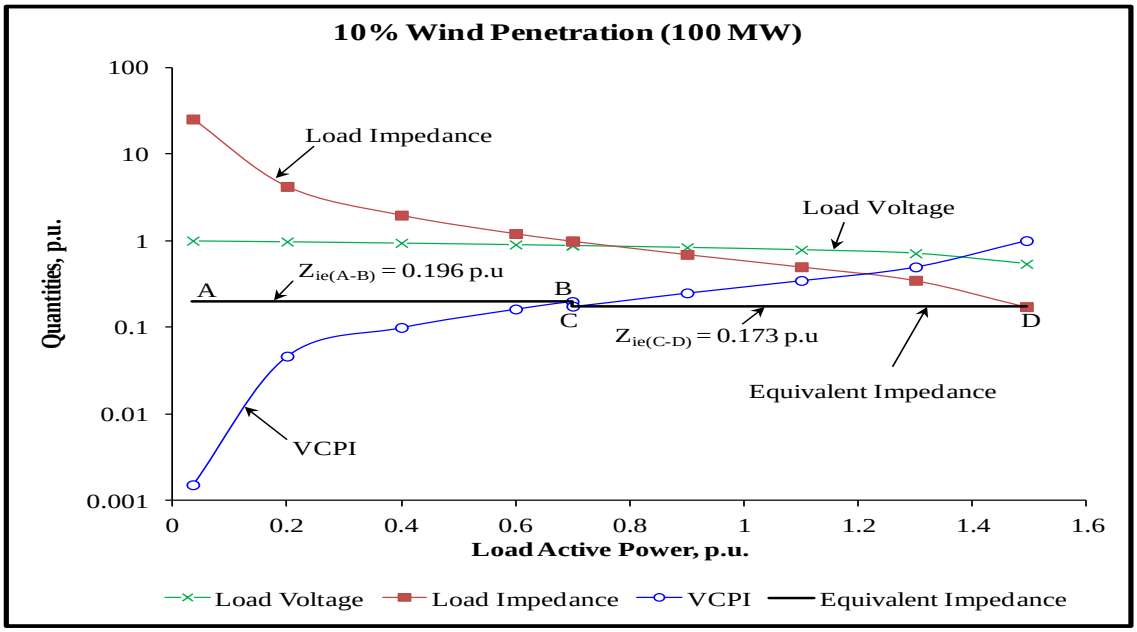

Figure 4.24: The variation of quantities with the load at bus 16 (IEEE-30 bus system) with 10% wind penetration. The wind speed is assumed to be constant and the wind farm is at maximum output.

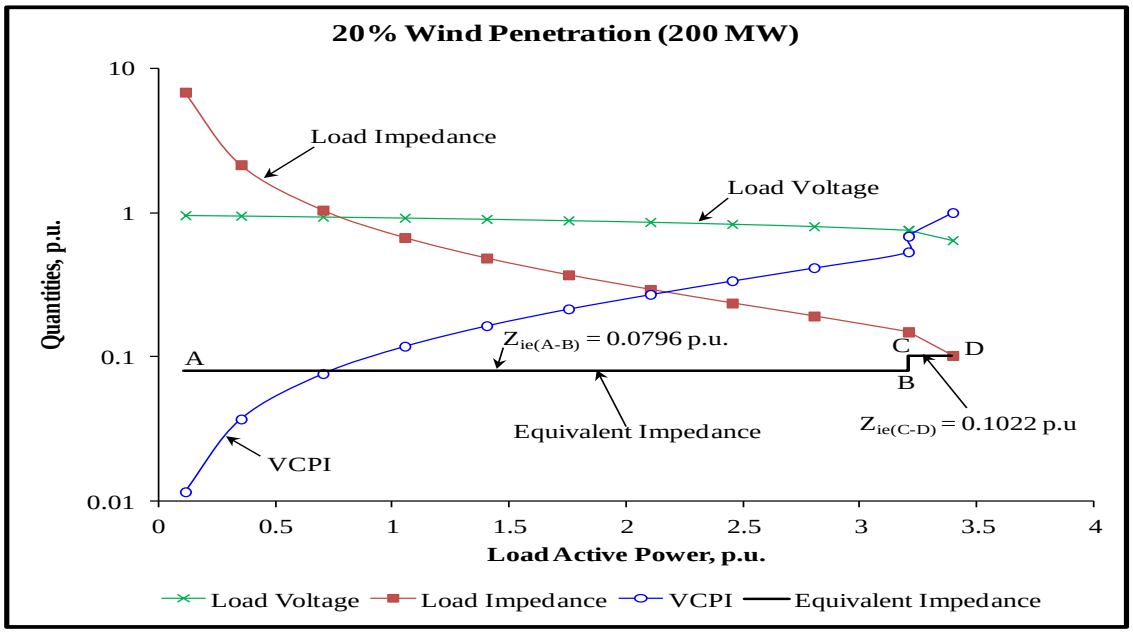

Figure 4.25: The variation of quantities with the load at bus 12 (IEEE-30 bus system) with 20% wind penetration. The wind speed is assumed to be constant and the wind farm is at maximum output.

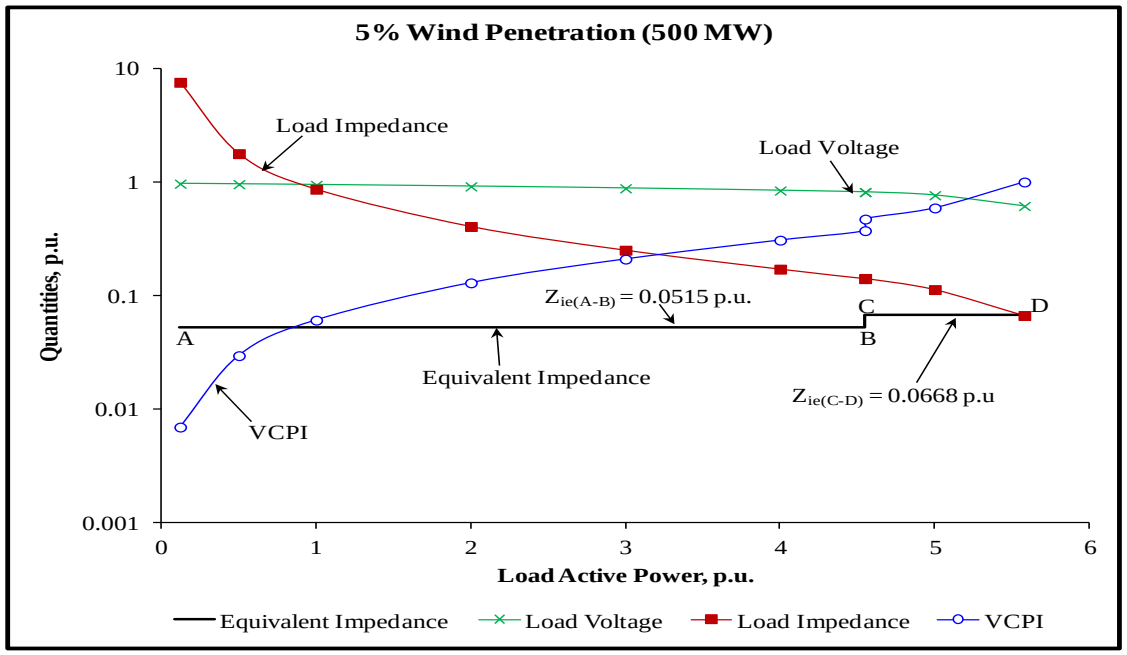

Figure 4.26: The variation of quantities with the load at bus 58 (IEEE-118 bus system) with 5% wind penetration. The wind speed is assumed to be constant and the wind farm is at maximum output.

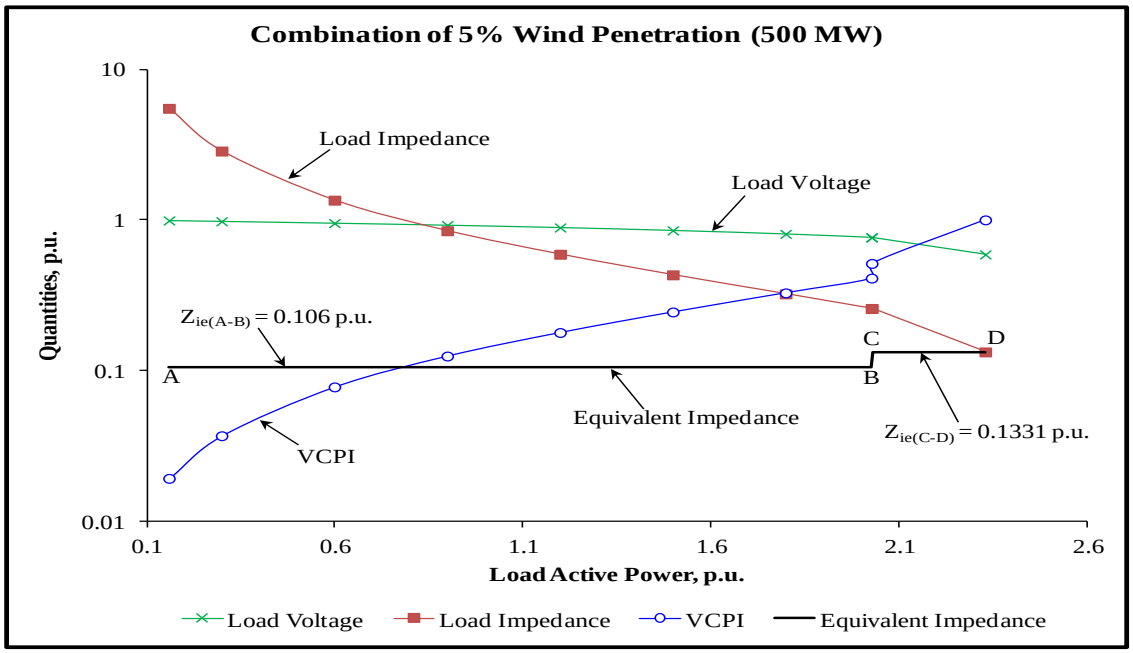

Figure 4.27: The variation of quantities with the load at bus 44 (IEEE-118 bus system) with combination of 5% wind penetration. The wind speed is assumed to be constant and the wind farm is at maximum output.

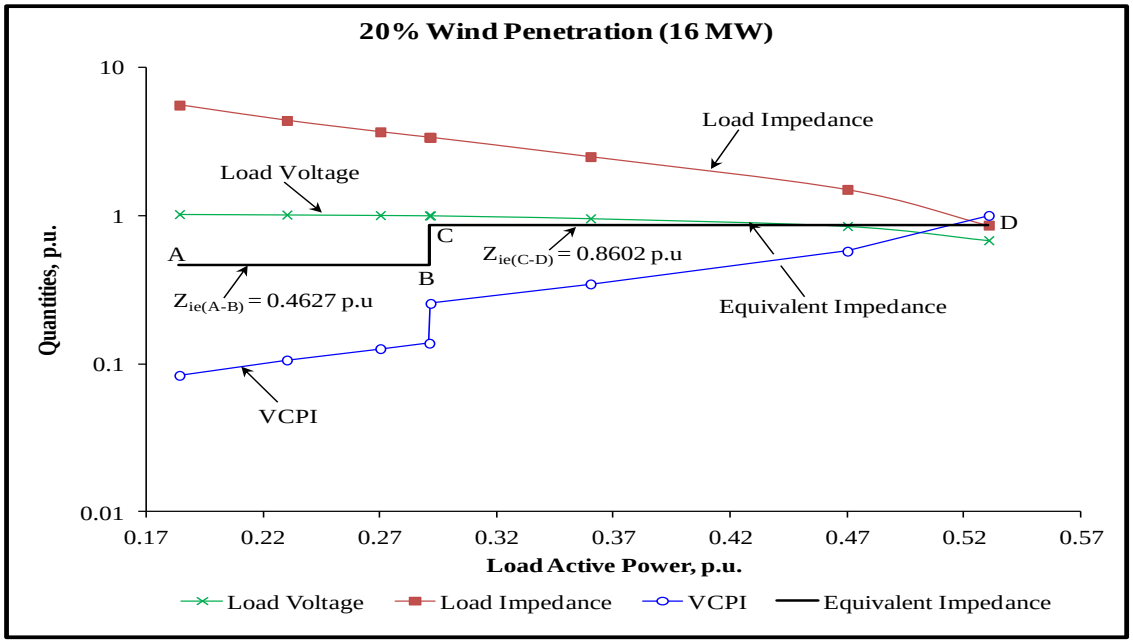

Figure 4.28: The variation of quantities with the load at bus 51 (61-radial distribution network) with 20% wind penetration. The wind speed is assumed to be constant and the wind farm is at maximum output.

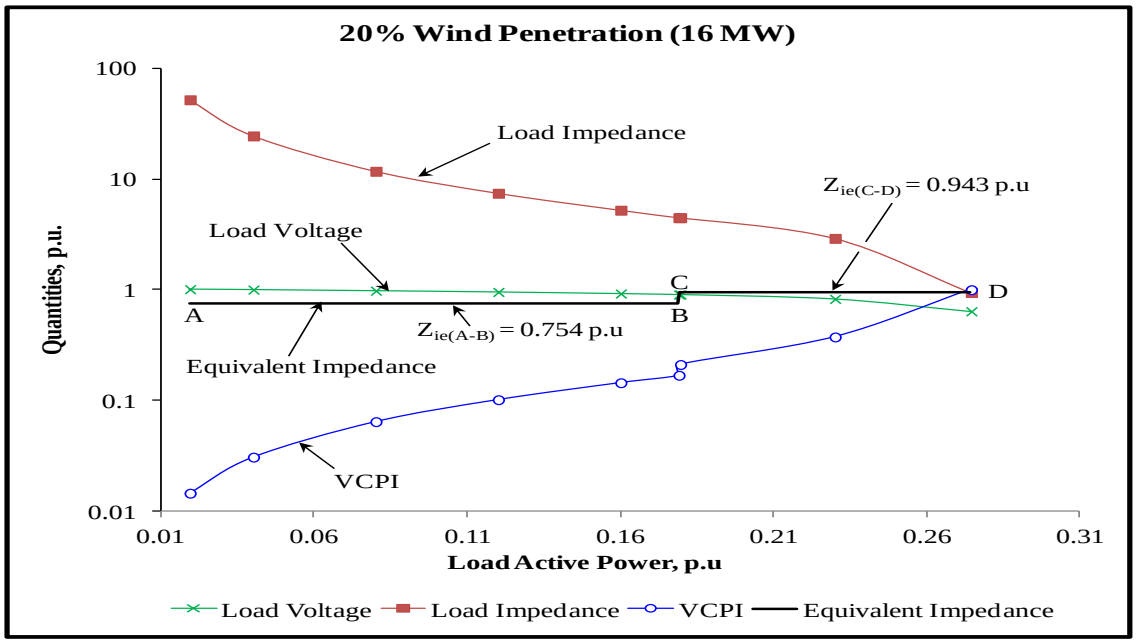

Figure 4.29: The variation of quantities with the load at bus 50 (61-radial distribution network) with 20% wind penetration. The wind speed is assumed to be constant and the wind farm is at maximum output.

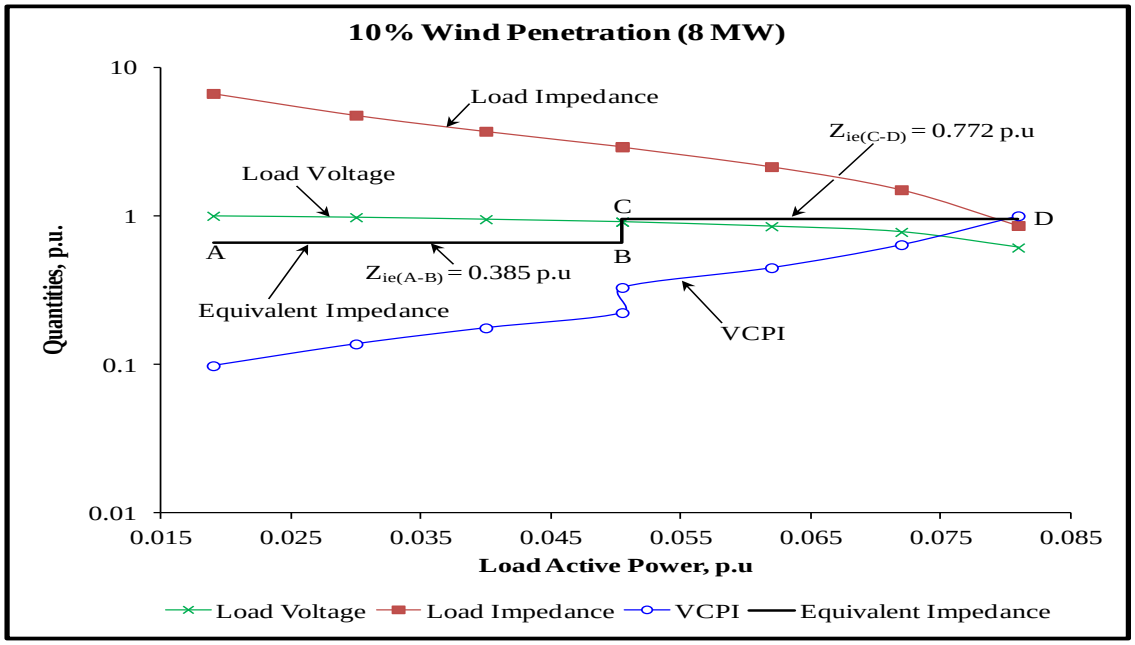

Figure 4.30: The variation of quantities with the load at bus 45 (61-radial distribution network) with 10% wind penetration. The wind speed is assumed to be constant and the wind farm is at maximum output.

4.11 Conclusion

This chapter has described some voltage collapse analytical metods, all of which have the objective of calculating the proximity to the voltage collapse point. One common point in these methods is that the majority of them use the tranditional load flow equations and extract information from the Jacobian Matrix. One important factor to consider in a voltage collapse scenario is load variation. To perform comprehensive studies to estimate the system strength, the load change must be cosidered both in terms of real and/or reactive power. This chapter has also devloped a VCPI calculation method which takes into consideration the reactive power limitation of wind generators in the system. The method identifies a new reference bus when necessary, which is a requirement to determine the new equivalent system impedance. Due to the reactive power limitation of wind generators, this equivalent system impedance is not constant. The method uses PV-PQ sensitivity and "referencing" techniques to determine the system equivalent impedance. The voltage collapse proximity indicator is the ratio of the system equivalent impedance to the load equivalent impedance. The value of the VCPI varies from zero at no load to 1.0 at maximum loadability. The VCPI behaves nearly linearly with the load variation and the voltage variation is small for lightly loaded systems and hence the load equivalent impedance variation is marginal. However, for a heavy loaded system, any small increase in demand induces a severe voltage drop, which in turn causes a large increase in the voltage collapse proximity indicator.

The results show that the system equivalent impedance value was changed when the wind generator reached its reactive power limit. The validity and effectiveness of this method is demonstrated with the application of different network configurations. The applicability of this method is verified by its ability to predict the buses which will experience voltage collapse in the context of system loadability when the load changes. Several results have been obtained for different cases, taking into account the reactive power limitation of wind generators and wind penetration levels. This clearly demonstrates the validity and effectiveness of the methodology. The VCPI will be used in the next chapter (Chapter 5) to investigate the impact of wind generation on system

voltage stability by considering the penetration level of wind generation, its intermittent nature and wind generator location.

Chapter 5

Impact of Wind Generation Intermittency and Penetration on System Voltage Stability

5.1 Introduction

A practical power system is complicated and its operating conditions can be highly variable. Power system characteristics are influenced by many factors, such as distributed generation (solar cell and wind power) and transmission system structure. There has been considerable interest and development in the use of wind generation as part of the generation mix. With the wind power penetration level increasing or set to increase in many systems worldwide, operational issues are beginning to emerge due to the intermittent nature of wind power output. One of these issues is power system stability. Power system stability may be broadly defined as the property of a power system that enables it to remain in a state of operating equilibrium after being subjected to a disturbance [57]. Depending on the physical nature of the resulting mode of instability, power system stability can be classified into three categories: rotor angle stability, frequency stability, and voltage stability. When a power system connects with a wind farm, voltage stability is one of the most important factors as it affects both the wind farm and operation of the system.

Due to the variability and limited predictability of wind speed, the output of wind turbines cannot be controlled to the same extent as conventional generation technologies. Currently, conventional generation plays a key role in maintaining the power balance between generation and demand. This thesis is to find that the impact of wind power generation on power system voltage stability is either positive or negative, depending on wind penetration level, the intermittent nature of wind power output, wind

location, and wind generator type. This chapter proposes a new assessment methodology regarding wind generation impact on voltage stability of power systems, taking into consideration wind generation intermittency and load variations. In this methodology, a voltage collapse proximity indicator (VCPI) based on network loadability is used to investigate the contribution of wind generation to voltage stability.

It is necessary to simulate and determine how much wind generation (DFIG) can affect power system voltage stability under different conditions and scenarios. In order to research and analyse the impact in more detail and under practical operation conditions, the proposed method is applied to simulation scenarios for different wind speed data, different penetration levels of wind energy, and different system models including IEEE-14-Bus system, IEEE-30-Bus system and 61-radial distribution network.

5.2 Unit Commitment and Economic Dispatch

Scheduling of generation units is done based on load forecasts and the economics and technical characteristics of the available generation units. This involves the calculation of optimal selection of units for power generation for a certain period of time (minutes to hours to days) [106] called unit commitment. Important parameters in unit commitment include start-up and shut-down cost, minimum up- and downtimes, and operating cost. Economic dispatch performs the actual distribution of total load between committed units, which is optimized for each operating state while taking into account all economic and technical aspects of the units. The outputs of unit commitment and economic dispatch (UC–ED) are generation unit operation-schedules. From these, an estimation of the associated use of fossil fuels and emission of greenhouse gases can be calculated as well.

5.3 Proposed Method: A New Assessment of Wind Generation Impact on Voltage Stability by Considering Wind Intermittency and Load Variations

This section proposes a new assessment of wind generation impact on voltage stability of power systems, taking into consideration wind generation intermittency and load variations. For this methodology, a voltage collapse proximity indicator was developed (see chapter 4) and used to investigate the impact of wind generation on voltage stability in transmission networks and distribution networks.

This methodology utilizes a Time Step Simulation Optimal Power Flow (TSSOPF), which is available in standard simulation software such as Power World Simulator which allows the incorporation of the effects of variable wind generation on system voltage stability. The method was validated on several power system networks, including IEEE benchmarks and UKDGS networks.

The proposed method has three main inputs, as shown in Fig. 5.1. The wind power inputs are the time series values of the wind generation connected to the network in MW at one hour intervals. This data was obtained from a utility operating in a United Kingdom wind farm for a one month period at one hour intervals [105]. The input of conventional generators indicates their availability, considering their capacity rating and quantity. The load model input is the forecasted load profile applied to the transmission network.

The flow chart for the proposed methodology is shown in Fig. 5.1. Each stage in the flow chart represents a critical aspect of the methodology, which can be described in the following steps:

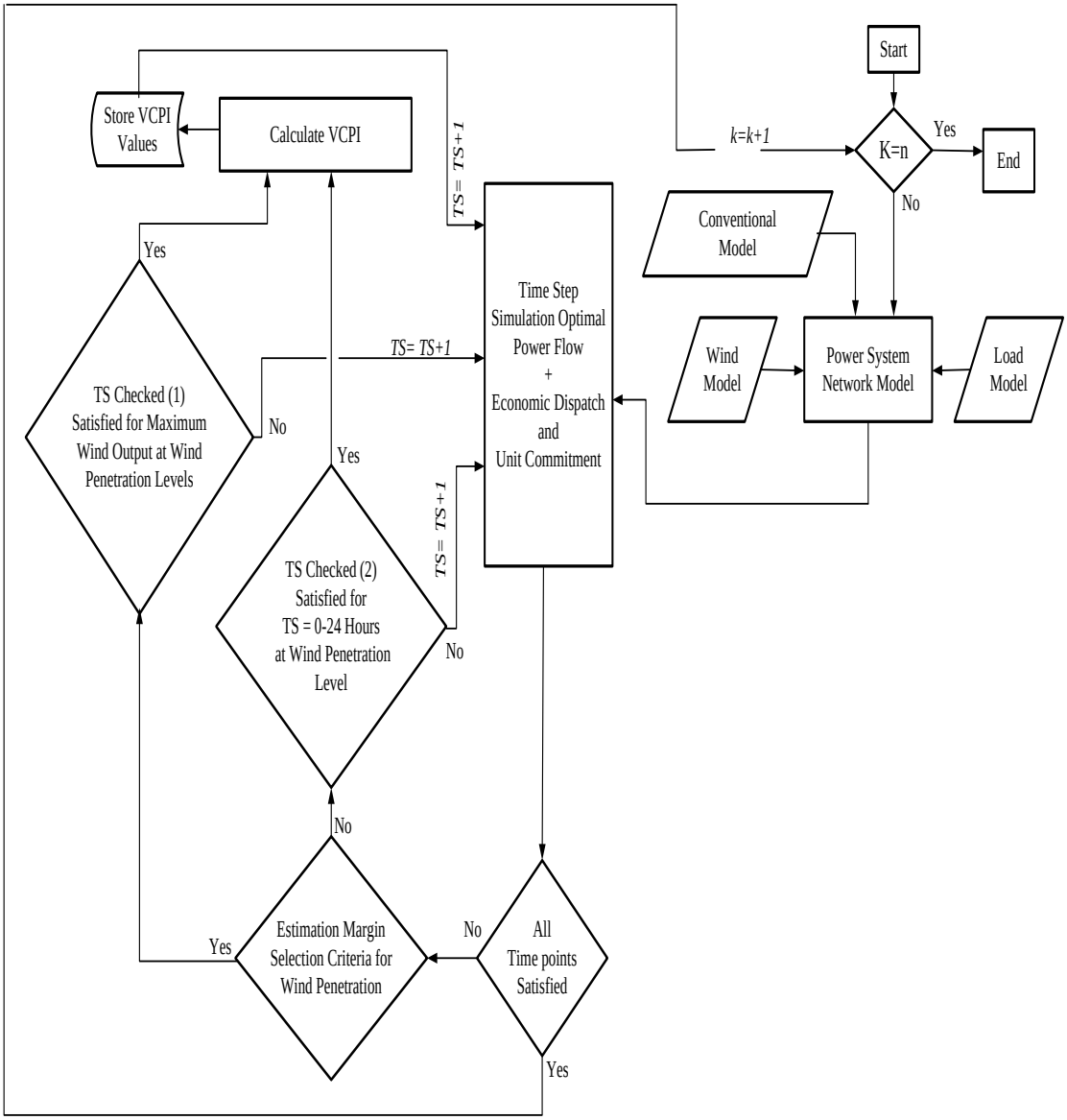

Figure 5.1: Flow chart describing the methodology used in the analysis.

Step 1: Obtain input data and time–series analysis

This step involves obtaining the three inputs to the simulator. These inputs represent wind generation active power output, conventional generators' active power output, and load profile in MW:

- The wind power output data in MW is connected to the network at different wind penetration levels, from 10% to 30% in steps of 10%, for one month. The penetration level of the wind generation is determined as a percentage of the installed capacity of the conventional generators in the network. The study takes into account the impact of both the level of wind generation and the wind variability on the system voltage stability. This is then compared with the base case without wind generation. The wind power output is highly stochastic, as shown in Figure 5.2, for a three-day output at one hour intervals. This plot highlights the variability of wind generator output for the different locations.

- The conventional generators are assumed to be thermal with given installed capacity in MW, and then used as the reference for calculating the penetration level of the wind generator.

- The load model is based on a single day load profile data; this profile is repeated for one month. The same load profile is used for all wind penetration levels so as to enable comparison of the simulation results.

- A time-series analysis is used in the simulation for modelling the load demand and variability of the wind generation in the system [106]. Each point in the time series represents an operating point that can be used as an input for optimal power flow. In this manner, several simulations are obtained on an hourly basis for the load profile. Due to the daily profile of load and the variability of wind over a day, a time step of one hour is used and applied for one month. This means that at least 720 power flow simulations need to be solved.

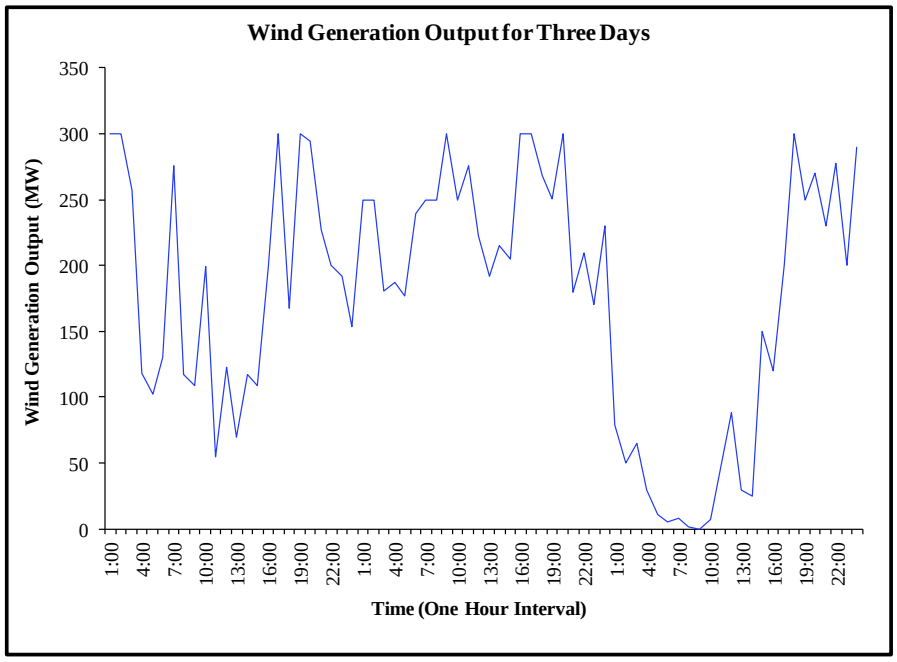

Figure 5.2: Typical plot of wind power output for three days.

Step 2: OPF incorporating wind generation

With the introduction and development of renewable energy sources, especially wind energy, there is a need to incorporate wind generation costs into the classical optimal power flow (OPF) problem [107]. The economic dispatch (ED) of a wind-thermal system involves the allocation of generation among wind plants and thermal plants so as to minimize total production costs. The sum of outputs from the available wind and thermal generators must equal the system load plus system losses. In addition, certain constraints may be placed on the generator model. These constraints typically take the form of minimum and maximum generator outputs. Generally, the problem can be formulated as follows [107]:

The fuel cost of thermal generation units are represented quadratic functions as

$$(P_{Gi}) = a + b(P_{Gi}) + c(P_{Gi}^2) \tag{5.1}$$

Where $f_t(P_{Gi})$ is the cost of a thermal generator; a, b, c are the characteristic parameter cost coefficients of the thermal generator; and P_{Gi} is the real power output of the thermal

generator. In a deregulated market, wind generation will have a cost that is based on special contractual agreements (i.e. fixed schedule or economic schedule) for buying or selling between each independent power producer and the transmission network operator (TNO). The output of a wind generator is constrained by an upper and lower limit. The operation costs of wind generation units can be represented as the function of wind farm scheduled power output [108].

$$f_w(P_{WGj} = C_w(P_{WGj}) + C_{p,w}(P_{WGj(available)} - P_{WGj}) + C_{r,w}(P_{WGj} - P_{WGj(available)}) \quad (5.2)$$

Where $f_w(P_{WGj})$ is the cost of the wind generator, P_{WGj} is scheduled wind power from the wind generator, $P_{WGj(available)}$ is the available wind power from the wind generator, and C_w is the cost function for the wind generator (this factor will typically take the form of a payment to the wind farm operator for the wind power actually generated). $C_{p,w}$ is the penalty cost function for not using all available power from the wind power generator, and $C_{r,w}$ is the required reserve cost function relating to uncertainty of wind generation.

The objective function includes not only the operation costs of the thermal generation units but also the operation costs of wind generation units operating in the system. They can be stated as follows [107]:

$$\text{Minimize: } f_T(P_{Gi}, P_{WGj}) = f_t(P_{Gi}) + f_w(P_{WGj}) \quad (5.3)$$

Where $f_T(P_{Gi}, P_{WGj})$ is the cost of a thermal generator and wind generator outputs, P_G is the power output from a thermal generator, and P_{WGj} is the schedule wind power from a wind generator.

Minimization of the above function is subject to system constraints. The system constraints for the problem can be shown as follows:

- The system load flow constraints:

$$\Delta P_i = P_{G_i} - P_{D_i} - V_i \sum_{j=1}^{NB} V_j [G_{ij} \cos(\delta_i - \delta_j) + B_{ij} \sin(\delta_i - \delta_j)] = 0 , \qquad i \in NB$$

$$\Delta Q_i = Q_{G_i} - Q_{D_i} - V_i \sum_{j=1}^{NB} V_j [G_{ij} \sin((\delta_i - \delta_j) - B_{ij} \cos(\delta_i - \delta_j)] = 0 , \qquad i \in NB$$

- Unit capacity constraint of thermal generator:

$$P_{G_i}^{min} \leq P_{G_i} \leq P_{G_i}^{max}, \qquad i \in NG$$

$$Q_{G_i}^{min} \leq Q_{G_i} \leq Q_{G_i}^{max}, \qquad i \in NG$$

- Unit capacity constraint of wind generator:

$$P_{WG_j}^{min} \leq P_{WG_j} \leq P_{WG_j}^{max} \qquad j \in NWG$$

$$Q_{WG_j}^{min} \leq Q_{WG_j} \leq Q_{WG_j}^{max} \qquad j \in NWG$$

- Compensator performance for shunt capacitor:

$$Q_{C_j}^{min} \leq Q_{C_j} \leq Q_{C_j}^{max}, \qquad j \in NC$$

- Bus generator voltage constraints:

$$V_{G_i}^{min} \leq V_{G_i} \leq V_{G_i}^{max}, \qquad i \in NG$$

- Bus load voltage constraints:

$$V_{D_j}^{min} \leq V_{D_j} \leq V_{D_j}^{max}, \qquad j \in ND$$

- Line capacity limit constraints:

$$F_{ij}^{min} \leq F_{ij} \leq F_{ij}^{max}, \qquad j \in NL$$

Where NG, NWG, NC, ND, and NL are the total number of thermal generators, the total number of wind generators, the total number of shunt capacitor compensators, the total number of loads, and the total number of branches, respectively; and P_{WG}, P_{WG}^{min}, and P_{WG}^{max} are the wind generator scheduled power output and its lower and upper limits, respectively.

Step 3: Balancing load and variable generation

As a wind generator's power output and system loading change at each time-step in the simulation, it is necessary to maintain a balance between the total generation and load in the system. This can be achieved by re-dispatching the conventional units in the system. This can be accomplished by using economic dispatch and unit commitment together. By combining the active power outputs generated from thermal generator P_G with wind generator P_{WG}, and by combining the reactive power outputs generated from thermal generator Q_G with wind generator Q_{WG} and shunt capacitor Q_C, two matrices containing the active power and the reactive power generated at all units in the system over 720 hours can be written as follows:

$$\begin{bmatrix} P_1^h \\ P_2^h \\ \vdots \\ P_N^h \end{bmatrix} = \begin{bmatrix} P_{G_1}^h \\ P_{G_2}^h \\ \vdots \\ P_{G_N}^h \end{bmatrix} + \begin{bmatrix} P_{WG_1}^h \\ P_{WG_2}^h \\ \vdots \\ P_{WG_N}^h \end{bmatrix} \qquad \text{Where} \quad h = 1, 2, 3, \ldots 720$$

$$\begin{bmatrix} Q_1^h \\ Q_2^h \\ \vdots \\ Q_N^h \end{bmatrix} = \begin{bmatrix} Q_{G_1}^h \\ Q_{G_2}^h \\ \vdots \\ Q_{G_N}^h \end{bmatrix} + \begin{bmatrix} Q_{WG_1}^h \\ Q_{WG_2}^h \\ \vdots \\ Q_{WG_N}^h \end{bmatrix} + \begin{bmatrix} Q_{C_1}^h \\ Q_{C_2}^h \\ \vdots \\ Q_{C_N}^h \end{bmatrix} \qquad \text{Where} \quad h = 1, 2, 3, \ldots 720$$

The complex power (S^h) delivered from all unit generators in the system over 720 hours can then be represented by:

$$\begin{bmatrix} S_1^h \\ S_2^h \\ \vdots \\ S_N^h \end{bmatrix} = \begin{bmatrix} P_1^h \\ P_2^h \\ \vdots \\ P_N^h \end{bmatrix} + j \begin{bmatrix} Q_1^h \\ Q_2^h \\ \vdots \\ Q_N^h \end{bmatrix} \qquad \text{Where} \quad h = 1, 2, 3, \ldots 720$$

The real and reactive power balance in the system over 720 hours can be written as:

$$\sum_{t=1}^{Nh} \left(\sum_{i=1}^{NG} P_{G_i}^h + \sum_{j=1}^{NWG} P_{WG_j}^h \right) = \sum_{t=1}^{Nh} \left(\sum \left(P_{Load}^h + P_{Loss}^h \right) \right), \qquad \begin{matrix} i \in NG \\ j \in NWG \\ t \in Nh \end{matrix}$$

$$\sum_{t=1}^{Nh} \left(\sum_{i=1}^{NG} Q_{G_i}^h + \sum_{j=1}^{NWG} Q_{WG_j}^h + \sum_{j=1}^{NC} Q_{C_j}^h \right) = \sum_{t=1}^{Nh} \left(\sum \left(Q_{Load}^h + Q_{Loss}^h \right) \right), \qquad \begin{matrix} i \in NG \\ j \in NWG \\ j \in NC \\ t \in Nh \end{matrix}$$

Where Nh is the total number of hours.

The active power available from wind generator P_{WG} is given by the expression below [68];

$$P_{WG} = \frac{1}{2}\rho . A . C_p . V_w^3$$

Where ρ is the air density, A is the turbine swept area, C_p is the cofeeicient of performance of the turbine, and V_w is the wind speed.

The net reactive power of a doubly fed induction generator (DFIG), when operated with a pre-determined power factor (φ), can be approximated by:

$$Q_{WG} = P_{WG} . \tan(\varphi_{WG})$$

However, as in most cases where DFIG contributes to AC voltage control as required in most of the present grid codes, DFIG net reactive power exchange with grid will be determined by the machine's AC voltage controller.

Step 4: Time step selection based on system conditions of interest and VCPI calculation

Two sets of scenarios are selected on which the VCPI calculations are performed. The first scenario is related to the maximum power output of wind generation (P_{WG}^{max}) for each wind penetration level. In this case, the wind data is monitored for the maximum output to identify the time step at which this occurs. The VCPI is then calculated at that simulation time step. It is assumed that the wind speed during this time step is constant and the load is then gradually increased at a certain single bus until the collapse point, while other load buses in the system remain unchanged.

The second scenario is related to wind variability at a specified time range within a one month period. In this case, the voltage collapse proximity indicator is calculated for each time step. This case concentrates on large and sudden changes in the

wind power injected into the network caused by wind conditions during peak load. The choice of these times and wind generation outputs provides results that are indicative of the impact of wind variability on the system voltage stability. The VCPI is calculated at each time step by using the developed methodology that was described and presented in Chapter 4.

5.4 The Impact of Wind Generation on Voltage Stability in Power Systems

As the use of wind generation in power systems is increasing rapidly it is having a more noticeable impact on the manner in which these power systems operate. An important issue in the integration of large-scale wind farms is the impact of power systems on voltage stability. When large wind farms are connected to a transmission network (110kV-220kV), or connected to a distribution network (33kV-11kV), voltage stability is a concern as it affects system operation. For example, the key issue for a wind farm is lack of reactive power support, which causes voltage instability in the power system. Its effect can be more severe when there is a large amount of power injected from the wind farm. In order to investigate the impact of wind generation on power system voltage stability, a variety of network configurations are used in this section for analyzing. Section 5.4.1 discusses the impact on voltage stability in a transmission network and low-voltage distribution network.

5.4.1 Case Studies and Results

In order to evaluate the impact of wind generation intermittency, and the penetration and location on voltage stability in transmission networks, an IEEE-14 bus system, IEEE-30 bus system and UKGDS 61-bus radial distribution network are applied to the proposed method. The results of this study show that system voltage stability is affected positively or negatively depending on the penetration level, location of wind generation connection, fluctuation of wind generator output and type of wind generator.

5.4.1.1 Modified IEEE-14 Bus Test System

A single line diagram of the IEEE-14 bus system is shown in Figure 4.6 and detailed data of the system are shown in Appendix A. The modified test system was analyzed using AC Optimal Power Flow (OPF). All simulations were carried out in the Power World Simulation environment. The test system was modified by connecting wind generation to the system at different buses, with different connection scenarios at different wind penetration levels, and the farm consisted of several variable speed doubly fed induction generator (DFIG) wind turbines, each of 1.5 MW. In this assessment, the DFIG was modelled as a PV bus and operated with maximum and minimum power factors of 0.95 leading (capacitive VAr) and 0.95 lagging (inductive VAr).

The different connection scenarios of wind generation were:

- First scenario: one wind farm connected to strong area at bus 4.
- Second scenario: one wind farm connected to weak area at bus 12.
- Third scenario: two wind farms were connected to bus 4 and bus 12 simultaneously with a combination of different penetration levels.

For each connection scenario, three wind penetration (WP) scenarios (10%, 20% and 30%) were considered to evaluate the effect of wind penetration level and wind farm location on voltage stability. Only the first connection scenario, with a 30% wind penetration level, was considered to assess the impact of wind generation fluctuation output on voltage stability during system loadability.
The three wind penetration level scenarios for the case studies are shown in Table 5.1.

Table 5.1: Penetration level of wind generation scenarios for IEEE-14 bus system.

Scenarios	Scenario 1	Scenario 2	Scenario 3
Wind Penetration (%)	(10% WP)	(20% WP)	(30% WP)
(MW)	130 MW	260 MW	390 MW

The one day load profile used in the simulation is given in Table 5.2. The one day load data are only a representative sample of the one month load profile data used for the simulation at one hour intervals. The same load profile was used for all wind penetration level scenarios and wind connection scenarios, to enable comparison of results. Due to the size of the data used for the simulation, the total one month data has been saved under the file name "Load 14-bus" on a CD attached to this thesis. A one week plot of the load profile is also shown in Figure 5.3; this depicts the variation of the total system load over the simulation period. The output of the wind generator in MW (connected to bus 4 at different wind penetration (WP) levels from 10% to 30% in steps of 10% for one month) used in the simulation has also been saved under the file name "WG output" on the CD attached to this thesis.

The penetration level of the wind generator is determined as a percentage of the capacity of the conventional generators in the network. The total generation output from the wind turbines connected to the test system is varied every hour to represent the stochastic behavior of wind generation. The wind generation is varied from 10% to 30% of the total connected load in the network for each of the scenarios. The voltage collapse proximity indicator (VCPI) is calculated under different conditions for evaluating the impact of wind generation on voltage stability. A one day wind generator input to the network at one hour intervals is given in Table 5.3 at different penetration levels used in the simulation. The penetration level percentages refer to the value of wind generation as a function of total conventional generating capacity. The conventional generators are assumed to be thermal; their capacities and the buses to which they are connected are given in Appendix A. The total installed capacity is 1300 MW, which is used as the reference value for calculating the penetration percentages of the wind generator.

Table 5.2: A one day load profile for IEEE-14 bus system.

Load Bus	**2**	**3**	**4**	**5**	**6**	**9**	**10**	**11**	**12**	**13**	**14**
Peak (MW)	**84**	**300**	**152**	**25**	**36**	**94**	**29**	**12**	**20**	**43**	**48**
	21.7	94.1	47.7	7.599	11.1	29.4	8.9	3.4	6.0	13.4	14.8
	21.7	94.1	47.7	7.5	11.1	29.4	8.9	3.4	6.0	13.4	14.8
	32.5	141.3	71.6	11.4	16.8	44.2	13.4	5.2	9.1	20.2	22.3
	32.5	141.3	71.6	11.4	16.8	44.2	13.4	5.2	9.1	20.2	22.3
	33.7	146.3	74.2	11.8	17.4	45.8	13.9	5.4	9.4	20.9	23.1
	33.7	146.3	74.2	11.8	17.4	45.8	13.9	5.4	9.4	20.9	23.1
	46.1	200.5	101.7	16.1	23.8	62.7	19.1	7.4	12.9	28.7	31.7
	46.1	200.5	101.7	16.1	23.8	62.7	19.1	7.4	12.9	28.7	31.7
	52.7	229.1	116.2	18.4	27.2	71.7	21.8	8.5	14.8	32.8	36.2
	52.7	229.1	116.2	18.4	27.2	71.7	21.8	8.5	14.8	32.8	36.2
	36.6	159.2	80.7	12.8	18.9	49.8	15.1	5.9	10.3	22.8	25.1
	36.6	159.2	80.7	12.8	18.9	49.8	15.1	5.9	10.3	22.8	25.1
	39.7	172.5	87.5	13.9	20.5	54.0	16.4	6.4	11.1	24.7	27.2
	39.7	172.5	87.5	13.9	20.5	54.0	16.4	6.4	11.1	24.7	27.2
	68.9	299.1	151.7	24.1	35.5	93.6	28.5	11.1	19.3	42.8	47.2
	68.9	299.1	151.7	24.1	35.5	93.6	28.5	11.1	19.3	42.8	47.2
	83.7	363	184.5	29.3	43.2	113	34.7	13.5	23.5	52.	57.5
	83.7	363	184.5	29.3	43.2	113	34.7	13.5	23.5	52.	57.5
	64	280	142.2	22.6	33.3	87.7	26.7	10.4	18.1	40.5	44.3
	64	280	142.2	22.6	33.3	87.7	26.7	10.4	18.1	40.5	44.3
	34.3	149.2	75.4	12.0	17.7	46.7	14.2	5.5	9.6	21.3	23.5
	34.3	149.2	75.4	12.0	17.7	46.7	14.2	5.5	9.6	21.3	23.5
	30.3	131.6	66.7	10.6	15.6	41.2	12.5	4.8	8.5	18.8	20.8
	30.3	131.6	66.7	10.6	15.6	41.2	12.5	4.8	8.5	18.8	20.8

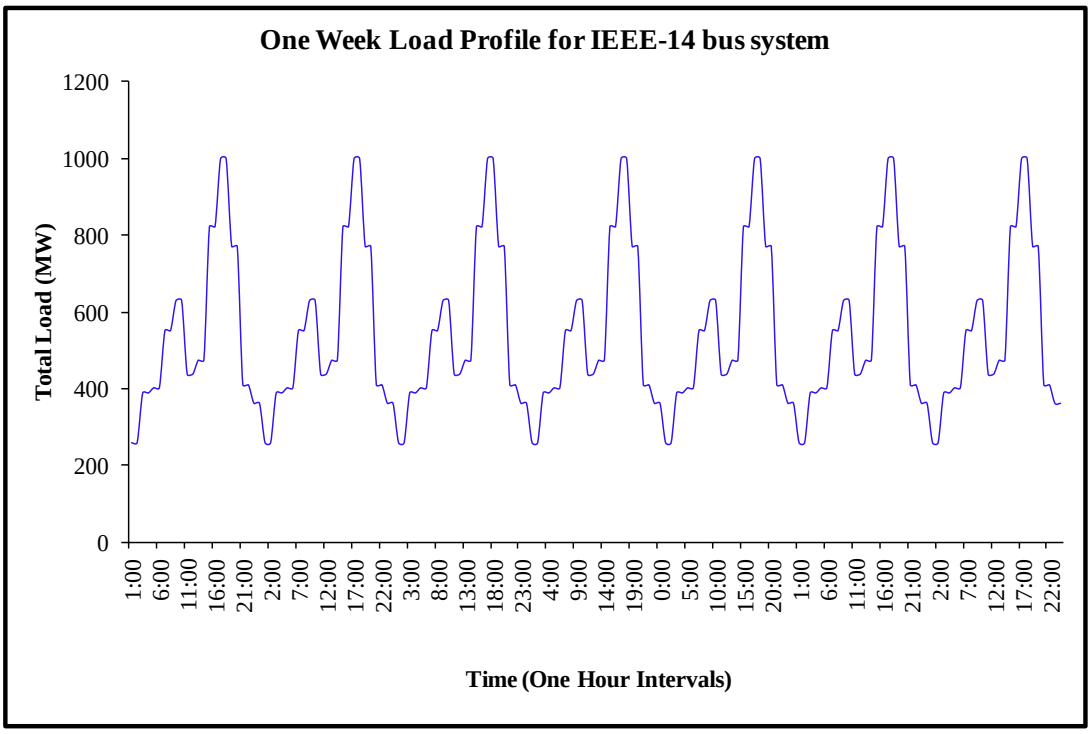

Figure 5.3: One week load profile plot.

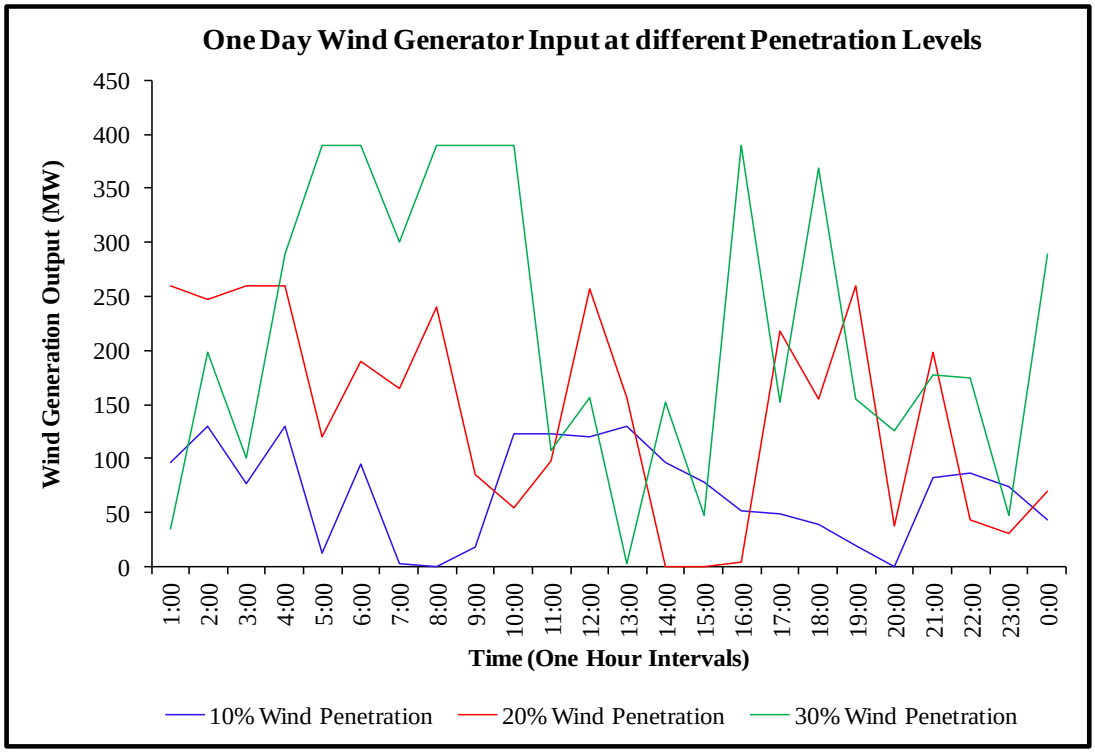

Figure 5.4: One day wind generator input at 10%, 20% and 30% penetration levels.

Table 5.3: Wind generator input data for one day in MW for IEEE-14 bus system.

Time (Hour)	10% (WP)	20% (WP)	30% (WP)
01:00:00	96.9	260	34.7
02:00:00	130	247.2	198
03:00:00	76.6	259.9	100
04:00:00	130	259.9	289
05:00:00	12.5	119.4	390
06:00:00	95.3	190.2	390
07:00:00	3.4	164.4	300
08:00:00	0	240.2	390
09:00:00	17.8	84.7	390
10:00:00	123.4	54.2	390
11:00:00	123.2	97.9	108
12:00:00	119.7	257	157
13:00:00	130	157	2.6
14:00:00	97	0	152.4
15:00:00	77.6	0	47.9
16:00:00	51	3.7	390
17:00:00	48.3	217.8	152.3
18:00:00	39.6	155.2	369
19:00:00	19.1	260	155.2
20:00:00	0	38.2	125.9
21:00:00	82	198	177
22:00:00	86.6	43.8	174.5
23:00:00	73.5	30.2	46.8
00:00:00	43.8	70.1	289

The inputs to the modified IEEE-14 bus system in the Power World Simulator were the variable loads, wind generation, and output from the thermal generators to reflect the actual response of the system. These inputs were connected to the test system at one hour simulation time steps for a total period of one month, and the system voltage stability was analyzed and VCPI calculated from different standpoints. These were the level of wind penetration (WP) (i.e. 10% to 30%), the dispersion of wind generation (i.e. one location at strong bus, one location at weak bus and two locations as a combination with wind penetration levels), and the intermittency of wind generation output

(fluctuation of wind generation output). In order to show the impact of wind generation on voltage stability, the simulation results of all wind generation scenarios were compared with the base case (no wind generation connected to the system).
The results and related discussions are presented in the following sections.

5.4.1.1.1 The Effect of Wind Penetration Level

This section will evaluate the effect of different wind penetration levels on voltage stability in the transmission network. A voltage collapse proximity indicator (VCPI), based on network loadability, is employed to investigate the contribution of wind generation to voltage stability. As mentioned above, each simulation run used one hour data of load and wind generation. The VCPI is calculated for each wind penetration level (10%, 20% and 30%) then each case is compared to the VCPI when no wind is connected to the network.

The simulation is carried out by connecting the wind generator at bus 4, the strongest bus in the system. In this case, the wind data is monitored for the maximum output of each wind penetration level, then the time step at which this occurs is identified. It is assumed that the wind speed during this time step is constant. The load is then gradually increased at a single bus until the collapse point, while other load buses in the system remain unchanged. The voltage collapse proximity indicator is calculated at this time step.

Buses 14, 10 and 9 are selected individually for each penetration level. Buses 14, 10 and 9 of the IEEE-14 bus system are selected for evaluation because these are critical buses and prone to voltage instability. The results presented here are for evaluating the impact of wind generation on the system and the VCPI is calculated for each bus. Figures 5.5, 5.6 and 5.7 illustrate the impact of different wind penetration levels on the voltage stability of the IEEE-14 bus system, when one wind farm is connected to the network at bus 4. Figures 5.5, 5.6 and 5.7 show a plot of the VCPI of

buses 14, 10 and 9, respectively, when no wind generation is connected to the network and when wind generation is connected to bus 4 with 10%, 20% and 30% wind penetration levels. As shown, the value of VCPI is increased as the load at the concerned bus is increased. Consequently, the voltage collapse proximity indicator reaches the value of 1.0, beyond which is the voltage collapse point.

The VCPI of bus 14 reaches a value of 1.0 as the load at bus 14 reaches maximum loading at 1.308 p.u for the base case (no wind), 1.321 p.u for 10% WP (wind penetration), 1.334 p.u for 20% WP, and 1.341 p.u for 30% wind penetration, as shown in Figure 5.5. It can be seen from the results in this figure that the system voltage stability is improved with all wind penetration levels when DFIG is connected to the stronger bus and the higher the penetration level the better.

Figure 5.6 shows the variation of the VCPI of bus 10 with load at all wind penetration levels. Compared to the base case when no wind was connected to the system, the VCPI of bus 10 reached the value of 1.0 when the demand reached maximum loading at 1.638 p.u for the base case, 1.694 p.u for 10% WP, 1.725 p.u for 20% WP, and 1.744 p.u for 30% wind penetration level. The system voltage stability with wind generation (DFIG) was much better compared to the base case.

As shown in Figure 5.7, the VCPI variation with load at bus 9 with 30% WP was given more maximum loading than other wind penetration levels. It can be seen that the results show an improvement in the voltage stability by connecting a doubly fed induction generator (DFIG) to the network when the system is based on system loadability. Moreover, the voltage stability is improved with higher wind penetration levels.

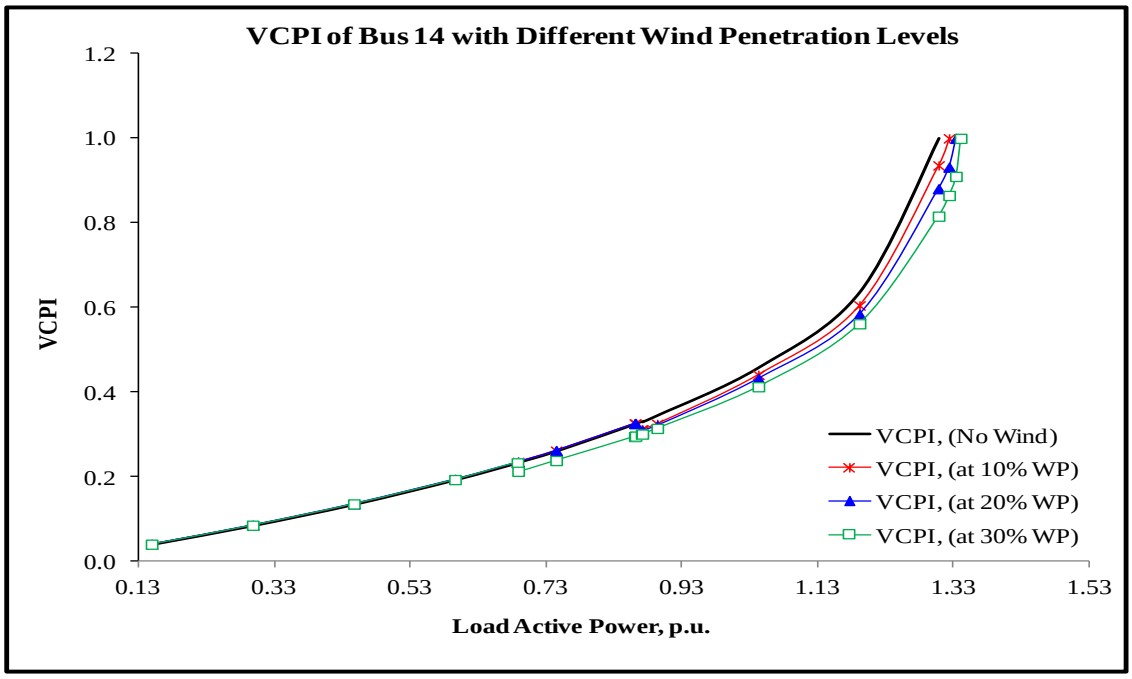

Figure 5.5: VCPI of bus 14 (IEEE-14 bus system) at different wind penetration levels when the load at bus 14 is varied at constant power factor; the wind farm is connected to bus 4 only.

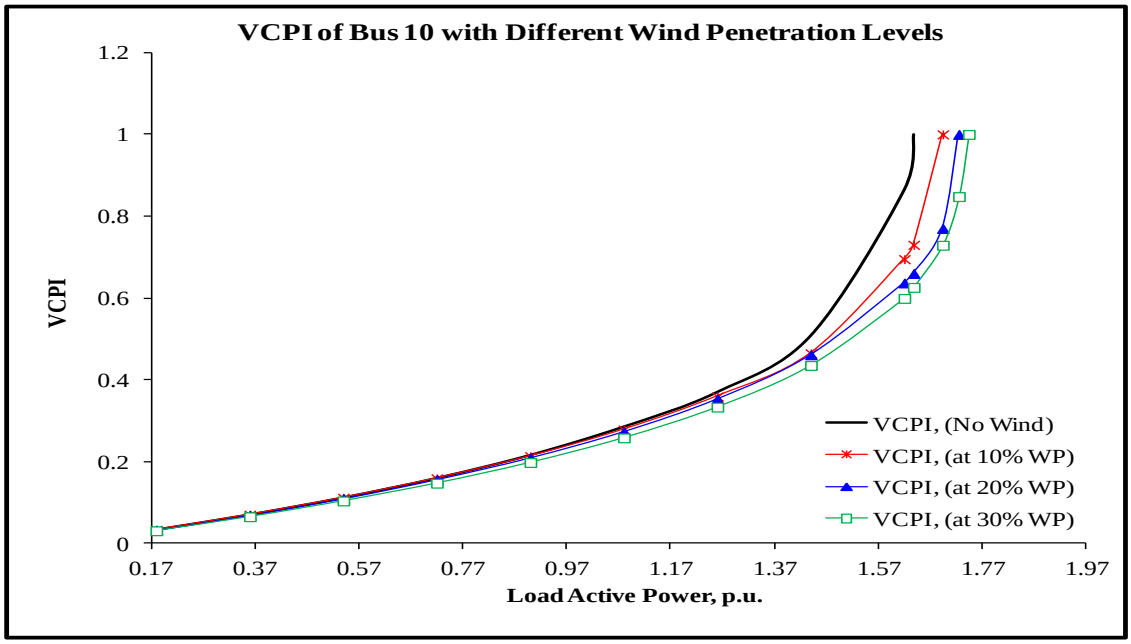

Figure 5.6: VCPI of bus 10 (IEEE-14 bus system) at different wind penetration levels when the load at bus 10 is varied at constant power factor; the wind farm is connected to bus 4 only.

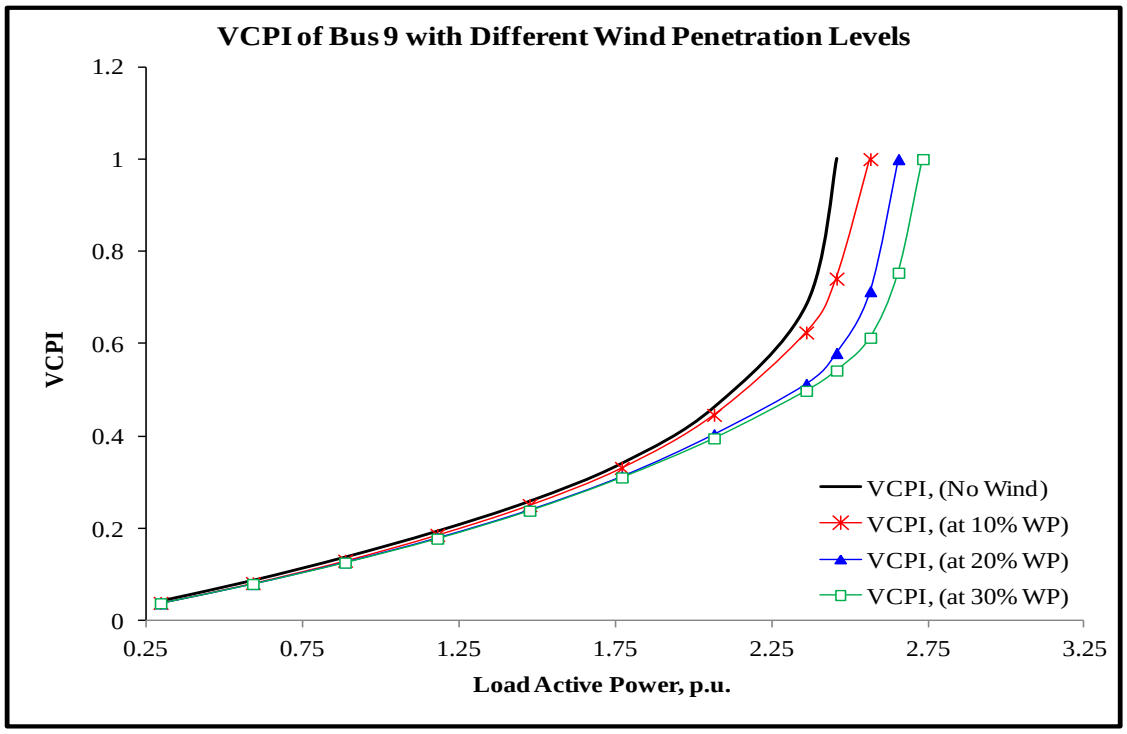

Figure 5.7: VCPI of bus 9 (IEEE-14 bus system) at different wind penetration levels when the load at bus 9 is varied at constant power factor; the wind farm is connected to bus 4 only.

5.4.1.1.2 The Effect of Wind Farm Location

This section aims to discuss the effect of wind farm location on IEEE14-bus system voltage stability. In addition, a voltage collapse proximity indicator, based on network loadability, is used to study the impact of wind farm location on voltage stability. In this section, results for 3 wind generation connection scenarios are considered and compared to the base case when no wind generator is connected to the network. One wind farm is located at bus 4 in the first connection scenario, then the same wind farm is connected to bus 12 in the second scenario.

In the third connection scenario, the wind farm is connected to buses 4 and 12 simultaneously with a combination wind penetration level. The simulation will be processed under 20% and 30% penetration level of wind generation. Table 5.4 shows the wind penetration level and locations connected at these buses.

Table 5.4: The 30% wind penetration level and different locations.

% Wind Penetration (WG4)	% Wind Penetration (WG12)	% of Combination Wind Penetration	
		(WG4, WG12)	% of Total
20% (260 MW)	20% (260 MW)	10% (130 MW), 10% (130 MW)	20% (260 MW)
30% (390 MW)	30% (390 MW)	15% (195 MW), 15% (195 MW)	30% (390 MW)

As mentioned in section 5.4.1.2 above, each simulation run uses one hour data of load and wind generation. By using the proposed method, the voltage collapse proximity indicator is calculated for a certain load bus for the maximum output of each wind penetration level at a specific time step simulation. Buses 14 and 10 are selected separately for investigating each scenario of wind penetration and wind location. The results are presented here to assess the impact wind farm location has on system voltage stability. Figures 5.8, 5.9, 5.10 and 5.11 show the variation of the VCPI of buses 14 and 10 with load at 20% and 30% wind penetration levels. Wind farms are connected to the network according to the three different connection scenarios defined previously and compared to the base case (i.e. when no wind is connected to the system).

It can be seen from Figure 5.8 that the VCPI of bus 14 reaches the value 1.0 as the load at bus 14 reaches maximum loading at 1.308 p.u for the base case (no wind), 1.334 p.u for 20% wind penetration when wind generation is connected at bus 4 (strong bus), 1.201 p.u for the same wind penetration when wind generation is connected at bus 12 (weak bus), and 1.304 p.u for 20% combination wind penetration when wind generation is connected to buses 4 and 12. Compared to the base case, the voltage stability is improved only when wind generation is connected to a stronger bus. The reverse is true when wind generation is connected to a weaker bus or multiple locations of wind farms at the same wind penetration level. FACTS devices such as SVC and STATCOM are required to support voltage stability when DFIG is located at a weaker bus.

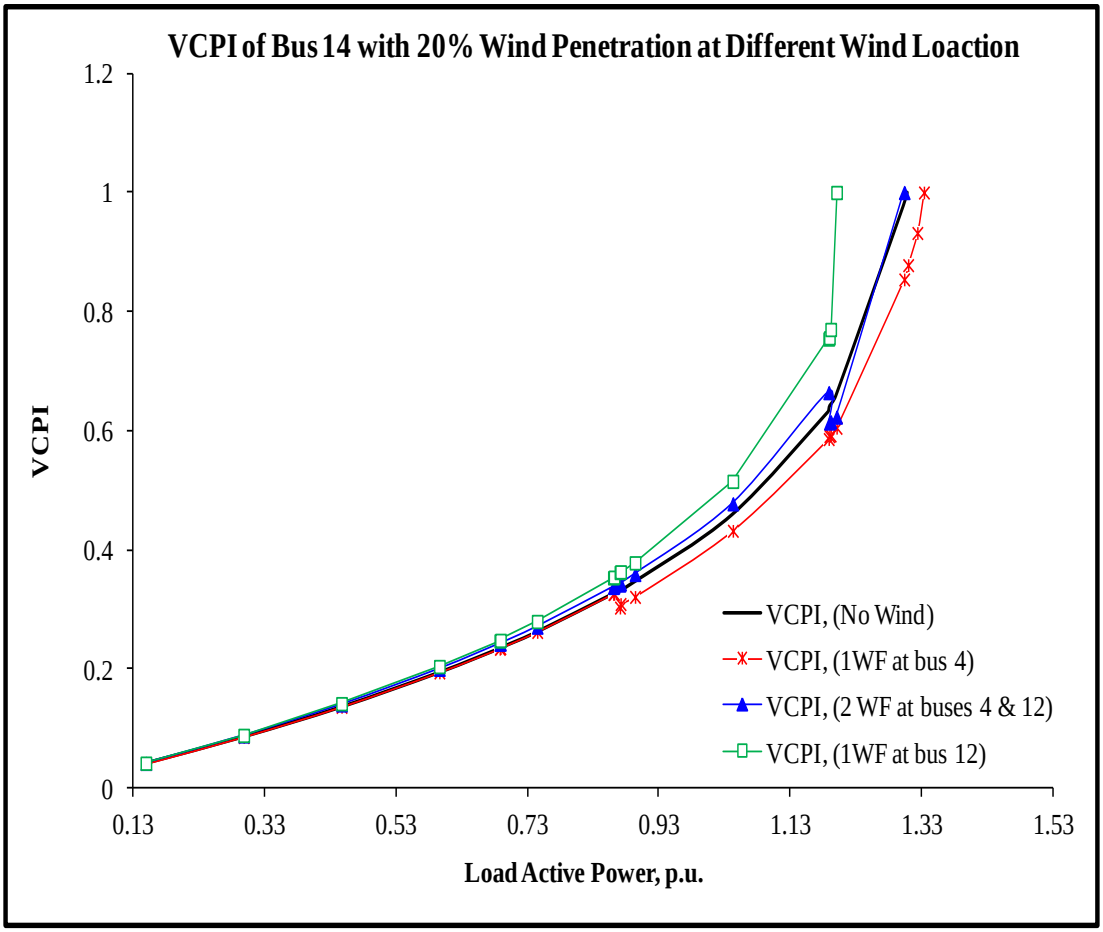

Figure 5.8: The variation of load with the VCPI of bus 14 (IEEE-14 bus) at 20% wind penetration level; the wind farm is connected to a network at different connection scenarios.

Figure 5.9 shows that the variation of the VCPI with load at bus 10 with 20% penetration level. The VCPI reaches the value of 1.0 when the load at the bus reaches maximum loading at 1.638 p.u for the base case, 1.725 p.u when the wind generator is at bus 4, 1.571 p.u when the wind generator is at bus 12, and at 1.68 p.u when the two wind farms are connected at buses 4 and 12 with a combination of wind penetration levels. The results show that, from the voltage stability point of view, the doubly fed induction generator being connected to a stronger bus (bus 4) is a better option and will improve system voltage stability more than when the wind generator is connected to other buses, as shown by the VCPI.

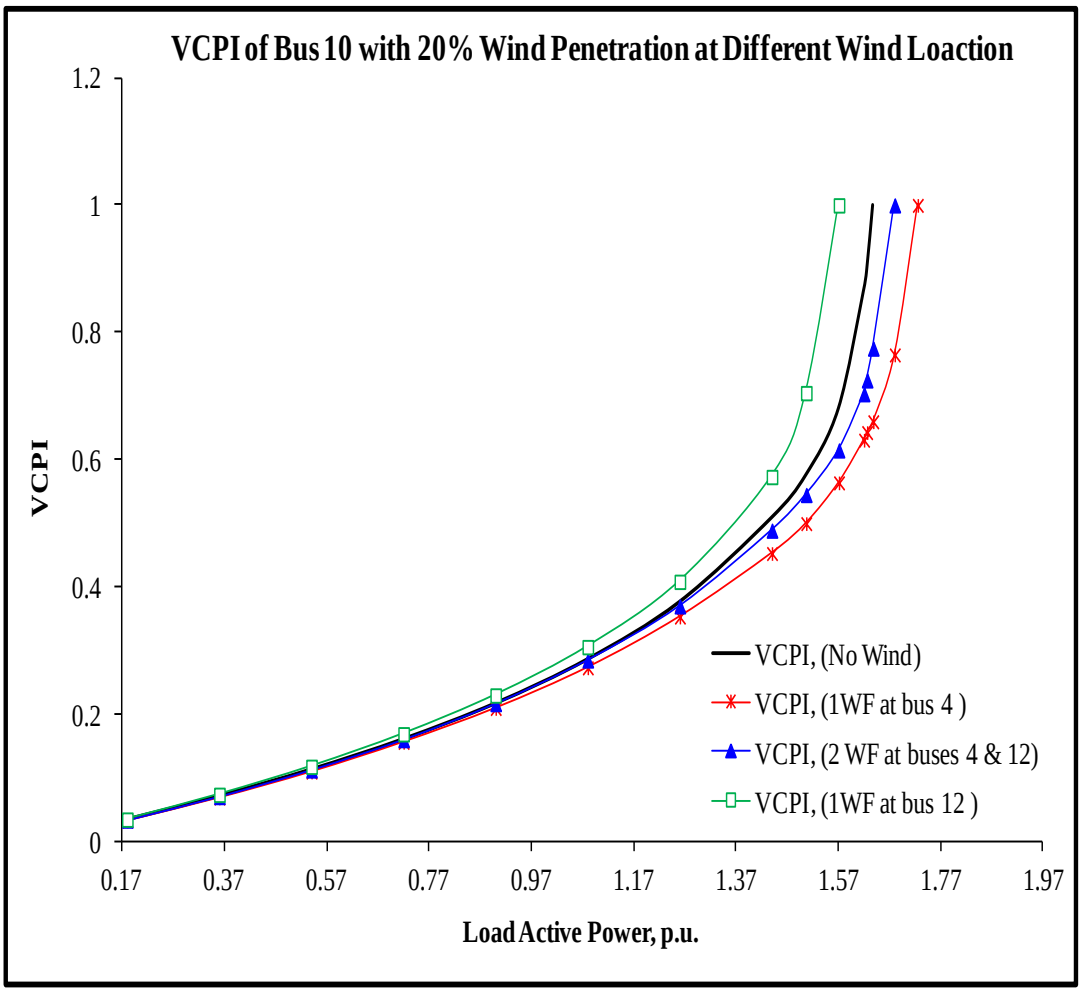

Figure 5.9: The variation of load with the VCPI of bus 10 (IEEE-14 bus) at 20% wind penetration level; the wind farm is connected to a network at different connection scenarios.

Figures 5.10 and 5.11 show that at the high wind penetration level, the system voltage stability is better for one connection location when the wind farm is connected to a stronger bus compared to other location scenarios according to the VCPI point at maximum loading for buses 14 and 10. Reactive power compensation (e.g. SVC) may still be necessary, especially if a large penetration of DFIG is connected to a weak area.

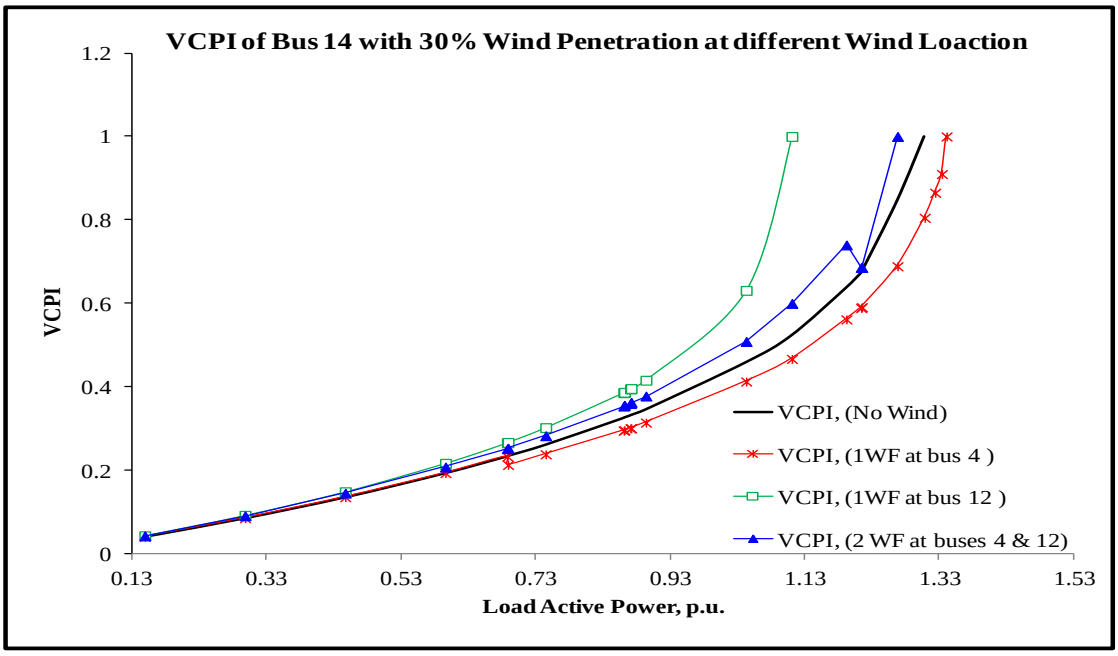

Figure 5.10: The variation of load with the VCPI of bus 14 (IEEE-14 bus) at 30% wind penetration level, when wind farm connected to a network at different connection scenarios.

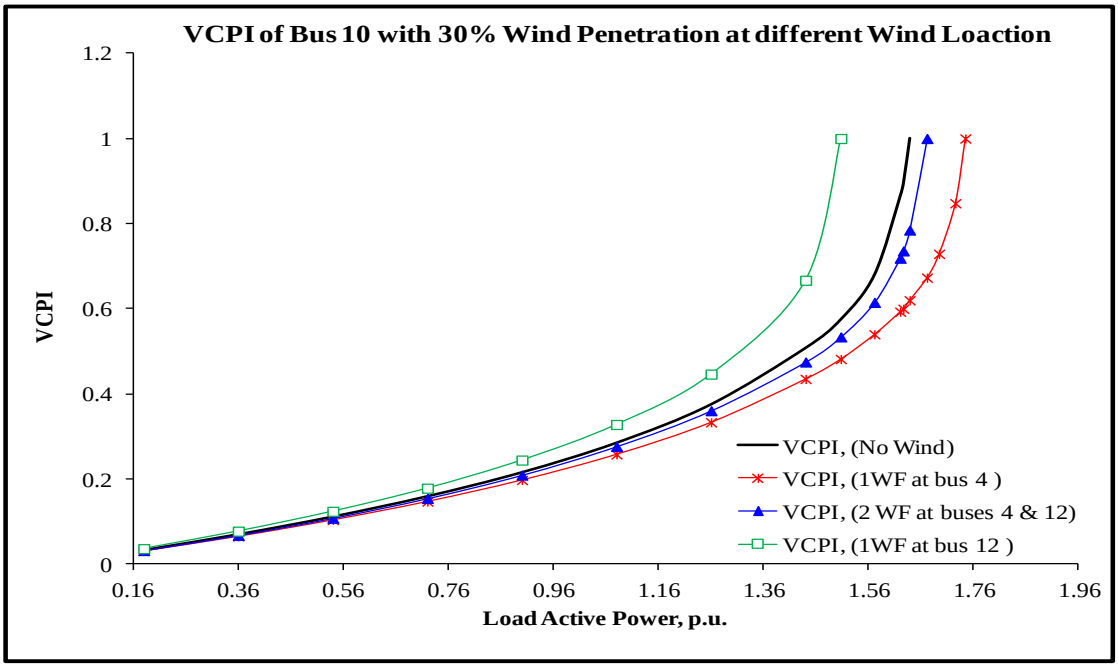

Figure 5.11: The variation of load with the VCPI of bus 10 (IEEE-14 bus) at 30% wind penetration level; the wind farm is connected to a network at different connection scenarios.

5.4.1.1.3 The Effect of Fluctuation of Wind Generation Output

This study concentrates on peak load when large and sudden changes in power are injected into the network from the wind generation output. In this case study, the simulation is conducted using the same system (IEEE-14 bus system), operated under 30% wind energy penetration level. Only one wind generator at bus 4 is considered for evaluating the impacts from intermittency of wind generation output. The values of the wind power output, conventional generators output and load model are used as inputs to the simulator and variables for a single month period. A one hour interval is used for the simulation time step function. This implies that for a 24 hour period, 24 time points will need to be used to calculate the value of VCPI for each time point. Buses 10 and 14 of the IEEE-14 bus are selected for evaluating the impact because they are critical and prone to voltage instability. It is assumed that some total loads at some time points in the load profile are the same. For example, the values of a peak load at 17:00 and 18:00 pm are the same. Figure 5.12 shows a plot of the load profile for buses 10 and 14 for 24 hours.

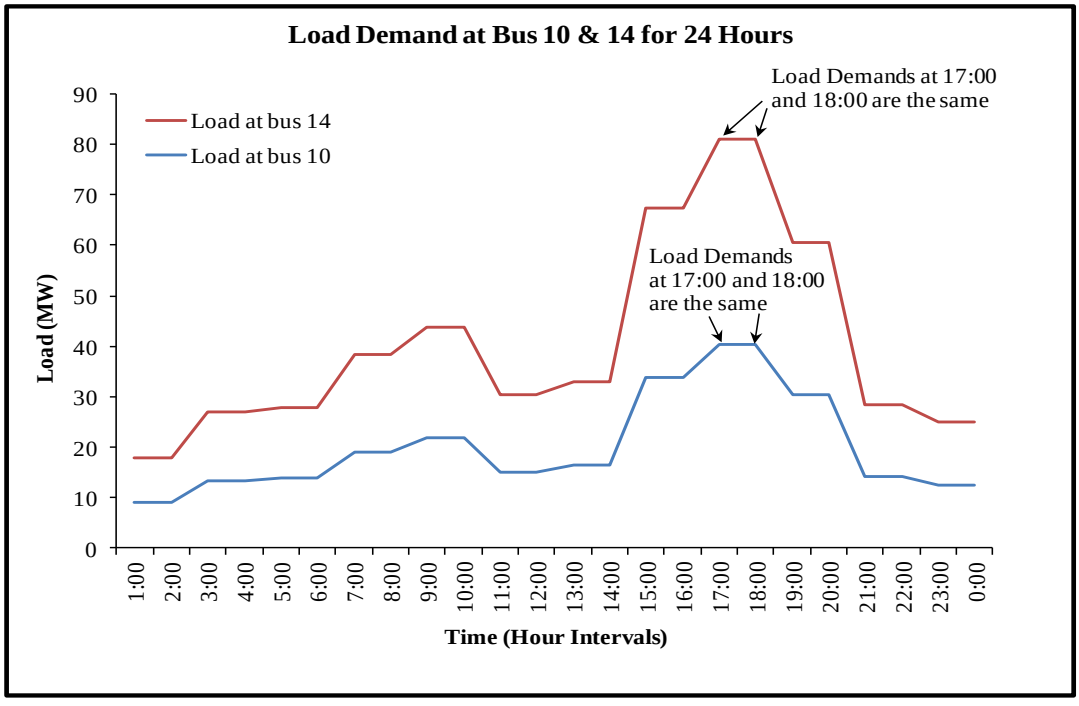

Figure 5.12: Load profile (MW) for buses 10 and 14 for 24 hours.

Figure 5.13 and 5.14 shows a plot of the VCPI values and the load at buses 14 and 10, respectively. The fluctuation of wind generation output at 30% penetration level when wind generation is connected to the network at bus 4 is also illustrated. As shown in Figure 5.13, the peak load value of bus 14 at 17:00 and 18:00 is the same, and the value 0.2607 of VCPI at bus 14 is recorded at peak load when DFIG is at maximum output of 390 MW at 17:00. However, the value of VCPI increases to 0.336 at the same peak load at 18:00 when large and sudden changes in the wind power are injected into the network due to weather conditions. The DFIG output is 3.67 MW for weather conditions at 18:00. This means that the intermittency of wind generation output could potentially lead to a voltage instability problem during peak load according to the VCPI values shown in the figure.

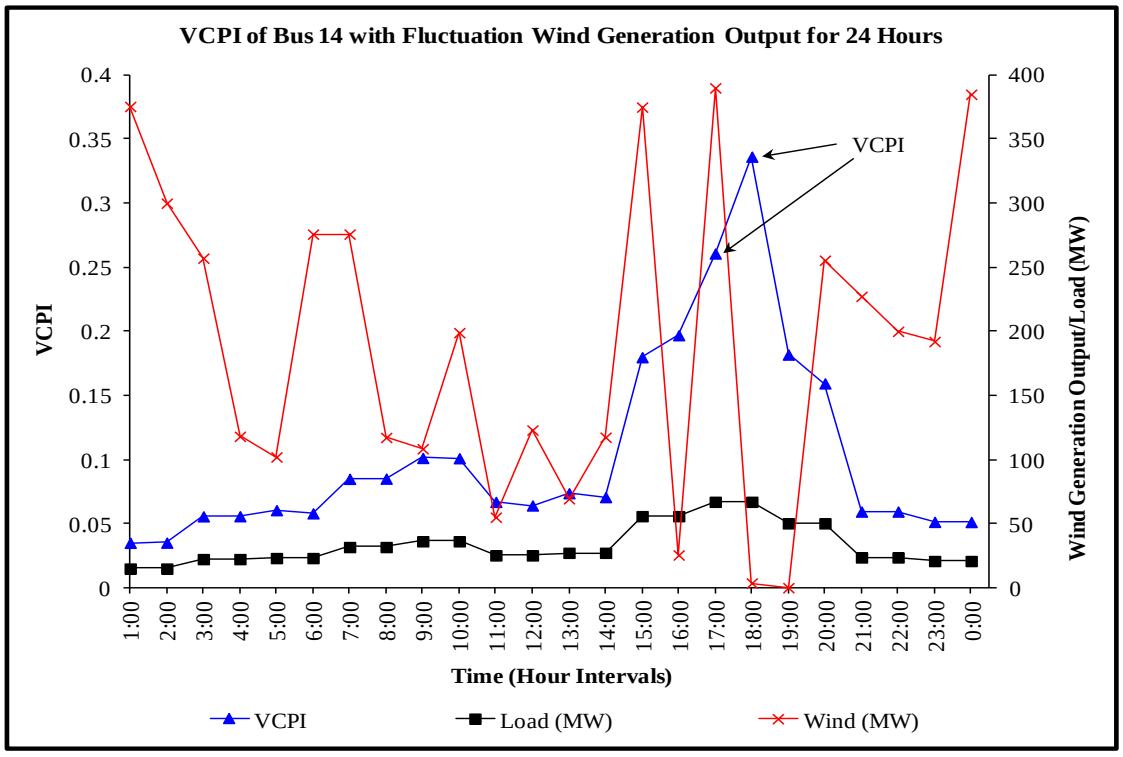

Figure 5.13: The VCPI values and load curve at bus 14 (IEEE-14 bus system) with fluctuation wind generation output for 24 hours; only one wind generation is connected at bus 4.

The value of VCPI at bus 10 is calculated and found to be 0.0979 at a peak load when wind generation is at maximum output. The value of VCPI increases to 0.1303 at the same peak load in the following time steps, when there is a large decrease in power output from wind generation, as shown in Figure 5.14. Large wind generation output fluctuations, especially during high system loadability, can lead to system voltage collapse according to the VCPI values.

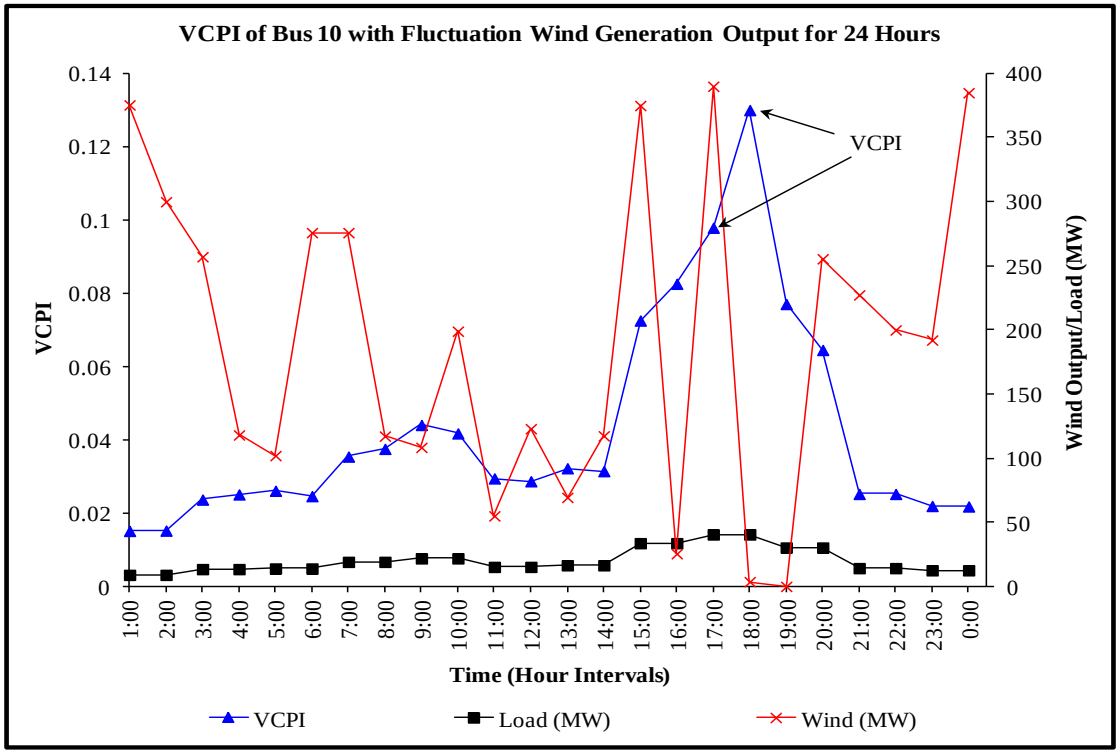

Figure 5.14: The VCPI values and load curve at bus 10 (IEEE-14 bus system) with fluctuation wind generation output for 24 hours; only one wind generation is connected at bus 4.

5.4.1.2 Modified IEEE-30 Bus Test System

In order to test the findings of section 5.3.1.1 using a bigger system, an IEEE-30 bus test system was modified by connecting one wind generation to bus 14, and on a second simulation run, wind generation was connected to bus 28. Then in the multiple locations scenario, wind generation was connected to buses 6 and 28 with different

penetration level combinations applied, as shown in Table 5.3. The wind generator input data for a day on the IEEE-30 bus system is shown in Figure 5.15. The single line diagram of the IEEE-30 bus system is shown in Figure 4.7. The total generation capacity was 1000 MW and the system peak load was 820 MW.

Table 5.5: Penetration level of wind generation scenarios for IEEE-30 bus system.

% Wind Penetration (WG14)	% Wind Penetration (WG12)	% of Combination Wind Penetration	
		(WG4, WG12)	% of Total
10% (100 MW)	10% (100 MW)	5% (50 MW), 5% (50 MW)	10% (100 MW)
20% (200 MW)	20% (200 MW)	10% (100 MW), 10% (100 MW)	20% (200 MW))
30% (300 MW)	30% (300 MW)	15% (150 MW), 15% (150 MW)	30% (300 MW)

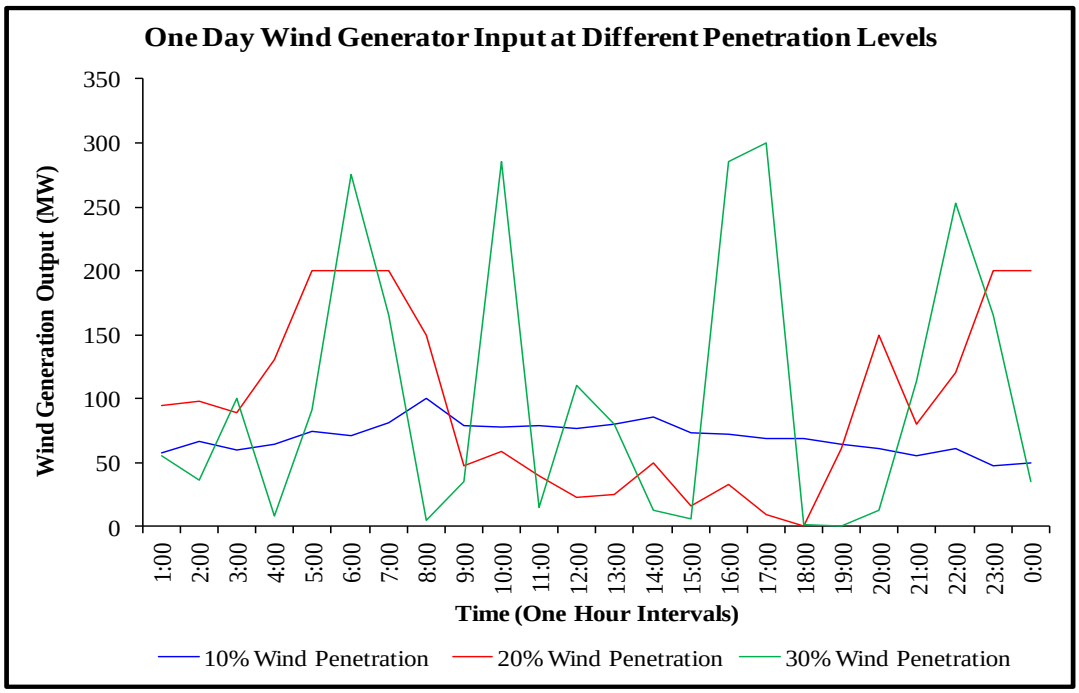

Figure 5.15: One day wind generator input at 10%, 20% and 30% penetration levels.

The inputs to the simulator are the wind generator power output from the wind farm, the output from the conventional generators, and the load profile for a simulation period of one month at one hour intervals. This procedure is repeated for each of the wind penetration levels and for each wind connection scenario. Similar to the IEEE-14 case in

section 5.3.1.1, the VCPI is calculated from different standpoints and used to evaluate the effect of wind penetration level, wind farm location, and the fluctuation of wind generation output on system voltage stability.

5.4.1.2.1 The Effect of Wind Penetration Level

Similar to the results for the IEEE-14 bus system, the VCPI is calculated for each wind penetration level (10% to 30%), then each case is compared to the VCPI when no wind is connected to the network. The wind data is monitored for the maximum output of each wind penetration level, and then the time step at which this occurs is identified. It is assumed that the wind speed during this time step is constant. The load is then gradually increased at a single bus until the collapse point, while other load buses in the system remain unchanged. The voltage collapse proximity indicator is calculated at this time step. Figures 5.16, 5.17 and 5.18 show a plot of the VCPI of buses 30, 24 and 19, respectively, when no wind generation is connected to the network and when wind generation is connected to bus 28 (as a strong bus) with 10%, 20% and 30% wind penetration levels.

As mentioned in Chapter 4, the voltage collapse occurs as the voltage collapse proximity indicator reaches a value of 1.0. The VCPI of bus 30 reaches a value of 1.0 as the load at bus 30 reaches maximum loading at 0.505 p.u for the base case (no wind), 0.5102 p.u for 10% WP (wind penetration), 0.511 p.u for 20% WP, and 0.516 p.u for 30% wind penetration, as shown in Figure 5.16. It can be seen in Figures 5.16-18 that the system voltage stability is improved with all wind penetration levels when the DFIG based wind farm with voltage controlled mode is integrated into the IEEE-30 bus at a stronger bus compared to the case with no wind. Moreover, 30% wind penetration level gives better improvement in system voltage stability compared to other cases according to the voltage collapse point at maximum loading for buses 30, 24 and 19, respectively.

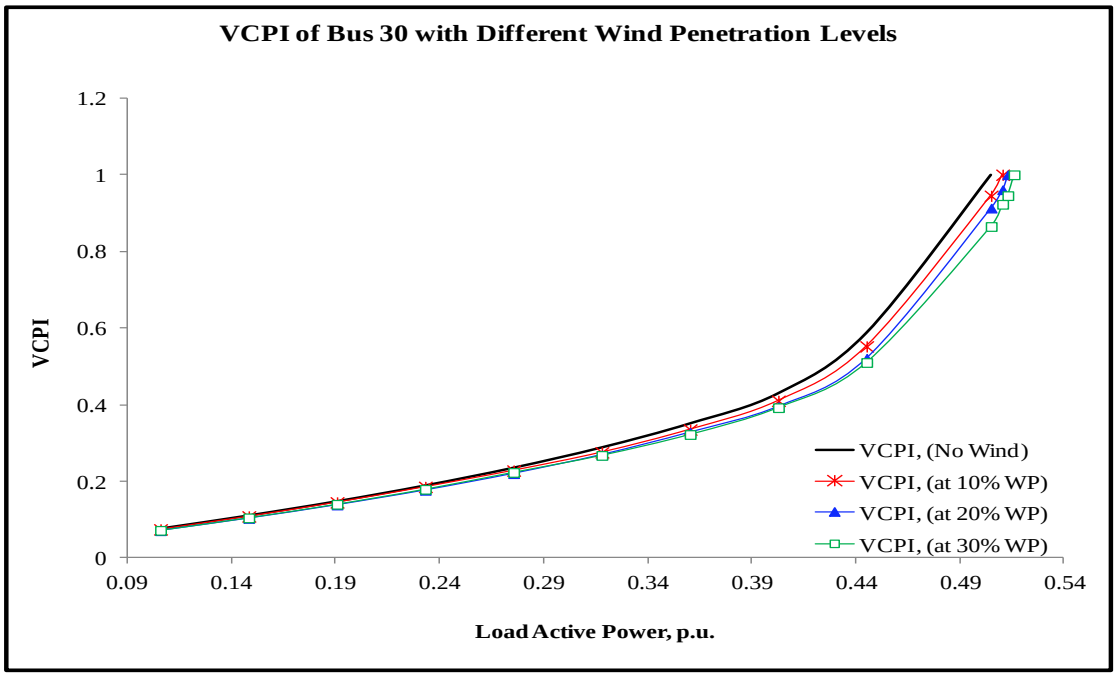

Figure 5.16: VCPI of bus 30 (IEEE-30 bus system) at different wind penetration levels when the load at bus 30 is varied at constant power factor; the wind farm is connected to bus 28 only.

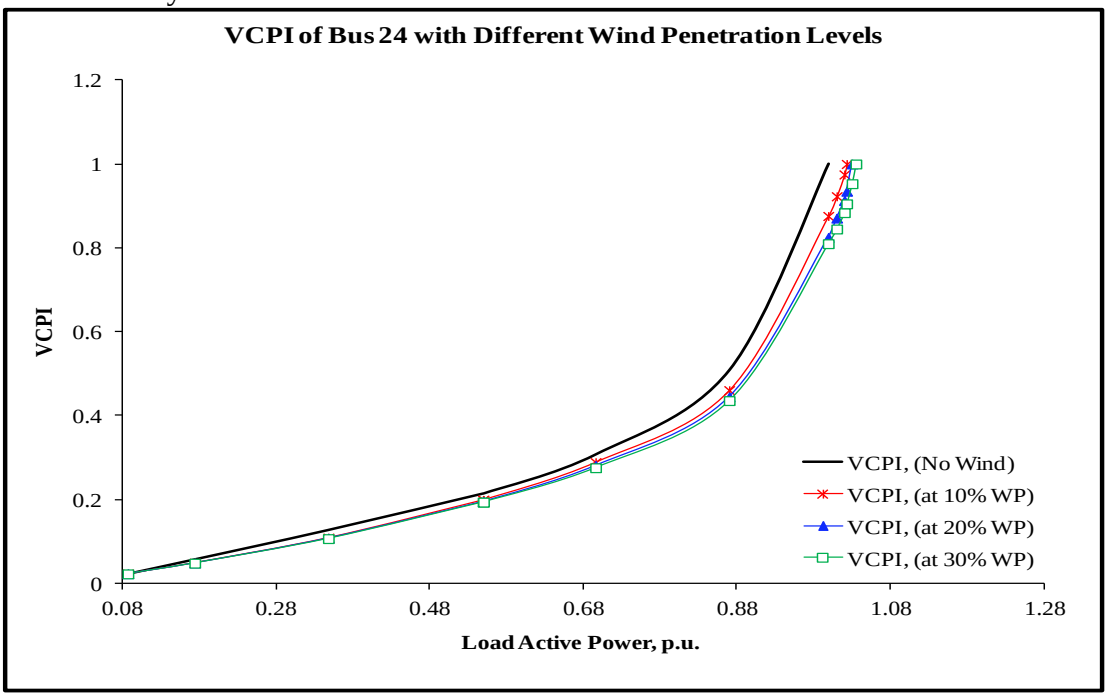

Figure 5.17: VCPI of bus 24 (IEEE-30 bus system) at different wind penetration levels when the load at bus 24 is varied at constant power factor; the wind farm is connected to bus 28 only.

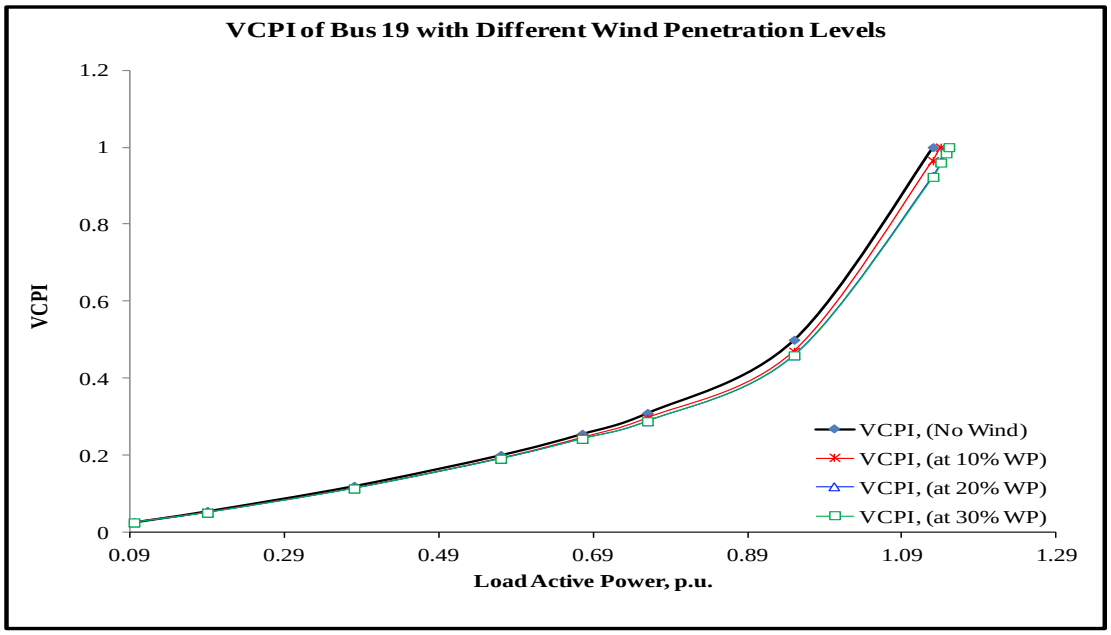

Figure 5.18: VCPI of bus 19 (IEEE-30 bus system) at different wind penetration levels when the load at bus 19 is varied at constant power factor; the wind farm is connected to bus 28 only.

5.4.1.2.2 The Effect of Wind Farm Location

The reason for connecting the wind farm at different buses is to show the effect of wind farm location on voltage stability from different areas in the network, and also to choose a suitable connection point bus for the wind farm which can improve the system voltage stability. As mentioned in Chapter 2, variable speed wind turbines equipped with voltage source converters have the capability of generating or absorbing reactive power and can be used as reactive power sources to control the voltage at grid terminals.

Results for 4 scenarios at IEEE-30 bus system are considered and compared in this section. No wind case is evaluated first to set a base case, then 3 wind farm location scenarios are used. These are a single wind farm located at the strong bus (bus 28), a single wind farm located at the weak bus (bus 14), and 2 wind farms connected at buses 6 and 28, which are evaluated with a combination of wind penetration levels. For each connection scenario, 20% and 30% wind penetration levels are considered and applied to

the proposed method. A voltage collapse proximity indicator, based on network loading, is calculated and used to investigate the impact wind farm location has on system voltage stability. Load buses 30 and 19 are selected separately for investigating each wind generation scenario. The VCPI values calculated from the simulation are plotted on Figures 5.19, 5.20, 5.21 and 5.22. Compared to the no wind case, the system voltage stability improves by connecting the wind farm (DFIG) to the strong bus 28, as seen by comparing the voltage collapse point at maximum loading in Figures 5.19-22. However, the results show that the system is more unstable when the wind farm is connected to the weak bus 14 according to the VCPI values at maximum loading compared to the no wind case, as shown in Figures 5.19-22. When DFIG is located at the weak bus 14, some bus voltages fall due to the reactive power consumed by DFIG, and appropriate reactive power support is required at the wind connection point or at weak areas in order to support and enhance the system voltage stability. The results also show that system voltage stability is better for a strong single location of wind generation compared to multiple locations.

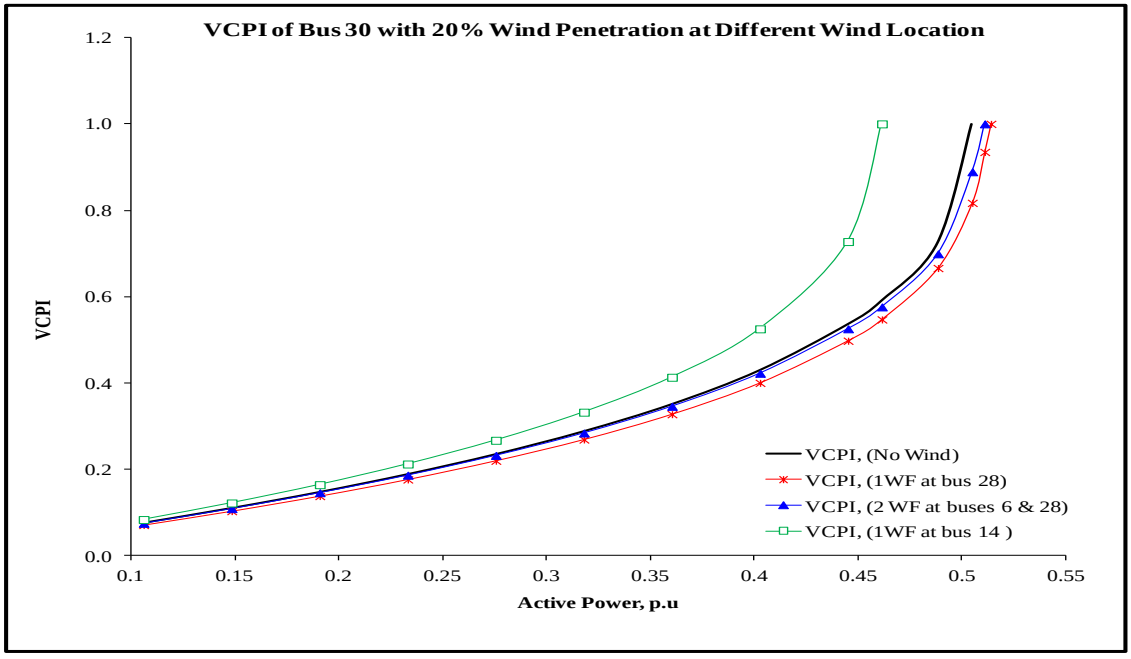

Figure 5.19: The variation of load demand with the VCPI of bus 30 (IEEE-30 bus) at 20% wind penetration level; the wind farm is connected to a network at different connection scenarios.

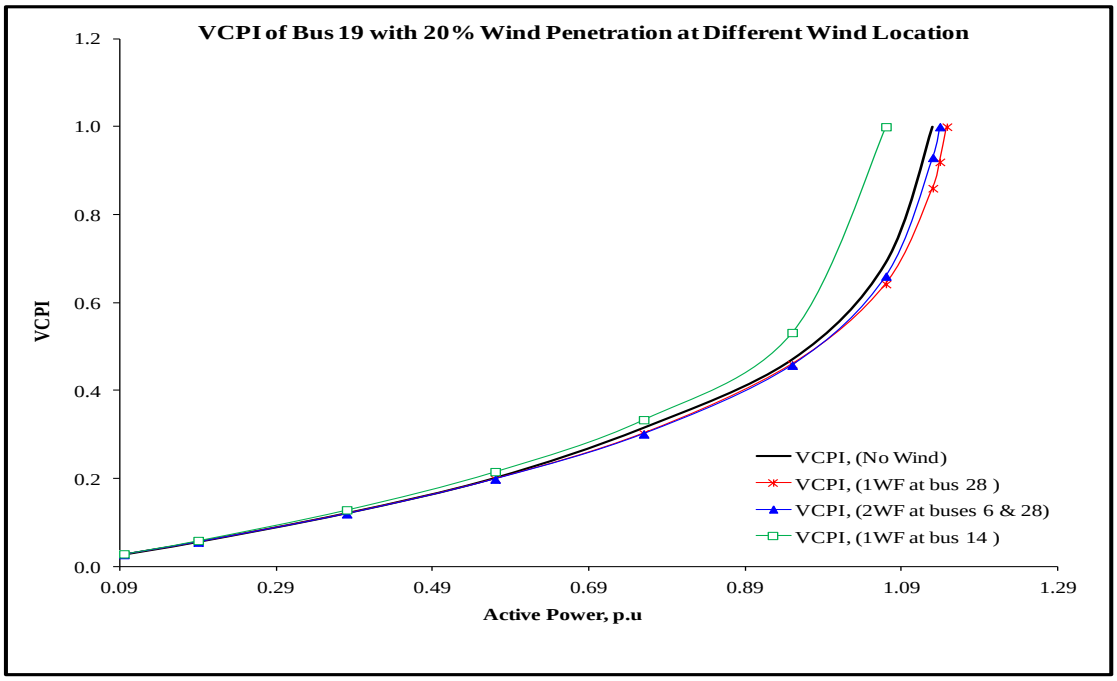

Figure 5.20: The variation of load demand with the VCPI of bus 19 (IEEE-30 bus) at 20% wind penetration level; the wind farm is connected to a network at different connection scenarios.

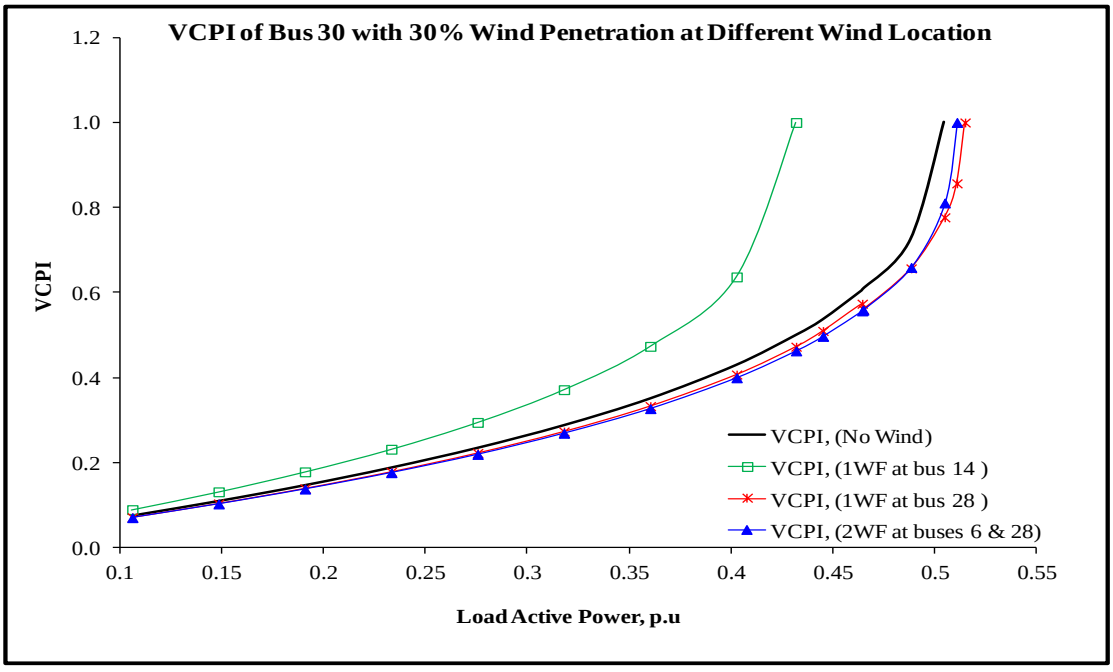

Figure 5.21: The variation of load demand with the VCPI of bus 30 (IEEE-30 bus) at 30% wind penetration level; the wind farm is connected to a network at different connection scenarios.

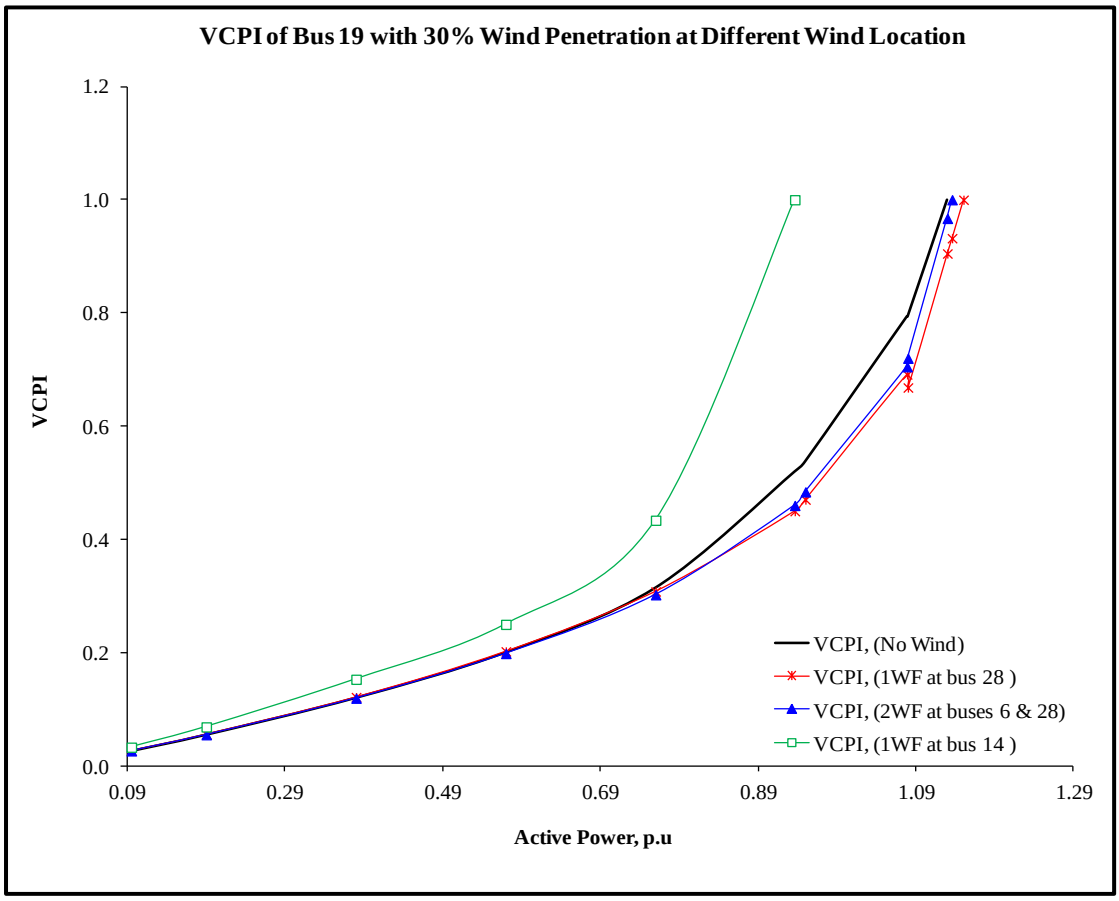

Figure 5.22: The variation of load demand with the VCPI of bus 19 (IEEE-30 bus) at 30% wind penetration level; the wind farm is connected to a network at different connection scenarios.

5.4.1.2.3 The Effect of Fluctuation of Wind Generation Output

The aim of this section is to study the impact of wind generation intermittency on voltage stability when system load is at its peak. The system is based on the IEEE-30 bus system, which is operated with 30% wind energy penetration level and only one wind generator at bus 28. It is considered for evaluating the impact from intermittency of wind generation output. One hour intervals are used in the time step function. This means that for a 24 hour period, the value of VCPI is calculated at 24 time points. Bus 30 is selected for study, because it is sensitive to voltage instability. It is assumed that the peak load at 17:00 and 18:00 are the same. A plot of the load profile for bus 30 for 24 hours is shown in Figure 5.23.

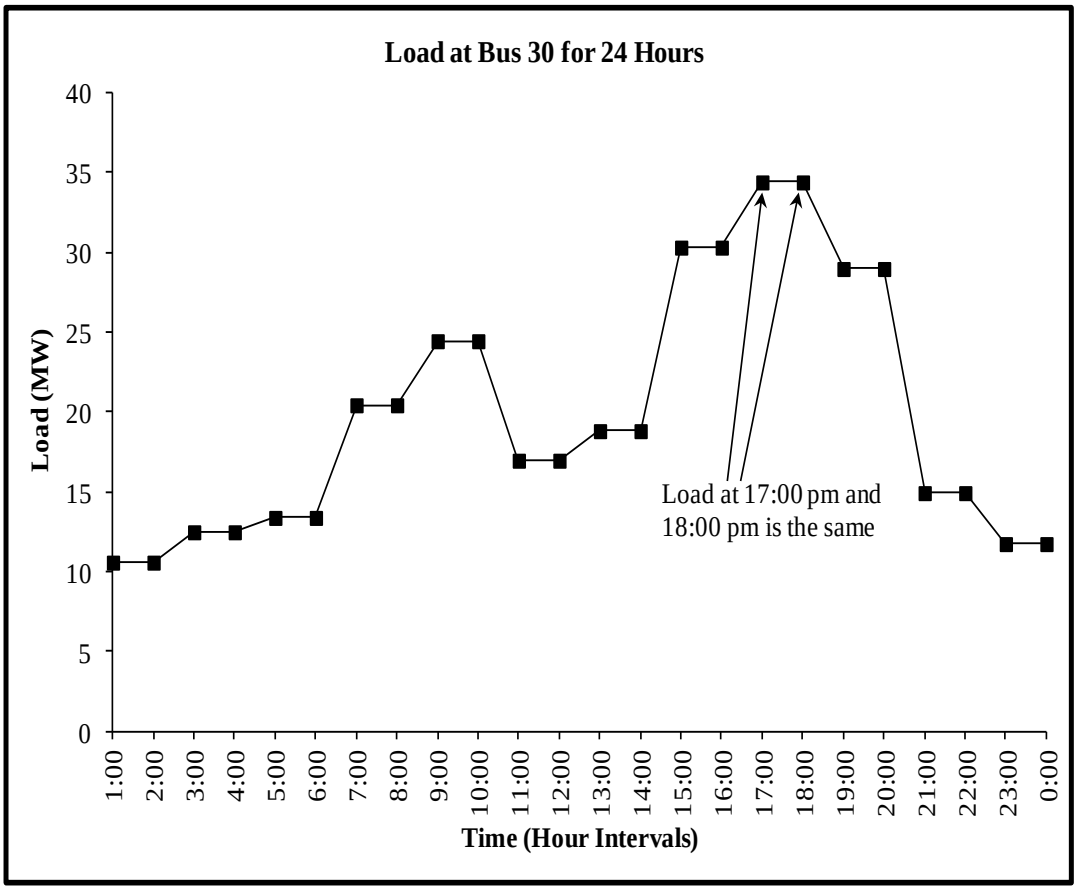

Figure 5.23 A plot of the load profile for bus 30 (IEEE-30 bus system) for 24 hours.

The value of VCPI at bus 30 is calculated and found to be 0.568 at peak load (at 17:00) as wind generation is at maximum output (300 MW). The value of VCPI increases to 0.814 at the same peak load in the following time step (18:00) when there is a large and sudden decrease in wind injected into the system caused by wind conditions, as shown in Figure 5.24. Unfortunately, large wind generation output fluctuations, especially during high system loading, can lead to serious voltage instability problems according to VCPI values. System protection devices are required and load shedding may be necessary to protect the system from the risk of voltage collapse due to large and sudden changes in the power injected into the network during system peak load.

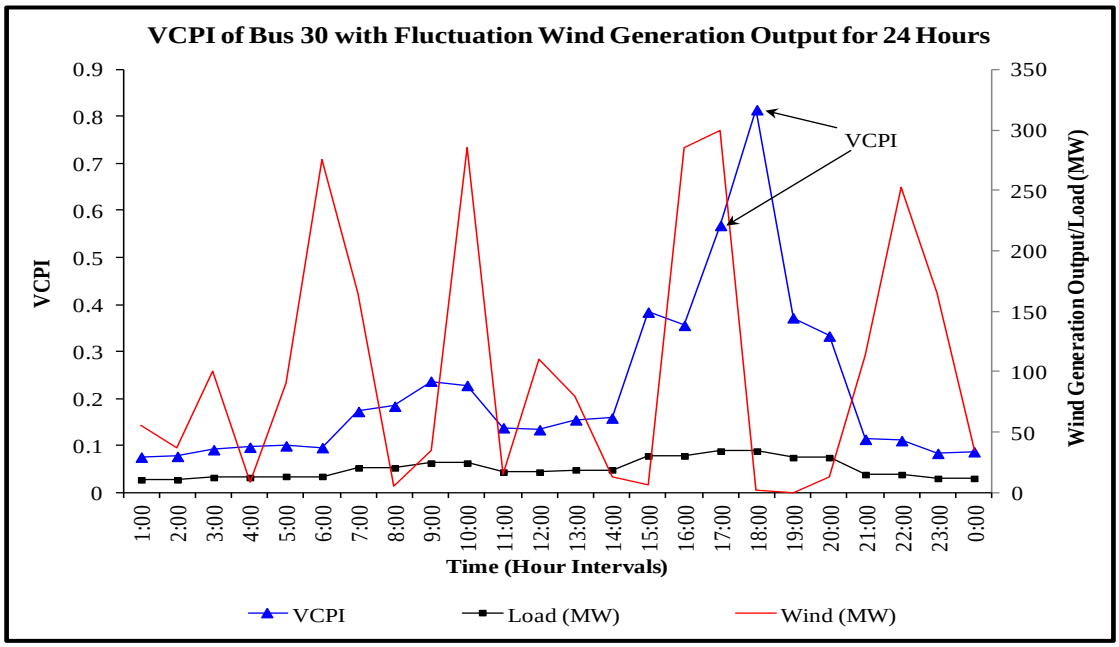

Figure 5.24: The VCPI values and load curve at bus 30 (IEEE-30 bus system) with fluctuation wind generation output for 24 hours; only one wind generation is connected at bus 28.

5.4.1.3 A 61-bus Radial Distribution Network

In order to test the proposed method on a low-voltage distribution network, a 61-bus radial distribution network has been modelled in PowerWorld®Simulator. Wind generation is connected at different locations of the network and these locations are identified as critical points. The level of wind penetration is varied systematically to assess the influence on voltage stability. Also, the impact takes into consideration the intermittent nature of wind generation. Additionally, a voltage collapse proximity indicator, based on network loadability, is employed to investigate the contribution of wind generation to voltage stability. Figure 4.9 shows the 61-bus radial distribution network with two thermal generators which supply power to the 18 load points through a 132/33/11 kV substation. The total generation capacity is 80 MW. The farm consists of several variable speed doubly fed induction generator (DFIG) wind turbines, each of 1.5 MW. In this assessment, DFIG is modelled as a PV bus and operated with maximum and minimum power factors of 0.95 leading (capacitive VAr) and 0.95 lagging (inductive

VAr). The different connection scenarios of wind generation are as follows: in the first scenario one wind farm connected to bus 12, in the second scenario the same wind farm is located at bus 35, and in the third scenario two wind farms are connected to buses 12 and 28, respectively, with different combinations of penetration levels. Table 3.3 shows the combinations of penetration levels and locations connected at buses 12 and 28. A typical wind generation input for two consecutive days at one hour intervals is plotted in Figure 5.25.

Table 5.6: Different wind penetration levels and different locations for UKGDS 61-bus.

% Wind Penetration (WG12)	% Wind Penetration (WG35)	% of Combination Wind Penetration	
		(WG12, WG28)	% of Total
10% (8 MW)	10% (8 MW)	5% (4MW), 5% (4 MW)	10% (8 MW)
20% (16 MW)	20% (16 MW)	10% (16 MW), 10% (16 MW)	20% (16 MW))
30% (24 MW)	30% (24 MW)	15% (12 MW), 15% (12 MW)	30% (24 MW)

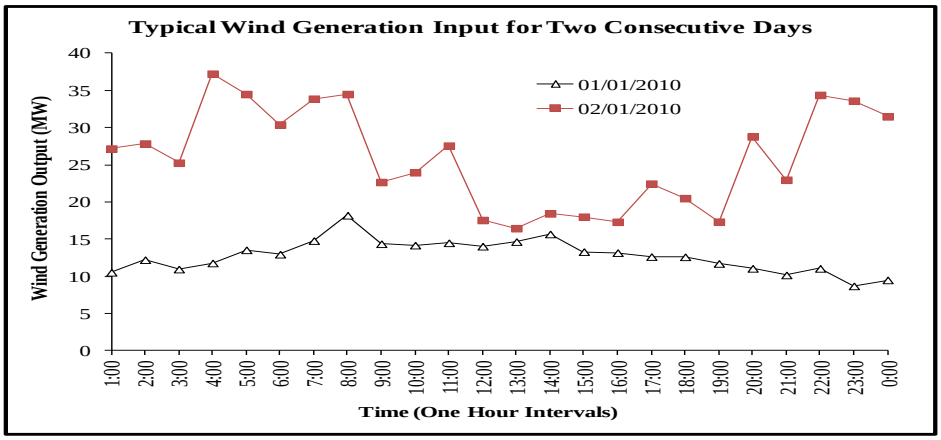

Figure 5.25: A typical wind generation input for two consecutive days.

The inputs to the modified test system in the Power World® Simulator are the variables. These inputs are connected to the test system at one hour time steps continuously for one month. The wind generation is varied from 10% to 30% of the total connected load in the network; for each of the scenarios, the voltage collapse proximity indicator (VCPI) is calculated. The impact results of wind generation outputs on system voltage stability are presented in the following sections.

5.4.1.3.1 The Effect of Wind Penetration Level

Similar to simulation procedures conducted on the IEEE-14 bus and IEEE-30 bus systems, the analysis concentrates on maximum wind generator output for each penetration level. In this simulation, only one wind farm is located at bus 12, with wind penetration levels from 10% to 30%. Similar to the IEEE-14 case, the VCPI is calculated at specific time step simulation in which the maximum wind generation output occurs. Figures 5.26, 5.27 and 5.28 show a plot of the VCPI of buses 58, 51 and 45, respectively, at different wind penetration levels. The study concentrates on the voltage collapse point and maximum loading, and the collapse point is used as a proximity indicator to show the impact of wind generation. It can be seen from the figures that the VCPI reaches a value of 1.0 at the maximum admissible load.

The VCPI of bus 58 reaches the value of 1.0 as the load at bus 58 reaches maximum loading at 0.0883 p.u for the base case (no wind), 0.093 p.u for 10% WP, 0.0981 p.u for 20% WP, and 0.1053 p.u for 30% wind penetration, as shown in Figure 5.5. It can be concluded from figures 5.26-28 that the system voltage stability is improved with all wind penetration levels when a DFIG based wind farm with voltage controlled mode is integrated into the 61-bus radial distribution network at the stronger bus. Furthermore, the 30% wind penetration level provides better improvement compared to other cases according to the voltage collapse point at maximum loading. In other words, a DFIG based wind farm with voltage controlled mode has improved the voltage collapse margin of the system at penetration levels 10% to 30%. Furthermore, higher penetration levels showed a larger improvement and there was a positive effect on voltage stability of the network when the penetration level increased.

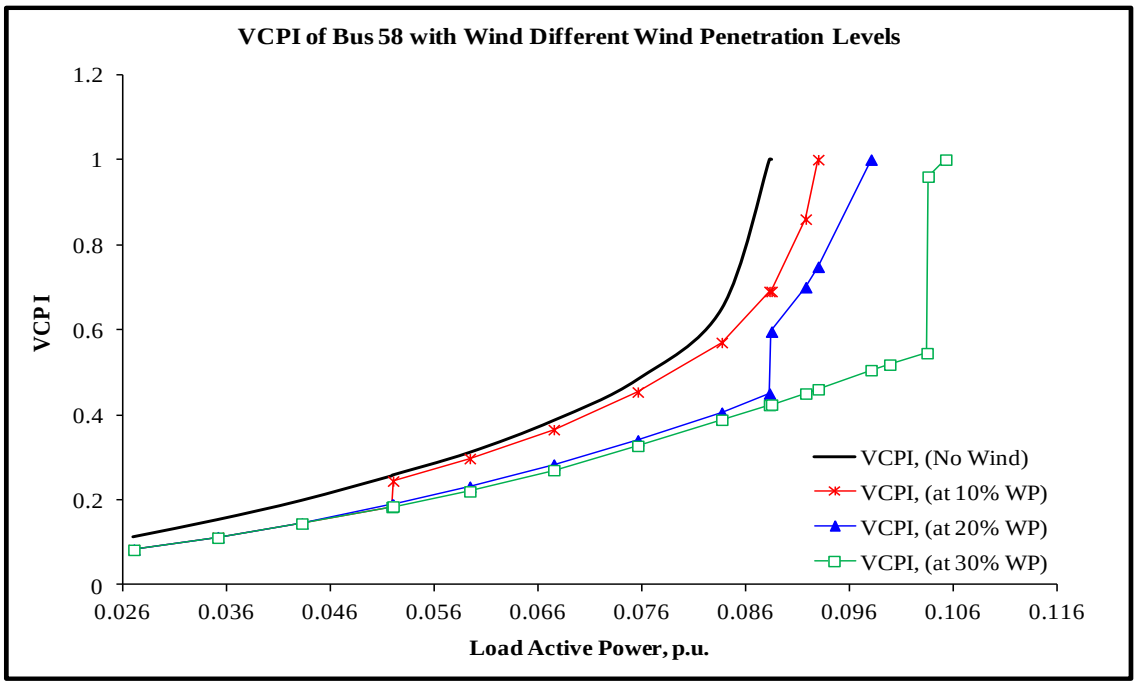

Figure 5.26: VCPI of bus 58 (UKGDS 61-bus radial distribution network) at different wind penetration levels when the load at bus 58 is varied at constant power factor; the wind farm is connected to bus 12 only.

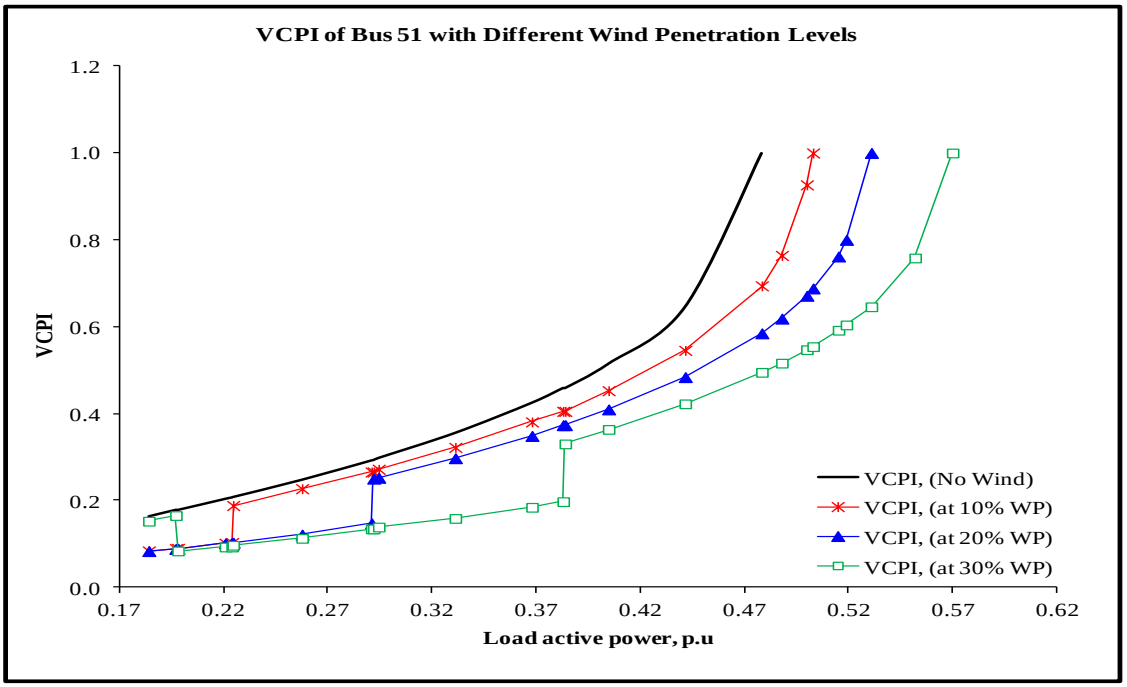

Figure 5.27: VCPI of bus 51 (UKGDS 61-bus radial distribution network) at different wind penetration levels when the load at bus 51 is varied at constant power factor; the wind farm is connected to bus 12 only.

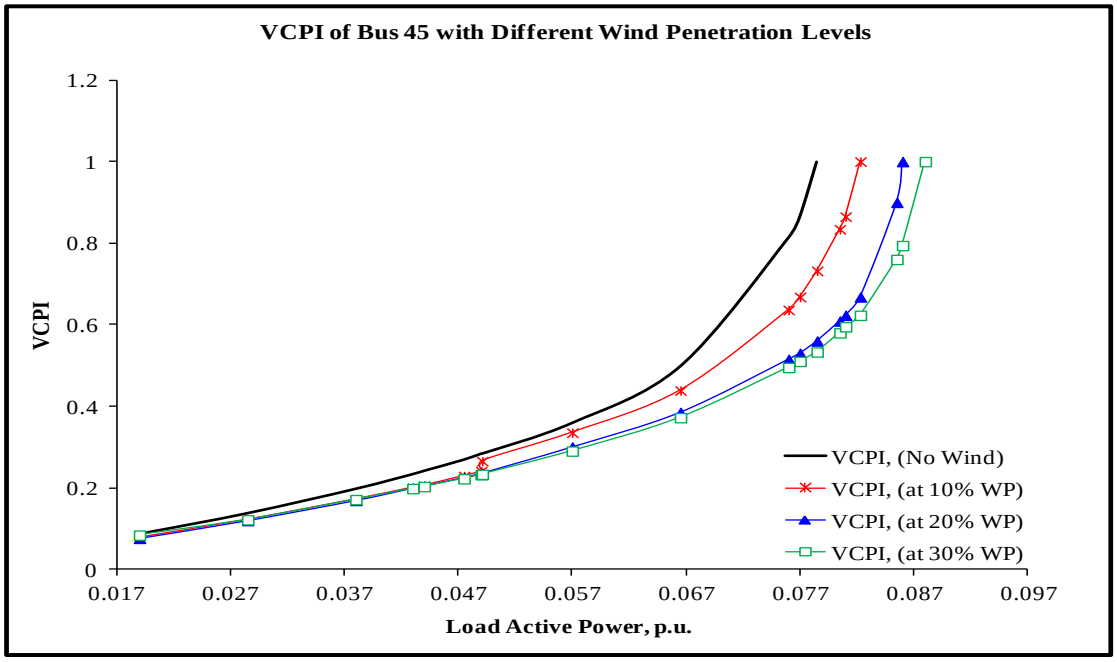

Figure 5.28: VCPI of bus 45 (UKGDS 61-bus radial distribution network) at different wind penetration levels when the load at bus 45 is varied at constant power factor; the wind farm is connected to bus 12 only.

5.4.1.3.2 The Effect of Wind Farm Location

In this section, three wind connection scenarios are used to investigate the impact of wind farm location on system voltage stability. These scenarios are as follows: in the first scenario one wind farm is connected to a strong bus 12, in the second scenario one wind farm is located at a weak bus 35, and in the third connection scenario two wind farms are connected to buses 12 and 28, with a combination of wind penetration levels. The reason for connecting the wind output at more than one bus is to show the effect of dispersing the wind power around the network. For each connection scenario, 20% and 30% wind penetration levels are considered and applied to the proposed method. A voltage collapse proximity indicator, based on network loadability is calculated and used to measure the impact. Load buses 58 and 45 are selected separately for investigating each wind generation scenario. The selection is based on the fact that a wide range of locations is covered to show the impact of wind generation output on the whole network. The VCPI values calculated are plotted on Figures 5.29,

5.30, 5.31 and 5.32. Compared to the no wind the case, system voltage stability is improved by connecting the wind farm (DFIG) to strong bus 12, as seen by comparing the VCPI value at the collapse point at maximum loading in Figures 5.29-32. On the other hand, the DFIG with voltage control mode might weaken the system voltage stability when DFIG is connected to weak bus 35, according to the voltage collapse point at maximum loading compared to the base case (no wind), as shown in Figures 5.29-32. It is clear from Figure 5.31 that the VCPI of bus 58 reaches the value of 1.0 as the load at bus 58 reaches maximum loading at 0.0883 p.u for the no wind case, and 0.086 p.u for 20% wind penetration as the wind farm is located at weak bus 35. Also, the results show that the system voltage stability may worsen with higher wind penetration as wind is connected to bus 35, and reactive power compensation such as shunt capacitor and SVC is required to be installed at the wind connection point at bus 35 or at weaker areas to support system stability. The results show that system voltage stability is better for a single strong location compared to multiple locations of wind farms.

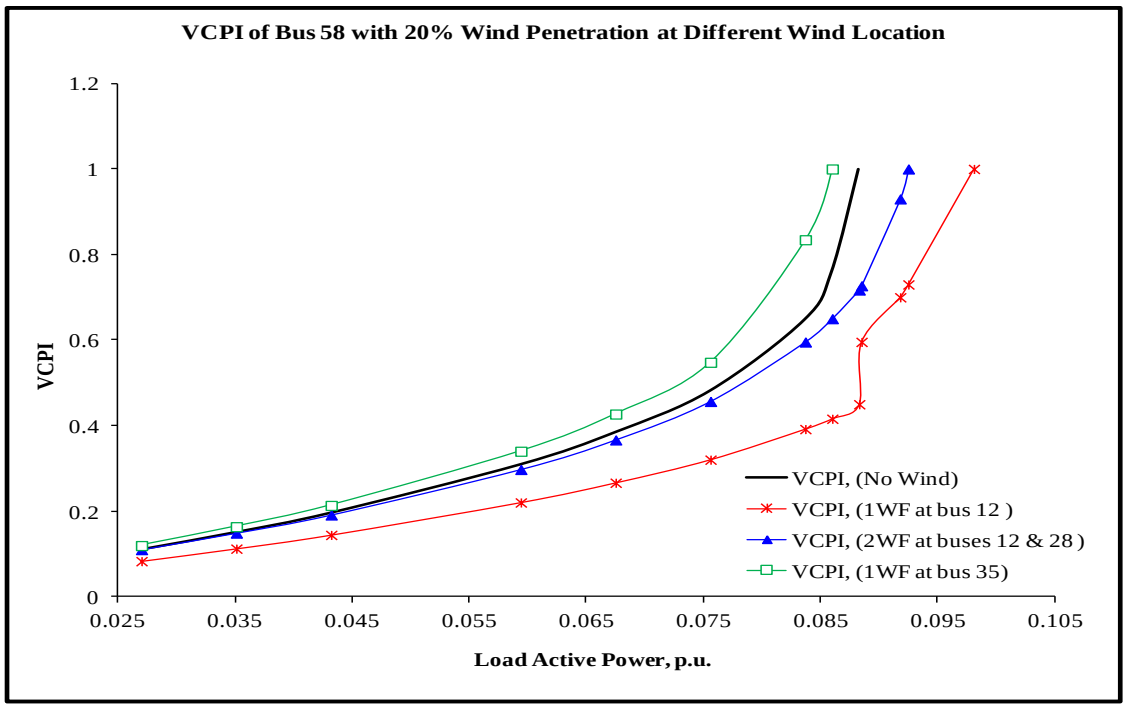

Figure 5.29: The variation of load demand with the VCPI of bus 58 (UKGDS 61-bus radial distribution network) at 20% wind penetration level, when the wind farm is connected to a network at different connection scenarios.

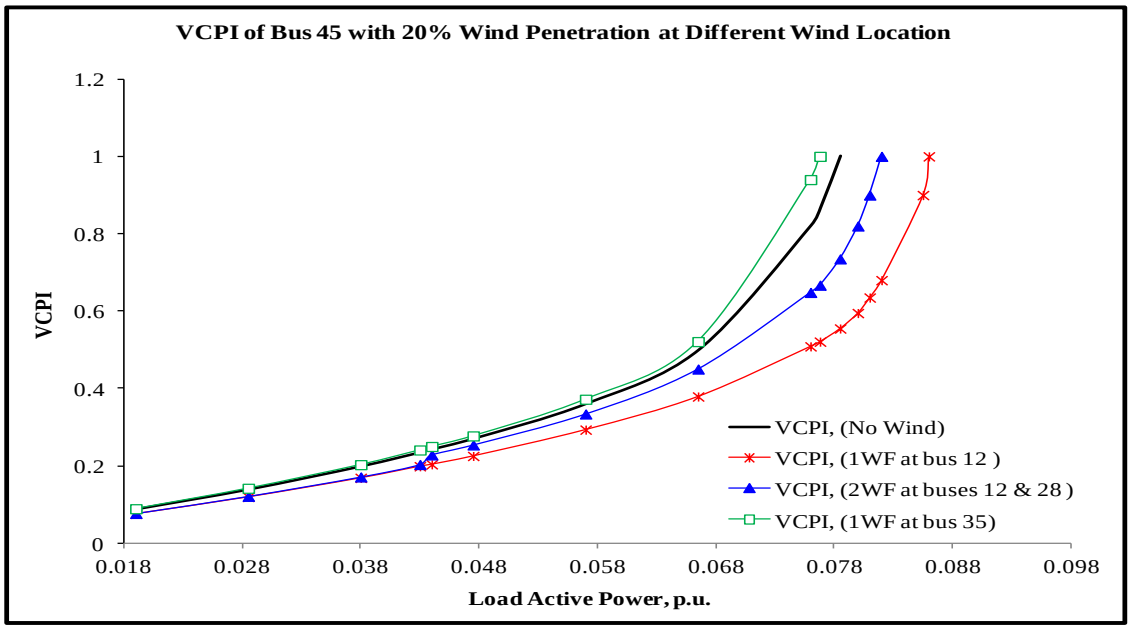

Figure 5.30: The variation of load demand with the VCPI of bus 45 (UKGDS 61-bus radial distribution network) at 20% wind penetration level, when the wind farm is connected to a network at different connection scenarios.

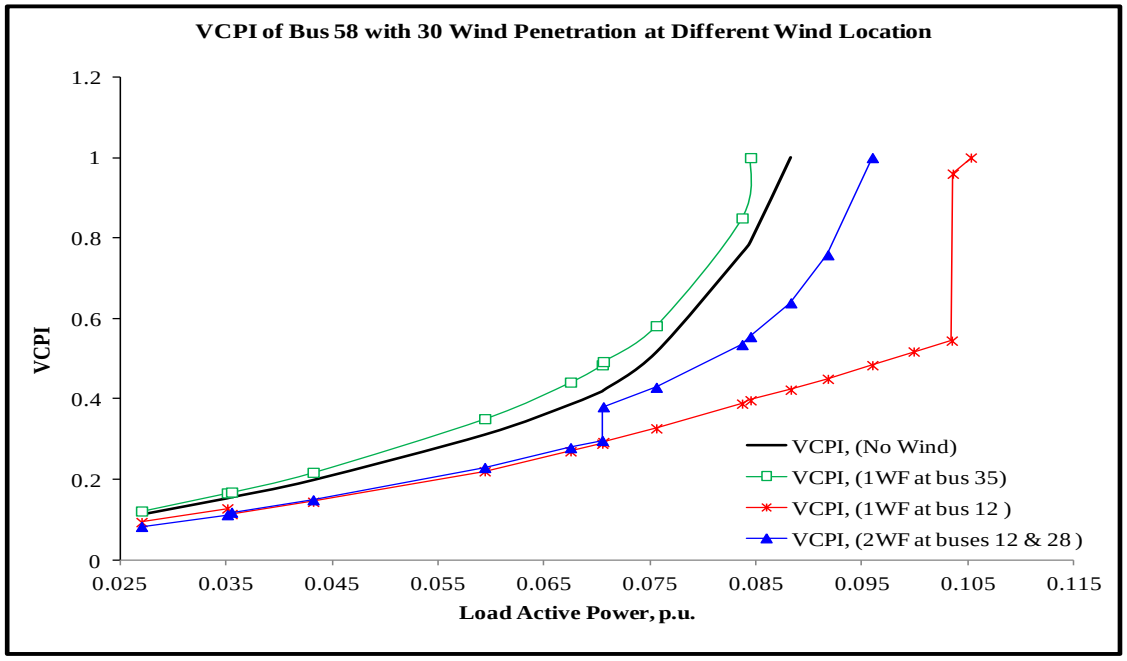

Figure 5.31: The variation of load demand with the VCPI of bus 58 (UKGDS 61-bus radial distribution network) at 20% wind penetration level, when the wind farm is connected to a network at different connection scenarios.

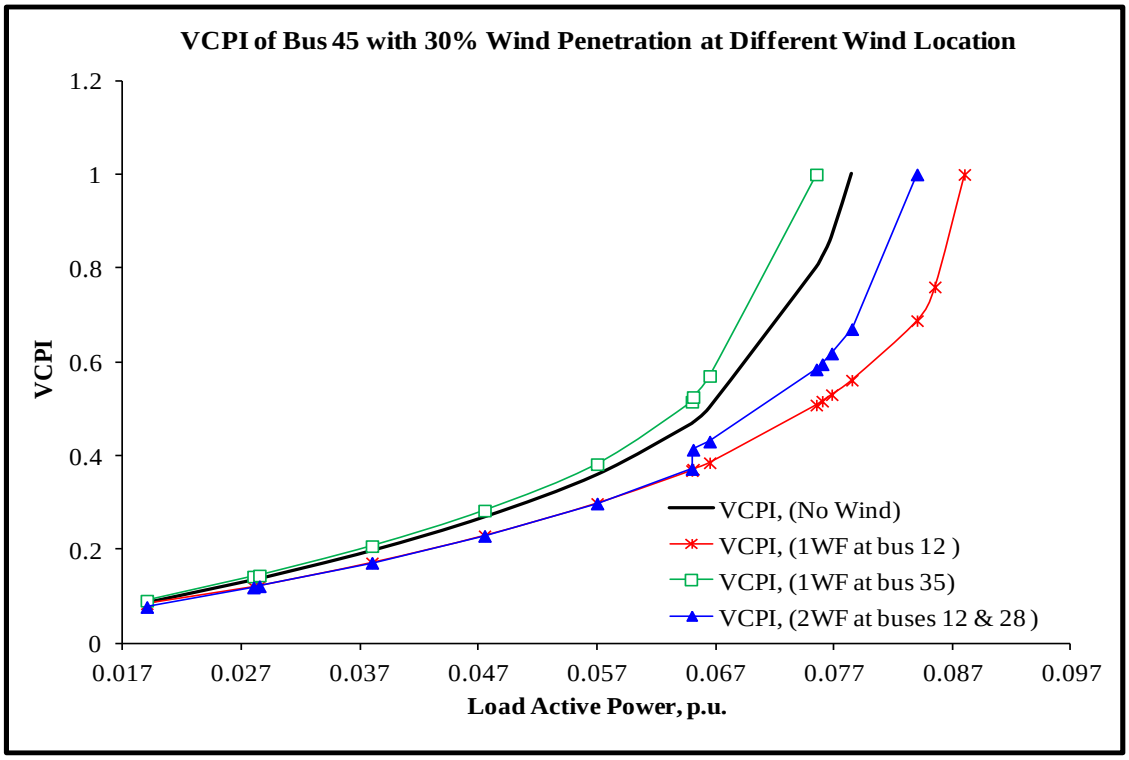

Figure 5.32: The variation of load demand with the VCPI of bus 45 (UKGDS 61-bus radial distribution network) at 30% wind penetration level, when the wind farm is connected to a network at different connection scenarios.

5.4.1.3.3 The Effect of Fluctuation of Wind Generation Output

The system is on a 61-radial distribution network, operated with 30% wind penetration level. Only one wind generator at bus 12 is considered for evaluating the impact of intermittency of wind generation output. Similar to the simulation procedure conducted on previous network cases, the inputs to the modified 61-bus radial distribution system in the simulator are the variables. The value of the VCPI is calculated and the results presented here are for a 24-hour period. The bus 51 is selected for study, since it is sensitive to voltage instability. It is assumed that the peak load at 17:00 and 18:00 are the same. A plot of the load for bus 51 for 24 hours is shown in Figure 5.33.

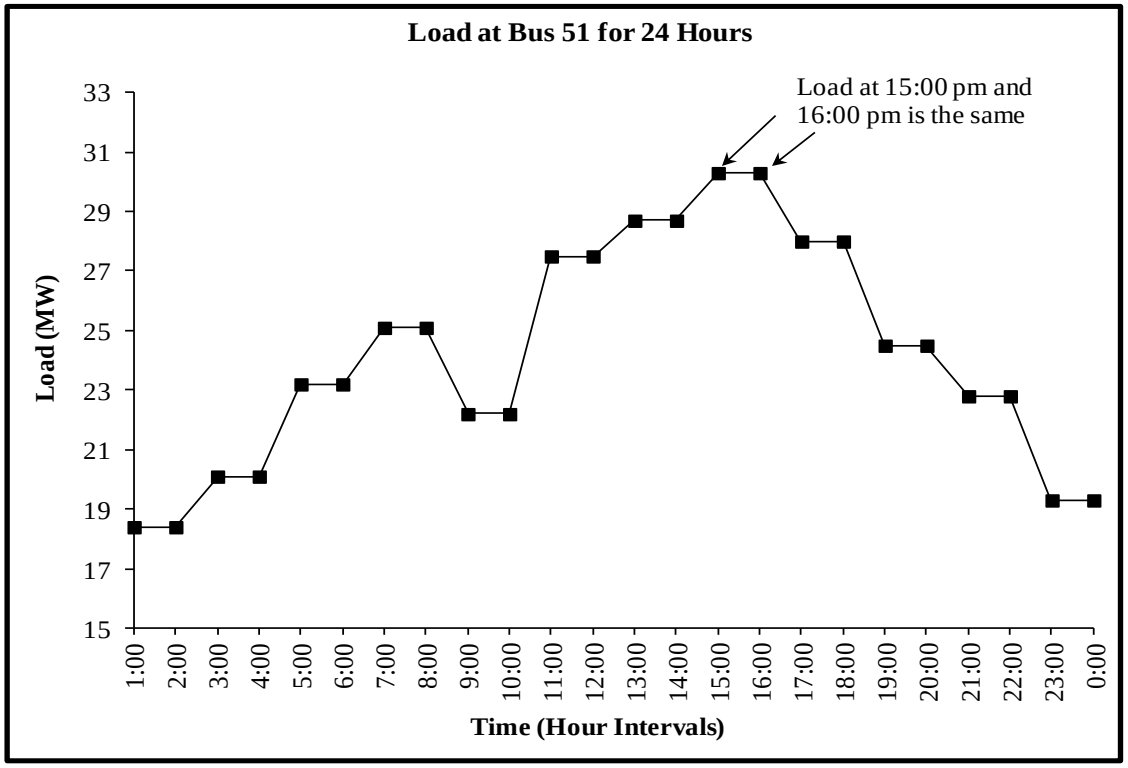

Figure 5.33: A plot of the load for bus 51 (UKGDS 61-bus radial distribution network) for 24 hours.

The study concentrates on peak load when large and sudden changes in power are injected into the network from wind generation output. The VCPI value of bus 51 is calculated at 15:00 at a certain value of wind generation output, then it is compared to the VCPI value of the same bus at the same loading when suddenly wind generation output changes at 16:00. As mentioned in Chapter 3, the system is close to voltage instability as the value of the VCPI is close to 1.0. The VCPI value of bus 51 is calculated and found to be 0.264 at a peak load at 15:00 when load bus 51 is at 30.34 MW and wind generation is at a maximum output of 24 MW. Then the value of VCPI increases to 0.317 at the same peak load in the following time step at 16:00, when there is a large decrease in power output from wind generation. It can be seen that the VCPI value increases due to intermittency of wind generation output, as shown in Figure 5.34. It can be concluded that any large and sudden change in the power injected into the network from wind generation output, especially during system peak load, can lead to

voltage instability according to increases in the VCPI at 16:00. System protection devices are necessary to protect the system from risk of voltage collapse due to large and sudden changes in wind power injected into the network during peak load.

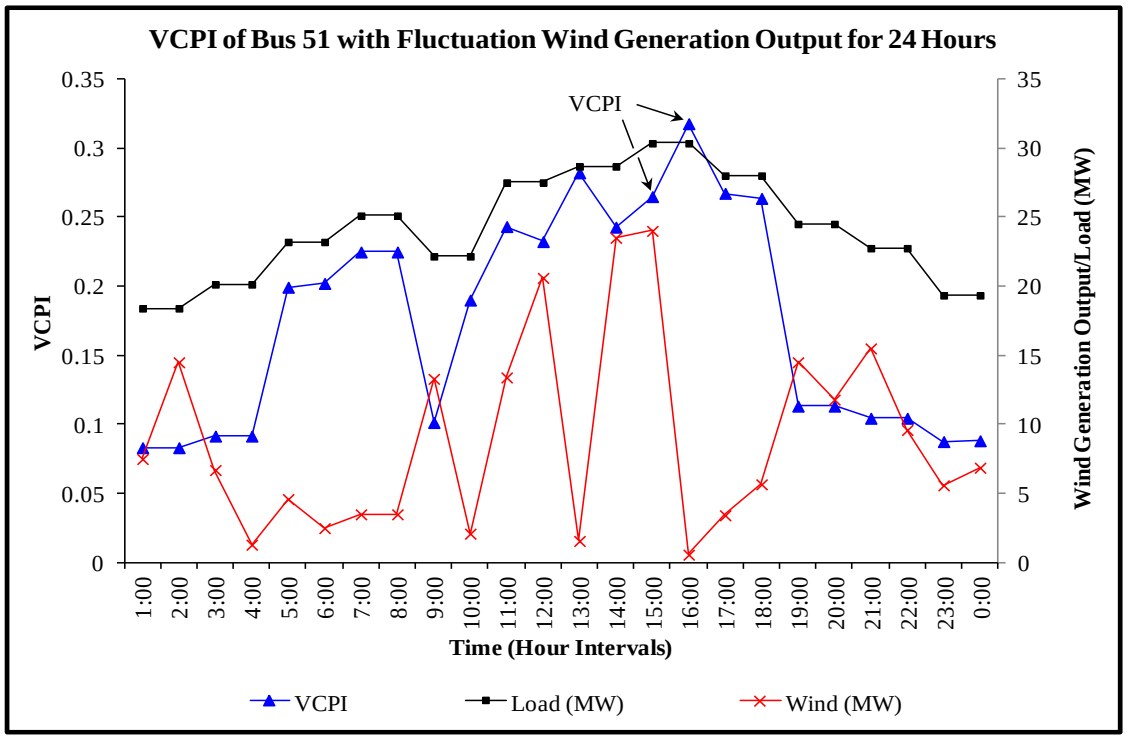

Figure 5.34: The VCPI values and load curve at bus 51 (UKGDS 61-bus radial distribution network) with fluctuation wind generation output for 24 hours; only one wind generation is connected at bus 12.

5.5 Conclusion

The integration of wind farms into existing electricity networks and the impact on networks has been presented in this chapter. Furthermore, case study results have been presented regarding the impact of wind generation on system voltage stability. The type of wind generator used was of variable speed with a doubly fed induction generator (DFIG) which was modelled on load flow studies as a PV bus and operated in voltage controlled mode. This chapter proposed a new method for evaluating the impact of wind generation on system voltage stability, taking into consideration the intermittent nature

of wind generation. Simulation was developed and presented for this method. In this methodology a voltage collapse proximity indicator was also calculated and employed to investigate the contribution of wind generation to voltage stability. Different penetration levels from 10% to 30% were used and different wind connection scenarios were used in the network to analyse the impact of wind generation. From the results presented in this chapter, it can be concluded that voltage stability is affected positively or negatively depending on penetration level, fluctuation of wind generator output, and location of wind generator connection. When wind generation was connected to a stronger bus it was able to improve system voltage stability and the higher the penetration level the better. The reverse was found to be true when wind generation was connected to a weaker bus, in which case reactive power compensation (e.g. SVC) may still be necessary, especially if a large penetration of DFIG is connected to a weak area. The results obtained show that system voltage stability was better for a single wind farm connection location connected to a stronger bus compared to multiple locations of wind farms for the same amount of wind penetration level. It can be concluded from the results that large wind generation output fluctuations, especially during high system loading, can lead to system voltage collapse. A protection system is required to protect systems from the risk of voltage collapse caused by intermittency of wind generation output during peak load. Developers and system operators can decide on the location and penetration levels of new wind farms to be connected to existing systems based on the proposed methodology used here, which calculates the system proximity to voltage collapse using the voltage collapse proximity indicator, which considers location, penetration level, and the intermittent nature of wind generators.

Chapter 6

Evaluating the Impact on Power Margins and System Losses due to Wind Generation Intermittency

6.1 Introduction

Nowadays, wind generation penetration levels in transmission networks have been increasing. The increase in integration is mainly due to environmental concerns and the push for carbon-free power generation. In some remote areas, economic factors can also be a contributing factor. The size of wind turbines and wind farms are increasing and the influence of wind generation on voltage stability and total power loss is becoming a major concern. Similar to some of the existing renewable generation, a major drawback of wind generation is its intermittent nature. As explained in Chapter 5, by using the voltage collapse proximity indicator (VCPI), the intermittent output of wind power resources can lead to a voltage instability problem.

In this chapter, another indicator is the power margin, which is used to measure the margin between the voltage collapse point and the current operating point. This chapter develops a comprehensive methodology for calculating the power margin based on wind generation variability. The power margin is used to measure the impact of wind generation on system voltage stability. The proposed method is applied to simulation scenarios for different wind speed data, different penetration levels of wind energy, and an IEEE-30 bus system is used as a sample test system where the wind sources are connected at different network locations. The commercial software Power World Simulator is used to obtain simulated results. In addition, the impact of wind generation

intermittency and the penetration on total real power losses based on system loadability is also investigated.

6.2 Proposed Methods for Power Margin based on Wind Generation Intermittency

This section will develop a methodology for calculating the power margin of transmission networks that considers the time varying characteristics of power system generation components, penetration level of wind generation and the intermittent nature of the wind power. In this method the P-V curve is used to investigate the impact wind generation has on voltage stability in the transmission network. The study uses the power margin between the voltage collapse point and the current operating point as a proximity indication to assess the relative stability improvement or deterioration relative to the base case (i.e. without wind generation).

This methodology was carried out using Time Step Simulation Optimal Power Flow (TSSOPF), where inputs can be varied at any time during the simulation window. The Time step option allows the user to specify operating conditions and obtain optimal power flow solutions for a set of points in time. The proposed collapse margin method has three main inputs as shown in Fig.1. The wind power inputs is the time series values of the wind generation connected to network in MW at one hour intervals. This data was obtained from a utility operating in the United Kingdom from their wind farm for a one month period at one hour intervals [105]. The input of the thermal generators indicates their availability considering their capacity rating and quantity. The load model input is the forecasted load profile applied to the transmission network.

The flow chart for the proposed methodology is shown in Fig. 1. Each stage in the flow chart represents a critical aspect of the methodology and will be described in the following steps:

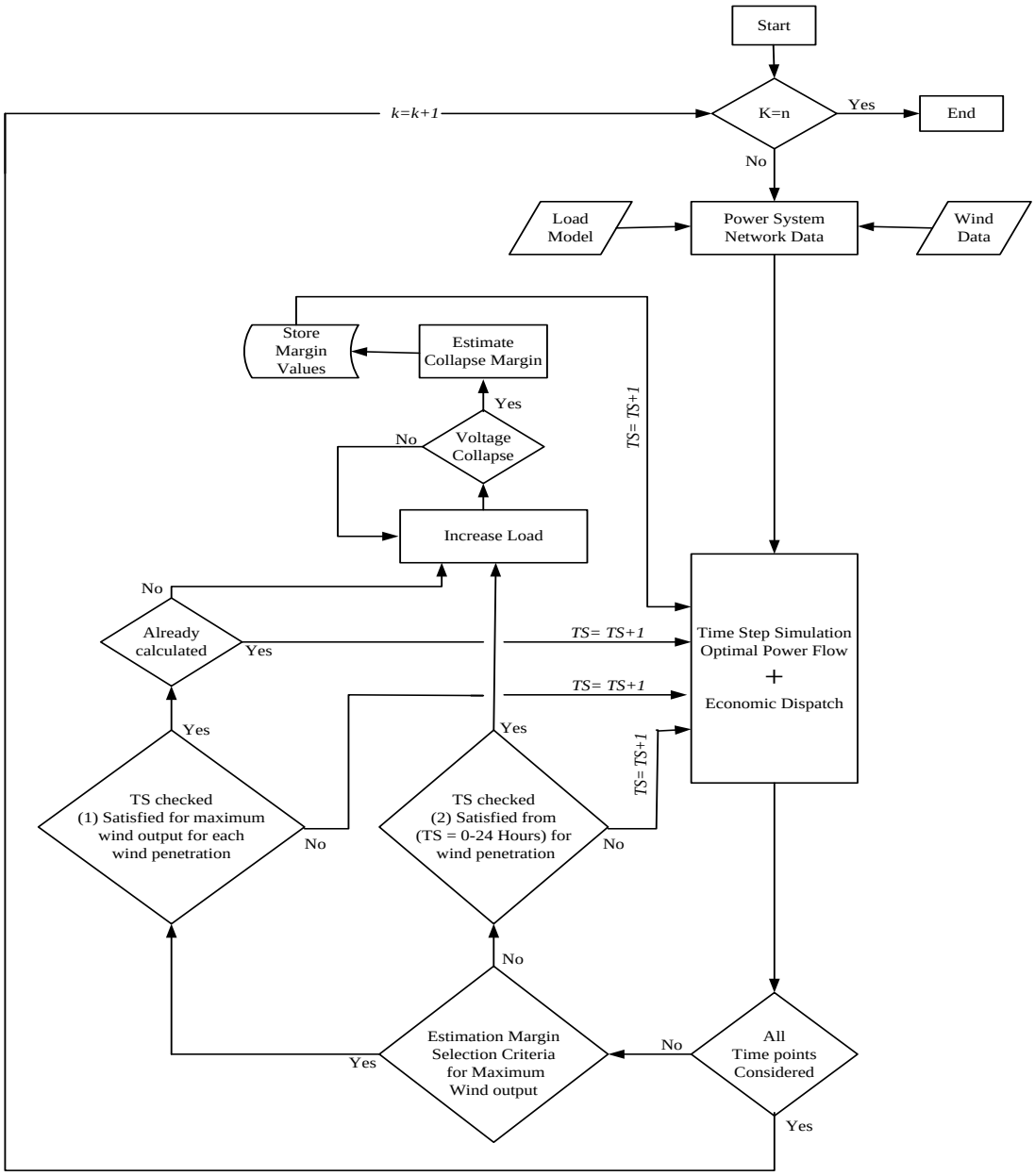

Figure 6.1: The flow chart for the proposed methodology of collapse margin.

Step 1: Obtain Input Data and Time –Series Analysis

This step involves obtaining the three input values to the simulator. These values represent wind power output, conventional generators output and the load model:

- The wind power output data in MW is connected to the network at different penetration levels.. The penetration level of the wind generator is determined as percentage of the installed capacity of the conventional generators in the network. The study takes into account the impact of both the level of wind generation and the wind variability on the system collapse margin and compares this to the base case (i.e. no wind).
- The conventional generators are assumed to be thermal; their installed capacity is in MW, and is used as the reference value for calculating the penetration percentage of the wind generator.
- The load model is based on a single day load profile data and is repeated for one month. The same load profile is used for all wind penetration levels, to enable us compare the simulation results.
- A time-series analysis is used in the simulation for modelling load demand and variable resources of wind generation [106]. The single power flow problem with mean values is expanded to multiple simulations with individual values for each time step. Due to the daily profile of load and the variability of wind over a day, a time step of one hour is used and applied for one month. This means that at least 720 power flow simulations need to be solved.

Step 2: OPF Incorporating Wind Generation

With the introduction and development of renewable energy sources especially wind energy; there is a need to incorporate wind generation cost into the classical optimal power flow (OPF) problem [107]. The economic dispatch (ED) of generation in a wind-thermal system involves the allocation of generation among wind plants and thermal plants so as to minimize the total production costs. The sum of outputs from the available wind and thermal generators must equal the system load plus any system losses. In addition, certain constraints may be placed on the generator model. Theses constraints typically take the form of minimum and maximum generator outputs.

Generally, the problem can be formulated as follows: [107]

The fuel cost of a thermal generation units are represented by quadratic functions as

$$f_t(P_{Gi}) = a + b(P_{Gi}) + c(P_{Gi}^2) \quad (6.1)$$

Where $f_t(P_{Gi})$ is the fuel cost of a thermal generator; a, b, c are the characteristic parameter cost coefficients of the thermal generator, and P_{Gi} is the real power output of the thermal generator.

In a deregulated market, the wind generation will have a cost that is based on the special contractual agreements (i.e. fixed schedule or economic schedule) for buying or selling between each independent power producer and the transmission network operator (TNO). The output of a wind generator is constrained by an upper and lower limit. The operation cost of the wind generation units can be represented as the function of wind farm scheduled power output [108].

$$f_w(P_{WGj} = C_w(P_{WGj}) + C_{p,w}(P_{WGj(available)} - P_{WGj}) + C_{r,w}(P_{WGj} - P_{WGj(available)}) \quad (6.2)$$

Where $f_w(P_{WGj})$ is the fuel cost of the wind generator, P_{WGj} is scheduled wind power from the wind generator, $P_{WGj(available)}$ is the available wind power from the wind generator, C_w is the cost function for the wind generator and this factor will typically take from a payment to the wind farm operator for the wind generated power actually used. $C_{p,w}$ is the penalty cost function for not using all available power from the wind power generator. $C_{r,w}$ is the required reserve cost function, relating to uncertainty of wind power.

The objective function includes not only the operation cost of the thermal generation units but also the operation cost of wind generation units operating in the system and can be stated as follows: [107]

$$\text{Minimize: } f_T(P_{Gi}, P_{WGj}) = f_t(P_{Gi}) + f_w(P_{WGj}) \tag{6.3}$$

Where $f_T(P_{Gi}, P_{WGj})$ is the fuel cost of a thermal generator and a wind generator outputs, P_G is the power output from a thermal generator and P_{WGj} is the schedule wind power from wind generator.

The minimization of the above function is subject to the system constraints. The system constraints for the problem are shown as follows:

- The system load flow constraints:

$$\Delta P_i = P_{G_i} - P_{D_i} - V_i \sum_{j=1}^{NB} V_j [G_{ij} \cos(\delta_i - \delta_j) + B_{ij} \sin(\delta_i - \delta_j)] = 0 , \qquad i \in NB$$

$$\Delta Q_i = Q_{G_i} - Q_{D_i} - V_i \sum_{j=1}^{NB} V_j [G_{ij} \sin((\delta_i - \delta_j) - B_{ij} \cos(\delta_i - \delta_j)] = 0 , \qquad i \in NB$$

- Unit capacity constraint of thermal generator:

$$P_{G_i}^{min} \le P_{G_i} \le P_{G_i}^{max}, \qquad i \in NG$$

$$Q_{G_i}^{min} \le Q_{G_i} \le Q_{G_i}^{max}, \qquad i \in NG$$

- Unit capacity constraint of wind generator:

$$P_{WG_j}^{min} \le P_{WG_j} \le P_{WG_j}^{max} \qquad j \in NWG$$

$$Q_{WG_j}^{min} \le Q_{WG_j} \le Q_{WG_j}^{max} \qquad j \in NWG$$

- Compensator performance for shunt capacitor:

$$Q_{C_j}^{min} \leq Q_{C_j} \leq Q_{C_j}^{max}, \qquad j \in NC$$

- Bus generator voltage constraints:

$$V_{G_i}^{min} \leq V_{G_i} \leq V_{G_i}^{max}, \qquad i \in NG$$

- Bus load voltage constraints:

$$V_{D_j}^{min} \leq V_{D_j} \leq V_{D_j}^{max}, \qquad j \in ND$$

- Line capacity limit constraints:

$$F_{ij}^{min} \leq F_{ij} \leq F_{ij}^{max}, \qquad j \in NL$$

Where NG, NWG, NC, ND, NL are the total number of thermal generators, the total number of wind generators, the total number of shunt capacitor compensators, the total number of loads and the total number of branches respectively; *k* is an indicator load condition of wind generation; P_{WG}, P_{WG}^{min}, P_{WG}^{max} are the wind generator scheduled power output and its lower and upper limits, respectively.

Step 3: Balancing Load and Variable Generation.

As a wind generator's power output and system loading change at each time-step in the simulation, it is necessary to maintain the balance between the total generation and load in the system. This will be achieved by re-dispatching the conventional units in the system. This can be achieved by using economic dispatch and unit commitment together. By combining the active power outputs generated from

thermal generator (P_{Gi}) with wind generator (P_{WGj}), also by combining the reactive power outputs generated from a thermal generator (Q_{Gi}) with a wind generator (Q_{WGj}) and a shunt capacitor (Q_{Cj}), two matrices containing the active power and the reactive power generated at all units in the system during 720 hours can be written as follows:

$$\begin{bmatrix} P_1^h \\ P_2^h \\ \vdots \\ P_N^h \end{bmatrix} = \begin{bmatrix} P_{G_1}^h \\ P_{G_2}^h \\ \vdots \\ P_{G_N}^h \end{bmatrix} + \begin{bmatrix} P_{WG_1}^h \\ P_{WG_2}^h \\ \vdots \\ P_{WG_N}^h \end{bmatrix} \qquad \text{Where} \quad h= 1, 2, 3,\ldots 720$$

$$\begin{bmatrix} Q_1^h \\ Q_2^h \\ \vdots \\ Q_N^h \end{bmatrix} = \begin{bmatrix} Q_{G_1}^h \\ Q_{G_2}^h \\ \vdots \\ Q_{G_N}^h \end{bmatrix} + \begin{bmatrix} Q_{WG_1}^h \\ Q_{WG_2}^h \\ \vdots \\ Q_{WG_N}^h \end{bmatrix} + \begin{bmatrix} Q_{C_1}^h \\ Q_{C_2}^h \\ \vdots \\ Q_{C_N}^h \end{bmatrix} \qquad \text{Where} \quad h= 1, 2, 3,\ldots 720$$

The complex power (S^h) delivered from all unit generators in the system along 720 hours can then be represented by:

$$\begin{bmatrix} S_1^h \\ S_2^h \\ \vdots \\ S_N^h \end{bmatrix} = \begin{bmatrix} P_1^h \\ P_2^h \\ \vdots \\ P_N^h \end{bmatrix} + j \begin{bmatrix} Q_1^h \\ Q_2^h \\ \vdots \\ Q_N^h \end{bmatrix} \qquad \text{Where} \quad h= 1, 2, 3,\ldots 720$$

The real and reactive power balance in the system during 720 hours can be written as:

$$\sum_{t=1}^{Nh}\left(\sum_{i=1}^{NG} P_{G_i}^{h} + \sum_{j=1}^{NWG} P_{WG_j}^{h}\right) = \sum_{t=1}^{Nh}\left(\sum\left(P_{Load}^{h} + P_{Loss}^{h}\right)\right), \qquad \begin{matrix} i \in NG \\ j \in NWG \\ t \in Nh \end{matrix}$$

$$\sum_{t=1}^{Nh}\left(\sum_{i=1}^{NG} Q_{G_i}^{h} + \sum_{j=1}^{NWG} Q_{WG_j}^{h} + \sum_{j=1}^{NC} Q_{C_j}^{h}\right) = \sum_{t=1}^{Nh}\left(\sum\left(Q_{Load}^{h} + Q_{Loss}^{h}\right)\right), \qquad \begin{matrix} i \in NG \\ j \in NWG \\ j \in NC \\ t \in Nh \end{matrix}$$

Where Nh is the total number of hours.

The active power available from a wind generator(P_{WG}), is given by the expression below [68];

$$P_{WG} = \frac{1}{2}\rho . A . C_p . V_w^3$$

Where ρ is the air density, A is the turbine swept area, C_p is the cofeeicient of performance of the turbine, and V_w is the wind speed. The net reactive power of a doubly fed induction generator (DFIG) when operated with a pre-determined power factor (φ) can be approximated by:

$$Q_{WG} = P_{WG} . . \tan(\varphi_{WG})$$

However, as in most of cases where DFIG contributes to AC voltage control as required in most of the present grid codes, DFIG net reactive power exchange with grid will be determined by the machine's AC voltage controller.

Step 4*:* Time step selection based on system conditions of interest and estimation of collapse margin

Two sets of scenarios are selected on which power margin calculations are performed. The first scenario is related to the maximum power output of wind

generation (P_{WG}^{max}) for each penetration level. In this case, the wind data is monitored for the maximum output to identify the time step at which this occurs. It is assumed that the wind speed during this time step is constant. Then the P-V curve is obtained by gradually increasing both active and reactive powers at a certain single bus until the load flow ceases to converge (i.e. voltage collapse), and it is used to measure the margin of collapse. The collapse margin is measured as the distance between the current operating point and the maximum loading point in the P-V curve. This is done to draw the P-V curve to establish the strength of the system voltage stability, i.e. the maximum power that can be transferred to the bus. The voltage collapse point and the collapse margin for different wind penetration levels are then identified. The calculated collapse margin is then stored for comparison with the base case.

The second scenario is related to wind variability at a specified time range within a one month period. In this case, the collapse margin is estimated under variable wind generation outputs. However, only a penetration level of 30% is considered during this period. Similar to the first case, the time step at which these conditions are met is identified and the calculation is carried out at that specific time step. The choice of time range and wind variability provides results that are indicative of the impact of wind variability on the system stability margin.

6.3 Case Study and Results

In order to evaluate the impact of the wind generation intermittency and the penetration on the system collapse margin in the transmission network, an IEEE-30 bus is applied to the proposed method. In this section, the P-V curve is studied at different wind scenarios. The voltage collapse point and the current operating point are used for proximity indication.

6.3.1 Modified IEEE-30 bus test system

A one-line diagram of the IEEE-30-bus system is shown in Figure 4.7 and the detailed data of the system is shown in Appendix B [104]. The modified test system is analyzed using an AC Optimal Power Flow (OPF). The test system is modelled on the

Power World Simulator, which has been modified in the first simulation run by connecting wind generation on bus 28. In the second simulation run, wind generation is connected to bus 14. In the third connection scenario, the wind generator is connected to buses 6 and 28 simultaneously with a combination of different penetration levels. Table 5.5 shows the combinations of penetration levels. The wind generator is assumed to be a doubly fed induction generator (DFIG) which has reactive power control capability. In this assessment, the DFIG is modelled as a PV bus and operated with maximum and minimum power factors of 0.95 leading (capacitive VAr) and 0.95 lagging (inductive VAr). These power factors can be attained with an aggregate DFIG model having reactive power capability of (± MVAr) for the MW wind farm. The total system generation capacity is 1000 MW.

6.3.2 Simulation Procedure

The simulation is carried out using the Power World Simulator time-step simulation option, where inputs can be varied at any time in the simulation window. Wind turbines are connected to the IEEE 30-bus system at different locations and at different MW outputs. The different connection scenarios of wind generation are mentioned in section 6.3.1. The inputs to the modified test system in the Power World Simulator are the variable loads, wind generation and output from the thermal generators. These inputs are connected to the test system at one hour time steps continuously for a simulation time of one month. Moreover, the total generation output from the wind turbines is varied every one hour to represent the stochastic behaviour of wind generation. The wind generation is varied from 10% to 30% of the total connected load in the network for each of the scenarios. All results and discussions in the following section are based on data from one month's load and profile of wind generation.

In this section, the system voltage stability is investigated by using a P-V curve with different wind generation outputs. The P-V curve is analysed to identify the collapse margin or voltage collapse point. The collapse margin measures the distance from the current operating point to the maximum loading in the P-V curve. The system

voltage stability is analysed from three different standpoints: the level of wind penetration (i.e. 10% to 30%), the intermittency of wind generation output (fluctuation of wind generation output), and the location of wind generator as a single location or as two locations. All results and discussions in the following section are based on data from one month's load and profile of wind generation.

6.3.3 The Effect of Wind Penetration Level

As mentioned in section 6.3.2 above, each simulation run uses one hour data of load and wind generation. One month's data is used for ease of presentation. The same load profile is used for all wind penetration levels. In order to assess the impact of wind generation on the voltage stability, one scenario of described wind generation connection with different penetration levels is studied and the results compared with the base case without any wind generation. The simulation runs by connecting one wind generation on bus 28 as the stronger bus in the system.

In this case, the wind data is monitored for the maximum output for each wind penetration level, then the time step at which this occurs is identified. It is assumed that the wind speed during this time step is constant. The load is then gradually increased at a single bus until the collapse point, while other load buses in the system remain unchanged. In this time step the P-V curve is done and plotted to establish the strength of the system voltage stability, i.e. the maximum power that could be transferred to a certain load bus.

We have identified the voltage collapse point and the collapse margin at this time step simulation. Load buses 30, 21, 15, 12, 10 and 4 are selected individually for each penetration level. The results presented here are for evaluating the impact of wind generation on the system and the P-V curve is plotted for each bus. Buses 30, 21, 15, 12, 10 and 4 of the IEEE-30 bus system are selected for evaluation because some of them are critical buses and prone to voltage instability. Figures 6.2-6.7 illustrate the impact of different wind penetration levels on the voltage stability of the IEEE-30 bus system. Figure 6.2 shows bus 30's P-V curve when the wind farms are connected to strong bus 28, compared to the base case when no wind is connected to the system. As shown, the

system collapse margin is 323.4 MW for the base case (no wind) and the system collapse margin increases to 323.9 MW for 10% WP (wind penetration), 324.4MW for 20% WP, and 325 MW when the wind penetration level is 30% WP. Figure 6.7 shows a plot of bus 4 P-V curves for wind penetration from 10% to 30%. Compared to the base case, 10%, 20% and 30% wind penetration levels increase the system collapse margin. In this figure it can be seen that the system collapse margin is 992.8 MW for the base case (no wind), and the collapse margin increases to 1072 MW for 10% WP, 1122.9 MW for 20% WP, and 1150.8 MW when the percentage of wind capacity is 30% (300 MW). The results from all figures indicate that the system collapse margin is improved with all wind penetration levels and the system collapse margin is better for the higher penetration level. The DFIG has a positive effect on the voltage stability of the network when the penetration level increases when the DFIG is connected to a strong bus.

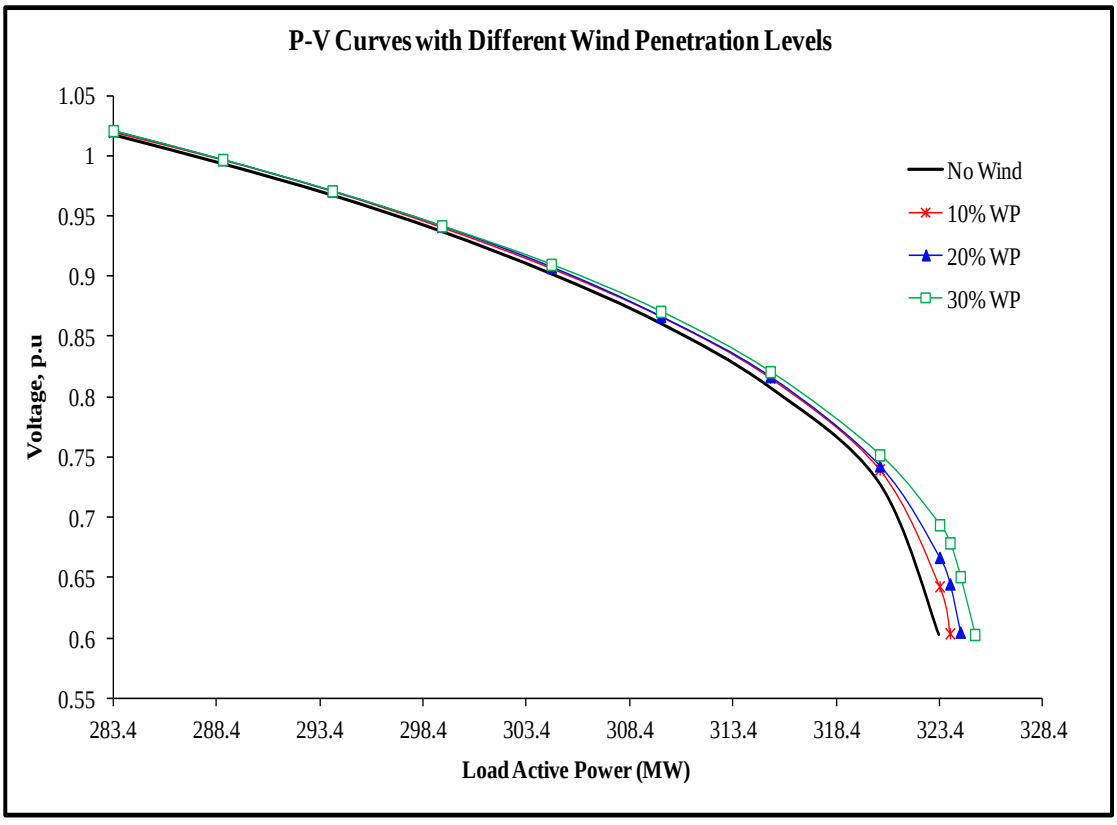

Figure 6.2: P-V curves at bus 30; analysis of IEEE-30 bus system with different wind penetration levels when wind farms connected to bus 28.

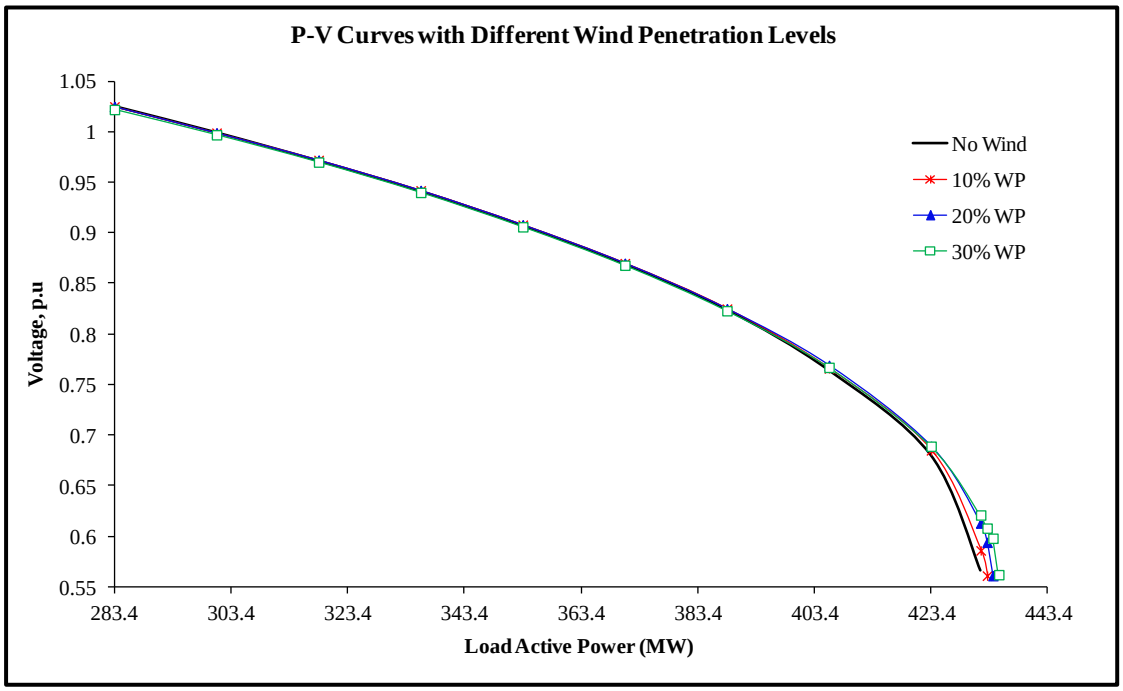

Figure 6.3: P-V curves at bus 21; analysis of IEEE-30 bus system with different wind penetration levels when wind farms connected to bus 28.

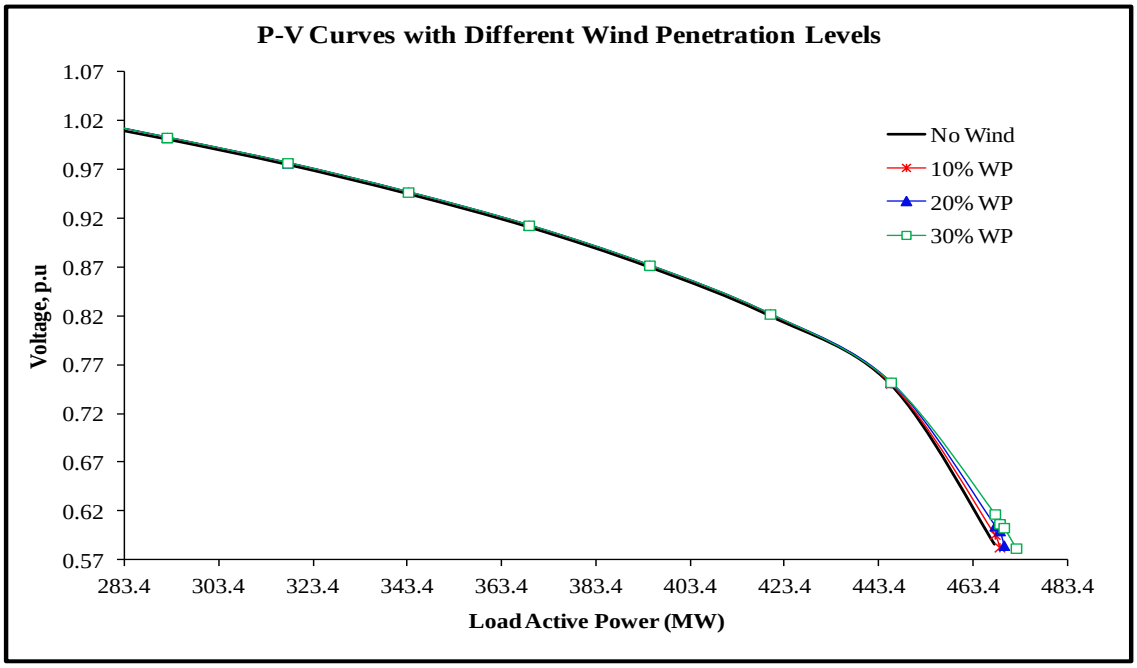

Figure 6.4: P-V curves at bus 15; analysis of IEEE-30 bus system with different wind penetration levels when wind farms connected to bus 28.

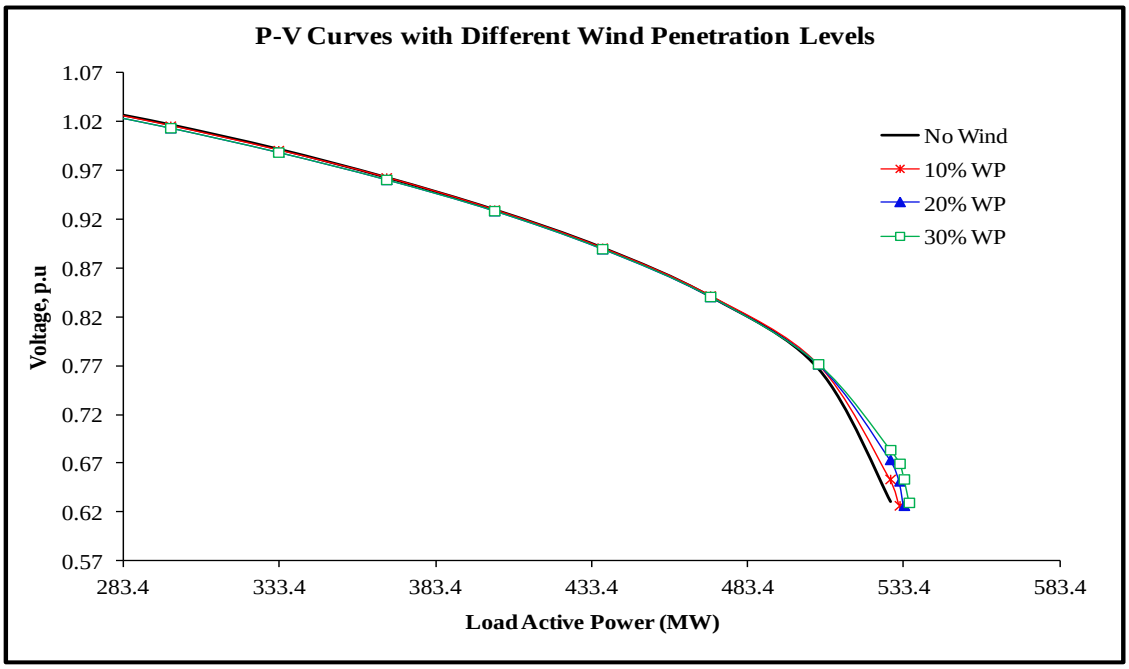

Figure 6.5: P-V curves at bus 12; analysis of IEEE-30 bus system with different wind penetration levels when wind farms connected to bus 28.

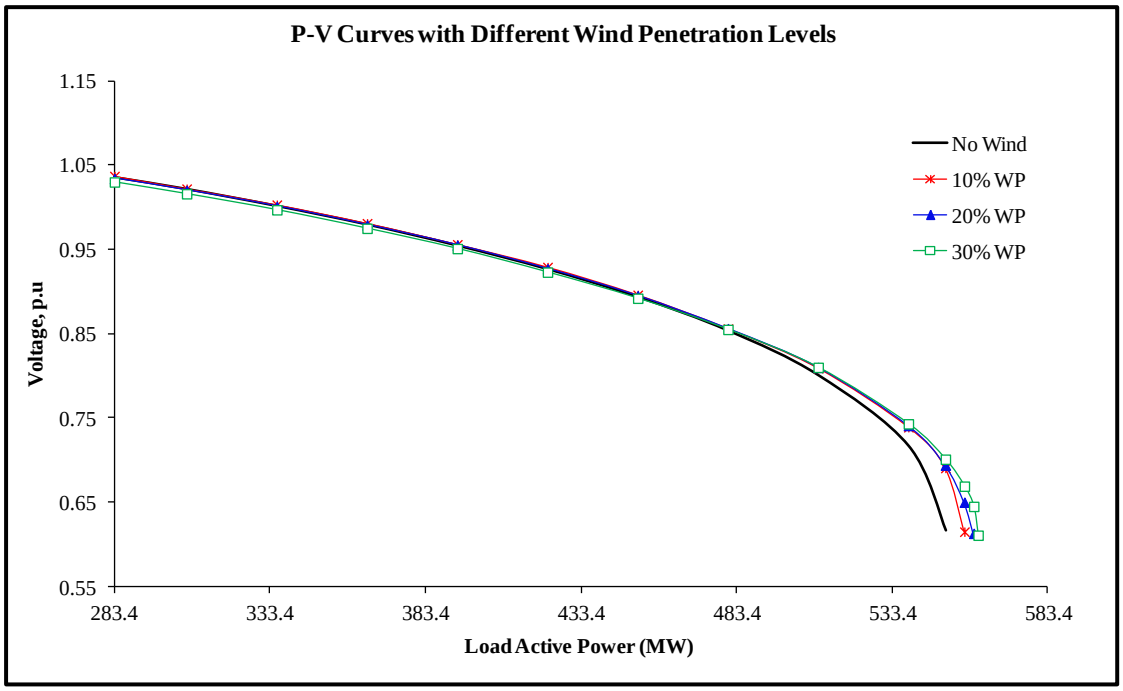

Figure 6.6: P-V curves at bus 10; analysis of IEEE-30 bus system with different wind penetration levels when wind farms connected to bus 28.

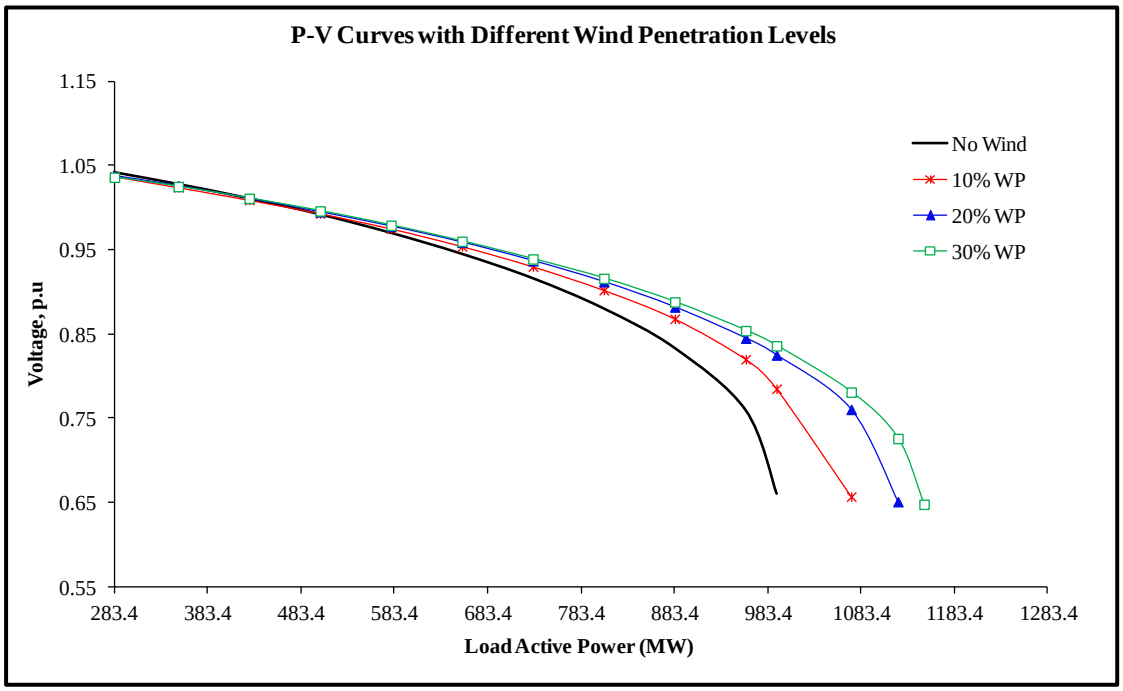

Figure 6.7: P-V curves at bus 4; analysis of IEEE-30 bus system with different wind penetration levels when wind farms connected to bus 28.

6.3.4 The Effect of Wind Farm Location

This section aims to discuss the effect of wind farm location on the system collapse margin in the transmission network. Results for four scenarios are considered and compared in this section. No

wind case is evaluated first to set a base case and three wind farm location scenarios are then evaluated. The connection scenarios of wind farms are:

1 WF: one wind farm connected at bus 28 as a strong bus.

1 WF: one wind farm connected at bus 14 as a weak bus.

2 WF: two wind farms connected at buses 6 and 28, respectively, with a combination of wind penetration levels.

The reason for connecting the wind output at more than one bus is to show the effect of dispersing the wind power around the network. As mentioned above in the simulation procedure, the total generation output from the wind turbines connected to the test system is varied every hour to represent the stochastic behaviour of wind generation. In order to investigate the effect, only 20% WP (wind penetration) is applied to the proposed method for each of the wind connection scenarios. The analysis is concentrated at maximum wind generator output for each penetration level. The P-V curve of a certain load bus is plotted for maximum wind generator output at the specific time step simulation during simulation runs. In this specific time step, it is assumed that the wind speed is constant during the time step and the single load bus is gradually increased until collapse point, while other load buses in the system remain constant.The margin between the voltage collapse point and the current operating point is used as a proximity indication. Load buses 30, 21, 10 and 4 are selected separately for investigating each wind generation connection scenario. The selection is aimed at covering the whole network to show the impact of wind generation output. Figures 6.8, 6.9, 6.10 and 6.11 show plots of bus 44 P-V curves, bus 21 P-V curves, bus 10 P-V curves, and bus 4 P-V curves, respectively, for 20% WP (wind penetration) when the wind farm is connected to the system at different connection scenarios.

As shown in Figure 6.8, the system collapse margin is 323.4 MW for the base case and the system collapse margin increases to 323.95 MW with two wind farms (DFIG). The system collapse margin increases to 324.4 MW when one wind farm is located at strong bus 28. However, compared to the no wind case, the system collapse margin decreases to 319 MW when one wind farm is connected to weak bus 14. Results in Figure 6.10 show the P-V curves of bus 10; the system collapse margin is 550.5 MW for the no wind case, and then the system collapse margin is measured and found to increase to 558 from the no wind case when two wind farms are connected to the system and to 559.8 MW when a single wind farm is located at strong bus 28. However, if the wind farm is connected to bus 14 as a weak bus, the system collapse margin is decreased to 544.1 MW compared to the collapse margin of the no wind case.

From the results presented in the figures, it can be concluded that the system collapse margin of the transmission system improves at 20% penetration level when the DFIG with voltage control mode is connected to a strong bus according to the voltage collapse point and collapse margin compared to the base case (no wind), as shown in Figures 6.8-6.11. The figures also indicate that the system collapse margin is better for one location of wind generation at strong bus 28 compared to the two locations 6 and 28 with a combination of wind penetrations. However, the wind farm does not improve the voltage collapse margin and has a negative effect on voltage stability of the network when the DFIG is connected at weak bus 14.

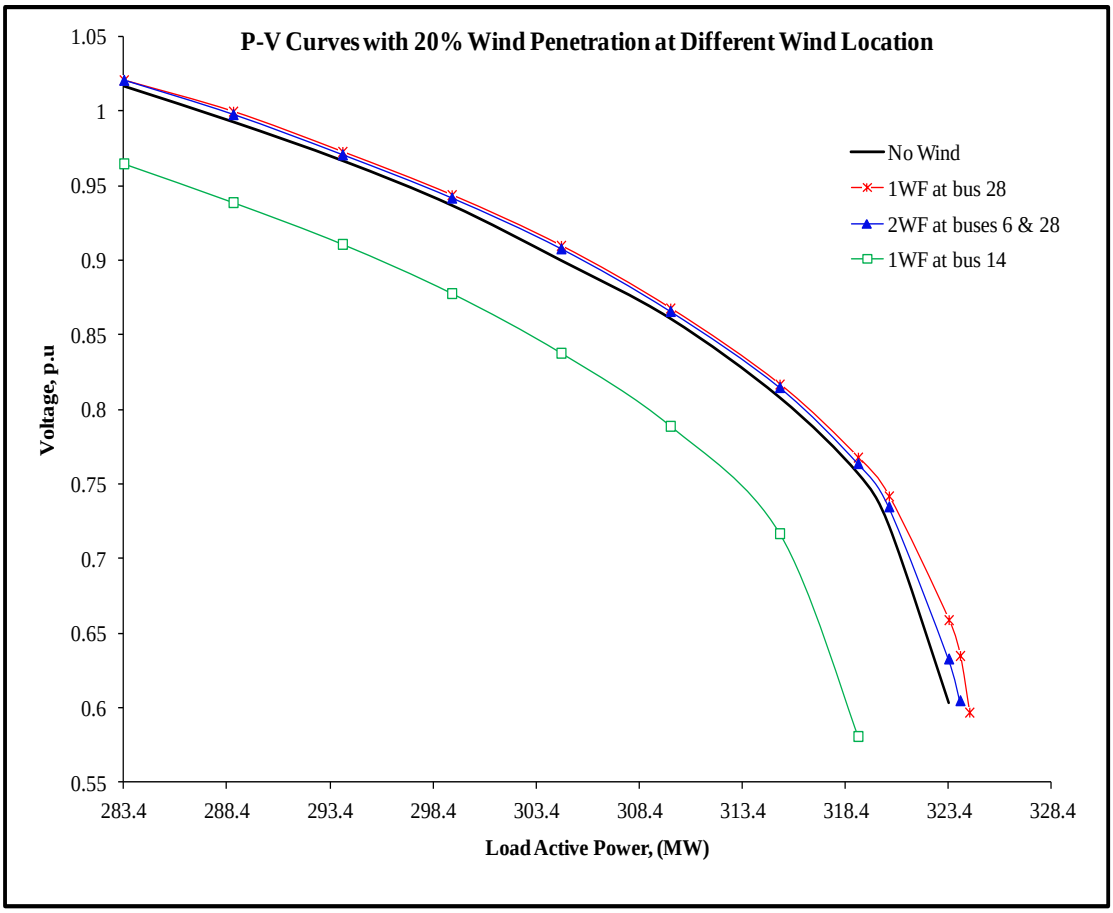

Figure 6.8: P-V curves at bus 30; analysis of IEEE-30 bus system with 20% wind penetration levels when wind farms connected to the network at different connection scenarios.

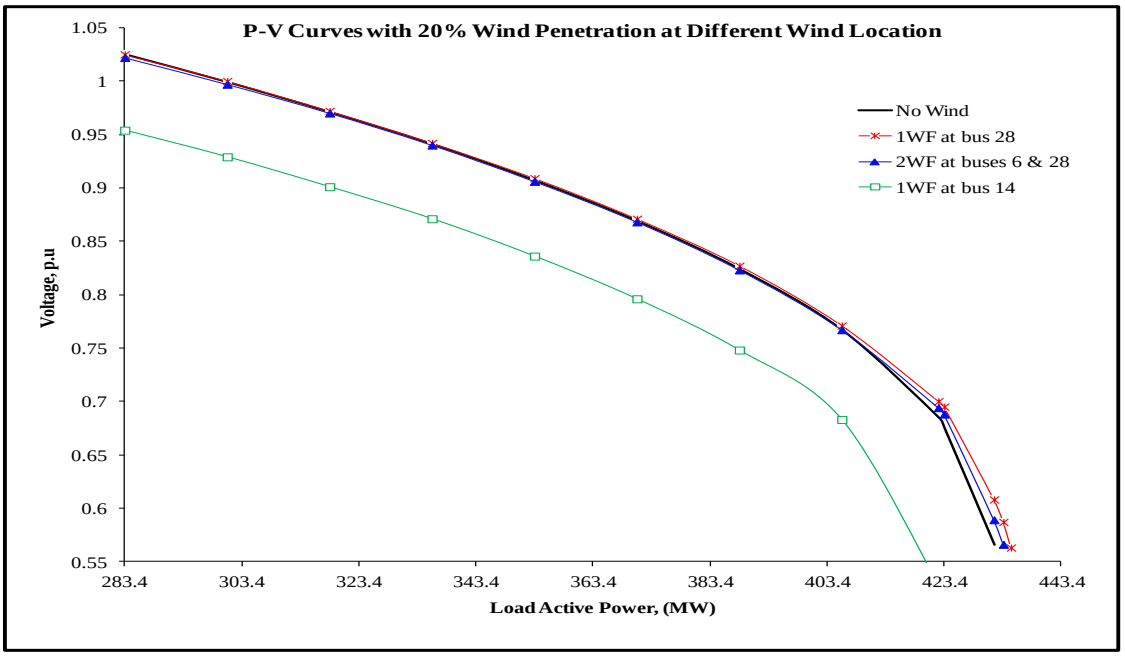

Figure 6.9: P-V curves at bus 21; analysis of IEEE-30 bus system with 20% wind penetration levels when wind farms connected to the network at different connection scenarios.

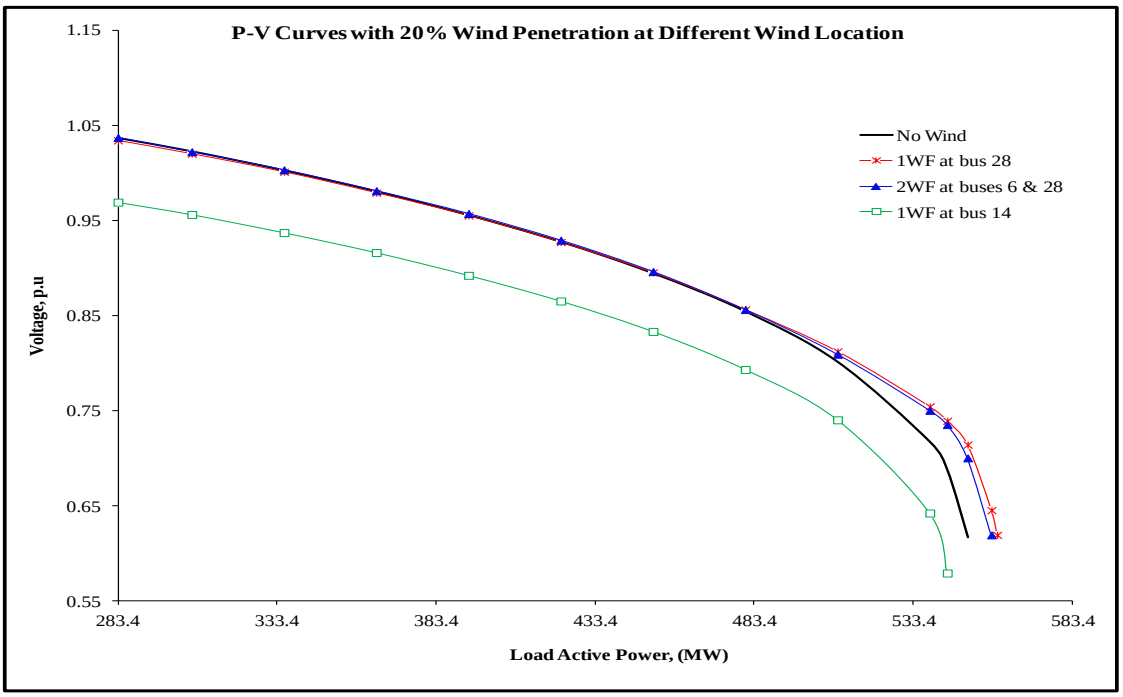

Figure 6.10: P-V curves at bus 10; analysis of IEEE-30 bus system with 20% wind penetration levels when wind farms connected to the network at different connection scenarios.

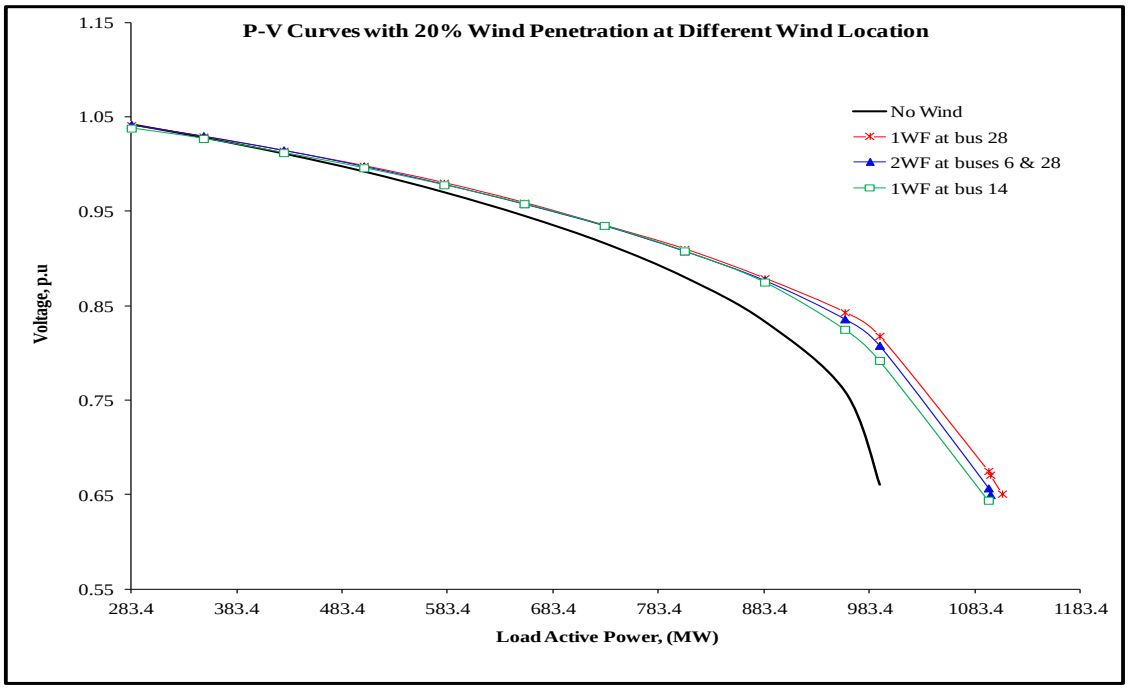

Figure 6.11: P-V curves at bus 4; analysis of IEEE-30 bus system with 20% wind penetration levels when wind farms connected to the network at different connection scenarios.

6.3.5 The Effect of Fluctuation of Wind Generation Output

The aim of this section is to study the impact of wind generation intermittency on the system collapse margin. In this case study, the simulation is conducted using the IEEE-30 bus system, which is operated with 30% wind penetration level. Only one wind generator at bus 28 is considered for evaluating the impacts from intermittency of wind generation output. Similar to the simulation procedure outlined in the previous sections, the inputs to the modified test system in the simulator are variable for a single month period. A one hour interval is used for the simulation time step function. The wind data is monitored for specific conditions when sudden wind generation output changes from the maximum to the lowest wind generator output, then the time steps at which these conditions occur are identified. The maximum and lowest values are found to be 300 MW at 1:00 and 7.5 MW at 2:00, respectively, on the seventh day of the month, as shown Figure 6.12. The P-V curve is plotted separately for each value. The P-V curve of

bus 30 is plotted first for 300 MW at 1:00, then the P-V curve of the same bus is plotted for 7.5 MW at 2:00 by repeating the simulation procedure using the same wind data used in the first analysis. It is assumed that the wind speed during this time step is constant. The load is then gradually increased at bus 30 until the collapse point, while other load buses in the system remain unchanged. Then the P-V curve is plotted during this specific time step. Figure 5.13 shows a P-V plot of bus 30 with two different values of wind generation output. As shown in Figure 5.13, the value of the system collapse margin decreases from 325 MW when the DFIG is at maximum output of 300 MW to 323.1 MW when DFIG output is at 7.5 MW, which is less than the system collapse margin of the base case (no wind). According to the no wind case, the system collapse margin is 323.4 MW.

From the results presented in the section, it can be concluded that the fluctuation of wind generation outputs has a negative effect on the collapse margin of the network, especially when there is a large decease in the wind power injected into the network. This means that according to the analysis results in this section, the intermittency of wind generation might weaken the system voltage stability.

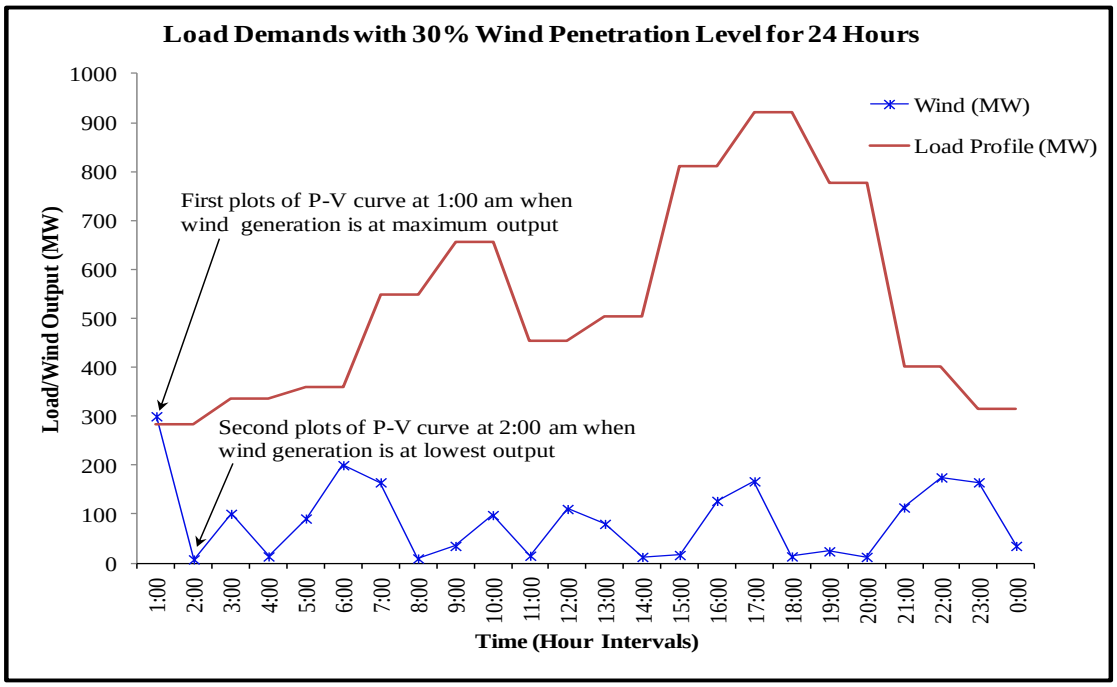

Figure 6.12: Load profile with 30% wind penetration level for one day.

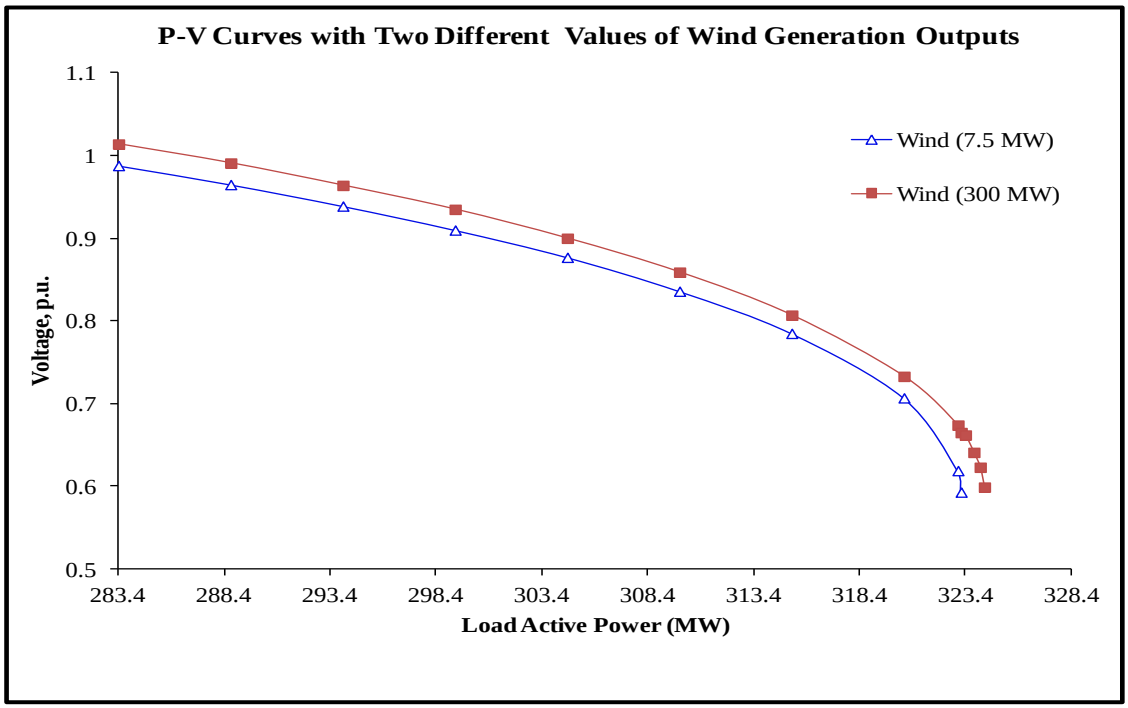

Figure 6.13: P-V curves at bus 30; analysis of IEEE-30 bus system with two values of wind generation outputs when one wind farm connected to bus 28.

6.4 Evaluating the Impact of Wind Generation Intermittency and the Penetration on System Losses based on System Loadability

Interest in the integration of wind farms into transmission and distribution networks has increased in various countries throughout the world, as economic and environmental factors drive new technologies to be more efficient and less polluting than their earlier counterparts. As the penetration level of wind generation increases, transmission network performance has to be analyzed in detail. This work investigates the effects of generation intermittency and the penetration on system MWh losses in the transmission network. An analysis method is used to assess system losses that considers the time varying characteristics of the power system generation components, penetration level of wind generation, and the variable nature of wind power, using the time step option in the Power World Simulator. The analysis method has three major inputs, as shown in Figure 6.14. The wind power input is the time series values of the wind generation connected to the network in MW at one hour intervals. These data were obtained from a utility

operating in the United Kingdom from a wind farm for a one month period and at one hour intervals. The input of the conventional generators is their availability considering their capacity and quantity, while the load model input is the forecasted load profile applied to the network for the evaluation of system losses due to the intermittency of wind generation.

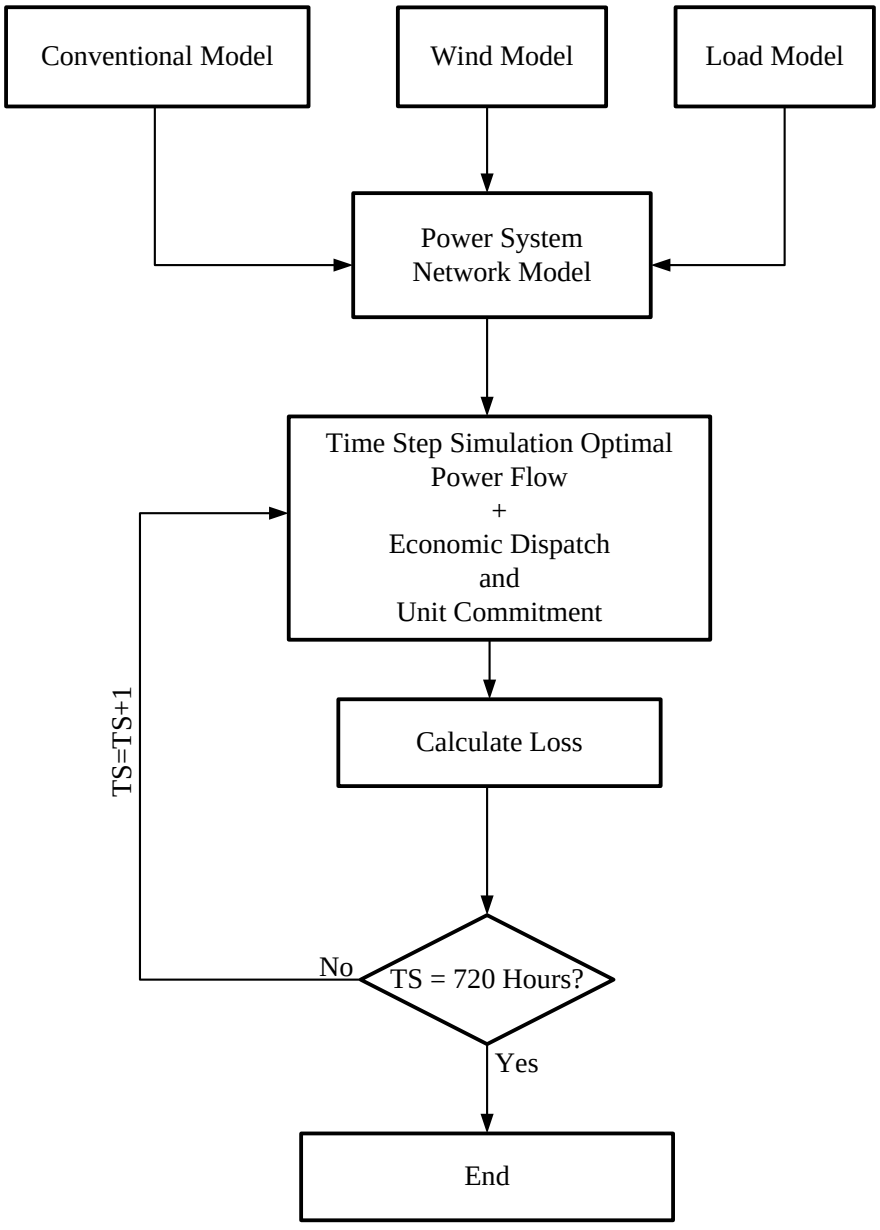

Figure 6.14: Flow chart of system loss calculation approach.

In order to investigate the impact of wind generation on system losses when connected at the transmission level, a modified IEEE-30 bus test system is used. A single-line diagram of the IEEE-30 bus system is shown in Figure 4.7 and detailed data on the system is shown in Appendix B [104]. Wind turbines are connected to the transmission system at different locations and with different MW outputs. The different connection scenarios of wind generation are:

1WF: one wind farm connected at strong bus 28.

1WF: one wind farm connected at weak bus 14.

2WF: two wind farms connected at buses 6 and 28, respectively, and simultaneously with a combination of different wind penetration levels.

The three wind penetration level scenarios for the case studies are shown in Table 6.1.

Table 6.1: Penetration level of wind generation scenarios for IEEE-30 bus system.

Scenarios	Scenarios 1	Scenarios 2	Scenarios 3
Wind Penetration (%)	(10% WP)	(20% WP)	(30% WP)
(MW)	100 MW	200 MW	300 MW

The inputs to the modified test system in the Power World Simulator are the variable loads, wind generation and output from the thermal generators. These inputs are connected to the test system at one hour time steps continuously for a simulation time of one month. However, the results presented here are for a 24 hour period. Table 6.2 shows the wind power input data for different wind penetration levels with a one day load period. The system real losses are analyzed from different standpoints. These are the level of wind penetration (WP) (i.e. 0% to 30%), the location of wind generation (i.e. one location at strong bus, one location at weak bus, and two locations as a combination with wind penetration levels), and the intermittency of wind generation output (fluctuation of wind generation output).

Table 6.2: Wind power input data for different wind penetration with one day load period

Time (Hour)	Total Loads (MW)	10%WP (100 MW)	20% WP (200 MW)	30% WP (300 MW)
01:00:00	283.4	96.9	24.96	55.5
02:00:00	283.4	67.7	57.7	37
03:00:00	302.5	13.5	174.5	100.5
04:00:00	302.5	78.4	162.4	8
05:00:00	358.8	51.5	104.3	91
06:00:00	358.8	48.3	45.6	275.5
07:00:00	500	39.6	119.4	165.2
08:00:00	500	9.1	190.2	5.5
09:00:00	615.5	0	164.4	35.7
10:00:00	615.5	24.6	143.4	167.4
11:00:00	454.6	86.6	84.7	15.3
12:00:00	454.6	73.5	54.2	110.5
13:00:00	504.3	43.8	97.9	80.7
14:00:00	504.3	12.5	200	12.5
15:00:00	745.5	45.6	157	6.5
16:00:00	745.5	74.3	123.2	285.7
17:00:00	850.1	100	200	300
18:00:00	850.1	68.9	96.4	7.5
19:00:00	695	45.3	130.5	0
20:00:00	695	46.7	38.2	12.4
21:00:00	450	23.5	13.5	113.6
22:00:00	450	19.5	43.8	176.3
23:00:00	314.9	87.7	30.2	165.1
00:00:00	314.9	56.4	70.1	35.9

In order to show the impact of wind generation on system MWh losses, the simulation results of all wind generation scenarios are compared with the base case (no wind generation connected to the system). The system MWh losses of the network are calculated for every one hour of the simulation and recorded for analysis. Figure 6.15 shows a plot of the system load (MW) and the corresponding system MWh losses when

no wind generation is connected to the network. It can be seen that the total system losses increase as the system load increases, and the maximum value (149.48 MW) of system MWh losses is recorded at peak load at 17:00 and 18:00, respectively, as shown in Figure 6.15.

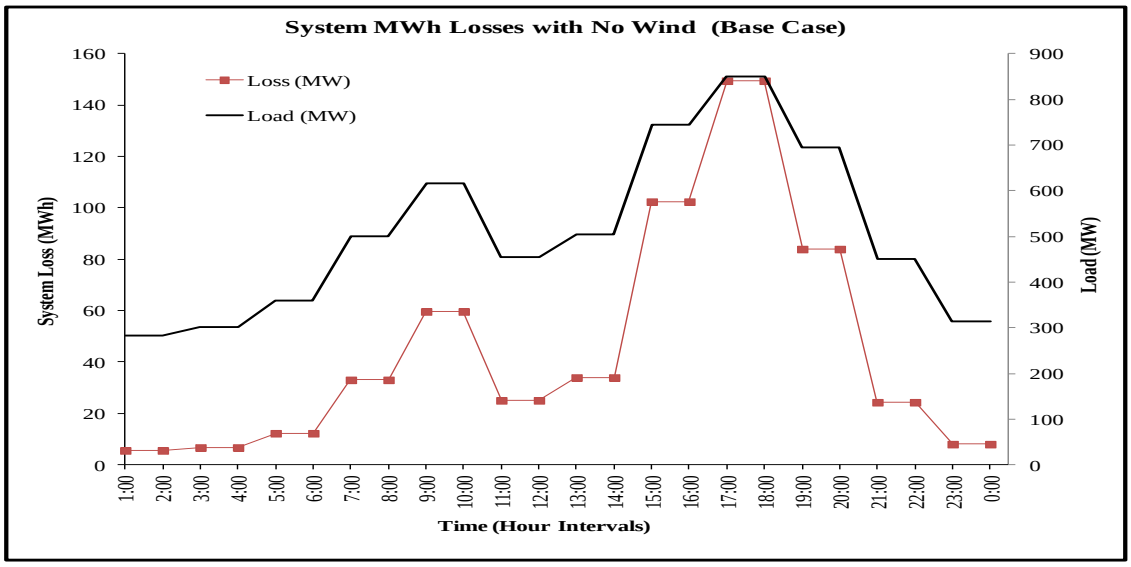

Figure 6.15: System MWh losses of IEEE-30 bus system with no wind generation.

In order to investigate the impact of wind penetration level on system MW losses, only one wind farm is connected to strong bus 28 at different wind penetration levels from 10% to 30% in steps of 10% for one month in the simulation. The wind generator is assumed to be a doubly fed induction generator (DFIG) which has reactive power control capability. In this assessment, the DFIG is modelled as a PV bus and operated with maximum and minimum power factors of 0.95 leading (capacitive VAr) and 0.95 lagging (inductive VAr). The analysis concentrates on maximum wind generator output for each penetration level when system loading is at its peak.

Figures 6.16, 6.17 and 6.18 illustrate the impact of different wind penetration levels on the system MW losses of an IEEE-30 bus system. As shown in Figure 6.16, the system MW losses decrease to 109.4 MW at a peak load at 17:00 when wind generation is at a maximum output of 100 MW (10% WP) compared to the no wind case (149.48 MW). When the wind penetration level increases to 20% and 30%, the system witnesses

a significant decrease in system MWh losses compared to the no wind case when the system loading is at peak load, as shown in Figures 6.17 and 6.18, respectively. It can be seen that the value of system MWh losses decreases with the connection of wind generation from 149.48 MW in the case of no wind generation to 84.89 MW for 20% wind penetration (WP) and 59.44 MW for 30% WP, as shown in Figures 6.17 and 6.18, respectively. This means that the DFIG based wind farm with voltage controlled mode has a good effect on decreasing the system MWh losses when the system is based on system loadability, especially when the wind farm is connected to a strong bus or closest to the central generation.

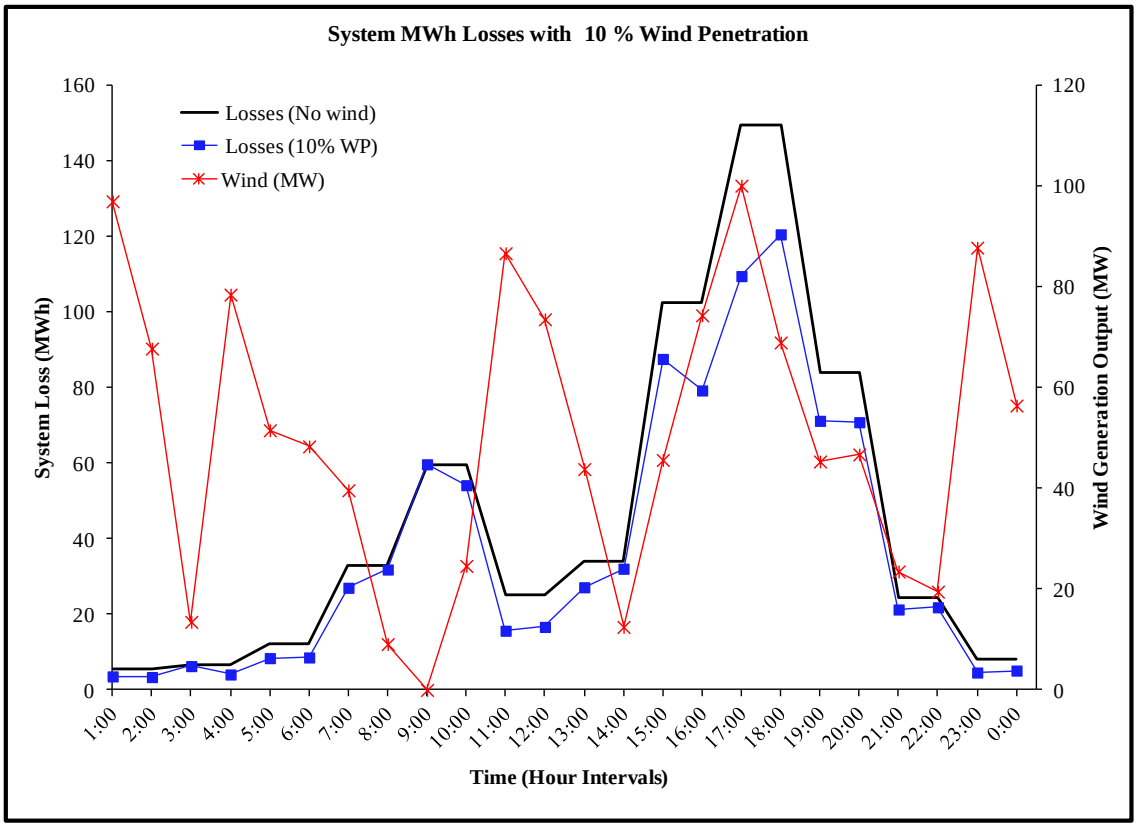

Figure 6.16: System MWh losses of IEEE-30 bus system with 10% wind penetration level, when a single wind farm is connected to bus 28.

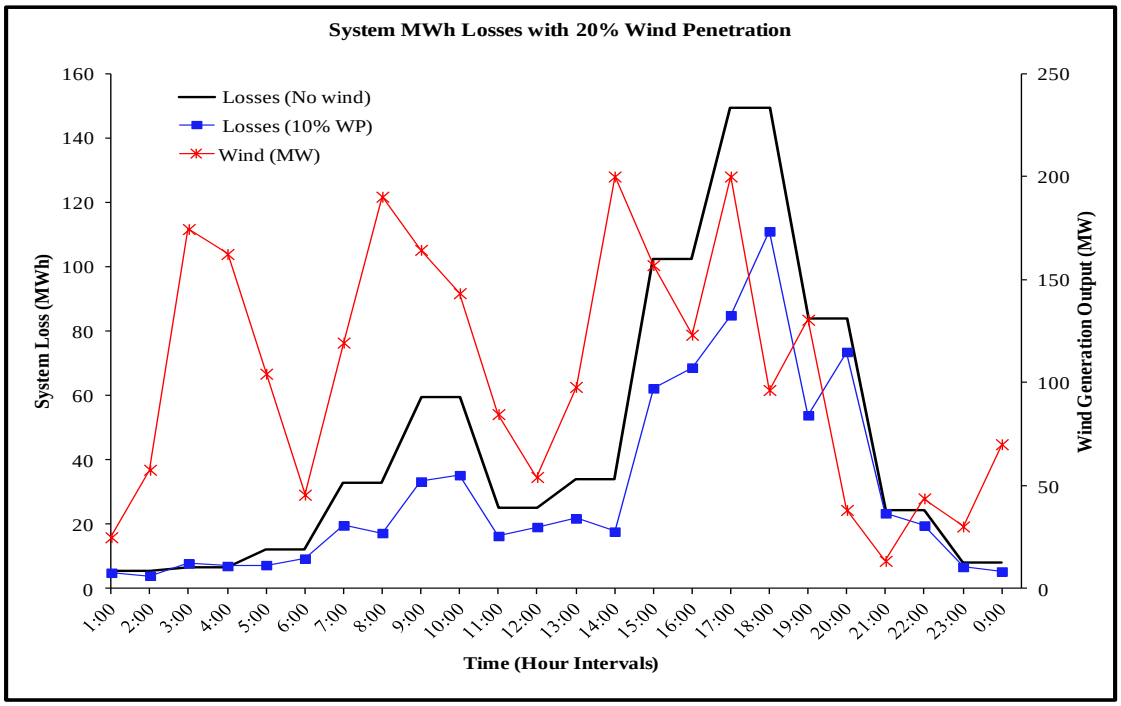

Figure 6.17: System MWh losses of IEEE-30 bus system with 20% wind penetration level, when a single wind farm is connected to bus 28.

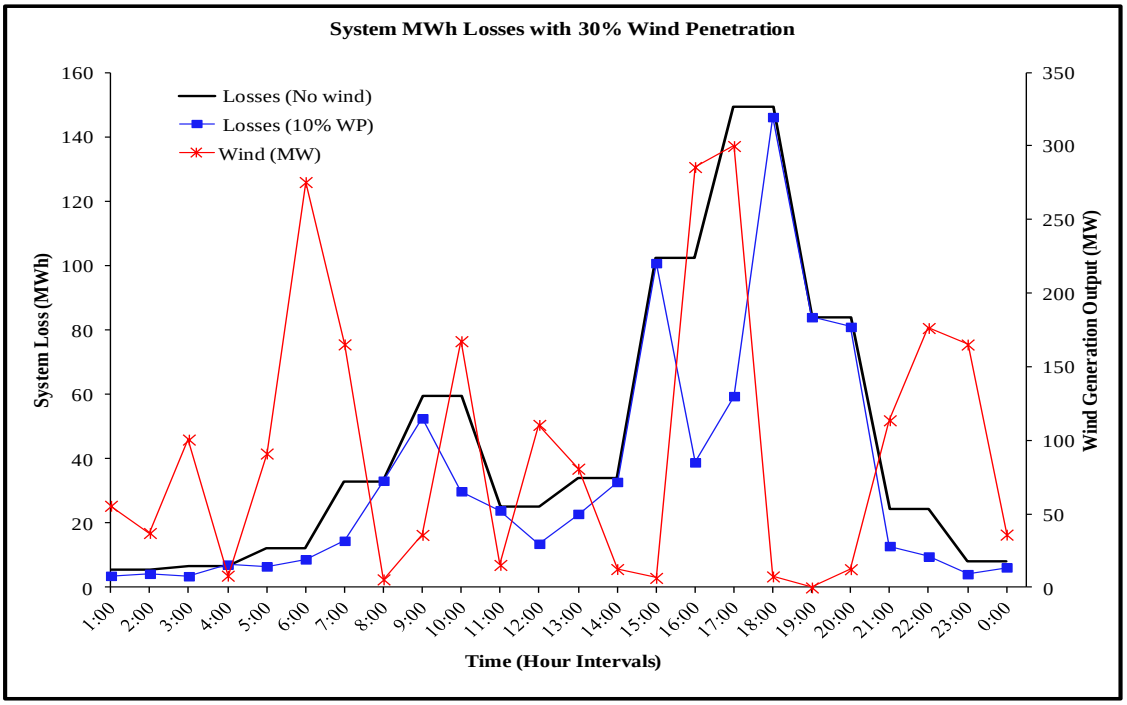

Figure 6.18: System MWh losses of IEEE-30 bus system with 30% wind penetration level, when a single wind farm is connected to bus 28.

The objective of connecting wind generation at different locations is to investigate the effect of location site on system MWh losses. There are three wind farm connection scenarios: a strong area at bus 28, a weak area at bus 14, and two locations at buses 6 and 28 as dispersion of wind generation. The system MWh losses are analysed for two different wind generation levels (20% and 30%). The results presented here are for a 24 hour period. The system MWh losses of the network are calculated for every one hour of the simulation and are recorded. As shown in Figure 6.19, the value of the system MW losses decrease with the connection of wind generation from 149.48 MW at the peak load period in the case of no wind generation to 80.06 MW for the connection case (1 wind farm is connected to a strong bus 28), 84.89 MW for the connection case (2 wind farms are connected to buses 6 and 28) and 129.6 MW as one wind farm is connected to a weak bus 14 when the percentage of wind capacity was 20% (200 MW). It can be seen that for 20% wind penetration level, the total system real power losses are reduced significantly for both wind connection scenarios compared to the base case. From a total system real power loss point of view, a single wind farm being connected to a strong bus is a better option and will reduce the real power losses more than other connection scenarios.

When the wind penetration level increases from 20% to 30%, the total system MW losses are reduced more for both wind connection scenarios (for one strong location and for multiple locations) compared to the base case and when the wind generation is 30% (300 MW). The system MW losses are recorded as 59.4 MW when the wind farm is connected to the strong bus and 62 MW for 2 wind locations. The system witnesses a significant reduction in system MW losses for higher wind penetration levels as the system becomes more heavily loaded, as shown in Figure 6.20. However, when the wind penetration level, connected to weak bus 14, increases to 30%, the system MW losses are increased to 166.1 MW, which is a slight increase compared to the no wind case (149.48 MW). This means that a higher wind penetration might increase the system MW losses during system loadability (at the peak load) when the wind farm is connected to a weak area.

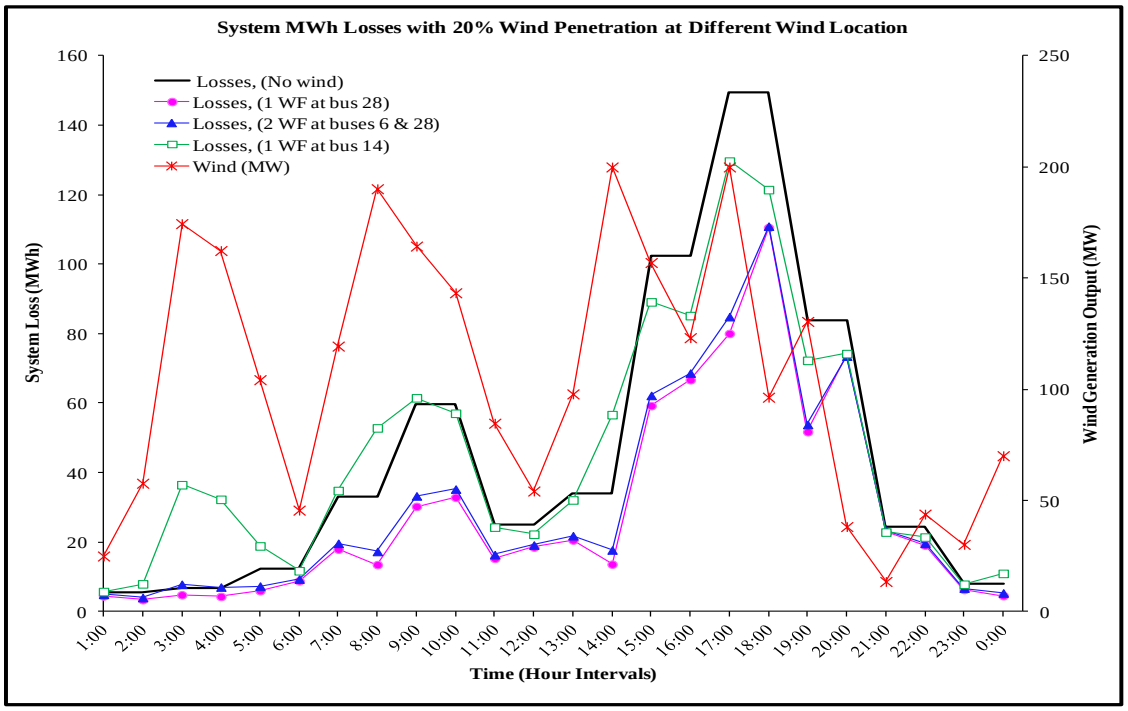

Figure 6.19: System MWh losses of IEEE-30 bus system with 20% wind penetration level, when wind farm is connected to the network at different connection scenarios.

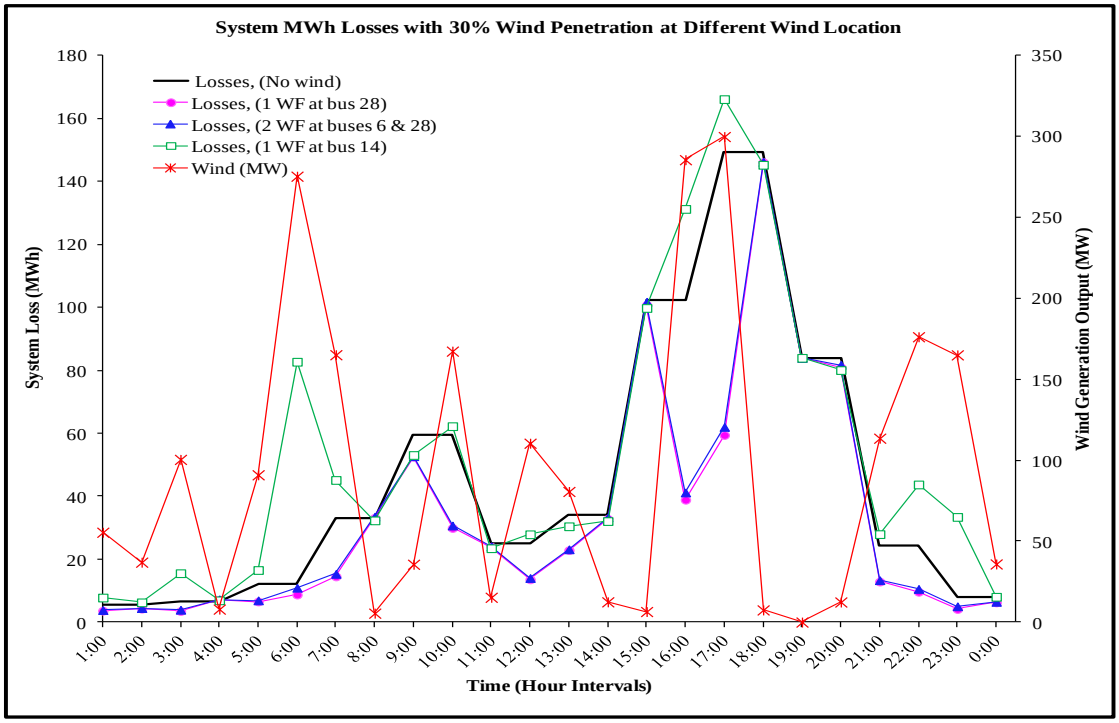

Figure 6.20: System MWh losses of IEEE-30 bus system with 30% wind penetration level, when wind farm is connected to the network at different connection scenarios.

In order to investigate the effect of fluctuation of wind generation output on system MWh losses, only one wind farm (connected to bus 28) is considered in the study. The study concentrates on peak load when large and sudden changes in power are injected into the network from wind generation. The system MW losses are calculated at 17:00 (300 MW) of wind generation output, then compared to the losses value at the same loading when wind generation output suddenly changes to 7.5 MW at 18:00. Figure 6.21 shows that the system losses value of the IEEE-30 bus system has been calculated and found to be 9.4 MW at peak load at 17:00 when wind generation is at a maximum output of 300 MW. Then the value of system MWh losses increases to 146.1 MW at the same peak load in the following time step at 18:00, when there is a large decrease in power output from wind generation (7.5 MW). It can be seen in Figure 6.21 that the system MW losses value increases due to intermittency of wind generation output.

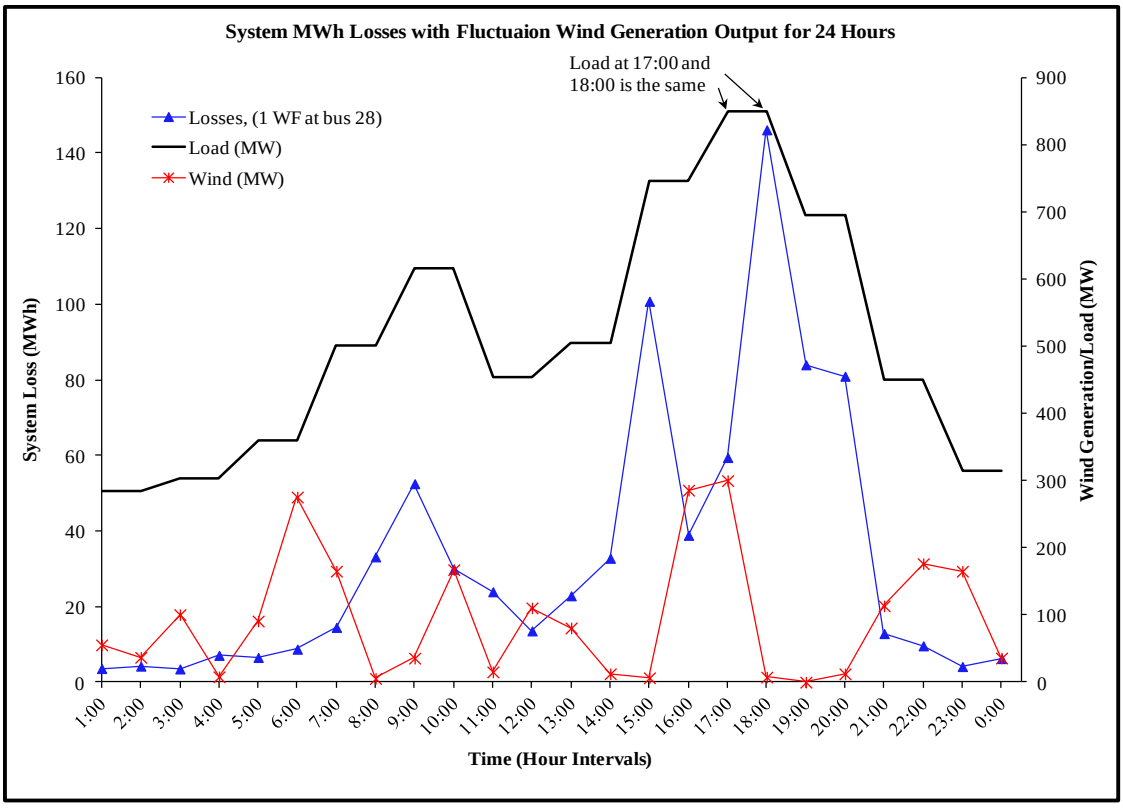

Figure 6.21: The system MWh losses values and load curve of IEEE-30 bus system with fluctuation wind generation output for 24 hours; only one wind generation is connected at bus 28.

6.5 Conclusion

This chapter has investigated the impact of wind generation intermittency and its penetration levels and dispersion of wind farms on the transmission network. This includes the impact on power margin and system MW losses. A DFIG based wind farm with a voltage controlled mode was integrated into an IEEE-30 bus system. Different connection scenarios of wind farms were considered; a single location (a strong bus and a weak bus) and dispersion of wind farms in two locations. This chapter has developed a method for calculating the power margin based on wind generation intermittency. The indicator of the power margin has been used in this chapter to measure the impact of wind generation on system voltage stability. From the results presented in the chapter, it can be concluded that the system collapse margin improves with wind penetration level and the system collapse margin is better for higher penetration levels. Also, the system power margin is better for a single strong location of wind generation compared to two locations of wind generation with a combination of wind penetrations. On the other hand, wind generation does not improve the system collapse margin when the wind farm is connected to a weak bus or weak area. The DFIG based wind farm with voltage controlled mode has a positive effect on voltage stability of a network when the penetration level increases and when the DFIG is connected to a strong bus or close to central generation. However, the DFIG has a negative effect on voltage stability of a network when the DFIG is located at a weak area.

The results presented in this chapter show that the fluctuation of wind generation outputs have a negative effect on the system power margin of a network, especially when a large decrease in the wind power is injected into the network. This means that the intermittency of wind generation might weaken the system voltage stability, according to the result analysis in this chapter. The impact of wind generation on system MW losses based on system loadability has also been investigated. The results analysed show that the wind penetration level in a transmission network is capable of reducing system MW losses when the network is based on system loadability. In addition, the results show that a single strong location for a wind farm with higher wind penetration

levels can achieve a significant reduction in system MW losses when the system loading is high. However, the results show that real power losses increase if the wind farm is located at a weak area with higher wind penetration levels when the system is highly loaded.

Chapter 7

Conclusions and Future Work

7.1 Conclusions

In line with the objectives of the study, this thesis has presented a new problem facing the electricity industry, namely the integration of sources of renewable generation, especially those with stochastic outputs, and how they are likely to affect system voltage stability with increasing penetration levels of wind generation. This thesis has investigated the problem of longer-term voltage instability when the reactive power limitation of wind generators is taken into consideration when a system reaches its maximum loading. A voltage collapse proximity indicator (VCPI) based on network loadability has been derived by taking into consideration the reactive power limitation of the wind generator. Also, this thesis has investigated the impact of wind generation intermittency, as well as the impact of penetration and wind generation location on system voltage stability. In addition, this thesis has investigated the impact of wind generation intermittency and penetration on the system transmission losses based on system loadability. The original contribution can be summarized:

1. The study has developed a voltage collapse proximity indicator (VCPI) calculation method which takes into consideration the reactive power limitation of wind generators in the system. Secondly,

2. The thesis has proposed a new assessment methodology related to the impact of wind generation on voltage stability of power systems, taking into consideration wind generation intermittency and load variations. In this methodology, a voltage collapse proximity indicator (VCPI) based on network loadability is used to investigate the contribution of wind generation to the system voltage stability.

3. The thesis has developed a comprehensive methodology for calculating the power margin based on wind generation variability. The power stability margin is used to measure the impact of wind generation on system voltage stability.

The thesis began by presenting a general review of wind generation, concentrating on the relevant technologies in use today for electricity generation. The aim was to put forward an understanding of the rapid developments taking place around the world in relation to the use of wind generation and the likely consequences this will have on the operation of electricity systems. The main reasons for the rapid development in wind generation of electricity are environmental, economic and related to the security of supply. A detailed discussion was presented on its present status and the potential of wind generation technologies around the world. The development of wind turbine technologies over the past twenty-five years has put wind generation to the forefront of renewable electricity generation. This thesis has presented a detailed analysis of different wind turbine technologies in use, their advantages and disadvantages, and their capacities. The stochastic power output of wind generation brings a new set of problems related to voltage stability of power systems. For analysis purposes, in this study the type of wind generator used was of variable speed, namely a doubly fed induction generator (DFIG) which was modelled on load flow studies as a PV bus and operated in voltage controlled mode.

This thesis has also presented the concept of voltage stability. This has included basic definitions related to voltage stability and a brief discussion of voltage instability incidents to help demonstrate the causes and circumstances surrounding voltage collapse. This thesis has also provided a descriptive analysis of the relationship between power (active and reactive) and voltage at the receiving-end. The following findings have been made: voltage stability is related to load areas and load characteristics; voltage stability depends on the relationship between power transfer and receiving-end voltage; the power factor plays a significant role in the voltage-power characteristics of the system; and the reactive power margin of the power system can be obtained from the study of the Q-V curves. Some voltage collapse analytical metods have been described,

all of which have the objective of calculating the proximity to the voltage collapse point. One common point in these methods is that the majority of them use tranditional load flow equations and extract information from the Jacobian Matrix.

This research involved an investigation of a voltage collapse proximity indicator (VCPI) and determination of the critical state from any of the operating points that consider the wind generator reactive power limits. The VCPI calculation method has been developed in this thesis, taking into consideration the reactive power limitation of wind generators in the system. The method identifies a new reference bus when necessary, which is a requirement to determine the new equivalent system impedance. Due to the reactive power limitation of wind generators, this equivalent system impedance is not constant. The method uses PV-PQ sensitivity and 'referencing' techniques to determine the system equivalent impedance**.** The relationship between the voltage collapse proximity indicator and the load power, the voltage and the system equivalent impedance, takes into consideration the reactive power limitation of wind generators in the system, as assessed in Chapter 4. The results presented in Figures 4.18-30 show that the system equivalent impedance remains constant until the reference bus (wind generation) reaches its reactive power limit. After this, new system equivalent impedance is calculated, which also remains constant until the collapse point. The voltage collapse proximity indicator is the ratio of the system equivalent impedance to the load equivalent impedance. The value of the VCPI varies from zero at no load to 1.0 at maximum loadability. In other words, it measures the proximity to voltage collapse in terms of power loadability for every load connected to the network. It is the ratio of the system equivalent impedance to the load equivalent impedance. This ratio conforms with the theory of longer-term voltage stability defined by the IEEE power system engineering committee [14] as the ability of the system to maintain voltage so that when load admittance is increased, the load power will increase, and so both power and voltage are controllable. The VCPI states that the maximum power is reached when the load impedance is equal to the system equivalent impedance. The VCPI behaves nearly linearly with the load variation, as shown in Figures 4.18-30, and the voltage variation is

small for lightly loaded systems and hence the load equivalent impedance variation is marginal. However, for a heavy loaded system, any small increase in demand induces a severe voltage drop, which in turn causes a large increase in the voltage collapse proximity indicator.

This thesis has evaluated the impact of wind generation on system voltage stability, taking into consideration wind generation intermittency and load variations. Two different proximity indications have been used to investigate the contribution of wind generation to voltage stability in the power system, one of which is a voltage collapse proximity indicator (VCPI) based on network loadability. The second indicator is the power margin, which is used to measure the margin between the voltage collapse point and the current operating point. Generally, the results presented in this thesis show that voltage stability can be affected positively or negatively depending on penetration level, fluctuation of wind generator output, and location of wind generator connection. When wind generation was connected to a stronger bus it was able to improve system voltage stability and the higher the penetration level the better. The reverse was found to be true when wind generation was connected to a weaker bus, in which case reactive power compensation (e.g. SVC) may still be necessary, especially if a large penetration of the DFIG is connected to a weak area. The results obtained show that system voltage stability is better for a single wind farm connected to a stronger bus compared to multiple locations of wind farms for the same amount of wind penetration level. It can be concluded from the results that large wind generation output fluctuations, especially during high system loading, can lead to system voltage collapse. A protection system is required to protect systems from the risk of voltage collapse caused by intermittency of wind generation output during peak load. The improvement of voltage stability results shows a direct correlation to both the penetration level and the location of the wind generation. Developers and system operators can decide on the location and penetration levels of new wind farms to be connected to existing systems based on the proposed methodologies, which calculate the system proximity to voltage collapse using both the

voltage collapse proximity indicator and the system stability margin, which considers location, penetration level, and the intermittent nature of wind generators.

Finally, this study has provided simulation and analysis of the impact of wind generation intermittency and penetration levels on system losses in a transmission network. The results analysed show that wind penetration level and wind location in the transmission network can reduce the system MW losses when the network is based on system loadability. In addition, the results indicate that a single strong location of a wind farm with higher wind penetration levels can achieve a significant decrease in the system MWh losses when the system loading is high. However, the results show that real power losses increase if the wind farm is located at a weak area with higher wind penetration levels when the system is highly loaded. As mentioned previously, the proposed methodologies have been tested on a variety of network configurations, ranging from a 3-bus system to an IEEE 118-bus system. It has also been tested on buses at different locations of a network, from remote to those that are close to generation. Finally, a number of sets of results have been obtained from different wind conditions, including different wind power generation penetration level conditions, different wind generation locations, and intermittent wind power.

7.2 Future Work

In any research work, there are always areas for possible improvement. This section suggests possible improvements or further ways to test the proposed method for evaluating the impact of wind generation on system voltage stability.

(a) The proposed method for evaluating the impact of wind generation on system voltage stability was applied to IEEE test systems and the UKGDS test system. It would be worthwhile for utilities to apply the proposed method to real networks and compare the results obtained with those presented in this thesis in relation to IEEE test systems and the UKGDS test system.

(b) The focus of this thesis was mainly on a variable speed doubly fed indication generator (DFIG) which was modelled as a PV bus. Hence, a further step would be to implement methods that consider other types of wind generators, such as a fully rated converter and a DFIG modelled as a PQ bus in the power flow. Moreover, it is necessary to consider reactive power compensation (e.g. SVC, STATCOM) and evaluate the impact.

(c) It would be interesting to test the validity of the proposed methods in relation to other renewable energy sources, such as photovoltaics, and evaluate their impact on system voltage stability.

(d) It would be useful to develop and use other proximity indications to evaluate the impact of wind generation on system voltage stability and compare the results obtained with those presented in this thesis.

References

[1] B.M. Weedy, B.J. Cory, Electric Power System, Forth Edition, UK: John Wiley & Sons, Ltd, 1998.

[2] Thomas. Ackermann, Goran. Andersson, Lennart. Soder, "Distributed Generation Definition," Electric Power Systems Research, Vol. 57, pp195-204, December 2000.

[3] D. Gautam, "Impact of Increased Penetration of DFIG Based Wind Turbine Generators on Rotor Angle Stability of Power System", PhD thesis, Arizona State University, December 2010.

[4] World Wind Energy Association, Available online at http://www.wwindea.org/home/index.php/ Last accessed March 2012.

[5] K. Hanjalic, R.Van de Krol, A. Lekic, "Sustainable Energy Technologies: Operations and Prospects," Springer Verlag, 2008.

[6] M.H. Albadi, E.F. El-Saadany, "Impact of Wind Power Variability on Generation Costs-An Overview," The Journal of Engineering Research, Vol.7 No. 2, pp. 24-31, April 2010.

[7] J. G. Slootweg, "Wind Power Modelling and Impact on Power System Dynamics," PhD thesis, Delft University of Technology, The Netherlands, 2003.

[8] J. Soens, "Impact of Wind Energy in a Future Power Grid," PhD thesis, Katholieke Universiteit Leuven, Belgium 2005.

[9] I.S. Naser, Olimpo Anaya-Lara, K. L. Lo, "Study of the Impact of Wind Generation on Voltage Stability in Transmission Networks," IEEE DRPT, The 4th International Conference on Electric Utility Deregulation and Restructuring and Power Technologies. 6th-9th July, 2011, Shandong, China.

[10] IEEE System Dynamic Performance Subcommittees, "Voltage Stability of Power Systems: Concepts, Analytical Tools and Industry Experience", IEEE Document 90TH-0358-2-PWR, 1990.

[11] V. Balamourgan, T.S. Sidhu, M.S. Sachdev, "Technique for On Prediction of Voltage Collapse", IEE Proc-Generation, Transmission, Distribution, 2004, 151(4)453-460.

[12] J. Bialek, “Are blackouts contagious?” IEE Power Engineer, pp. 10-13, Dec/Jan, 2003/04. Available at www.see.ed.ac.uk/~jbialek/IEE%20Power%20Engineer%20blackouts.pdf

[13] L. Chunyan, S. Yuanzhuny, C. Xiangyi, “Recommendations to improve Power System Security: Lessons Learned from the Europe Blackout on Nov 4th 2006”, UPEC 2007, Brighton, UK.

[14] “Voltage Stability of Power Systems: Concepts, Analytical Tools and Industry Experience”, IEEE Catalog Number 90TH0358-2.

[15] W. Casson, H.J. Sheppard, “Technical and Economical Aspects of the Supply of Reactive Power in England and Wales”, Proc.IEE 108 A, pp. 507-526, March 1961.

[16] V.A. Venikov, V.A. Strov, V.I. Idelchick, V.I. Tarasov, “Estimation of Electrical Power System Steady State Stability in Load Flow Calculations”, IEEE Transaction on Power Apparatus and Systems, Vol. PAS-94, No.3, pp. 1034-1040, May 1975.

[17] Vu. Khoi, M.B. Miroslav, N. Damir, M. S. Murari, “Use of Local Measurements to Estimate Voltage Stability Margin”, IEEE Transactions on Power Systems, Vol.14, No.3, August 1999.

[18] S. Minami, S. Morii, S. Kawamoto, “Voltage Stability Analysis for Bulk Power System by P-V and Q-V Curves Considering Dynamic Loads”, Proc. of ICEE, No.0-013, Japan 2008.

[19] C. Reis, A. Andrade, F.P. Maciel, “Voltage Stability Analysis of electrical Power System”, POWERENG 2009, Lisbon Portugal, March 2009.

[20] F. Echavaren, E. Lobato, L. Rouco, “Steady-State Analysis of the Effect of Reactive Generation Limit in Voltage Stability”, pp 1292-1299. ELSEVIER2009.

[21] Van Cutsem, “A Method to Compute Reactive Power Margins with Respect to Voltage Collapse”, IEEE Transaction on Power Systems, Vol. 6, No. 2, pp. 145-156, February 1991.

[22] A.C. Zambroni de Souza, A.P.A da Silva, J.L.A. Jardim, L.C.A. Ferreira, “A New Contingency Analysis Approach for Voltage Collapse Assessment”, ELSEVIER2003, Electrical Power and Energy Systems, No.25, pp.781-785, 2003.

[23] A. Augugliaro, L. Dusonchet, S. Mangione, “Voltage collapse proximity indicators for radial distribution networks”, Proceedings of the 9th International Conference on Electrical Power Quality and Utilization, pp. 1-6, 9-11 October, 2007, Barcelona, Spain.

[24] M.V. Suganyadevia, C.K. Babulal, "Estimating of loadability margin of a power system by comparing voltage stability indices", Proceedings of the International. Conference on Control, Automation, Communication and Energy Conservation, pp. 1-4, 4-6 June, 2009, Erode, India.

[25] Chebbo, M. Irving, M. Sterling, "Voltage Collapse Proximity Indicator: Behaviour and Implications", IEE Proc., Pt. C, Vol. 139, No.3, pp.241-252, May 1992.

[26] R. Alammari, "A New Simplified Approach to the Long-Term Voltage Stability and Security in Electrical Power Systems", PhD Thesis, Strathclyde University, Glasgow, February 1996.

[27] Vu. Khoi, M. M. Begovic, D. Novosel, M.M. Saha, "Use of Local Measurements to Estimate Voltage-Stability Margin", IEEE Transaction on Power Systems, Vol.14, No. 3, pp. 1029-1035, August 1999.

[28] V. Balamourougun, T. S. Sidhu, M.S. Sachdev, "Technique for Online Prediction of Voltage Collapse", IEE Proc, Generation. Transmission. Distribution, Vol. 151, No.4, pp. 453-460, July 2004.

[29] H. Wei, Z. Guohua, Y. Jingyan, L. Zongqi, Z. Jianhua, "An Approach for Estimating static Voltage Collapse", Power Engineering Conference, IPEC 2005.

[30] Y. Wang, W. Li, J. Lu, "A New Node Voltage Stability Index Based on Local Voltage Phasors", Electric Power System Research, Vol.79, No. 1, pp. 265-271, January 2009.

[31] C.W. Taylor, "Power System Voltage Stability", Mc Graw-Hill, New York, USA, 1994.

[32] E. Muljad, C.P. Butterfield, B. Parson, A. Ellis, "Effect of Variable speed wind Turbine Generator on Stability of a Weak Grid", IEEE Transactions on Energy Conversion, Vol. 22, No. 1, March 2007.

[33] H. Muller, M. Poller, Ch. Eping, J. Stenzel, "Impact of Large Scale Wind Power on Power System Stability", Power and Transmission Network for offshore Wind Farms, Fifth International Workshop, Glasgow, UK, April 2005.

[34] L. T. Ha, T. K. Saha, "Investigation of Power Loss and Voltage Stability Limits for Large Wind Farm Connections to a Subtransmission Network", IEEE Power Engineering Society General Meeting, Colorado, USA, June 2004.

[35] C. Han, A.Q. Huang, M.E. Baran, S. Bhattacary, L. Anderson, A. Edris, "STATCOM Impact Study on the Integration of a Large Wind Farm into Weak Loop Power System", IEEE Transaction on Energy Conversion, Vol. 23, No. 1, March 2008.

[36] C. Wong, D. Mader, "Voltage Stability Studies Using Real-Time Simulation Computing", System Theory, SSST2008, 40th Southeastern Symposium on, pp. 410-419, March 2008.

[37] W. Freitas, J. C. M. Vieira, L. C. P. da Silva, "Long-Term Volatge Stability of Distribution System with Induction Generators", IEEE 2005, Power Engineering Society General Meeting, pp. 2910-2913, Vol. 3, 12-16 June 2005.

[38] Y. Chi, Y. Liu, W. Wang, H. Dai, "Voltage Stability Integration into Transmission Network", International Conference on Power System Technology, PowerCon 2006, pp. 1-7, October 2006.

[39] N. R. Ullah, T. Thiringer, "Variable Speed Wind Turbines for Power System Stability Enhancement", IEEE Transactions on Energy Conversion, Vol. 22, No. 1, pp. 52-60, 2007.

[40] Z. Chan, Y. Huand, F. Blaabjerg, "Stability Improvement of Induction Generator-based Wind Turbine System", IET Renewable Power Generation, Vol. 1, No. 1, pp. 81-93, March 2007.

[41] T. T. Chuong, "Voltage Stability Investigation of Grid Connected Wind Farm", World Academy of Science, Engineering and Technology, 2008.

[42] S. Abdelkader, "Voltage stability Assessment for Systems with Large Wind Power Generation", UPEC 2009, pp. 14-17, Glasgow, UK, 1-4 September, 2009.

[43] M. Alonso, H. Amaris, "Voltage Stability in Distribution Networks with DG", 2009 IEEE Bucharest Power Conference, Bucharest, Romania, June 28th-July 2nd, 2009.

[44] J. Eriksson, "In 2011 World Wind Power Capacity Reaches New Heights", IPS New Report, March 18, 2012. Available at: http://www.renewablepowernews.com/archives/3005

[45] Danish Wind Industry Association, "Describing Wind Variations: Weibull Distribution", 19 September, 2003. Available at: http://www.windpower.org/en/tour/wres/weibull.htm

[46] HE. Dexin, "Small Wind World Report 2012: Summary", World Wind Energy Association, Available at http://www.wwindea.org/home/index.php/

[47] Global Wind Energy Council, “A report of the Global Wind Energy Outlook”, GWEC, 12 October, 2010, Available at

http://friendsofwind.ca/wind-power-could-provide-15th-of-worlds-electricity-by-2030/

[48] European Wind Energy Association, Available online at http://www.ewea.org/

Last accessed; March 2012.

[49] British Wind Energy Association, “Onshore and Offshore Wind Energy Targets”, 2007, Available at http://www.bwea.com/planning/index.html.

[50] European Wind Energy Association, “Wind Power Capacity and Production Report”, 2011, Available at http://en.wikipedia.org/wiki/Wind_power#Wind_energy

[51] Li. Junfeng, G. Hu, “China Wind Power Report 2007”, China Environmental Science, Beijing, January, 2007.

[52] “Wind Electricity Installed Capacity". International Energy Statistics, (EIA), Retrieved2011-04-24.Available at http://www.eia.doe.gov/cfapps/ipdbproject/iedindex3.cfm?tid=2&pid=37&aid=7&cid=CH,&syid=2004&eyid=2008&unit=MK. .

[53] “China Could Replace Coal with Wind". Ecogeek.org. Retrieved 2010-01-31. Available at http://ecogeek.org/wind-power/2948-china-could-replace-coal-with-wind.

[54] Climate Action Network, “Why haven’t the USA and Australia jointed the Kyoto Protocol?”, 2005, Available at: htt://www.climatenetwork.org/climate-change-basics/usa-and-australia

[55] “Wind Powering America: Installed U.S. Wind Capacity and Wind Project Locations". U.S. Department of Energy. January 19, 2012. Retrieved January 19, 2012, Available at:

http://www.windpoweringamerica.gov/wind_installed_capacity.asp.

[56] E.ON Delivers 335-MW of Wind in Texas, 23 September, 2008.

[57] "Strengthening America’s Energy Security with Offshore Wind", U.S. Department of Energy, February 2011.

Available at: http://www.nrel.gov/docs/fy11osti/49222.pdf

[58] Bundesministerium für Wirtschaft und Technologie (February 2012), "Die Energiewende in Deutschland". Berlin. p. 4. Available at:

http://www.bmwi.de/Dateien/BMWi/PDF/energiewende-in-deutschland,property=pdf,bereich=bmwi,sprache=de,rwb=true.pdf.

[59] "Alpha-Ventus Report", 2009, Available at: http://www.alpha-ventus.de/

[60] "BWEA Statistical Overview of Wind Farms 2012", 2012, Available at: http://www.bwea.com/statistics/

[61] "Wind Power Energy in Libya 2012" the Ministry of Electrical and Renewable Energy, Available at:

http://www.gecol.ly/aspx/main.aspx

[62] L. Shuhi, T. A. Haskew, "Energy Capture Conversion and Control Study of DFIG Wind Turbine under Weibull Wind Distribution", In Power & Energy Society General Meeting, pp. 1-9, PES IEEE, 2009.

[63] I. M. D. Alegri, "Connection Requirements for Wind Farms: A Survey on Technical Requirements and Regulation", Renewable and Sustainable Energy Reviews, Vol. 11, No. 8, pp. 1858-1872, October 2007.

[64] S. Chondroiannis, "Modeling and GB Grid Code Compliance Studies of Offshore Wind Farms with Doubly-Fed Induction Generators", In Power Electronics, Machines and Drives, The 3rd IET International Conference on, pp. 22-26, 2006.

[65] "The Grid Code", No. 3, Vol 12. Available at http://www.nationalgrid.com/uk/Electricity/Codes/gridcode/gridcodedocs/

[66] G. L. Johnsson, "Wind Energy Systems" Englewood Cliffs, N. J., USA, Prentice-Hall, 1985.

[67] T. Thiringer, J. Linders, "Control by Variable Rotor Speed of a Fixed-pitch Wind Turbine Operating in a Wide Speed Range", IEEE Transactions Power Conversion, Vol. 8, No. 3, pp. 520-526, September 1993.

[68] "Wind Electricity Generation: Technical Brief", Practical Action.

Available at: practicalaction.org/docs/technical.../wind_electricity_generation.pdf -

[69] S. M. Muyeen, M. H. Ali, R. Takahashi, T. Murata, A. Sakahara, E. Sasano, "Comparative Study on Transient Stability Analysis of Wind Turbine Generator System

Using Different Drive Train Models", IET Renewable Power Generation, Vol. 1, No. 2, pp. 131-141, June 2007.

[70] R. Billinton, L. Gan, "Wind Power Modeling and Application in Generation Adequacy Assessment", IEEE Conference Proceedings Communications Computers and Power in Modern Environment. WESCANEX93, pp.100-106, May 1993.

[71] P. Giorsetto, K. Utsurog, "Development of a New Procedure for reliability Modelling of Wind Turbine Generators" IEEE Transactions, Power on Apparatus and Systems, Vol. PAS-102, pp. 134-143, January 1983.

[72] H. Li, Z. Chen, "Overview of Different Wind Generator Systems and Their Comparisons", IET Renewable Power Generation, Vol.2, No.2, pp. 123-138, June 2008.

[73] B. Fox, D. Flym, L. Bryans, N. Jenkins, D. Milborrow, M. O'Malley, R. Watson, O. Anaya-Lara, "Wind Power Integration: Connection and System Operation Aspect", IET Power and Energy, Series 50 IET, 2007.

[74] W. L. Kling, J. G. Slootweg, "Wind Turbines as Power Plants".

[75] T. Burton, D. Sharpe, N. Jenkins, E. Bossanyi, "Wind Energy Handbook", Tohn Wiley and Sons Ltd, 2001.

[76] P. W. Carlin, A. S. Laxson, E. B. Muljadi, "The History and State of the Art of Variable-Speed Wind Turbine Technology", Tech. Rep. National Renewable Energy Laboratory, 2001. Available at: http://www.nrel.gov/docs/fy01osti/28607.pdf

[77] L. Holdsworth, X. G. Wu, J. R. Ekanayake, N. Jenkins, "Comparison of Fixed-Speed and Doubly-Fed Induction Wind Turbine during Disturbances", IEE Proceedings Part C, 150 (3), pp.343-352, 2003.

[78] B. H. Chowdhury, S. Chellapilla, "Double-Fed Induction Generator Control for Variable Speed Wind Power Generation", ELSEVIER 2005, Electric Power System Research 76, pp. 786-800, 20 December 2005.

[79] J. G. Slootweg, S. W. H. de Haan, H. Polinder, W. L. Kling, "General Model for Representing Variable Speed Wind Turbines in Power System Dynamics Simulations" IEEE Transactions on Power System, Vol. 18,No. 1, February 2003.

[80] R. Richter, "Electrische Machinen", 2 nd ed, Basel/Stuttgart: Verlag Birkhauser, 1954, German.

[81] N. R. Ullah, T. Thiringer, "Variable Speed Wind Turbines for Power System Stability Enhancement", IEEE Transactions on Energy Conversion, Vol. 22, No. 1, pp. 52-60, March 2007.

[82] V.S. Pappala, S. N. Singh, M. Wilch, I. Erlich, "Reactive Power Management in Offshore Wind Farms by Adaptive PSO", International Conference on Intelligent Systems Application to Power Systems, (ISAP), pp. 1-8, November 2007.

[83] P. Kundur, J. Paserba, V. Aijarapu, G. Andersson, A. Bose, C. Canizares, N. Hatzizrgyiou, D. Hill, A. Stankovic, C. Taylor, T. V. Cutsem, V. Vittal, "Definition and Classification of Power System Stability", IEEE Transactions on Power Systems, Vol. 19, No. 2, pp. 1387-1401, May 2004.

[84] P. Kundur, "Power System Stability and Control", Mc Graw-Hill, New York, USA, 1994.

[85] IEEE Power System Engineering Committee, "Voltage Stability of Power Systems: Concepts, Analytical Tools, and Industry Experience", IEEE Publication 90 TH0358-2-PWR, 1990.

[86] Van. T. Cutsem, C. Vournas, "Voltage Stability of Electric Power Systems", Kluwer Academic Publishers, Boston, USA, 1998.

[87] D.J. Hill, I. A. Hiskens, D. Popovic, "Load Recovery in Voltage Stability Analysis and Control", Bulk Power System Phenomena III, Voltage Stability Security and Control, ECC, Davos, pp. 579-595, 1994.

[88] CIGRE Task Force 38, 02, 10, "CIGRE Technical Brochure: Modelling of Voltage Collapse Including Dynamic Phenomena", Electra, No. 147, pp. 71-77, April 1993.

[89] A. Atputharajah, K.S. Tapan, "Power System Blackouts-Literature Review" Fourth International Conference on Industrial and Information Systems, ICIIS 2009, 28-31 December 2009, Srilanka.

[90] "Blackout on August 14, 2003", Final Report February by New York Independent System Operator, February 2005.

[91] L. Chunyan, S. Yuanzhuny, C. Xiangyi, "Recommendations to improve Power System Security: Lessons Learned from the Europe Blackout on Nov 4th 2006", UPEC 2007, Brighton, UK.

[92] IEEE Task Force on Load Representation for Dynamic Performance, "Load Representation for Dynamic Performance Analysis", IEEE Tran. On Power Systems, Vol. 8, No. 2, pp. 472-482, May 1993.

[93] G. J. Berg, "Power-System Load Representation", Proceeding IEE, Vol. 120, No. 3, pp.344-348, March 1973.

[94] Y. Sekine, H. Ohtsuki, "Cascaded Voltage Collapse", IEEE Trans. on Power Systems, Vol. 5, No. 1, pp. 250-256, February 1990.

[95] D. J. Hill "Nonlinear Dynamic Load Models with Recovery for Voltage Stability Studies", IEEE Trans. on Power Systems, Vol. 8, No. 1, pp. 166-176, February 1993.

[96] N. Flatabo, R. Ogendal, T. Carlsen, "Voltage Stability Condition in a Power Transmission System Calculated by Sensitivity Methods", IEEE Transactoin on Power Systems, Vol. 5, No. 4, pp. 1286-1293, November 1990.

[97] B. Gao, G. K. Morrison, P. Kundur, "Voltage Stability Evaluation Using Modal Analysis", IEEE Transaction on Power Systems, Vol. 7, No. 4, pp. 1529-1536, November 1992.

[98] T. Q. Tuan, J. Fandino, N. Hadjsaid, J. C. Sabonnadiere, H. Vu, "Emergency Load Shedding to Avoid Risks of Voltage Instability Using Indicators", IEEE Transaction on Power Systems, Vol. 9, No. 1, pp. 341-351, February 1994.

[99] Y. L. Chen, W. B. Liao, S. C. Wang, K. Y. Shen, S. C. Tuan, "Voltage Collapse Proximity Indicators of a Power System", UPEC2001, Swansea, Wales, 12-14 September 2001.

[100] A. R. Mukhedkar, H. Nouri, "Comparative Study and Performance Analysis of Online Static Voltage Collapse Indices in Interconnected Systems", UPEC2001, Swansea, Wales, 12-14 September 2001.

[101] B. Singh, S. N. Singh, "Voltage Stability Assessment of Grid-Connected Offshore Wind Farms" Wind Energy, 2009 John Wiley & Sons. Ltd, Vol. 12, pp. 157-169, January 2

[102] Y. Mansour, P. Kundur, "Analysis and Control System Techniques for Electric Power Systems", Vol. 42, Part 2 of 4, Academic Press Inc, pp. 111-161, 1991.

[103] P. Kessel, H. Glavitsch, "Estimating the Voltage Stability of a Power System", IEEE Transaction on Power Delivery, (PWRD-1), Vol. 1, No. 3, pp. 345-352, July 1986.

[104] “Power Systems Test Case Archive” available at:

http://www.ee.washington.edu/research/pstca/

[105] UKGDS, “United Kingdom Generic Distribution System” 2009.

http://www.sedg.ac.uk/Workshop%2018%20Oct%202005/Poster%20-%20UKGDS%20and%20Typical%20Networks.pdf

[106] T. Boehme, A. Wallace, G.P. Harrison, “Applying Time Series to Power Flow Analysis in Networks with High Wind Penetration”, IEEE Transactions on Power Systems, Vol. 22, No. 3, pp. 951-957, August 2007.

[107] C. L. Chen, T.Y. Lee, R. M. Jan, “Optimal Wind-Thermal Coordination Dispatch in Isolated Power Systems with Large Integration of Wind Capacity”, ELSEVIER, Energy Conversion & Management, Vol. 47 pp. 3456-3472, February 2006.

[108] J. Hetzer, D. C. Yu, K. Bhattarai, “An Economic Dispatch Model Incorporating Wind Power”, IEEE Transactions on Energy Conversion, Vol. 23, No. 2, June 2008.

[109] http://dictionary.reference.com/browse/probability+density+function

Appendix A: IEEE 14-Bus Test System

i. Bus Data and Load Flow Results

Bus No.	Bus Voltage		Generation		Load	
	Magnitude (p.u.)	Angle (Deg.)	Real (MW)	Reactive (MVAr)	Real (MW)	Reactive (MVAr)
1	1.05	0	233.44	-42.97	0	0
2	1.05	-5.33	40	66.67	21.7	12.7
3	1.05	-13.45	0	69.38	94.2	19
4	1.0166	-10.46	0	0	47.8	3.9
5	1.01572	-8.89	0	0	7.6	1.6
6	1.05	-14.45	0	5.79	11.2	7.5
7	1.04096	-13.57	0	0	0	0
8	1.05	-13.57	0	5.39	0	0
9	1.03734	-15.21	0	0	29.5	16.6
10	1.03201	-15.37	0	0	9	5.8
11	1.03736	-15.05	0	0	3.5	1.8
12	1.03502	-15.34	0	0	6.1	1.6
13	1.03023	-15.42	0	0	13.5	5.8
14	1.01591	-16.34	0	0	14.9	5

ii. Transformer Data

Transformer	Between Buses	Tap Setting
1	4-7	0.978
2	4-9	0.969
3	5-6	0.932

iii. Shunt Capacitor Data

Bus No.	Susceptance (p.u.)
9	0.2045

iv. Line Data

Line Between Buses		Line Impedance		Half Line Charging Susceptance (p.u.)
From	To	R (p.u.)	X (p.u.)	
1	2	0.0194	0.0592	0.0264
5	1	0.054	0.223	0.0246
2	3	0.047	0.198	0.0219

2	4	0.0581	0.1763	0.0187
5	2	0.0569	0.1739	0.017
3	4	0.067	0.171	0.0173
5	4	0.0133	0.0421	0.0064
4	7	0	0.20912	0
4	9	0	0.55618	0
5	6	0	0.252	0
6	11	0.09498	0.1989	0
12	6	0.12291	0.25581	0
6	13	0.06615	0.13027	0
7	8	0	0.17615	0
9	7	0	0.11001	0
10	9	0.03181	0.0845	0
14	9	0.12711	0.2703	0
10	11	0.08205	0.19207	0
12	13	0.22092	0.19988	0
14	13	0.17093	0.34802	0

Appendix B: IEEE 30-Bus Test System

i. Bus Data and Load Flow Results

Bus No.	Bus Voltage		Generation		Load	
	Magnitude (p.u.)	Angle (Deg.)	Real (MW)	Reactive (MVAr)	Real (MW)	Reactive (MVAr)
1	1.05	0	138.79	-39.13	0	0
2	1.05	-3	57.6	15.13	21.7	12.7
3	1.044	-4.77	0	0	2.4	1.2
4	1.04165	-5.72	0	0	7.6	1.6
5	1.05	-9.38	24.6	48.53	94.2	19
6	1.04224	-6.66	0	0	0	0
7	1.03798	-8.27	0	0	22.8	10.9
8	1.05	-6.77	35	51.16	30	30
9	1.03677	-8.29	0	0	0	0
10	1.03641	-10.19	0	0	5.8	2
11	1.05	-6.33	17.9	6.99	0	0
12	1.03142	-9.21	0	0	11.2	7.5
13	1.05	-7.96	16.9	14.12	0	0
14	1.01906	-10.16	0	0	6.2	1.6
15	1.01706	-10.32	0	0	8.2	2.5
16	1.02615	-9.93	0	0	3.5	1.8
17	1.02791	-10.33	0	0	9	5.8
18	1.01153	-11	0	0	3.2	0.9
19	1.01145	-11.2	0	0	9.5	3.4
20	1.01689	-11.01	0	0	2.2	0.7
21	1.02467	-10.66	0	0	17.5	11.2
22	1.02544	-10.66	0	0	0	0
23	1.01324	-10.83	0	0	3.2	1.6
24	1.0167	-11.13	0	0	8.7	6.7
25	1.03035	-11.12	0	0	0	0
26	1.0129	-11.53	0	0	3.5	2.3

27	1.04738	-10.84	0	0	0	0
28	1.03824	-7.09	0	0	0	0
29	1.02804	-12.01	0	0	2.4	0.9
30	1.01686	-12.85	0	0	10.6	1.9

ii. Transformer Data

Transformer	Between Buses	Tap Setting
1	4-12	1.0129
2	6-9	1.0155
3	6-10	0.9629
4	28-27	0.9581

iii. Shunt Capacitor Data

Bus No.	Susceptance (p.u.)
10	0.204
24	0.041

iv. Line Data

Line Between Buses		Line Impedance		Half Line Charging Susceptance (p.u.)
From	To	R (p.u.)	X (p.u.)	
1	2	0.0192	0.0575	0.0528
1	3	0.0452	0.1852	0.0408
2	4	0.057	0.1737	0.0368
2	5	0.0472	0.1983	0.0418
2	6	0.0581	0.1763	0.0374
3	4	0.0132	0.0379	0.0084
4	6	0.0119	0.0414	0.009
4	12	0	0.256	0
5	7	0.046	0.116	0.0204
6	7	0.0267	0.082	0.017
6	8	0.012	0.042	0.009
6	9	0	0.208	0
6	10	0	0.556	0
6	28	0.0169	0.0599	0.013
8	28	0.0636	0.2	0.0428
9	10	0	0.11	0
9	11	0	0.208	0
10	17	0.0324	0.0845	0
20	10	0.0936	0.209	0
10	21	0.0348	0.0749	0
10	22	0.0727	0.1499	0
12	13	0	0.14	0
12	14	0.1231	0.2559	0
12	15	0.0662	0.1304	0
12	16	0.0945	0.1987	0

14	15	0.221	0.1997	0
15	18	0.107	0.2185	0
15	23	0.1	0.202	0
16	17	0.0824	0.1932	0
18	19	0.0639	0.1292	0
19	20	0.034	0.068	0
21	22	0.0116	0.0236	0
22	24	0.115	0.179	0
23	24	0.132	0.27	0
24	25	0.1885	0.3292	0
25	26	0.2544	0.38	0
25	27	0.1093	0.2087	0
28	27	0	0.396	0
27	29	0.2198	0.4153	0
27	30	0.3202	0.6027	0
29	30	0.2399	0.4533	0

Appendix C: IEEE 118-Bus Test System

i. Bus Data and Load Flow Results

Bus No.	Bus Voltage		Generation		Load	
	Magnitude (p.u.)	Angle (Deg.)	Real (MW)		Magnitude (p.u.)	Angle (Deg.)
1	0.95717	-98.43	51	27	0	0
2	0.97222	-97.87	20	9	0	0
3	0.96902	-97.53	39	10	0	0
4	0.998	-93.8	30	12	-9	-15.52
5	1.00207	-93.35	0	0	0	0
6	0.99	-96.08	52	22	0	15.77
7	0.98932	-96.52	19	2	0	0
8	1.015	-88.34	0	0	-28	62
9	1.04278	-81.08	0	0	0	0
10	1.05	-73.5	0	0	450	-50.88
11	0.9851	-96.36	70	23	0	0
12	0.99	-96.88	47	10	85	88.35
13	0.96824	-97.73	34	16	0	0
14	0.98359	-97.59	14	1	0	0
15	0.97	-97.86	90	30	0	6.82
16	0.98393	-97.19	25	10	0	0
17	0.99519	-95.39	11	3	0	0
18	0.973	-97.58	60	34	0	28.15
19	0.962	-98.01	45	25	0	-14.22
20	0.95701	-97.16	18	3	0	0
21	0.95784	-95.59	14	8	0	0
22	0.96915	-93.06	10	5	0	0
23	0.99954	-88.18	7	3	0	0
24	0.992	-88.43	0	0	-13	-13.46
25	1.05	-81.2	0	0	220	49.83
26	1.015	-79.42	0	0	314	9.72
27	0.968	-93.65	62	13	-9	3.66

28	0.96158	-95.29	17	7	0	0
29	0.9632	-96.18	24	4	0	0
30	0.98566	-90.35	0	0	0	0
31	0.967	-96.03	43	27	7	4.66
32	0.963	-94.21	59	23	0	-16.64
33	0.97098	-98.34	23	9	0	0
34	0.984	-97.53	59	26	0	-18.34
35	0.98047	-97.98	33	9	0	0
36	0.98	-97.98	31	17	0	7.56
37	0.99074	-97.06	0	0	0	0
38	0.96257	-92.29	0	0	0	0
39	0.97031	-99.69	27	11	0	0
40	0.97	-100.32	20	23	-46	26.9
41	0.96667	-100.42	37	10	0	0
42	0.985	-97.88	37	23	-59	21.94
43	0.97223	-97.66	18	7	0	0
44	0.97256	-95.25	16	8	0	0
45	0.98089	-93.56	53	22	0	0
46	1.005	-90.91	28	10	19	-1.29
47	1.01729	-88.78	34	0	0	0
48	1.02063	-89.46	20	11	0	0
49	1.025	-88.46	87	30	204	111.94
50	1.00134	-90.31	17	4	0	0
51	0.96738	-92.69	17	8	0	0
52	0.95737	-93.57	18	5	0	0
53	0.94626	-94.34	23	11	0	0
54	0.955	-93.29	113	32	48	-23.02
55	0.952	-93.71	63	22	0	4.83
56	0.954	-93.45	84	18	0	-18.66
57	0.97084	-92.5	12	3	0	0
58	0.95936	-93.31	12	3	0	0
59	0.985	-90.61	277	113	155	83.99
60	0.99322	-87.14	78	3	0	0
61	0.995	-86.25	0	0	160	-41.63
62	0.998	-86.99	77	14	0	0.6
63	0.96905	-87.42	0	0	0	0
64	0.98389	-85.76	0	0	0	0
65	1.005	-82.75	0	0	391	79.53
66	1.05	-83.5	39	18	392	16.79
67	1.01985	-85.89	28	7	0	0
68	1.00319	-82.81	0	0	0	0
69	1.035	-80.19	0	0	504.4	-79.11
70	0.984	-87.3	66	20	0	6.71
71	0.98685	-87.68	0	0	0	0
72	0.98	-88.62	0	0	-12	-11.16
73	0.991	-87.89	0	0	-6	9.63
74	0.958	-88.27	68	27	0	-8.82
75	0.96868	-87.04	47	11	0	0
76	0.95	-88.18	68	36	0	14.75
77	1.006	-83.03	61	28	0	-77.91
78	1.00333	-83.43	71	26	0	0
79	1.00924	-83.32	39	32	0	0
80	1.04	-81.59	130	26	477	162.51
81	0.99674	-82.33	0	0	0	0
82	1	-83.23	54	27	0	33.39
83	0.99287	-82.28	20	10	0	0
84	0.98262	-80.09	11	7	0	0

85	0.985	-78.7	24	15	0	-15.22
86	0.98671	-80.07	21	10	0	0
87	1.015	-79.81	0	0	4	10.99
88	0.98777	-75.94	48	10	0	0
89	1.005	-72.14	0	0	607	19.63
90	0.985	-76.7	78	42	-85	44.44
91	0.98	-76.48	0	0	-10	-13.03
92	0.99	-75.64	65	10	0	-55.98
93	0.98621	-78.94	12	7	0	0
94	0.99165	-81.34	30	16	0	0
95	0.98351	-82.44	42	31	0	0
96	0.99713	-82.77	38	15	0	0
97	1.0137	-82.53	15	9	0	0
98	1.02353	-82.94	34	8	0	0
99	1.01	-83.12	0	0	-42	-17.57
100	1.017	-81.97	37	18	252	67.66
101	0.99119	-80.17	22	15	0	0
102	0.98897	-77.25	5	3	0	0
103	1.01	-85.65	23	16	40	35.36
104	1	-88.64	38	25	0	18.6
105	1	-89.8	31	26	0	76.73
106	0.98418	-89.85	43	16	0	0
107	0.952	-92.18	28	12	-22	-24.08
108	0.98734	-90.71	2	1	0	0
109	0.98241	-91.06	8	3	0	0
110	0.973	-91.64	39	30	0	-19.36
111	0.98	-90	0	0	36	-1.84
112	0.975	-94.74	25	13	-43	41.51
113	0.993	-95.52	0	0	-6	34.89
114	0.96009	-94.54	8	3	0	0
115	0.96002	-94.55	22	7	0	0
116	1.005	-83.25	0	0	-184	50.34
117	0.98241	-96.92	20	8	0	0
118	0.95347	-88.03	33	15	0	0

ii. Transformer Data

Transformer	Between Buses	Tap Setting
1	8-5	0.985
2	30-17	0.96
3	26-25	0.96
4	38-37	0.935
5	63-59	0.96
6	64-61	0.985
7	65-66	0.935
8	68-69	0.935
9	81-80	0.935

iii. Shunt Capacitor Data

Bus No.	Susceptance (p.u.)
5	0.401
34	0.135

37	0.245
45	0.096
46	0.101
48	0.156
74	0.11
79	0.201
82	0.2
83	0.0986
105	0.2
107	0.0544
10	.0568

iv. Line Data

Line Between Buses		Line Impedance		Half Line Charging Susceptance (p.u.)
From	To	R (p.u.)	X (p.u.)	
1	2	0.0303	0.0999	0.025
1	3	0.0129	0.0424	0.0108
2	12	0.0187	0.0616	0.0158
3	5	0.0241	0.108	0.0284
3	12	0.0484	0.16	0.0406
4	5	0.0018	0.008	0.0021
4	11	0.0209	0.0688	0.0174
5	6	0.0119	0.054	0.0142
8	5	0	0.0267	0
5	11	0.0203	0.0682	0.0174
6	7	0.0046	0.0208	0.0054
7	12	0.0086	0.034	0.0088
8	9	0.0024	0.0305	1.162
8	30	0.0043	0.0504	0.514
9	10	0.0026	0.0322	1.23
11	12	0.0059	0.0196	0.005
11	13	0.0225	0.0731	0.0188
12	14	0.0215	0.0707	0.0182
12	16	0.0212	0.0834	0.0214
12	117	0.0329	0.014	0.0358
13	15	0.0744	0.2444	0.0626
14	15	0.0595	0.195	0.0502
15	17	0.0132	0.0437	0.0444
15	19	0.012	0.0394	0.01
15	33	0.038	0.1244	0.032
16	17	0.0454	0.1801	0.0466
17	18	0.0123	0.0505	0.013
30	17	0	0.0388	0
17	31	0.0474	0.1563	0.0398
17	113	0.0091	0.0301	0.0077
18	19	0.0112	0.0493	0.0114
19	20	0.0252	0.117	0.0298
19	34	0.0752	0.247	0.0632
20	21	0.0183	0.0849	0.0216
21	22	0.0209	0.097	0.0246
22	23	0.0342	0.159	0.0404
23	24	0.0135	0.0492	0.0498
23	25	0.0156	0.08	0.0864

23	32	0.0317	0.1153	0.1174
24	70	0.1022	0.4115	0.102
24	72	0.0488	0.196	0.0488
26	25	0	0.0382	0
25	27	0.0318	0.163	0.1764
26	30	0.008	0.086	0.908
27	28	0.0191	0.0855	0.0216
27	32	0.0229	0.0755	0.0192
27	115	0.0164	0.0741	0.0197
28	29	0.0237	0.0943	0.0238
29	31	0.0108	0.0331	0.0084
30	38	0.0046	0.054	0.422
31	32	0.0298	0.0985	0.0252
113	31	0	0.1	0
32	113	0.0615	0.203	0.0518
32	114	0.0135	0.0612	0.0163
33	37	0.0415	0.142	0.0366
34	36	0.0087	0.0268	0.0056
34	37	0.0026	0.0094	0.0098
34	43	0.0413	0.1681	0.0422
35	36	0.0022	0.0102	0.0026
35	37	0.011	0.0497	0.0132
38	37	0	0.0375	0
37	39	0.0321	0.106	0.027
37	40	0.0593	0.168	0.042
38	65	0.009	0.0986	1.046
39	40	0.0184	0.0605	0.0156
40	41	0.0145	0.0487	0.0122
40	42	0.0555	0.183	0.0466
41	42	0.041	0.135	0.0342
42	49	0.0715	0.323	0.086
42	49	0.0715	0.323	0.086
42	49	0.0715	0.323	0.086
43	44	0.0608	0.2454	0.0606
44	45	0.0224	0.0901	0.0224
45	46	0.04	0.1356	0.0332
45	49	0.0684	0.186	0.0444
46	47	0.038	0.127	0.0316
46	48	0.0601	0.189	0.0472
47	49	0.0191	0.0625	0.016
47	69	0.0844	0.2778	0.071
48	49	0.0179	0.0505	0.0126
49	50	0.0267	0.0752	0.0188
49	51	0.0486	0.137	0.0342
49	54	0.0869	0.291	0.073
49	54	0.073	0.289	0.0738
49	54	0.073	0.289	0.0738
49	66	0.018	0.0919	0.0248
49	66	0.018	0.0919	0.0248
49	66	0.018	0.0919	0.0248
49	69	0.0985	0.324	0.0828
50	57	0.0474	0.134	0.0332
51	52	0.0203	0.0588	0.014
51	58	0.0255	0.0719	0.0178
52	53	0.0405	0.1635	0.0406
53	54	0.0263	0.122	0.031
54	55	0.0169	0.0707	0.0202

54	56	0.0027	0.0096	0.0074
54	59	0.0503	0.2293	0.0598
55	56	0.0049	0.0151	0.0038
55	59	0.0474	0.2158	0.0564
56	57	0.0343	0.0966	0.0242
56	58	0.0343	0.0966	0.0242
56	59	0.0803	0.239	0.0536
56	59	0.0825	0.251	0.0568
56	59	0.0825	0.251	0.0568
59	60	0.0317	0.145	0.0376
59	61	0.0328	0.15	0.0388
63	59	0	0.0386	0
60	61	0.0026	0.0135	0.0146
60	62	0.0123	0.0561	0.0146
61	62	0.0082	0.0376	0.0098
64	61	0	0.0268	0
62	66	0.0482	0.218	0.0578
62	67	0.0258	0.117	0.031
63	64	0.0017	0.02	0.216
64	65	0.0027	0.0302	0.38
65	66	0	0.037	0
65	68	0.0014	0.016	0.638
66	67	0.0224	0.1015	0.0268
68	69	0	0.037	0
68	81	0.0018	0.0202	0.808
68	116	0.0003	0.0041	0.164
69	70	0.03	0.127	0.122
69	75	0.0405	0.122	0.124
69	77	0.0309	0.101	0.1038
70	71	0.0088	0.0355	0.0088
70	74	0.0401	0.1323	0.0337
70	75	0.0428	0.141	0.036
71	72	0.0446	0.18	0.0444
71	73	0.0087	0.0454	0.0118
74	75	0.0123	0.0406	0.0103
75	77	0.0601	0.1999	0.0498
75	118	0.0145	0.0481	0.012
76	77	0.0444	0.148	0.0368
76	118	0.0164	0.0544	0.0136
77	78	0.0038	0.0124	0.0126
77	80	0.0294	0.105	0.0228
77	80	0.017	0.0485	0.0472
77	80	0.017	0.0485	0.0472
77	82	0.0298	0.0853	0.0817
78	79	0.0055	0.0244	0.0065
79	80	0.0156	0.0704	0.0187
81	80	0	0.037	0
80	96	0.0356	0.182	0.0494
80	97	0.0183	0.0934	0.0254
80	98	0.0238	0.108	0.0286
80	99	0.0454	0.206	0.0546
82	83	0.0112	0.0366	0.038
82	96	0.0162	0.053	0.0544
83	84	0.0625	0.132	0.0258
83	85	0.043	0.148	0.0348
84	85	0.0302	0.0641	0.0123
85	86	0.035	0.123	0.0276

85	88	0.02	0.102	0.0276
85	89	0.0239	0.173	0.047
86	87	0.02828	0.2074	0.045
88	89	0.0139	0.0712	0.0193
89	90	0.0238	0.0997	0.106
89	90	0.0518	0.188	0.0528
89	90	0.0518	0.188	0.0528
89	92	0.0393	0.1581	0.0414
89	92	0.0099	0.0505	0.0548
89	92	0.0099	0.0505	0.0548
91	90	0.0254	0.0836	0.0214
91	92	0.0387	0.1272	0.0327
92	93	0.0258	0.0848	0.0218
92	94	0.0481	0.158	0.0406
92	100	0.0648	0.295	0.0772
92	102	0.0123	0.0559	0.0146
93	94	0.0223	0.0732	0.0188
94	95	0.0132	0.0434	0.0111
94	96	0.0269	0.0869	0.023
94	100	0.0178	0.058	0.0604
95	96	0.0171	0.0547	0.0147
96	97	0.0173	0.0885	0.024
98	100	0.0397	0.179	0.0476
99	100	0.018	0.0813	0.0216
100	101	0.0277	0.1262	0.0328
100	103	0.016	0.0525	0.0536
100	104	0.0451	0.204	0.0541
100	106	0.0605	0.229	0.062
101	102	0.0246	0.112	0.0294
103	104	0.0466	0.1584	0.0407
103	105	0.0535	0.1625	0.0408
103	110	0.0391	0.1813	0.0461
104	105	0.0099	0.0378	0.0099
105	106	0.014	0.0547	0.0143
105	107	0.053	0.183	0.0472
105	108	0.0261	0.0703	0.0184
106	107	0.053	0.183	0.0472
108	109	0.0105	0.0288	0.0076
109	110	0.0278	0.0762	0.0202
110	111	0.022	0.0755	0.02
110	112	0.0247	0.064	0.062
114	115	0.0023	0.0104	0.0028

Appendix D: UKGDS 61-Radial Distribution Network

i. Bus Data and Load Flow Results

Bus No.	Bus Voltage		Generation		Load	
	Magnitude (p.u.)	Angle (Deg.)	Real (MW)	Reactive (MVAr)	Real (MW)	Reactive (MVAr)
1	1	0	39.78	23.24	0	0
2	0.95512	23.51	0	0	0	0

3	1.04927	27.47	0	0	0	0
4	1.04922	27.47	0	0	0	0
6	1.04338	27.34	0	0	0	0
7	1.04338	27.34	0	0	0	0
8	1.04101	27.29	0	0	0	0
9	1.041	27.29	0	0	0	0
10	1.02134	26.85	0	0	0	0
11	1.01495	25.37	0	0	0	0
12	0.99	24.37	0	0	0	0
13	0.9865	24.27	0	0	0	0
14	0.98627	24.24	0	0	0	0
15	0.96498	23.81	0	0	0	0
16	0.96477	23.8	0	0	0	0
17	0.96089	23.71	0	0	0	0
18	0.96089	23.71	0	0	0	0
19	0.97994	23.92	0	0	0	0
20	0.97994	23.92	0	0	0	0
21	1.0282	22.89	0	0	0	0
22	1.02822	22.89	0	0	0	0
23	0.98051	20.66	0	0	0	0
24	0.96964	20.33	0	0	0	0
25	0.96962	20.33	0	0	0	0
26	0.96526	20.23	0	0	0	0
27	0.95778	20.14	0	0	0	0
28	1.03326	28.08	0	0	0	0
29	1.0328	28.07	0	0	0	0
30	1.02796	28.39	0	0	0	0
31	1.02786	28.39	0	0	0	0
32	1.04499	27.6	0	0	0	0
33	1.04116	27.77	0	0	0	0
34	1.03358	28	0	0	0	0
35	1.02922	28.24	0	0	0	0
36	1.02422	28.68	0	0	0	0
37	1.02028	28.98	0	0	0	0
38	1	31.11	1.3	-8.49	0	0
39	0.9822	23.97	0	0	0	0
40	1.03175	26.43	0	0	0	0
41	1.01852	25.93	0	0	0	0
42	1.02918	26.48	0	0	0	0
43	0.96739	20.28	0	0	0	0
44	0.95256	23.22	0	0	0	0
45	0.99564	50.39	0	0	1.9	0.39
46	1.01776	54.28	0	0	1.5	0.3
47	1.01083	55.51	0	0	0.28	0.06
48	0.99761	55.14	0	0	0.32	0.06
49	1.00424	53.92	0	0	3.31	0.67
50	1.00892	54.25	0	0	1.93	0.39
51	1.01007	49.78	0	0	18.4	3.74
52	0.9841	50.59	0	0	1.9	0.39
53	0.99714	53.01	0	0	0.06	0.01
54	1.00649	53.23	0	0	0.06	0.01
55	1.01671	51.08	0	0	0.55	0.11
56	0.9964	49.87	0	0	0.04	0.01
57	1.0008	47.79	0	0	0.77	0.15
58	0.992	48.4	0	0	2.7	0.55
59	1.00956	48.44	0	0	2.85	0.58
60	0.98632	55.47	0	0	0.8	0.16

61	0.97578	57.84	0	0	0.21	0.04
62	1.00292	55.78	0	0	0.58	0.12

ii. Transformer Data

Transformer	Between Buses	Tap Setting
1	1-3	0.95
2	1-3	.95
3	2-45	0.95
4	4-46	1.01
5	7-47	1.02
6	9-48	1.03
7	13-51	0.955
8	14-51	0.955
9	16-52	0.96
10	18-53	0.96
11	20-54	0.97
12	44-22	0.97
13	23-58	0.95
14	25-56	0.97
15	26-57	0.95
16	27-59	0.95
17	29-60	1.03
18	31-61	1.025
19	35-62	1.01

iii. Line Data

Line Between Buses		Line Impedance		Half Line Charging Susceptance (p.u.)
From	To	R (p.u.)	X (p.u.)	
1	3	0	0.25	0
1	3	0	0.25	0
17	2	0.228	0.227	0
3	4	0	0.001	0
3	28	0.213	0.284	0
3	32	0.091	0.121	0
3	41	0.227	0.302	0
3	42	0.104	0.199	0
4	6	0.128	0.094	0
4	40	0.1	0.225	0
6	7	0	0.001	0
6	8	0.056	0.041	0
8	9	0.002	0.001	0
8	10	0.507	0.374	0
10	49	0.1514	1.6144	0
11	12	0.216	0.287	0
40	11	0.098	0.221	0
11	50	0.0917	1.0553	0
12	13	0.03	0.026	0.002

12	14	0.031	0.032	0.001
12	15	0.517	0.376	0
12	39	0.079	0.106	0
41	12	0.216	0.287	0
42	12	0.208	0.398	0
13	51	0.0343	0.8925	0
14	51	0.0343	0.8925	0
15	16	0.009	0.007	0
15	17	0.166	0.121	0
17	18	0	0.001	0
19	20	0	0.001	0
39	19	0.026	0.016	0.001
19	44	0.3	0.23	0.006
21	22	0	0.001	0
21	23	0.538	0.733	0
44	22	0.0728	0.1039	0
23	24	1.126	0.873	0.001
23	27	0.654	0.454	0
24	25	0.045	0.02	0
24	43	0.238	0.173	0
43	26	0.226	0.164	0
27	59	0.0944	1.0869	0
28	29	0.053	0.023	0
28	30	0.094	0.11	0.001
30	31	0.039	0.039	0
30	36	0.083	0.083	0
32	33	0.113	0.1	0.002
33	34	0.153	0.203	0
35	34	0.149	0.108	0
37	35	0.4	0.291	0
36	37	0.088	0.088	0
37	38	0.401	0.292	0